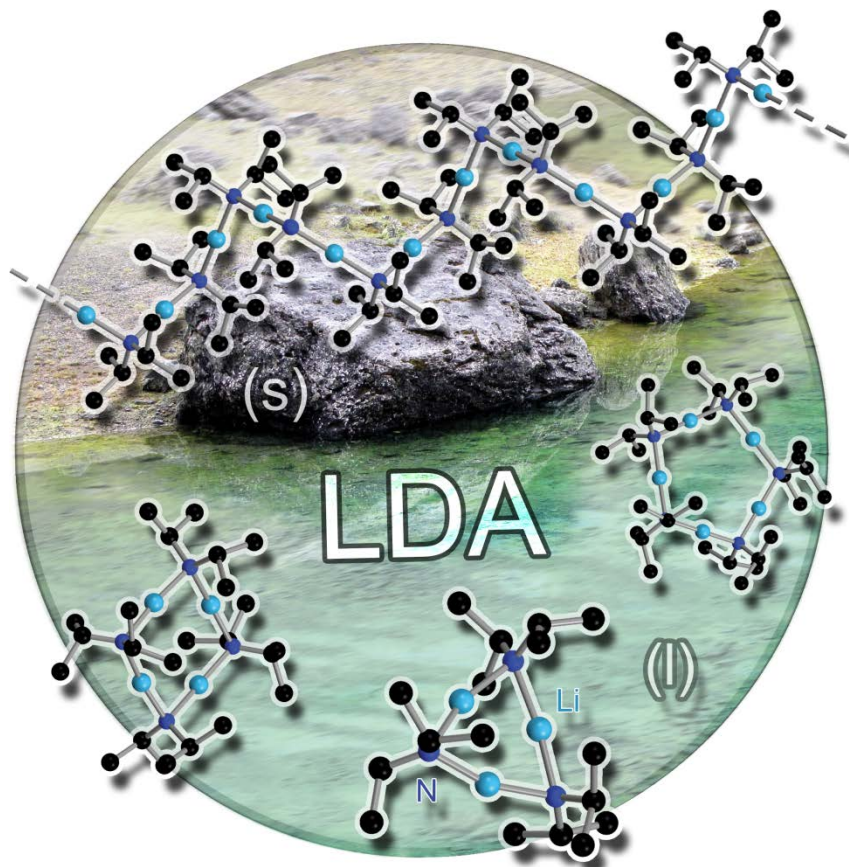


DOSY External Calibration Curve Molecular Weight Determination as a Valuable Methodology in Characterizing Reactive Intermediates in Solution



Frontispiece-Cover in *Angewandte Chemie Int. Ed.*

R. Neufeld, M. John, D. Stalke, *Angew. Chem. Int. Ed.*, **2015**, *54*, 6994–6998.

The Donor-Base-Free Aggregation of Lithium Diisopropyl Amide in Hydrocarbons Revealed by a DOSY Method

Dissertation zur Erlangung des Doktorgrades

„Doctor rerum naturalium“

der Georg-August-Universität Göttingen

im Promotionsprogramm Chemie

der Georg-August University School of Science (GAUSS)



vorgelegt von Roman Neufeld aus Pawlodar

Göttingen, 2016

Betreuungsausschuss

Prof. Dr. Dietmar Stalke, Institut für Anorganische Chemie

Prof. Dr. Sven Schneider, Institut für Anorganische Chemie

Mitglieder der Prüfungskommission

Referent: Prof. Dr. Dietmar Stalke

Korreferent: Prof. Dr. Sven Schneider

weitere Mitglieder der Prüfungskommission

Jun. -Prof. Selvan Demir, Institut für Anorganische Chemie

Prof. Ricardo A. Mata, Institut für Physikalische Chemie

Prof. Konrad Koszinowski, Institut für Organische und Biomolekulare Chemie

Dr. Michael John, Institut für Organische und Biomolekulare Chemie

Tag der mündlichen Prüfung: 14.03.2016

...for my lovely family

*There must be a beginning of any great matter, but the continuing
unto the end until it be thoroughly finished yields the true glory.*

Sir Francis Drake, 1587

Table of Contents

1	INTRODUCTION	1
1.1	Synthetically Useful Metal Amides	2
1.1.1	Structure of LDA	6
1.1.1	Structure of LiTMP	7
1.1.2	Structure of LiHMDS and its Havier Analoges	9
1.1.3	Structure of Hauser- and <i>Turbo</i> -Hauser Bases	12
1.2	Diffusion NMR Measurements	15
1.2.1	Aspects of Diffusion	15
1.2.2	The <i>Hahn</i> Spin-Echo Experiment	16
1.2.3	The Pulsed Gradient Spin-Echo (PGF-SE)-Experiment	17
1.2.4	The Pulsed Gradient Stimulated-Echo (PGF-STE)-Experiment	21
1.2.5	Advancements to the Stimulated-Echo	22
1.2.6	Extracting Diffusion Coefficients	23
1.2.7	Molecular Weight Determination	25
1.3	Scope of this Thesis	30
2	RESULTS AND DISCUSSION	32
2.1	Development of the DOSY-External Calibration Curve MW-Determination Methodology	32
2.1.1	Application of a Normalized Reference System with Fixed Diffusion Coefficients	32
2.1.2	External Calibration Curves (ECC) and Internal References	35
2.1.3	Quality of TOL- <i>d</i> ₇ and THF- <i>d</i> ₇ as Internal Reference	39
2.1.4	Influence of Shape	40
2.1.5	Influence of Concentration	41
2.1.6	Influence of Temperature	42
2.1.7	Influence of Halides and Molar Density	43
2.1.8	Influence of Deuterated Compounds	47
2.2	DOSY-ECC-MW-Determination of Organometallics and Metal Amides	47
2.2.1	Structure of LDA in THF Solution	47
2.2.2	Structure of LDA in Toluene Solution	48
2.2.3	Structure of Na-Indenide in THF Solution	52
2.2.4	Structure of [<i>t</i> -BuLi] ₄ [Me ₂ NC ₆ H ₄ Li] ₄ in Toluene Solution	54
2.2.5	Structure of MHMDS with Ammonia as Donorbase in Toluene Solution	55
2.2.6	Structure of Hauser Base ¹ Pr ₂ NMgCl in THF solution	62
2.2.7	Structure of <i>Turbo</i> -Hauser Base ¹ Pr ₂ NMgCl·LiCl in THF solution	70
2.2.8	Structure of <i>Turbo</i> -Hauser Base TMPMgCl·LiCl in THF solution	92
3	SUMMARY AND OUTLOOK	98

4	EXPERIMENTAL PART	104
4.1	Techniques and Experiments	104
4.1.1	Handling of Air- and Moisture Sensitive Compounds	104
4.1.2	NMR Experiments	104
4.1.3	Computational Details	105
4.2	Synthesis and Crystallization	106
4.2.1	Donor-Base-Free LDA	106
4.2.2	Na-Indenide	107
4.2.3	MHMDS-Ammoniacates (M = Li, Na, K, Rb and Cs)	107
4.2.4	¹ Pr ₂ NMgCl	108
4.2.5	¹ Pr ₂ NMgCl·LiCl	108
4.2.6	TMPMgCl·LiCl	109
4.3	Preparation of DOSY-NMR-Samples	110
4.3.1	Internal References	110
4.3.2	LDA	110
4.3.3	Na-Indenide	110
4.3.4	MHMDS-Ammoniacates (M = Li, Na and K)	111
4.3.5	¹ Pr ₂ NMgCl and ¹ Pr ₂ NMgCl·LiCl	111
4.3.6	TMPMgCl·LiCl	111
4.4	X-Ray Analysis	111
4.4.1	[NH ₃ ·LiN(SiMe ₃) ₂] ₂ ·TOL	112
4.4.2	[NH ₃ ·NaN(SiMe ₃) ₂] ₂	113
4.4.3	[NH ₃ ·KN(SiMe ₃) ₂] ₂	114
4.4.4	[NH ₃ ·RbN(SiMe ₃) ₂] ₂	115
4.4.5	(NH ₃) ₄ ·[NaN(SiMe ₃) ₂] ₂	116
4.4.6	[(THF)ClMg(μ- ¹ Pr ₂ N)] ₂	117
5	APPENDIX	118
6	REFERENCES	168
	DANKSAGUNG	176
	CURRICULUM VITAE	178

Abbreviations

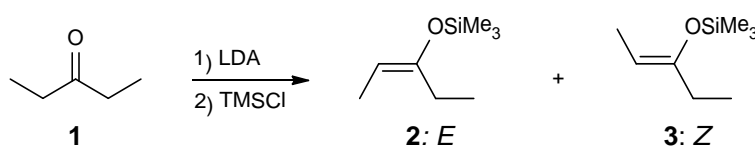
cHex	<i>cyclo</i> -hexyl
CIP	contact ion pair
DMF	<i>N,N</i> -dimethylformamide
DMSO	dimethyl sulfoxide
DOSY	diffusion ordered spectroscopy
Et	ethyl
Et ₂ O	diethyl ether
HOESY	heteronuclear overhauser enhancement spectroscopy
ⁱ Pr	<i>iso</i> -propyle
HMDS	1,1,1,3,3,3-hexamethyldisilazane
LDA	lithium diisopropylamide
LiTMP	lithium 2,2,6,6-tetramethylpiperidide
Me	methyl
MHMDS	alkalimetal 1,1,1,3,3,3-hexamethyldisilazide
ⁿ BuLi	<i>n</i> -butyllithium
NMR	nuclear magnetic resonance
Ph	phenyl
PMDETA	<i>N,N,N',N'',N'''</i> -pentamethyldiethylenetriamine
RF	radiofrequency
SSIP	solvent-separated ion pair
^t BuLi	<i>tert</i> -butyllithium
<i>sec</i>	secondary
TMP	2,2,6,6-tetramethylpiperidide
THF	tetrahydrofurane
TOL	toluene
TMEDA	<i>N,N,N,N</i> -tetramethylcyclohexane-1,2-diamine
TMEDA	<i>N,N,N',N'</i> -tetramethylethylene-1,2-diamine

Parts of this Ph. D. thesis have been published or submitted:

- [1] R. Neufeld, R. Michel, R. Herbst-Irmer, R. Schöne, D. Stalke, “*Introducing a Hydrogen Bond Donor Into a Non Nucleophilic Brønsted Base: Structural insights into Ammonia Coordinated Alkali Metal Hexamethyldisilazide (HMDS, Metal = Li, Na, K, Rb and Cs)*”, *Chem. Eur. J.* **2016**, submitted.
- [2] R. Neufeld, T. L. Teuteberg, R. Herbst-Irmer, R. A. Mata, D. Stalke, “*Solution Structures of Hauser Base ${}^i\text{Pr}_2\text{NMgCl}$ and Turbo-Hauser Base ${}^i\text{Pr}_2\text{NMgCl}\cdot\text{LiCl}$ in THF and the Influence of LiCl on the Schlenk-Equilibrium*”, *JACS* **2016**, accepted.
- [3] R. Neufeld, D. Stalke, “*Solution Structure of Turbo-Hauser Base $\text{TMPMgCl}\cdot\text{LiCl}$ in $\text{THF-}d_8$* ”, *Chem. Eur. J.* **2016**, submitted.
- [4] S. Bachmann, R. Neufeld, M. Dzemski, D. Stalke, “*New External Calibration Curves (ECCs) for the Determination of Molecular Weights in Various Common NMR Solvents*”, *Chem. Eur. J.* **2016**, accepted.
- [5] R. Neufeld, M. John, D. Stalke, “*The Donor-Base-Free Aggregation of Lithium Diisopropyl Amide in Hydrocarbons Revealed by a DOSY Method*”, *Angew. Chem.* **2015**, 127, 7100–7104; *Angew. Chem. Int. Ed.* **2015**, 54, 6994–6998.
- [6] R. Neufeld, D. Stalke, “*Accurate Molecular Weight Determination of Small Molecules via DOSY-NMR by Using External Calibration Curves with Normalized Diffusion Coefficients*”, *Chem. Sci.* **2015**, 6, 3354–3364.
- [7] R. Michel, T. Nack, R. Neufeld, J. M. Dieterich, R. A. Mata, D. Stalke, “*The Layered Structure of $[\text{Na}(\text{NH}_3)_4][\text{Indenide}]$ Containing a Square-Planar $\text{Na}(\text{NH}_3)_4^+$ Cation*”, *Angew. Chem.* **2013**, 125, 762–766; *Angew. Chem. Int. Ed.* **2013**, 52, 734–738.

1 INTRODUCTION

Besides synthetically useful organolithium compounds^[8] like MeLi, ⁿBuLi, ^tBuLi und PhLi, especially secondary organoamides (RR'N⁻) play a huge role in organic chemistry. In contrast to organolithiums which may be used as nucleophiles in useful addition or substitution reactions,^[9] sterically hindered *sec*-organoamides are predominantly used as powerful non nucleophilic Brønsted bases in synthetic chemistry.^[10] A variety of amidolithium compounds are commercially available. However, their chemical formula is often depicted as monomeric species, although it has been known for a long time that the actual structure is much more complicated. The aggregation of *sec*-amidolithium compounds differs in respect to their substituents. Studies in solution as well as in the solid state reveal several aggregation modes varying from monomers, cyclic dimers, trimers, tetramers and higher oligomers (see next chapter), furthermore dimeric units can associate laterally to form “ladder” like coordination polymers.^[11] Usually, disaggregated amidolithiums show similar to organolithiums an enhanced reactivity and a different chemoselectivity (Scheme 1-1).^[12] This is why the knowledge of the structure in the solid state and especially in solution where they operate is extraordinary important to deduce structure-reactivity relationships.^[13] In the following chapters a brief synthetical and structural overview of the most important *sec*-organoamides will be given. Finally, the use of self-diffusion measurements as a valuable tool for the determination of aggregation states will be introduced.



<i>Solvent</i>	<i>E/Z ratio</i>	<i>Yield [%]</i>	<i>Lit.</i>
Hexane	1.0:1.5	14	[12a]
THF	0.5:99.5	quant.	[12b]

Scheme 1-1. Enolization of 3-pentanone **1** with lithium diisopropylamide (LDA) in hexane and subsequent trapping with TMSCl affords silylenolates **2** and **3** in a *E/Z* ratio of 1.0:1.5 in very poor yields (14%).^[12a] In contrast, the same reaction carried out in THF gives highly stereoselectively the (*Z*)-3-trimethylsiloxy-2-pentane **3** in quantitative yield.^[12b] The change in reactivity and stereoselectivity is reflected in the different aggregation states of LDA in both solvents. In hexane LDA forms a distribution of at least three cyclic oligomers,^[5] while in THF it forms exclusively a disolvated dimer^[14] (for more information about the solution structure of LDA see chapter 1.1.1 and 2.2.2).

1.1 Synthetically Useful Metal Amides

The most important secondary amides used in synthetic chemistry are LDA **4**, LiTMP **5**, MHMDS **6** with $M = \text{Li, Na and K}$, Hauser bases **7** and **8** and their lithium chloride stabilized *Turbo*- analogues **9** and **10** (Fig. 1-1).

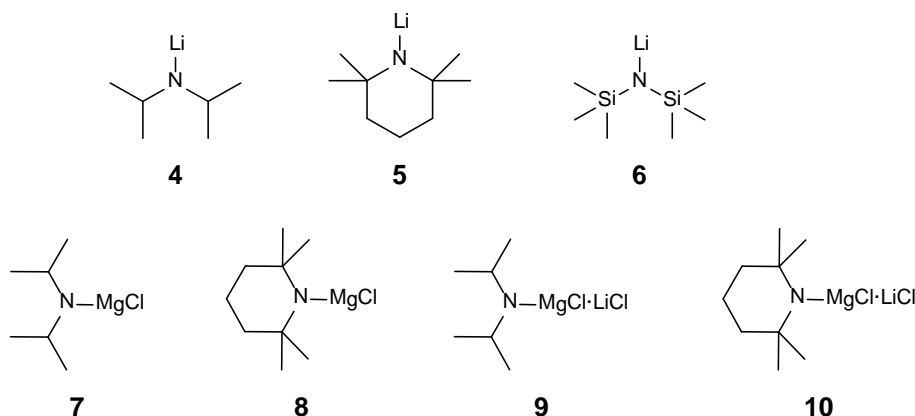
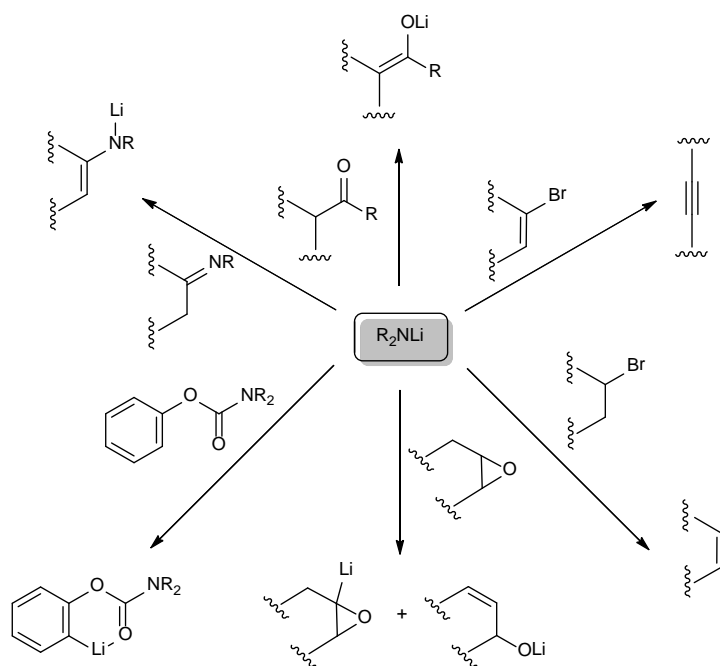


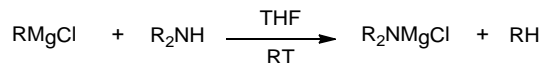
Fig. 1-1. Some of most important secondary amides in synthetic chemistry.

Commonly, alkalimetal amides are prepared by treating the secondary amine R_2NH with an alkyl lithium reagent (*e.g.* $^t\text{BuLi}$) in a cooled THF solution (-78°C). Diisopropylamide has a $\text{p}K_{\text{a}}$ value of 36.^[15] Its conjugate base is therefore suitable for the deprotonation of compounds with lower acidity.



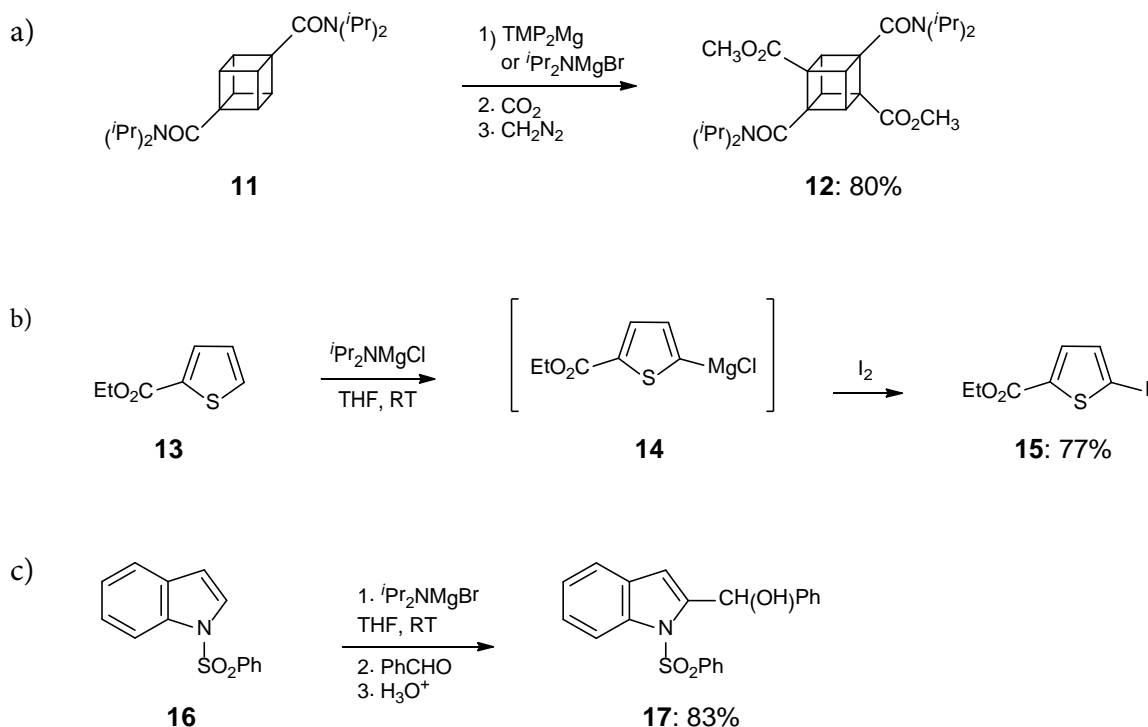
Scheme 1-2. Prominent reactions of lithium amides.^[13c]

Due to the steric demand of the amide ligand alkalimetal amides represent excellent reagents for the generation of enolates by abstraction of the acidic α -hydrogen atom of a carbonyl function. The most prominent reactions of lithium amides are summarized in Scheme 1-2. The high reactivity of organolithium compounds can also be considered their Achilles heel, since they are routinely used at low temperature (mostly -78°C). Additionally they often cause competing side reactions (*e.g.* *Chichibabin* reactions) and do not tolerate certain synthetically important functional groups like *e.g.* ester, carbonyl, nitrile, sulphoxide and halide. This is why in the past decades bis-amidomagnesium bases $[(\text{R}_2\text{N})\text{Mg}]$ and organomagnesium halides (at the simplest level described with the formula “ RMgX ”) have found profound improvements in synthetic chemistry. Compared with organolithium reagents the magnesium compounds have more covalent character and therefore less reactive metal-ligand bonds. This is why they display a higher functional group tolerance and a much greater chemoselectivity.^[16] Consequently they generally can be used at room temperature (RT) without significant side reactions. In the late 1940s *Hauser* and co-workers succeeded in the development of the amido Grignard reagent R_2NMgX , formally known as Hauser bases, by replacing the alkyl ligand of a Grignard with a secondary amide (Scheme 1-3).^[17]

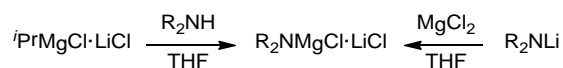


Scheme 1-3. Typical preparation of Hauser bases.

The breakthrough in synthetic protocols of Hauser bases culminates in the 1980s and 1990s, where *Eaton* and co-workers introduced $^i\text{Pr}_2\text{NMgBr}$ and TMP_2Mg , which were shown to *ortho*-magnesiate carboxamides (Scheme 1-4a).^[18] Later, *Kondo*, *Sakamoto* and co-workers reported the utility of $^i\text{Pr}_2\text{NMgX}$ ($\text{X} = \text{Cl}, \text{Br}$) as selective deprotonation reagents (exclusively at the 2-position) for heterocyclic thiophene^[19] and phenylsulphonyl-substituted indoles^[20] (Scheme 1-4b-c). An important driving force for such reactions is the presence of an *ortho*-directing group on the substrate, typically Lewis basic heteroatoms within or next to a double or triple bond. The principle of the functional group is known as “*Direct ortho Metallation*” (*DoM*) and has been elaborated by *Snieckus* and *Beak*.^[21]



Scheme 1-4. a) Compound **12** can be synthesized by α -magnesiation of carboxamide **11** with TMP_2Mg or $i\text{Pr}_2\text{NMgBr}$ followed by the subsequent reaction with CO_2 and CH_2N_2 .^[18] b) 2-carboethoxythiophene **13** was metalated at the *ortho* position by using an excess of $i\text{Pr}_2\text{NMgCl}$ (2 equiv). Afterwards the magnesiated intermediate **14** was treated with iodine to give iodothiophene **15** in 77% yield. c) Selective magnesiation of indole **16** in *ortho* position followed by the reaction with benzaldehyde give the substituted indole **17**.^[20]

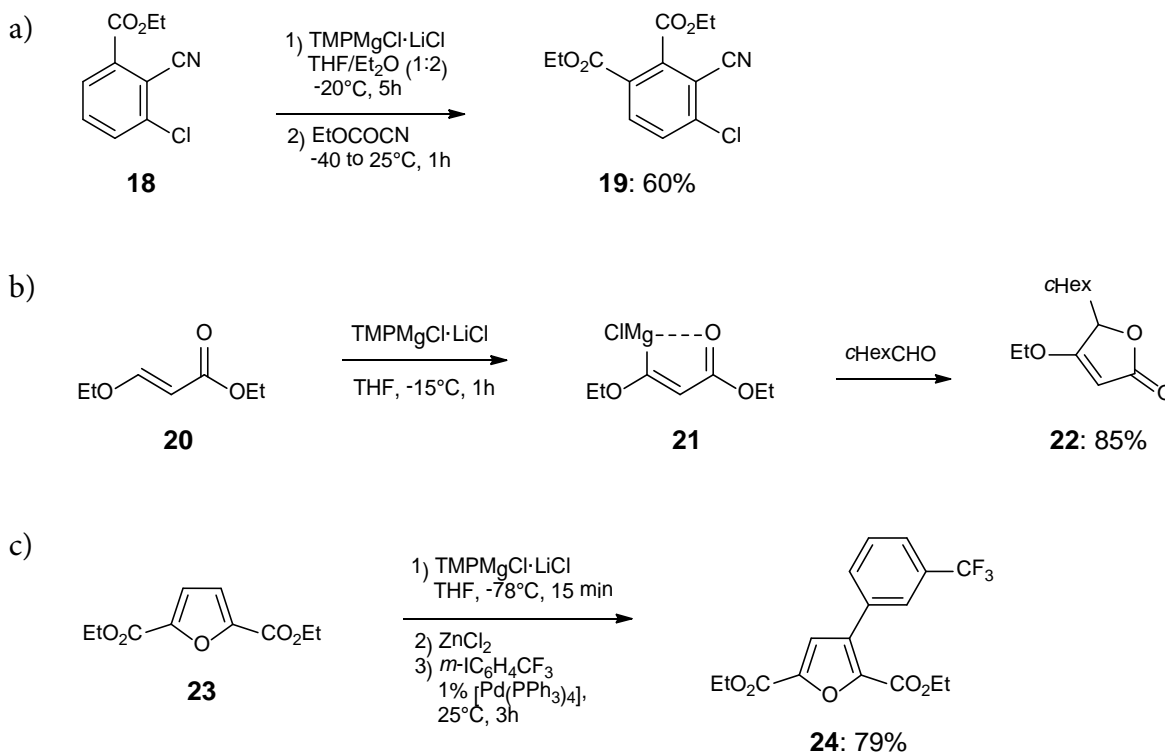


Scheme 1-5. Typical preparation of *Turbo*-Hauser bases.

A huge disadvantage of Hauser bases is their poor solubility in THF. In consequence, the metalation rates are slow and a huge excess of base is required (mostly 10 equiv.). This circumstance complicates the functionalization of the metalated intermediate with an electrophile. It is well known that numerous metallic salts are better soluble when LiCl is added to the solution.^[22] That feature led to the design of LiCl-solubilized *Turbo*-Hauser Bases $\text{TMPMgCl} \cdot \text{LiCl}$ **10** and the less bulky *Turbo*-analogue $i\text{Pr}_2\text{NMgCl} \cdot \text{LiCl}$ **9** (Scheme 1-5).^[23] Equipped with enhanced kinetic basicity,¹ these commercially available reagents

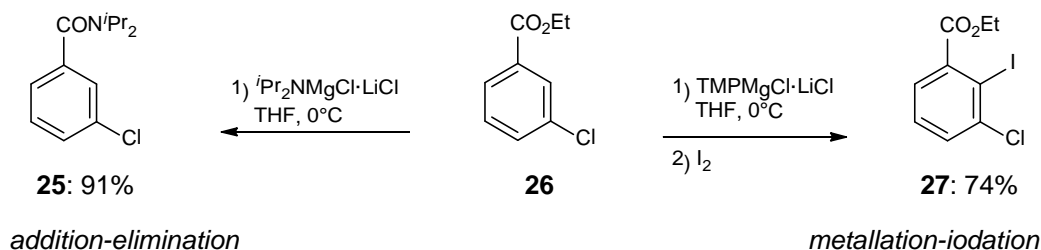
¹ For the sake of completeness it should be mentioned that in modern synthetic chemistry many other lithium chloride stabilized magnesium amide complexes like e.g. $(\text{TMP})_2\text{Mg} \cdot 2\text{LiCl}$, $\text{TMPZnCl} \cdot \text{LiCl}$, $(\text{TMP})_2\text{Zn} \cdot 2\text{LiCl}$ or mixed metal ate complexes like e.g. $(\text{TMP})_2\text{CuLi}$, $\text{R}_2\text{Zn}(\text{TMP})\text{Li}$, $\text{R}_3\text{Al}(\text{TMP})\text{Li}$ are also used as selective deprotonating reagents. For more information see e.g.: a) B. Haag, M. Mosrin, H. Ila, V. Malakhov, P. Knochel, *Angew. Chem.* **2011**, *123*, 9968–9999; *Angew. Chem. Int. Ed.* **2011**, *50*, 9794–9824. b) R. E. Mulvey, F. Mongin, M. Uchiyama, Y. Kondo, *Angew. Chem.* **2007**, *119*, 3876–3899; *Angew. Chem. Int. Ed.* **2007**, *46*, 3802–3824.

display a high reactivity even at room temperature (RT) as well as excellent regioselectivity and high functional group tolerance for a large number of aromatic and heteroaromatic substrates (Scheme 1-6).^[24]



Scheme 1-6. a) Metalation of ethyl 2-cyano,3-chlorobenzoate **18** with $\text{TMPMgCl}\cdot\text{LiCl}$ (**10**) and reaction with EtOCOCN gives the benzene derivative **19** in 60% yield.^[25] b) Compound **10** allows also selective deprotonations of 1,4 unsaturated compounds like e.g. the Michael acceptor **20**. The addition of compound **21** to $c\text{HexCHO}$ affords the unsaturated lactone **22** in 85% yield.^[26] c) Metalation of furane **23** and subsequent transmetalation with ZnCl_2 leads to a stable Zn -intermediate that can in presence of 1% $[\text{Pd}(\text{PPh}_3)_4]$ undergo a cross-coupling with an aryl iodide to give the functionalized furane **24**.^[27]

Interestingly, the diisopropylamido reagent ${}^i\text{Pr}_2\text{NMgCl}\cdot\text{LiCl}$ **9** can show a very different reactivity compared to its TMP counterpart **10** (Scheme 1-7). While **10** easily metalates ethyl-3-chlorobenzoate **26** in the C2 position to give after iodation benzene **27**, the same reaction carried out with **9** results in no metalation at all. Instead, an addition-elimination reaction occurs with the formation of *m*-chloro-*N,N*-diisopropylbenzamide **25**.^[28] The different reactivity can be attributed to the higher kinetic basicity of compound **10** compared to its homologous *i*Pr-Turbo-Hauser base **9**.^[23] Additionally, this contrasting behaviour could also be reflected in the aggregation state of both magnesium amides in THF solution that will be discussed in chapter 1.1.3.



Scheme 1-7. Contrasting reactivity of *Turbo*-Hauser bases $i\text{Pr}_2\text{NMgCl}\cdot\text{LiCl}$ **9** and $\text{TMPMgCl}\cdot\text{LiCl}$ **10** for the reaction with ethyl-3-chlorobenzoate **26** in THF solution at 0°C .^[28]

1.1.1 Structure of LDA²

LDA is one of the most prominent amide reagents that play a key role in organic synthesis, serving as a base par excellence for a broad range of deprotonation reactions.^[29] However, its donor-base free solid-state crystal structure **28** was only determined in 1991 by *Barnett et al.*^[30] It consists of an infinite helical chain with four units per turn in the helix (Fig. 1-2). In solution with monodentate donating solvents LDA exists as a single observable aggregate—the disolvated cyclodimer **29**.^[14] That Li_2N_2 dimer with one donor molecule coordinating each alkali metal atom, afford an overall lithium coordination number of three. Polydentate ligands give isostructural disolvated dimers with one exception: the TMCDA-solvated monomer **30**. This is why LDA is an ideal template for studying organolithium reactivity^[13c, 31] and LDA is one of the best explored lithium amides.^[10] Especially *Collum et al.* provided closer insights into LDA-mediated reaction mechanisms, solution kinetics, structure reactivity relationships, reaction rates and selectivity.^[12a, 32] However, the aggregation of LDA in donor-base free solvents was still unclear. In 1991 *Kim and Collum et al.* investigated $[\text{}^6\text{Li}]\text{LDA}$ and $[\text{}^6\text{Li}, \text{}^{15}\text{N}]\text{LDA}$ in hexane by ${}^6\text{Li}$ and ${}^{15}\text{N}$ NMR spectroscopy.^[12a] They observed a mixture of three major cyclic oligomers and suggested that they could correspond to cyclic dimers, trimers and higher oligomers. Unfortunately they were not able to quantify these observations because “*a severe overlap renders the effort required for a detailed study unjustifiable*”. A further characterization of these oligomers was not possible at that time.

² Includes revised parts of my publication: R. Neufeld, M. John, D. Stalke, *Angew. Chem.*, **2015**, *127*, 7100–7104; *Angew. Chem. Int. Ed.*, **2015**, *54*, 6994–6998.

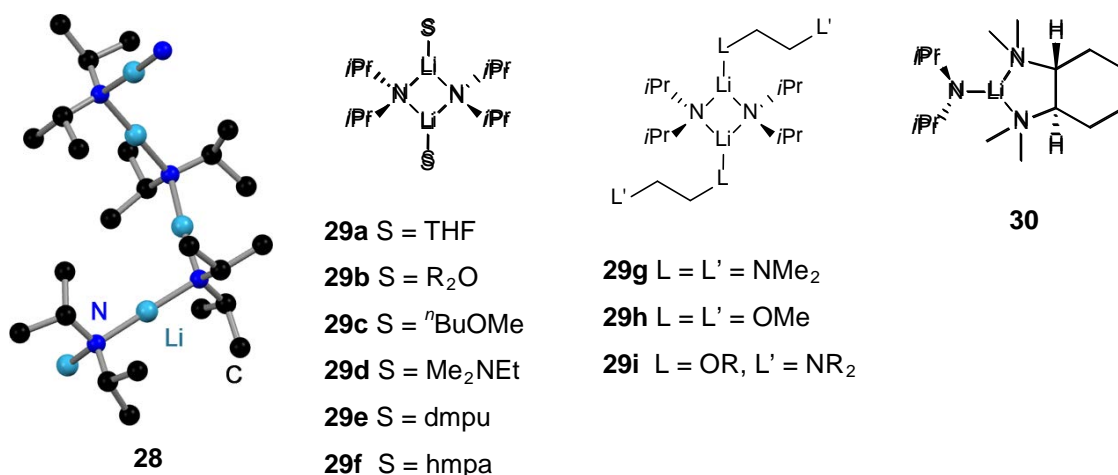


Fig. 1-2. Solid state structures (28)^[30] and solution structures (29, 30) of LDA.^[13c]

1.1.1 Structure of LiTMP

In 1983 *Lappert and Atwood et al.* revealed the solid state structure of unsolvated lithium 2,2,6,6-tetramethylpiperidide to be a cyclotetramer **32** (Fig. 1-3) with an essentially planar Li₄N₄-ring.^[33] Later, ⁶Li, ¹⁵N NMR and DOSY spectroscopic studies showed that in hydrocarbon solution cyclotetramer and -trimer co-exist in a balanced equilibrium.^[34] Three decades after *Lappert's* report, *Hevia and Mulvey et al.* finally characterized the concealed cyclotrimeric polymorph **31** in the solid state *via* X-ray crystallography.^[34a] In donating solvents LiTMP shows a much greater structural diversity. Beside the above mentioned cyclic oligomers LiTMP can form disolvated monomers **33** and **34**,^[35] di- and tetrasolvated dimers **35** and **36**,^[36] triple ions **37**^[37] and open dimers **38** and **39** (Fig. 1-4).^[38] The latter have shown to be important reactive intermediates since they contain vacant coordination sites for substrate precomplexation and a highly basic lone pair on the nitrogen atom.

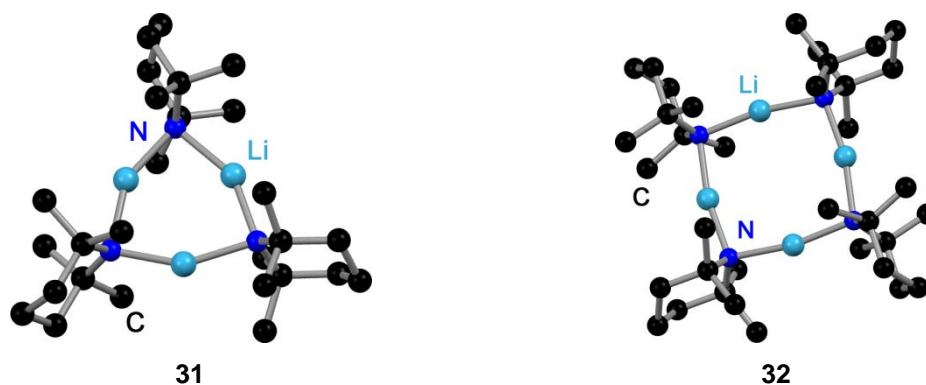


Fig. 1-3. Structure of LiTMP in the solid state and in hydrocarbons with hydrogen atoms omitted for clarity.

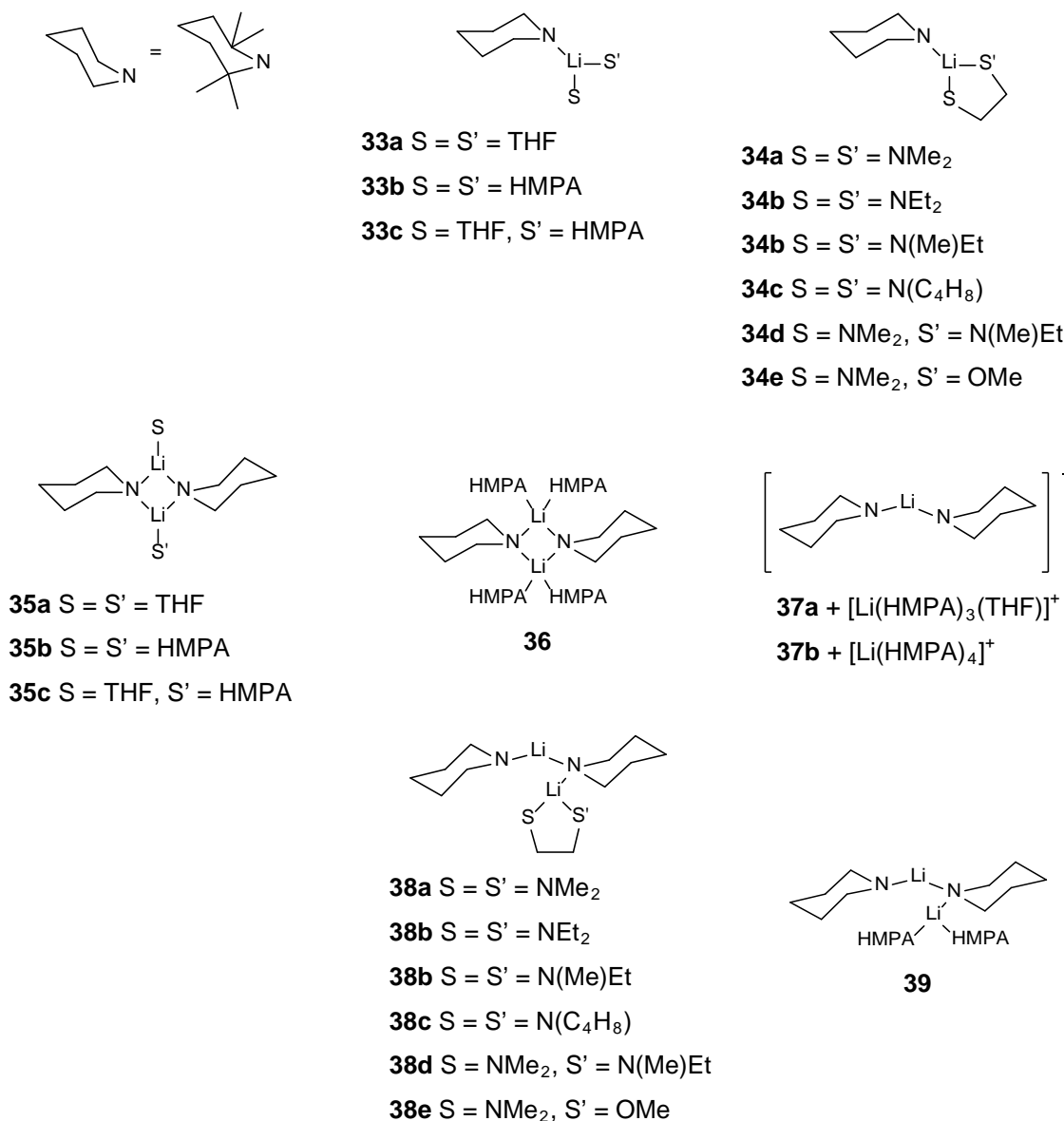


Fig. 1-4. Structural diversity of LiTMP in mono- and polydentate solvents.

The equilibrium between monomeric **34** and open dimeric **38** highly depends on the used chelating ligand and its concentration. *E.g.* the ratio of **34d** and **38d** is 1:3, while the ratio is completely inverted for species **34e** and **38e** (0.75 eq. of ligand, at -100°C in a 2:1 pentane:toluene solution).^[38a] Most of the solution studies have been carried out on the conformationally locked but isostructural 2,2,4,6,6-pentamethylpiperidide (LiPMP).^[38a]

1.1.2 Structure of LiHMDS and its Havier Analoges³

Besides LDA and LiTMP alkali metal 1,1,1,3,3,3-hexamethyldisilazides (MHMDSs), particularly Li-, Na- and KHMDS are very important reagents in many synthetic protocols.^[10] The high structural variance of MHMDS becomes apparent from the different aggregation motifs in the solid state, in the gas phase and in solution: The solid state structure of Li-^[39] and NaHMDS^[40] is a cyclic trimer (**40** in Fig. 1-5), whereas the latter also crystallizes as a linear coordination polymer (**42**).^[41] K-,^[42] Rb- and CsHMDS form dimeric structures (**44**, without donor base).^[43] In the gas phase LiHMDS adopts dimers^[44] (**44**, without donor base) and NaHMDS monomers^[45] (**43**, without donor base). The adducts of Li-,^[46] Na-^[47] and KHMDS^[42b, 48] with monodentate donor bases show dimeric (**44**) and polymeric structures (polymers of **44**, bridged by donor bases). Monomeric adducts (**43**) of Li-^[49] and KHMDS^[50] have been observed so far only with chelating bases like TMEDA and crown ethers. Rb- and CsHMDS were characterized as coordination polymers of dimers bridged by dioxane.^[47d] In solution LiHMDS shows a complex equilibrium of solvation and aggregation depending on the employed solvent. *Kimura* and *Brown* reported in 1971 that LiHMDS exists as a tetramer-dimer mixture in hydrocarbons and as dimer-monomer mixture in THF and Et₂O.^[51] Later, especially *Collum* and *Lucht* carried out deeply-rooted mechanistic studies to elucidate the aggregation of LiHMDS with various amine and ether ligands by ⁶Li, ¹⁵N, and ¹³C NMR spectroscopic studies.^[52] *Williard* and *Mulvey et al.* studied and characterized mixed Li-, Na- and KHMDS bases in the solid state and in solution.^[46a, 46c, 53] Compared to the wide synthetic application, both on laboratory and industrial scale, there still is not known much about the aggregation behavior of higher MHMDSs in solution.

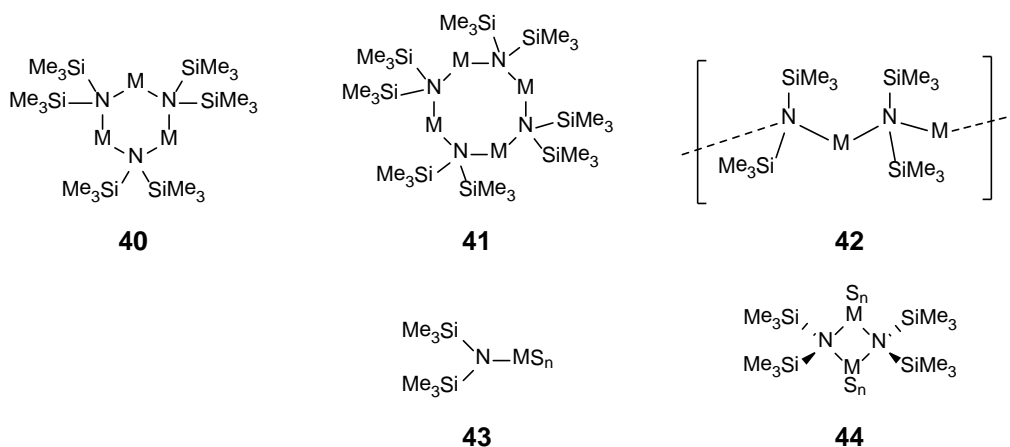


Fig. 1-5. Aggregation modes of MHMDS. S = donor base like *e.g.* THF with n = 1-3.

³ Includes revised parts of my publication: R. Neufeld, R. Michel, R. Herbst-Irmer, R. Schöne, D. Stalke, **2016**, submitted.

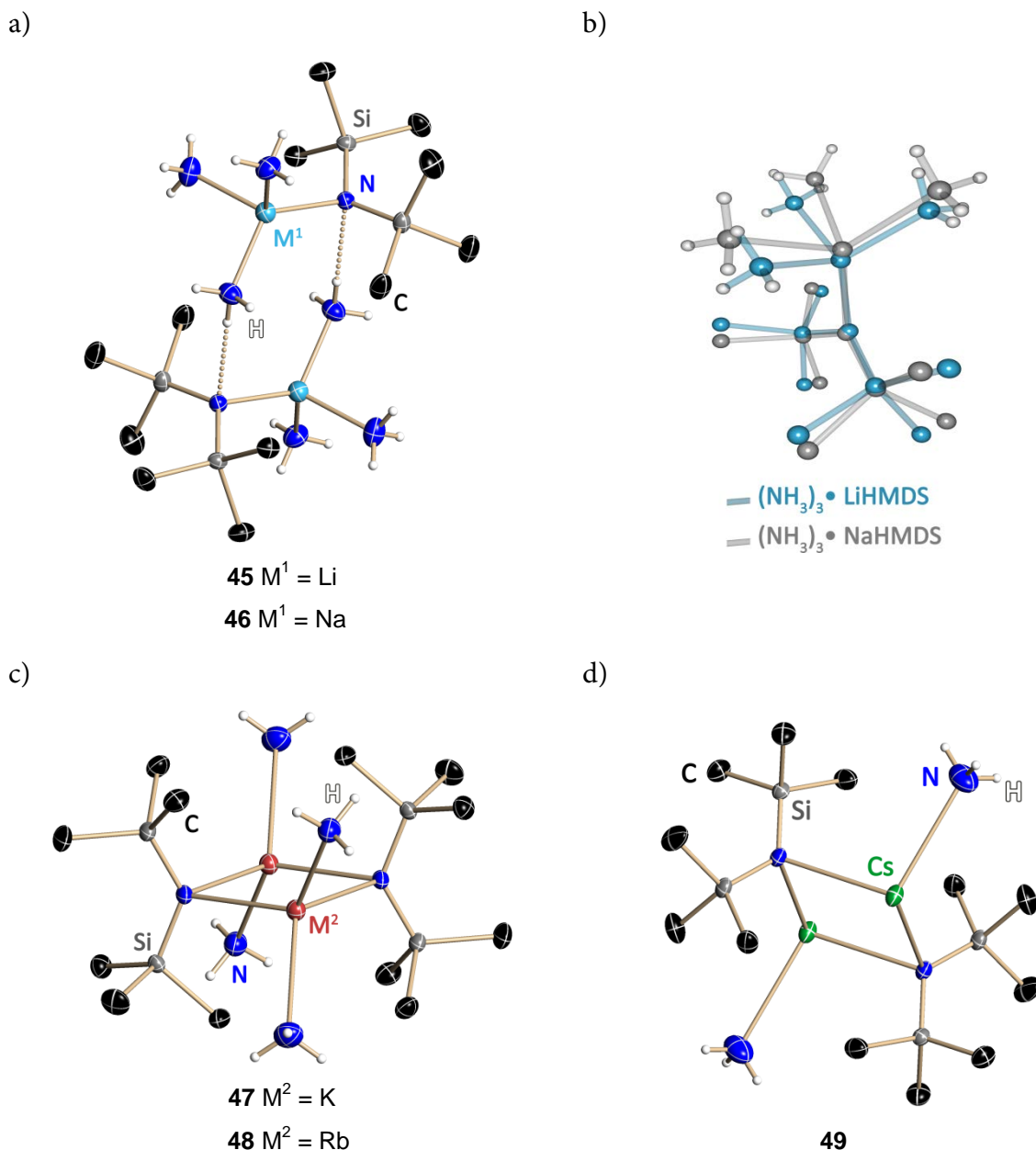
1.1.2.1 Structure of MHMDS with Ammonia as Donor Base⁴

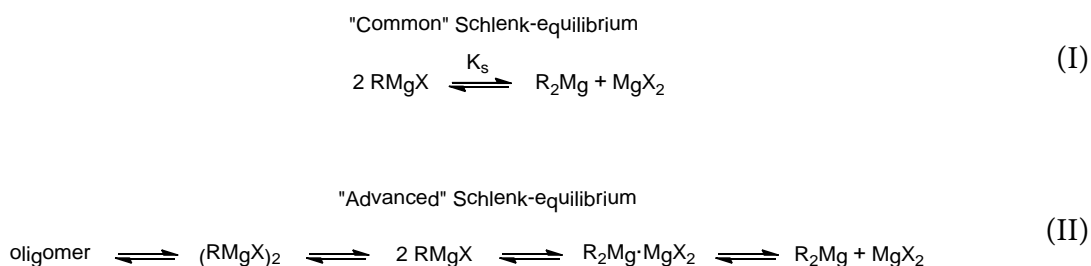
Fig. 1- 6. a) Hydrogen bonded monomers of two neighboring $(\text{NH}_3)_3 \cdot \text{M}^1 \text{N}(\text{SiMe}_3)_2$ [$M^1 = \text{Li}$ (**45**), Na (**46**)] molecules. b) Both compounds crystallize with the same aggregation motif, but in different space groups. **45** crystallizes in the monoclinic space group $C2/c$ and **46** in the primitive monoclinic space group $P2_1/c$. The superposition plot of the asymmetric units shows that both structures do not fit perfectly. Apart from the different $\text{M}-\text{N}_{\text{amide}}$ bond lengths both trimethylsilyl groups and the NH_3 molecules are twisted slightly with respect to another. c) Crystal structure of tetrasolvated $[(\text{H}_3\text{N})_2\text{M}^2\text{N}(\text{SiMe}_3)_2]_2$ [$M^2 = \text{K}$ (**47**), Rb (**48**)]. d) Crystal structure of disolvated CsHMDS dimer **49**. Anisotropic displacement parameters are depicted at the 50% probability level. Carbon bound hydrogen atoms are omitted for clarity.^[1]

⁴ Includes revised parts of my publication: R. Neufeld, R. Michel, R. Herbst-Irmer, R. Schöne, D. Stalke, *Chem. Eur. J.* **2016**, submitted.

Like others^[54] we decided for ammonia as a convenient solvent as we realized earlier that the structure determining effect by single ammonia molecules is much less pronounced than by *e.g.* bi- or tridentate donor bases and the probability to isolate monomeric contact ion pairs (CIPs) or even solvent separated pairs (SSIPs) is much higher.^[7, 55] *Page et al.* showed for example that ammonia is a promising candidate to replace dipolar aprotic solvents like *e.g.* DMSO and DMF in a number of industrial processes.^[56] NH₃ has a boiling point of -33 °C and a vapor pressure of 9 bar at 24 °C,^[57] so it is much easier to remove or rather to recover, compared to many toxic and harmful chelating solvents like *e.g.* PMDETA, unwanted in any pharmaceutical or natural product process. The physical properties of liquid ammonia are similar to those of liquid water. NH₃ is capable to solve many synthetically useful salts like *e.g.* LiNO₃, 244 g/100g at 25 °C because of its small dielectric constant (NH₃: 16.9, H₂O: 78.3 at 25 °C).^[58] With a *pK_a* value of 27.7 at 25 °C^[59] it is not exposed to fast auto protolysis like water (*pK_a* = 15.7 at 25 °C).^[60] A high dipole moment ($\mu = 1.47$),^[61] a small steric demand (compared to *e.g.* THF, Et₂O, etc.) and a high electron density at the nitrogen atom makes ammonia an advantageous donor base for many metal ions especially for alkali metal ions.^[7, 55b, 62] Instead of using neat liquid ammonia is also feasible to use it as an additive to classic solvents like THF or toluene by introducing gaseous NH₃ to the solution.^[7, 55b] Monomeric LiHMDS with monodentate donor bases was only characterized in solution. Anyway, since the first preparation of LiHMDS in 1959 by *Wannagat and Niederprüm*,^[63] all efforts to crystallize monomeric LiHMDS in the absence of chelating ligands failed. In 2016, *Neufeld et al.* succeeded for the first time the crystallization of the missing monomeric key compound.^[1] With ammonia as donor base trisolvated LiHMDS **45** and NaHMDS **46**, showing unique hydrogen bond interactions between two metal HMDS monomers, have been characterized. In addition, unprecedented tetrasolvated K- **47** and RbHMDS-dimers **48** as well as disolvated CsHMDS-dimer **49** with very close intermolecular Si-CH₃...Cs *s*-block "agostic" interactions have been prepared and characterized by single-crystal X-ray structure analysis.^[1]

1.1.3 Structure of Hauser- and *Turbo*-Hauser Bases⁵

Although there is a great deal of information on the utility of these reagents, very little is known regarding the nature of (*Turbo*-)Hauser bases in solution. One reason for that lack of information is that Hauser bases show a complex behaviour in solution. It was proposed^[64] that it could be similar to the Schlenk-equilibrium of Grignard reagents in ether solution, where more than one magnesium containing species exists.



Scheme 1-8. The Schlenk-equilibria.

A rearrangement of the organic ligand takes place and ends up in an equilibrium with the diorganomagnesium and the magnesiumdihalide (Eqn. I in Scheme 1-8).^[65] Later, molecular association studies also revealed oligomeric Grignard structures in diethyl ether. This fact complicated the simple Schlenk-equilibrium (I) so oligomeric species would have to be included (Eqn. II in Scheme 1-8).^[66] There are a few known solid state structures of Grignard complexes.^[67] It was found that the Mg atoms are predominantly tetrahedrally coordinated and dimeric species are bridged through halide atoms. Especially in the late 60s a lot of solution structure investigations have been done mainly by ebullioscopic-,^[66, 68] calorimetric^[69] and NMR^[70] measurements. The position of the Schlenk-equilibrium is considered to be dependent on the nature of the solvent, the steric of the organic substituent, the type of halogen involved and the temperature.^[71] In THF, all alkyl and arylmagnesium halides (Cl, Br, I) are found to be monomeric over a wide concentration range.^[66, 69] In diethyl ether, alkyl and aryl Grignard reagents are mostly monomeric at low concentrations (less than 0.5 M) and mostly dimeric at higher concentrations (0.5-1.0 M).^[68a]

⁵ Includes revised parts of my publication: R. Neufeld, T. L. Teuteberg, R. Herbst-Irmer, R. A. Mata, D. Stalke, *JACS* **2016**, submitted.

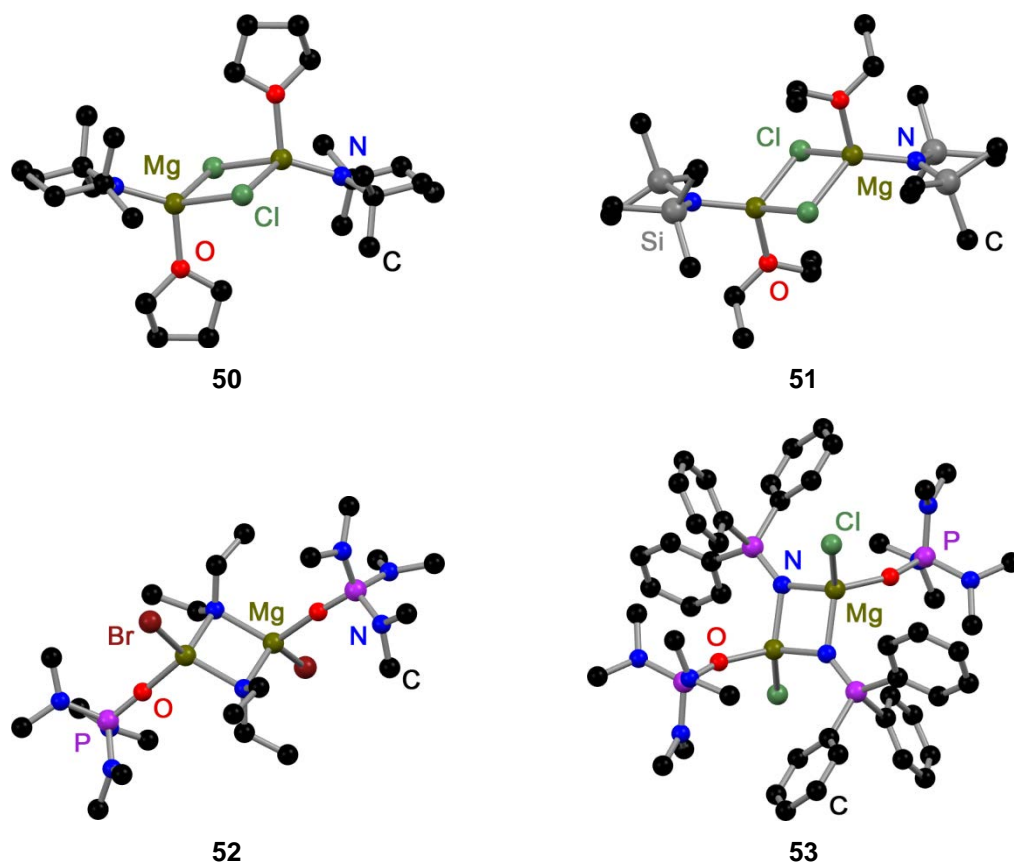
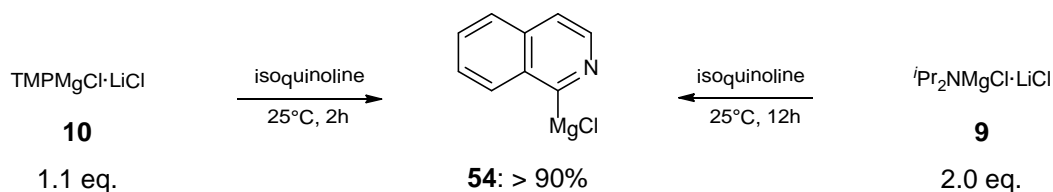


Fig. 1-7. Selected structures of dimeric Hauser bases in the solid state with hydrogen atoms omitted for clarity.

However, surprisingly there are no investigations concerning the aggregation of Hauser bases in solution. In the solid state TMP^[72] (**50**) and HMDS^[73] (**51**) Hauser bases as well as all Grignard dimers^[67a, 67b, 67e, 74] are bridged by halides (Fig. 1-7). In contrast to Grignard reagents, dimeric amido bridged (*Turbo*)Hauser bases exist, too.⁶ All have one feature in common: They are bridged by less bulky amido ligands like Et₂N^{-[73a]} (**52**), Ph₃P=N^{-[75]} (**53**) and ^{*i*}Pr₂N^{-[28]} (**9**) (Fig. 1-7 and Fig. 1-8). At least in the solid state, it can be concluded that the displacement to halide bridges may be influenced by bulky groups on the amide ligand.^[64] However, solid state structures may not necessarily maintain in solution. The impact of LiCl on the solution structure of Grignard reagents and Hauser bases is still unclear. Noteworthy is that the diisopropylamido reagent ^{*i*}Pr₂NMgCl·LiCl **9** shows a much lower reactivity than its TMP counterpart **10**. That difference in reactivity was shown by the deprotonation of isoquinoline in THF solution (Scheme 1-9). While TMPMgCl·LiCl **10** required only 2 h and 1.1 equivalents, **9** needed 12 h and 2 equivalents for comparable metalation (**54**).^[23]

⁶ Cambridge Structural Database CSD, version 5.36 (Updated Nov 2014), chelating amido ligands have been excluded.



Scheme 1-9. Contrasting reactivity of *Turbo*-Hauser base **9** and **10** for *ortho* metalation of isoquinoline.^[23]

The differing reactivity could be a result of unequal aggregation states reflected in a different solubility of both reagents. The solubility of $\text{TMPMgCl}\cdot\text{LiCl}$ **10** is 1.2 M, while that of $\text{Pr}_2\text{NMgCl}\cdot\text{LiCl}$ **9** is only half of it (0.6 M).^[23] Actually, in the solid state compound **10** exists as a monomeric dinuclear contact ion pair (CIP)^[72] and compound **9** as a dimeric tetranuclear CIP^[28] bridged by two amide ligands (Fig. 1-8). In both structures LiCl coordinates to the magnesium amides.

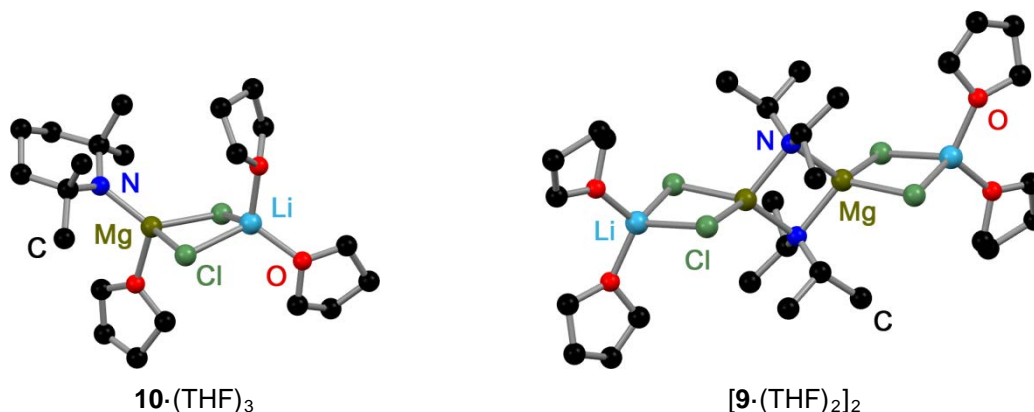


Fig. 1-8. Solid state structures of $\mathbf{10}\cdot(\text{THF})_3$ and $[\mathbf{9}\cdot(\text{THF})_2]_2$ with hydrogen atoms omitted for clarity.

However, it is not clear whether the structures aggregated by LiCl are really stable in solution or just transient species. *Knochel* has speculated that LiCl deaggregates RMgX oligomers^[23] and forms a more reactive bimetallic monomer $\text{RMgCl}\cdot\text{LiCl}$ that is supposed to give magnesiate character to the Grignard reagent in the sense of a solvent separated ion pair (SSIP) $[\text{Li}(\text{THF})_4]^+[\text{RMg}(\text{THF})\text{Cl}_2]^-$.^[76] *García-Álvarez* and *Mulvey et al.* analyzed^[28] crystals of **9** and **10** in $\text{THF}-d_8$ solution at -50°C by employing the diffusion coefficient formula weight (D-FW) analysis that was pioneered by *Williard et al.* (see chapter 1.2.7.2).^[77] Because of signal overlapping problems, the authors had to use inappropriate references, so the molecular weight (MW) determination was prone to a relatively high error of approximately $\pm 30\%$. This is why they were not able to “clearly establish the exact nature of the solution species”.^[28] However, the first key conclusion was that the molecular structure of both *Turbo*-Hauser bases were not retained in $\text{THF}-d_8$ solution and the second

was that aSSIP situation like it was proposed by *Knochel et al.*, described by negative charged magnesium ate complexes (like e.g. $[\text{RMg}(\text{THF})\text{Cl}_2]^-$) and free $[\text{Li}(\text{THF})_4]^+$ seemed most probable.^[28]

1.2 Diffusion NMR Measurements

Like already mentioned in the previous chapters, chemists have always had a vital interest in the size and aggregation state of molecules in solution. NMR measurements of self-diffusion coefficients have gained an increasing importance in this area. The physical observable that can be derived from these measurements is the diffusion coefficient D that is sensitive to size, shape and density of the molecular species.^[6] In the mid-1960s *Stejskal* and *Tanner* developed the pulsed field gradient spin-echo (PFG-SE) sequence that enables the measurement of diffusion coefficients in solution.^[78] However, it took at least 30 years until diffusion measurements have become routinely accessible through the introduction of conventional high-resolution NMR spectrometers that are equipped with pulsed field gradient probe heads. Field gradients are necessary to encode the physical location of a molecule and therefore to measure its diffusion in solution. In the beginning of the 1990s a huge varieties of NMR diffusion methods and applications have been developed and applied which were reviewed in several articles.^[79] These measurements include applications rising from the fields of biology and pharmacy,^[80] polymeric,^[81] organic^[82] and inorganic^[83] chemistry. In the following sections a theoretical background will be given starting from the aspects of diffusion, followed by measuring self-diffusion by applying different pulse sequences and finally the advanced process in molecular weight determination from diffusion NMR measurements will be discussed.

1.2.1 Aspects of Diffusion

Self-diffusion arises from random translational motion of molecules in homogeneous solutions (Brownian motion) driven by the thermal energy of the system. This motion may be characterized by the so called self-diffusion-coefficient D . The average displacement of a molecule in three dimensions is zero over time, but the mean square displacement is non-zero. The distance of a molecule travelled in a single direction is given by:

$$z_{\text{rms}} = \sqrt{2Dt} \quad (1)$$

where z_{rms} is the root mean square distance of an ensemble of molecules travelled in time t . This is why diffusion coefficients have units of m^2/s .

The probability (P) of finding a particle at position r , from the starting position r_0 , over a time t , results in a Gaussian function which is a solution to *Fick's second law*:

$$P(r_0, r, t) = A \exp\left(\frac{-(r - r_0)^2}{4Dt}\right) \quad (2)$$

where A represents a geometric volume normalization $A = (4\pi Dt)^{3/2}$.^[79b] The PFG-SE diffusion experiment works by expressing P in Eqn. (2) as a function of the nuclear spin phase ϕ , instead of the position r . The de-phasing caused by pulsed field gradients and the movement of the molecules during the time t , results after re-phasing in a NMR signal intensity attenuation that can be directly related to the diffusion coefficient D .^[79b]

As already mentioned, diffusion depends on size and shape of molecules which can be shown by the *Stokes-Einstein* equation:

$$D = \frac{k_b T}{6\pi\eta r_s} \quad (3)$$

where k_b is the Boltzmann constant, T the absolute temperature, η the solvent viscosity and r_s the Stokes radius of a spherical particle that has to be much larger than the solvent molecule in a fluid continuum.^[84] Often r_s is equalized with the hydrodynamic radius r_H of an equivalent sphere that diffuses with the same diffusion coefficient as the diffusing particle. However, this approximation has to be considered carefully. The scaling factor 6 in Eqn. (3) is invalid for smaller molecules, where the hydrodynamic radius of the solute tends towards that of the solvent molecule and therefore has to be corrected (a detailed description is presented in section 1.2.7.1).

1.2.2 The Hahn Spin-Echo Experiment

The NMR signal that is observed after an initial 90° pulse (Fig. 1-9 and Fig. 1-10b) decays with time due to variations in the magnetic field. Inhomogeneities in the external field due to intramolecular interactions lead the spins to precess at different rates that result in a loss of magnetization (dephasing due to T_2 spin-spin relaxation, Fig. 1-10c). However, this

dephasing effect can be removed by applying an additional 180° pulse around the y axis (after a time τ) that inverts the relative spin positions (Fig. 1-10d). Because each spin continues to process with its former frequency, all spins rephase perfectly at time 2τ forming a spin echo (SE, Fig. 1-10e).^[85]

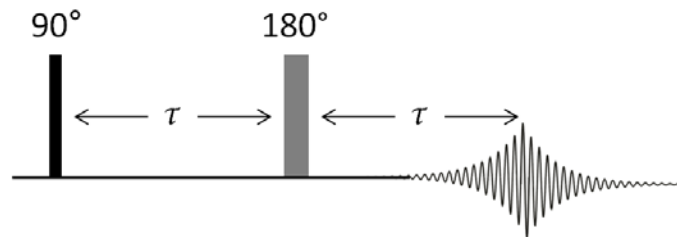


Fig. 1-9. Schematic presentation of the *Hahn* spin-echo pulse sequence.

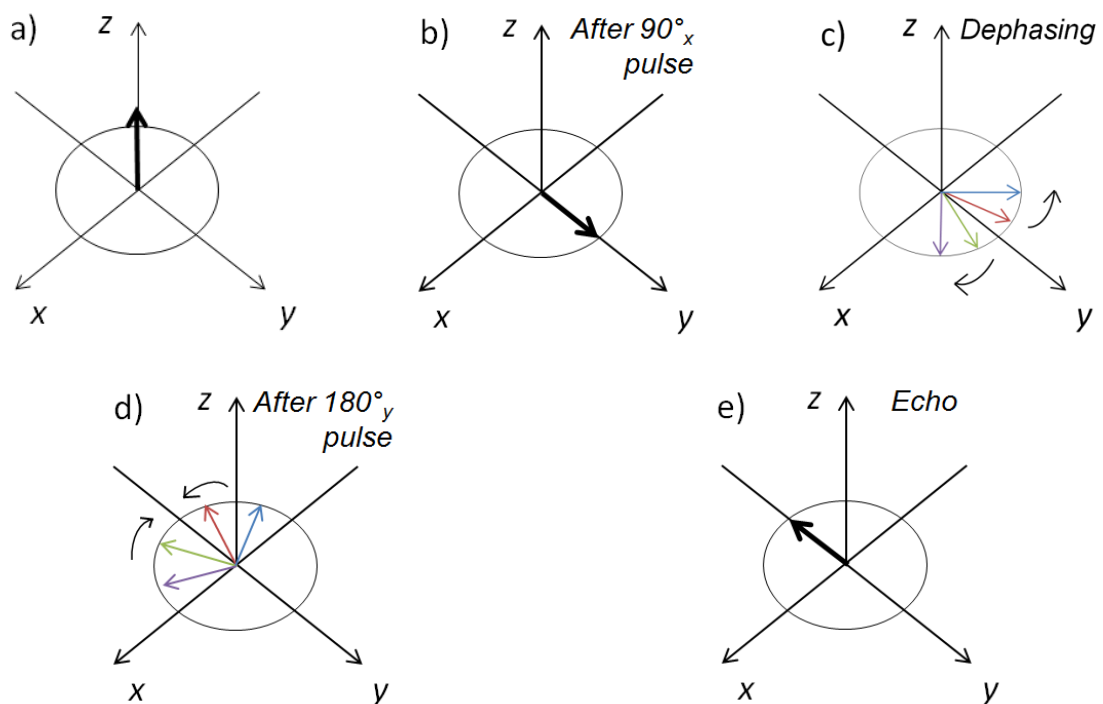


Fig. 1-10. Schematic representation of the *Hahn* spin echo (SE) pulse sequence and its effects on the spin system.

1.2.3 The Pulsed Gradient Spin-Echo (PFG-SE)-Experiment

Before starting with the diffusion experiments, first the effect of gradients on the nuclear spin frequency is described. A gradient is an external magnetic field B whose strength

changes with position. Today, most commercially available NMR spectrometers include self-shielded gradient coils for use *e.g.* in automatic shimming experiments. The additional magnetic field B_z is applied along the z -axis that can be described by:

$$G_z = \frac{\partial B_z}{\partial z} \quad (4)$$

Assuming that the B_z gradient is constant, the effective Larmor frequency ω_{eff} is:

$$\omega_{\text{eff}}(z) = \gamma(B_0 + G_z \cdot z) \quad (5)$$

where γ is the gyromagnetic ratio, B_0 the strength of the homogeneous, external static magnetic field and G_z the gradient strength of the additional inhomogeneous magnetic field. Eqn. (5) shows that the effective Larmor frequency increases when external gradient fields are applied. Due to the inhomogeneity of the latter, the spin frequency varies linearly along the z -axis over the whole sample (Fig. 1-11).^[79b]

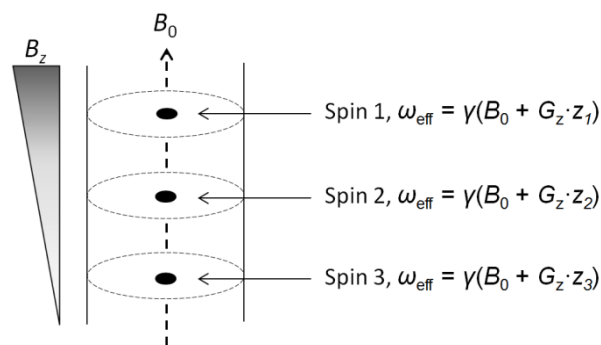


Fig. 1-11. The influence of the external gradient field on the Larmor frequency distribution. The total magnetic field is the sum of the homogeneous static magnetic field and the applied gradient field.

The *Hahn* spin-echo (SE) pulse sequence, in combination with pulse field gradients (PFG), results in a pulsed field gradient spin-echo (PFG-SE)-experiment that is the cornerstone of NMR diffusion experiments. In Fig. 1-12 a schematic picture of the PFG-SE sequence is displayed.

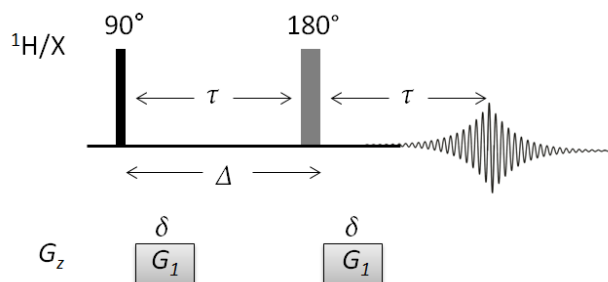


Fig. 1-12. The basic sequence for monitoring self-diffusion (PFG-SE sequence). The diffusion during the period Δ is obtained by measuring a series of experiments with increasing gradient strengths.

Without gradient pulses this sequence displays a standard spin-echo experiment (Fig. 1-9). When the first gradient G_z (encoding gradient) with the length δ is applied, the magnetization vector will impose a spatially dependent phase, which can be refocused by a second gradient of equal duration and magnitude. Due to the 180° pulse between them, the effect of the gradient pulses would cancel. However this is only true, if the spins of a molecule remain in the same physical position. If the molecule diffuses away from its initial position during the diffusion delay Δ , then the local field experienced during the second gradient (decoding gradient) does not exactly match with the first PFG. This scenario leads to an attenuation of the spin echo (SE) signal.

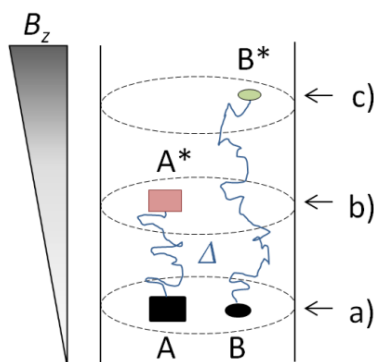


Fig. 1-13. Schematic representation of the spin echo signal attenuation through PFG and molecular diffusion. a) If no diffusion occurs than the spins of molecule A and B would refocus after the PFG-SE pulse sequence resulting in a full intensity of the spin echo. b) Due to diffusion, the local field experienced by molecule A does not match that experienced during the second gradient puls (A^*). The spins do not fully refocus. This provides a reduced magnetization in respect to the z-axis and therefore in a reduced SE intensity. c) Greater attenuation is observed for the faster diffusing molecule B that signal attenuation is even bigger than that of molecule A.

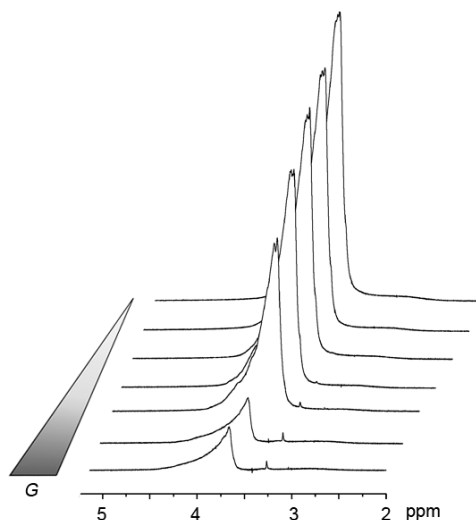


Fig. 1-14. Experimental 1D ^1H diffusion traces. The intensity decay is a result of a progressively increased gradient strength G .

To characterize diffusion rates, it is necessary to progressively increase the parameter Δ , δ or the strength of the gradient pulses G_z to monitor the change in the SE intensities. However, since longer diffusion times provide additional signal loss due to relaxation processes, it is more advantageous to vary the gradient strengths G instead of Δ and δ (Fig. 1-14).

At the end of a PFG-SE experiment, the observed signal intensity I_G is given by the so-called *Stejskal-Tanner* equation: ^[78]

$$I_G = I_0 \exp\left(-\frac{2\tau}{T_2}\right) \exp\left[-(\gamma\delta G)^2 D \left(\Delta - \frac{\delta}{3}\right)\right] \quad (6)$$

where I_0 is the signal intensity without the gradient spin-echo, τ , δ and Δ the delays as displayed in Fig. 1-12, T_2 is the transverse relaxation rate constant, γ is the gyromagnetic ratio, G is the gradient strength and D is the diffusion coefficient. For a typical PFG-SE experiment, where the gradient strength G is varied and the total echo time 2τ is constant a more useful equation is:

$$I_G = I_{G=0} \exp \left[-(\gamma \delta G)^2 D \left(\Delta - \frac{\delta}{3} \right) \right] \quad (7)$$

Since the constants γ , δ and Δ are known, the diffusion coefficient D can be calculated directly from linear or non-linear regression. Optionally the data can be presented in the pseudo-2D-DOSY format (Fig. 1-17 in chapter 1.2.6).

1.2.4 The Pulsed Gradient Stimulated-Echo (PFG-STE)-Experiment

In the above described PFG-SE-experiment the magnetization is transverse during diffusion. Therefore this sequence depends highly on transverse (spin-spin) relaxation times T_2 (see Eqn. (6)).

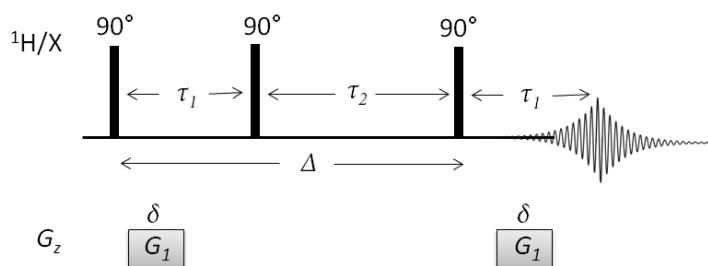


Fig. 1-15. PFG stimulated-echo (PFG-STE)-sequence

This relaxation loss can be very problematic, because very large molecules require long diffusion delays (Δ) and simultaneously show increased T_2 relaxation rates. In the alternative PFG stimulated-echo (PFG-STE)-sequence a second 90° pulse sets the magnetization along the z-axis during the diffusion encoding time (Fig. 1-15).^[86] In this period (τ_2) the relaxation is dictated by the potentially slower longitudinal (spin-lattice) relaxation rate T_1 , while T_2 relaxation is only present during the relatively short gradient periods τ_1 . After the diffusion period a third 90° pulse returns the magnetization with reversed sign to the transverse x-y-plane (Fig. 1-10), so the spin moments can refocus again. The observed signal intensity for the stimulated echo (STE) is given by:

$$I_G = \frac{I_0}{2} \exp\left(-\frac{2\tau_1}{T_2} - \frac{\tau_2}{T_1}\right) \exp\left[-(\gamma\delta G)^2 D \left(\Delta - \frac{\delta}{3}\right)\right] \quad (8)$$

When the gradient strength is the only varying parameter, again Eqn. (7) can be used to describe the STE-intensity. Compared with the PFG-SE-sequence (Eqn. (6)) it may be seen that the signal intensity is reduced by a factor 2 (Eqn. (8)), because shortly after the second 90° pulse a portion of the magnetization dissipates due to transverse relaxation.^[87] This is why the difference between $T_1 > T_2$ is important and the initial signal has to be strong enough to allow a sufficient PFG-STE-experiment.

1.2.5 Advancements to the Stimulated-Echo

Over the years, the PFG-STE sequence led to the development of advanced diffusion NMR pulse sequences with the aim to minimize lineshape distortions, to reduce experiment time and to suppress convection disturbance. In following, the benefits of some advanced pulse sequences will be displayed in a sense of a short overview:

- 1) **BPP-LED**: The key feature of this sequence is the replacement of single gradient pulses in the STE sequence by a pair of accurately matched pulses having different polarities that are separated by a 180° pulse. These so called bipolar pulse pairs (BPP) reduce eddy current distortions and minimize residual background gradients that lead to reduced lineshape disturbances.^[88] In addition the “longitudinal-eddy-current delay” (LED) pulse sequence reduces also effects of eddy currents in diffusion measurements by introducing an eddy current delay period prior to detection.^[89]
- 2) **ONE-SHOT**: The use of balanced asymmetrical bipolar gradient pairs in addition to purge gradients leads to rapid diffusion measurements and often to higher signal-to-noise ratios (compared to the BPP-LED pulse sequence).^[90]
- 3) **D-STE**: The so called “double-stimulated-echo” experiment is the most effective sequence that cancels the unwanted effect of convection during the diffusion measurement by dividing the total diffusion period in two STE sequences.^[91] However, the signal intensity is reduced by an additional factor of 2.

- 4) **Pure Shift:** The *Zangger-Sterk* pulse sequence suppresses multiplet structures in the spectral dimension that minimize signal overlap problems.^[92]

1.2.6 Extracting Diffusion Coefficients

Once the diffusion data set is collected (typically consisting as a set of 16-32 1D spectra) the diffusion coefficients of the species of interest have to be extracted from the data. The data analysis relies on fitting the attenuated intensity of a component as a function of the applied gradient strength. The diffusion coefficient D can be extracted either from non-linear Gaussian- (Fig. 1-16a), exponential- (Fig. 1-16b) or linear- (Fig. 1-16c) regression fits. However, because of a less accuracy of $\ln(I/I_0)$ the linear fits are less accurate than the non-linear fits.

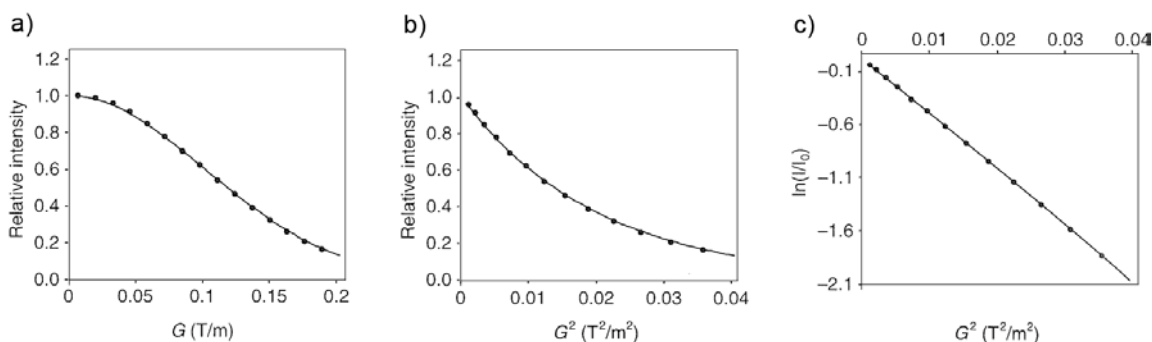


Fig. 1-16. Regression fit analysis to extract the diffusion coefficient by fitting a) I_G vs. G (Gaussian decay profile); b) I_G vs. G^2 (exponential decay profile) and c) $I_G/I_{G=0}$ vs. G^2 (linear decay profile).

A highly aesthetic presentation of the diffusion data is the pseudo 2D spectrum introduced by *Morris and Johnson* in 1992.^[93] The first dimension represents the regular chemical shifts δ and the second dimension gives the diffusion coefficients D of species separated by their particle size (Fig. 1-17). The authors referred this pseudo 2D experiment as “*Diffusion-Ordered NMR Spectroscopy*” (DOSY).^[93] Typically the diffusion coefficients are extracted from exponential fits that are described above, while the peak width reflects the magnitude of the fitting error. Since its invention in 1992, the DOSY “NMR Chromatography” experiment has gained huge popularity as an advanced tool for identifying individual species in a multicomponent solution (Fig. 1-18).

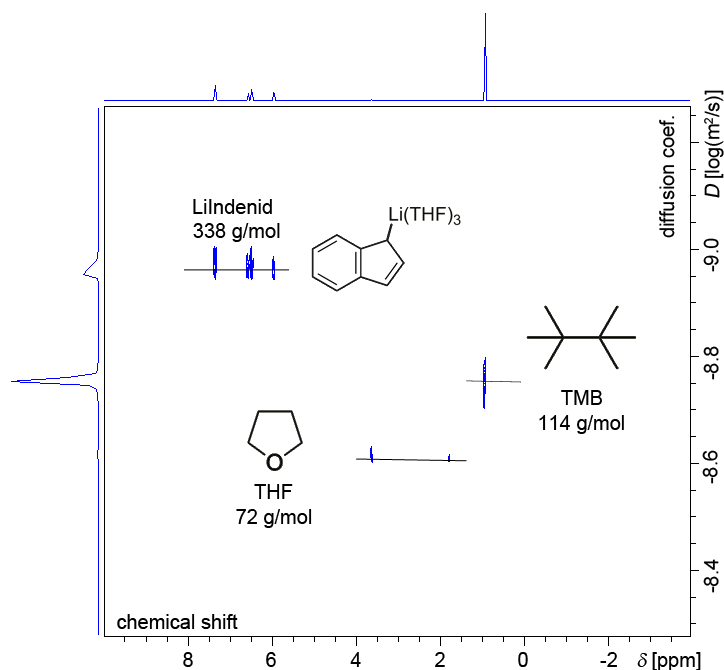


Fig. 1-17. Example of a pseudo 2D-DOSY-spectrum with three compounds with unequal sizes and therefore different diffusion coefficients.

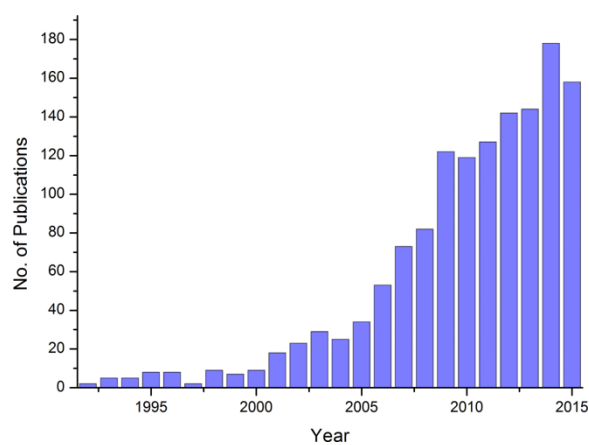


Fig. 1-18. Number of publications using the concept of DOSY.⁷

It is essentially important that signals show a desirable distribution, so no signal overlap is present. However, for weak overlap a range of more complicated mathematical procedures like *e.g.* CONTIN, DECRA and CORE are available. In cases of high signal overlap the apparent diffusion coefficient will be an intermediate result of both components. An alternative for signal overlapping problems may be the use of single shift pulse sequences^[92] or hybrid diffusion sequences such as COSY-IDOSY^[94], HSQC-IDOSY^[95] or TOCSY-DOSY^[96] (so called 3D-DOSY experiments; IDOSY means the implementation of an

⁷ Derived from a scifinder® search with the keyword “DOSY”.

INEPT transfer into a BPP-STE sequence, where the signal detection is performed on the heteroatom while the diffusion encoding is performed on ^1H magnetization).

1.2.7 Molecular Weight Determination

1.2.7.1 Molecular Weights Derived from the Stokes-Einstein Equation

Usually species are identified by comparing the hydrodynamic radius of a reference molecule with that of the solute. The hydrodynamic radius r_s of the solute can be directly calculated from the Stokes-Einstein equation:

$$r_s = \frac{k_b T}{6\pi\eta D_s} \quad (9)$$

where k_b is the Boltzmann constant, T the absolute temperature, η the solvent viscosity and D_s is the diffusion coefficient.^[84] For a quantitative relation of the hydrodynamic radius with the molecular weight (MW) of a particle the following equation can be used:^[97]

$$r_s = \left(\frac{3M\nu}{4\pi N_A} \right)^{\frac{1}{3}} \quad (10)$$

where N_A is the Avogadro constant, M is the MW and ν is the partial specific volume of the particle. Further it is possible to relate the diffusion coefficients of two molecules D_s and D_{ref} to their MWs M_s and M_{ref} .^[97]

$$\frac{D_s}{D_{\text{ref}}} = \left(\frac{M_{\text{ref}}}{M_s} \right)^{\frac{1}{3}} \quad (11)$$

However, equations (9) to (11) are only true for ideal spherical particles that have to be much larger than the solvent in a fluid continuum. For non-spherical molecules with a slightly larger size than the solvent, the additional factors c_s for size- and f_s for shape correction, respectively have been added to the Stokes-Einstein equation.^[79c]

$$r_s = \frac{k_b T}{c_s f_s \pi \eta D_s} \quad (12)$$

Gierer and *Wirtz* (Eqn. (13))^[98] and *Chen et al.* (Eqn. (14))^[99] derived the factor c_s as a function of r_{solv}/r_s by microfriictional theory and semi-empirically methods (Fig. 1-19a):

$$c_s(\text{GW}) = \frac{6}{\frac{3r_{\text{solv}}}{2r_s} + \frac{1}{1 + \frac{r_{\text{solv}}}{r_s}}} \quad (13)$$

$$c_s(\text{Chen}) = \frac{6}{1 + 0.695 \left(\frac{r_{\text{solv}}}{r_s}\right)^{2.234}} \quad (14)$$

The dependence of c on r_s taking methylene chloride as solvent is demonstrated in Fig. 1-19a. Further the shape of the molecule can be accounted for the shape factor f_s that was developed by *Perrin*:^[100]

For prolate ellipsoids:

$$f_s = \frac{\sqrt{1 - \left(\frac{b}{a}\right)^2}}{\left(\frac{b}{a}\right)^{\frac{2}{3}} \ln \frac{1 + \sqrt{1 - \left(\frac{b}{a}\right)^2}}{\left(\frac{b}{a}\right)}} \quad (15)$$

For oblate ellipsoids:

$$f_s = \frac{\sqrt{\left(\frac{b}{a}\right)^2 - 1}}{\left(\frac{b}{a}\right)^{\frac{2}{3}} \arctan \sqrt{\left(\frac{b}{a}\right)^2 - 1}} \quad (16)$$

where a is the major and b is the minor semiaxis of an ellipsoidal molecule. The dependence of a/b on f_s is demonstrated in Fig. 1-19b.

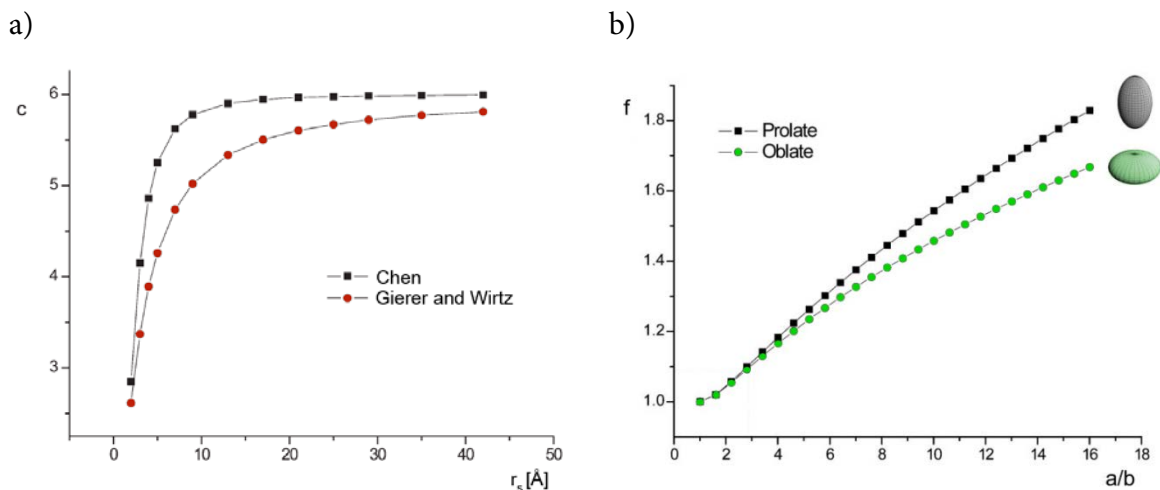


Fig. 1-19. a) Dependence of the size factor c on the hydrodynamic radius of the solute r_s using methylene chloride as solvent. According to *Chen* as well as to *Gierer and Wirtz* the size coefficient c tend to the value 6 with r_s values greater than 40 Å. b) Dependence of the ratio a/b on the shape factor f_s for prolate and oblate ellipsoidal molecules.^[79c]

Both, the *Gierer-Wirtz* as well the *Chen* modification assume the knowledge of the solvent radius r_{solv} . *Evans et al.* modified the *Gierer-Wirtz* Eqn. (13) by using the effective solvent density ρ_{eff} instead of the solvent radius r_{solv} assuming that all small molecules have the same effective density, the same shape, solvation and flexibility.^[101] The estimation of D is therefore given as:

$$D = \frac{k_b T \left(\frac{3\alpha + 1}{2 + 1 + \alpha} \right)}{6\pi\eta \left(\frac{3MW_s}{4\pi\rho_{\text{eff}}N_A} \right)^{\frac{1}{3}}}, \text{ with } \alpha = \left(\frac{MW_{\text{solv}}}{MW_s} \right)^{\frac{1}{3}} \quad (17)$$

Where η is the viscosity, MW_{solv} the molecular weight of the solvent and MW_s the molecular weight of the solute. The authors showed also that the MW-prediction of small molecules, like e.g. toluene, anthracene and cholesteryl acetate, using the unmodified Stokes-Einstein equation (9) produced an average root mean square error of RMS = 45%. The application of *Evan's* method increases the accuracy dramatically with an average error of RMS = 15% (Tab. 1-1 see *vide infra*).^[101]

1.2.7.2 Molecular Weights Derived from a Power Law

Besides the above mentioned Stokes-Einstein-modifications, especially the empirically derived power law is probably one of the most powerful classes of relations which correlate the MW and the diffusion coefficient according to:

$$D = K \cdot MW^\alpha \quad (18)$$

where D is the diffusion coefficient, MW the molecular weight of the solute and K and α are compound dependent constants. α is often related to the Flory exponent that comes from the fractal theory and can be described as a measure of compactness of a molecular shape. A Flory exponent of $-\alpha = 0.33$ notes that the space is totally filled and no holes are left. On the other hand a Flory exponent of $-\alpha = 1$ means that the molecule is completely one-dimensional and extends linearly like a rigid rod.^[81a] A double logarithmic plot of the diffusion coefficients from appropriate standards against their MWs leads to a linear calibration plot (Fig. 1-20) that can be used to calculate molecular masses from diffusion coefficients.

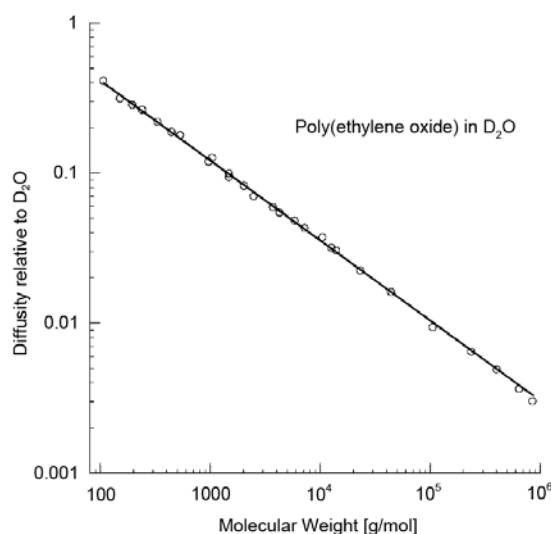


Fig. 1-20. A plot of diffusion vs. MW for a series of poly(ethylene oxide) samples in D₂O provides a linear relationship.^[81a]

This power law gives good results but is restricted to a specific class of compounds.^[81a] Especially the polymer community has applied this power law to estimate the MW distribution of polymer solutions such as globular proteins,^[81a] oligosaccharides,^[81b] polyethyleneoxides^[81c] and denatured peptides^[102] in various solvents.^[6] In 2007 *Crutchfield* and *Harris* showed that even small molecules correlate to the power law.^[103] In their work

they illustrated that using the power law a relatively good MW-determination was possible with an average error of 11% (Tab. 1-1). Unfortunately, the maximum error was still very high ($\pm 35\%$).^[103]

Tab. 1-1. RMS errors for MW-determination of small molecules (<1100 g/mol) by different methods.

<i>Method</i>	<i>RMS error / %</i>
Stokes-Einstein ^[101]	45
Gierer-Wirtz ^[101]	28
Chen ^[101]	18
Evans ^[101]	15
Crutchfield ^[103]	11

In diffusion measurements the absolute diffusion coefficient is affected by various sources of errors like *e.g.* diversities in temperature, fluctuation, convection, viscosity and concentration effects. In addition NMR device constants like *e.g.* gradient strength and pulse duration influence the absolute diffusion coefficient. To overcome this problem *Williard et al.* introduced several internal references (at least 3) with known MWs to the analyte sample.^[104] Since all of them experience the same physical environment the above mentioned distortions on the diffusion coefficient vanish for this specific NMR sample. By plotting the diffusion coefficients of the internal references against their MWs, an internal calibration curve (ICC) can be derived, which can be used to calculate the MW of the analyte. Using the so called “*Diffusion Coefficient–Formula Weight (D-FW) Analysis*” a few authors were able to characterize several organometallic compounds in solution.^[105] A great review on the practical use of this method is given in reference [77]. Unfortunately the ICC-method has some important disadvantages: on the one hand the ICC employs just a few references (mostly 3) and is often based on a small molecular weight distribution. On the other hand each ICC is only useful for one NMR sample. Another disadvantage is that all of the internal references have to fulfil several key factors:

- (a) They should be inert to the analyte in solution.
- (b) Their NMR signals should not overlap with other components.
- (c) The internal references should have no coordinating ability to the analyte.
- (d) All references should be well soluble in the solvent.
- (e) The internal references should have a well set molecular weight distribution.

Therefore, it is a big challenge to choose the appropriate internal references, because often at least one of the above-mentioned exigencies would not be met.

Since the authors did not take the shape of the references and the analyte into account, the accuracy the D-FW analysis is in the same range of *Crutchfield's* method with a maximum error of approximately $\pm 35\%$. For example the MW prediction of acetone- d_6 gives good results ($MW_{\text{calc}}(\text{acetone-}d_6) = 64 \text{ g/mol}$, $MW_{\text{det}}(\text{acetone-}d_6) = 67 \text{ g/mol}$, $MW_{\text{err}}(\text{acetone-}d_6) = 5\%$) but that of the very flat and expended molecule chrysene produces an error of -35% [$MW_{\text{calc}}(\text{chrysene-}d_{12}) = 240 \text{ g/mol}$, $MW_{\text{det}}(\text{chrysene-}d_{12}) = 158 \text{ g/mol}$, $MW_{\text{err}}(\text{chrysene-}d_{12}) = -35\%$].^[104a]

1.3 Scope of this Thesis

The aggregation and solvation numbers of organometallics and organoamides play a dominant role in reaction mechanisms and product forming. Therefore, the knowledge of reactive aggregates especially in solution where they operate is a prerequisite to understand how these molecules react and why they yield which products. Diffusion measurements and related molecular weight (MW) determinations proved to be very helpful tools for identifying reactive intermediates in solution. However, the available methods require either several mathematical corrections or the addition of multiple internal standards. However, especially for small molecules these methods provide a significant error in MW determination.

The main scope of this thesis was the development of a straight forward methodology which determines MWs from diffusion coefficients with viable accuracy.

The “original” Stokes-Einstein equation (9) has been modified by various correction factors. These take for example the size of the solute in respect to the solvent and the shape of the solute into account. In comparison, for power law derived MW determinations the analytes have been divided into specific classes of compounds, like *e.g.* proteins, polymers of glycosides or poly(ethylene oxides) and the class of “small molecules” with MWs $< 1100 \text{ g/mol}$. All of them show a linear relationship between MW and diffusion coefficient. However, the MW determination of small molecules still results in huge maximum errors of approximately $\pm 35\%$. Taking the shape and the density of small molecules into account could lead to improved accuracies and smaller errors. In addition,

the D-FW analysis pioneered by *Li* and *Williard et al.* is directed on multiple internal references which might interfere with the analyte. This is why the method is restricted to a handful internal references and many analytes cannot be examined due to signal overlap problems. Therefore, it would be highly beneficial if only one internal reference would be sufficient for accurate MW determinations. Furthermore, there are no investigations concerning the impact of molecule density and the absolute temperature on power law derived MW predictions.

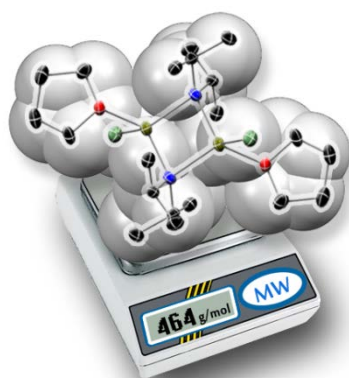


Fig. 1-21. Illustration: MW determination of dimeric Hauser base $[7\cdot\text{THF}]_2$ in THF solution.

Finally, the new developed MW determination methodology should be used to characterize the solution structure of prominent organometallics like *e.g.* LDA in toluene solution or Hauser bases (Fig. 1-21) and their *Turbo*-analogues in THF solution, whose solution structures were still unclear due to the absence of appropriate analytical methods.

2 RESULTS AND DISCUSSION

2.1 Development of the DOSY-External Calibration Curve MW-Determination Methodology⁸

2.1.1 Application of a Normalized Reference System with Fixed Diffusion Coefficients

Like already mentioned in the introduction, absolute diffusion coefficients are affected by various sources of errors like *e.g.* diversities in temperature, fluctuation, convection, viscosity and concentration effects. Additionally the NMR-device properties and constants like gradient strength and pulse duration have an influence on the absolute diffusion coefficient (Fig. 2-1). This is why the latter can only be compared under *ceteris paribus* conditions. To overcome the complications of these effects and to enable tabulated diffusion coefficients, the use of an internal standard is necessary. Those standards provide more resilient diffusion coefficients for any changes in the NMR sample. A ratio, often termed as relative diffusivity D_{rel} is defined as:

$$D_{\text{rel}} = \frac{D_{\text{x}}}{D_{\text{ref}}} \quad (19)$$

where ref and x correspond to the reference and analyte, respectively. This approach reduces the impact of viscosity, temperature, NMR-device properties and provides more robust data. Besides the abovementioned advantages this method has a disadvantage. Eqn. (19) produces relative diffusion values that always depend on the one reference molecule it has been referenced for. This reference has no strict or defined diffusion value. Therefore it would be more advantageous to employ relative diffusion coefficients with fixed diffusion values. Empirically derived results showed that logarithmic diffusion values are connected approximately linearly, independent of gradient and magnetic field strength, gyromagnetic ratio, gradient pulse duration, and changes in temperature or viscosity.

⁸ A revised version of my publication: R. Neufeld, D. Stalke, *Chem. Sci.* **2015**, 6, 3354–3364.

That is why the linear Eqn. (20) was empirically derived:

$$\log D_{x,\text{norm}} = \log D_{\text{ref,fix}} - \log D_{\text{ref}} + \log D_x \quad (20)$$

Where $\log D_{\text{ref,fix}}$ is the fixed value of the reference $\log D_{\text{ref}}$ the measured diffusion coefficient of the reference, $\log D_x$ the diffusion coefficient of analyte x and $\log D_{x,\text{norm}}$ the relative diffusion value of the analyte x normalized to the reference. Eqn. (20) ensures that all molecules get a normalized diffusion coefficient relative to the internal reference. For diffusion measurements for all TOL- d_8 solvates adamantane (ADAM) and for all THF- d_8 solvates 2,2,3,3-tetramethylbutane (TMB) was used as internal references (Table 2-1).

Table 2-1. $\log D_{\text{ref,fix}}$ values of the used internal references.

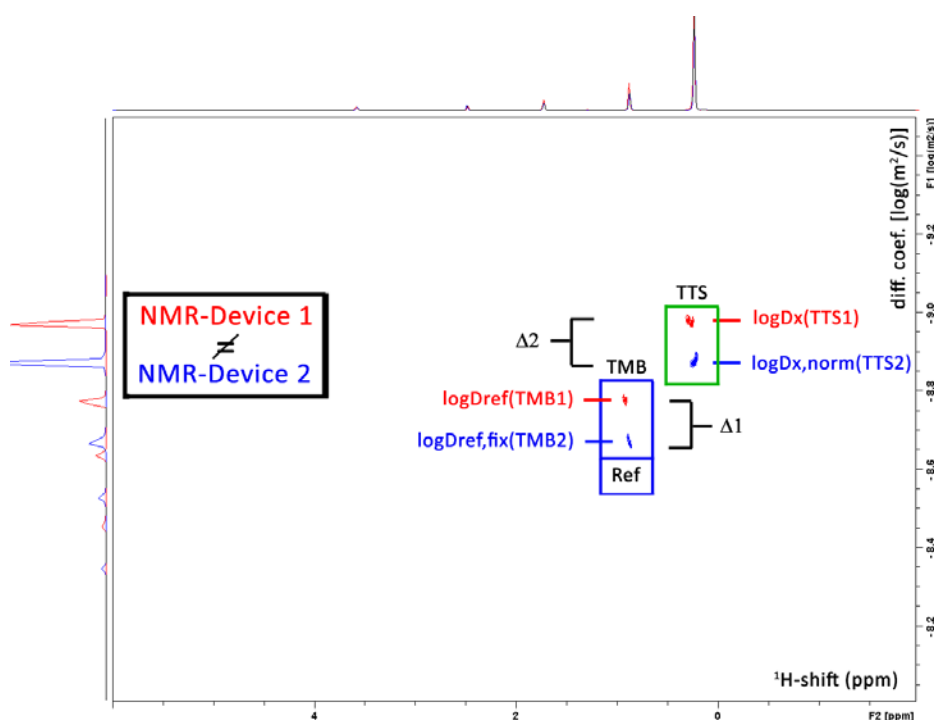
<i>internal reference</i>	$\log D_{\text{ref,fix}}$ ^{a)}
ADAM in TOL- d_8 ^{b)}	-8.8454
TMB in THF- d_8 ^{c)}	-8.7749

- a) Each diffusion coefficient was estimated by using the middle $\log D$ value of 15 DOSY measurements of 15 mM solutions at 25°C.
- b) ADAM has two signals in the $^1\text{H-NMR}$ -spectrum. For determining the diffusion coefficient, the signal of the $-\text{CH}_2$ groups with the highest intensity was used.
- c) The chemical shift of one ADAM signal is very close to the THF- d_7 signal at 1.73 ppm. Therefore TMB was used as internal reference for all THF- d_8 solvates.

The validity of Eqn. (20) was proved by measuring DOSY spectra of 18 model compounds on two different NMR spectrometer devices, where one spectrometer had calibrated and the other uncalibrated gradients. Although differences in gradient calibration, temperature and concentration automatically give deviations in absolute diffusion (Fig. 2-1), Eqn. (20) provides excellent results for the normalized diffusion coefficient $\log D_{x,\text{norm}}$ independent of the used NMR spectrometer with an average standard deviation of only $\sigma(\log D_{x,\text{norm}}) = 0.003$ in TOL- d_8 and 0.002 in THF- d_8 (A-Table 1 and A-Table 2 in the appendix).⁹ This experiment demonstrates the robustness of Eqn. (20) and the normalized diffusion coefficients.

⁹ Derived from 18 independent measurements of 18 molecules with MWs ranging from 70 g/mol (cyclopentane) to 623 g/mol (BINAP).

a)



b)

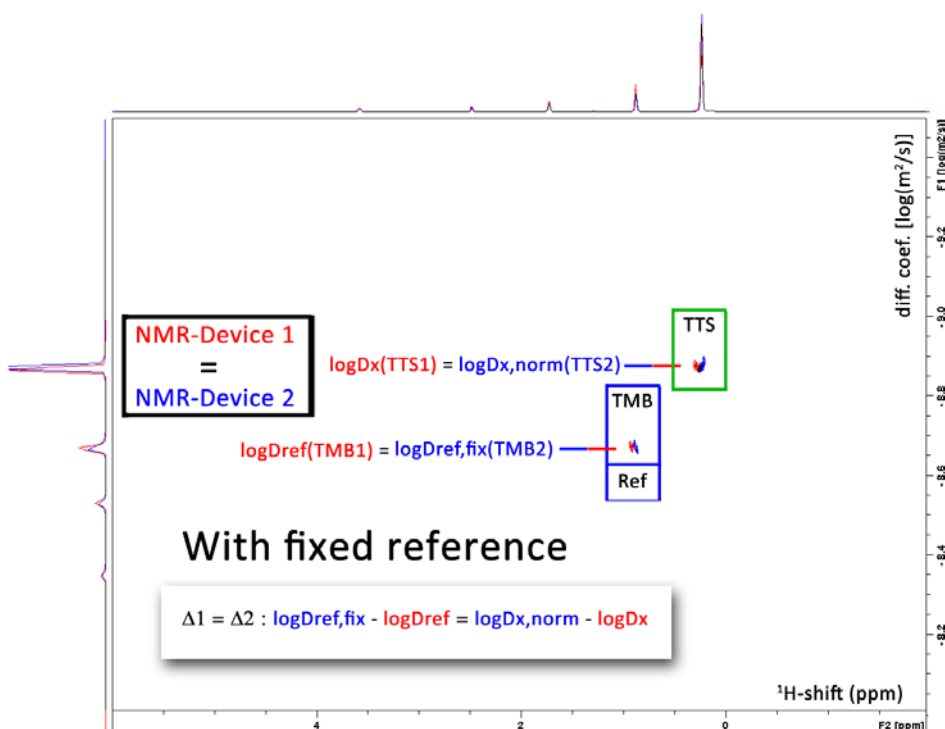


Fig. 2-1. Superposition plot of two DOSY spectra measured on two different NMR devices (red and blue). a) The absolute diffusion coefficients of $\text{Si}(\text{SiMe}_3)_4$ (TTS) are uneven $\log D(\text{TTS1}) \neq \log D(\text{TTS2})$ and $\log D(\text{TMB1}) \neq \log D(\text{TMB2})$ due to different gradient calibrations in the NMR devices and *e.g.* diversity in viscosity and/or temperature. b) The signal of the references has been shifted to a fixed value and the signals of TTS have been moved by the same increment of $\Delta 1 = \Delta 2$. With that referencing method it is possible to obtain the same diffusion values for analyte x independent of the used NMR device or changes in solution properties.

2.1.2 External Calibration Curves (ECC) and Internal References

The D-FW-determination developed by *Li and Williard et al.* relies on an internal calibration curve (ICC) that has been generated by a single DOSY measurement where all references are present in the same NMR sample. The calibration curves which will be presented in this work were generated by measuring 28 model compounds in independent NMR samples. This is why these calibration curves are named “external calibration curves” (ECC). These calibration curves have been plotted the common way by linearizing the power law (18) with taking the logarithm of both sides:^[104d]

$$\log D_{x,\text{norm}} = \log K + \alpha \log MW_{\text{calc}} \quad (21)$$

Plotting $\log D_{x,\text{norm}}$ versus $\log MW_{\text{calc}}$ of all model molecules in one diagram gives a linear correlation but with a significant deviation especially for the very low and higher weight molecules that prevents an accurate MW-determination (Fig. 2-2a).

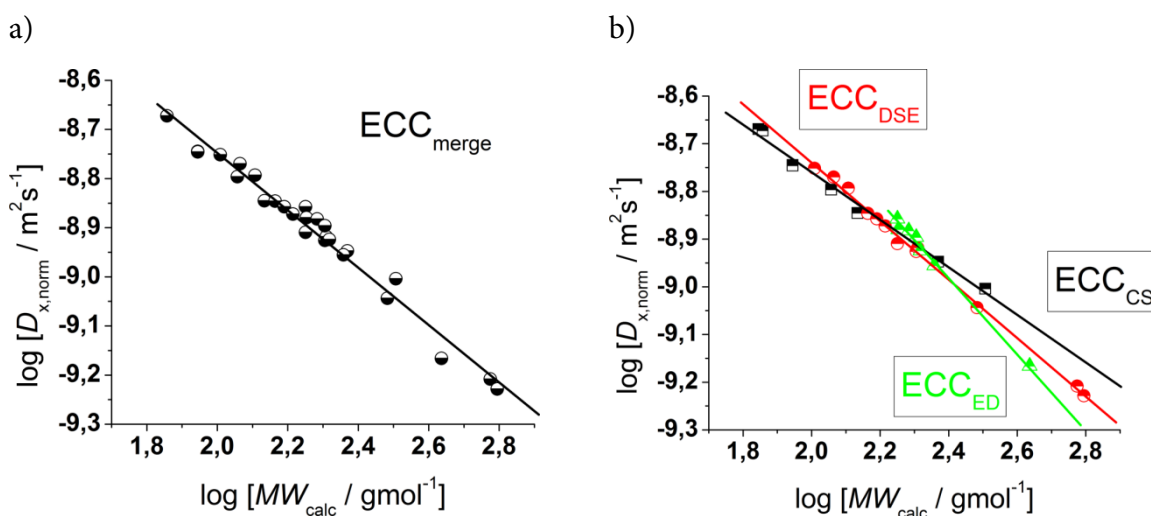


Fig. 2-2. ECC-plot: $\log D_{x,\text{norm}}$ vs. $\log MW_{\text{calc}}$ of 28 model compounds in TOL- d_8 . All compounds were normalized to $\log D_{\text{ref,fix}}(\text{ADAM}) = -8.8454$, see Table 2-1. a) The diffusion coefficients show a linear correlation. However, some compounds display significant deviations from a linear behavior (corr. $R^2 \leq 0.97$). b) Taking the shape (DSE, CS and ED) into account gives much better correlations between diffusion coefficients and MWs (corr. $R^2 \geq 0.99$). The same trend is observable in THF- d_8 solution.

To find a better correlation between diffusion coefficient and the MW three dimensional, shape optimized models of all model compounds were generated (A-Table 3 in the appendix). By comparing the diffusion coefficient of each molecule with its shape and compactness features, one can see a significant disparity.

The molecules can be classified in three different types:

- compact spheres (CS)
- dissipated spheres and ellipsoids (DSE)
- expanded discs (ED)

Of course the transitions between those types occur across a foggy line but there are clear systematic trends that can be rationalized. From Fig. 2-3 it is obvious, that CS have nearly the same radius in all dimensions with a high-density space like for example the compact molecules ADAM or $\text{Si}(\text{SiMe}_3)_4$.

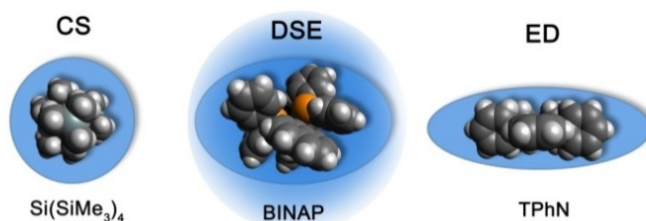


Fig. 2-3. Example molecules that were classified in the ECC as CS, DSE and ED like molecules.

However, the majority of small molecules diffuse like DSE. These are either spherical-like molecules that are less compact than CS (*e.g.* compounds with dative bonds like $[\text{Li}(\text{THF})_4]^+$) and/or ellipsoidal molecules like *e.g.* tetramethoxypropane or 2,2-bis(diphenylphosphino)-1,1-binaphthyl (BINAP). Small aromatic compounds like toluene, indene or naphthalene with $\text{MW} < 160 \text{ g/mol}$ diffuse also like DSE molecules. The significance of two dimensional shapes begins approximately at $\text{MW} > 178 \text{ g/mol}$. This is the region where the type of the ED begins, including molecules like anthracene (178 g/mol) or tetraphenyl naphthalene (TPhN, 433 g/mol). Depending on these different molecular types¹⁰ the ECC plot gives excellent linear fits (Fig. 2-2b) with a small error and very high R^2 values of $R^2 \approx 1$ (A-Figure 1 and A-Figure 2 in the appendix). These fits result in six different ECCs: ECC_{CS} , ECC_{DSE} and ECC_{ED} for each solvent ($\text{TOL-}d_8$ and $\text{THF-}d_8$). The linear fit parameters are summarized in Table 2-2. Merged calibration curves were also generated, for MW-determinations of compounds with unknown molecular shapes.

¹⁰ A fourth type of molecule shape is also thinkable that should distinguish from the already mentioned ones: rod shaped molecules. However, in this Ph.D. thesis the focus is on CS, DSE and ED molecules.

Table 2-2. Linear fit parameter for the four ECCs each for TOL- d_8 and THF- d_8 solutions

	TOL- d_8		THF- d_8	
	$-\log K$	$-\alpha$	$-\log K$	$-\alpha$
ECC_{CS}^S	7.7581	0.5018	7.7427	0.4943
ECC_{DSE}^S	7.5197	0.6098	7.5360	0.5824
ECC_{ED}^S	7.1008	0.7836	7.1205	0.7519
ECC_{merge}^S	7.4595	0.6318	7.4664	0.6095

When internal calibration curves (ICC) are used, then all references have to be in the same sample. The diffusion coefficients of those internal references show a linear dependency. In the above presented external calibration curves (ECC), (where each model compound has been measured with ADAM or TMB as single internal reference), a linear behavior is observable, too. These compounds behave as they were all measured in the same NMR sample. Therefore the idea occurred that beside ADAM and TMB, basically all model compounds could act as internal references for the ECCs, according to:

$$\log D_{x,\text{norm}} = \log D_{\text{ref,fix}}^* \quad (22)$$

Consequently DOSYs were measured with some model compounds (e.g. ADAM + Si(SiMe₃)₄ + naphthalene in TOL- d_8) in the same NMR sample. Every compound was used as internal reference by applying equation (22). In fact it is possible to determine accurate MWs of all compounds by using the normalized $\log D_{x,\text{norm}}$ value as fixed reference (Table 2-3). The MWs can be calculated by using the ECC-parameters from Table 2-2 and following equation:

$$MW_{\text{det}} = 10^{\left(\frac{\log D_{x,\text{norm}} - \log K}{\alpha}\right)} \quad (23)$$

And the deviation of the determined MW (MW_{det}) from the calculated MW (MW_{calc}) is estimated according to:

$$MW_{\text{err}} = \left[1 - \frac{MW_{\text{det}}}{MW_{\text{calc}}}\right] \cdot 100\% \quad (24)$$

Utilizing e.g. the residual proton signal TOL- d_7 as internal reference, ADAM, Si(SiMe₃)₄ and naphthalene can be determined with an average deviation of $\pm 5\%$. Or in other words, the “real” molecular weight was missed by only 5%, although a calibration curve was used which relies on the basis of many references that were not present in this NMR sample.

Table 2-3. Mixed composition of compounds (each 15 mM) in TOL-*d*₈ acting them self as internal reference for the DOSY-ECC-MW-determination.

Analyte	MW_{calc} [g/mol]	Ref 1 TOL- <i>d</i> ₇		Ref 2 ADAM		Ref 3 Si(SiMe ₃) ₄		Ref 4 Naphthalene	
		MW_{det} [g/mol]	MW_{err} [%]	MW_{det} [g/mol]	MW_{err} [%]	MW_{det} [g/mol]	MW_{err} [%]	MW_{det} [g/mol]	MW_{err} [%]
TOL- <i>d</i> ₇ ^{b)}	99	96	3	97	2	96	3	97	2
ADAM ^{a)}	136	144	-6	147	-8	144	-6	145	-7
Si(SiMe ₃) ₄ ^{a)}	321	304	5	309	4	303	5	305	5
Naphthalene ^{b)}	128	122	5	124	3	122	5	122	5

a) $\text{ECC}_{\text{CS}}^{\text{TOL}}$, b) $\text{ECC}_{\text{DSE}}^{\text{TOL}}$ were used to calculate the MW.

With the ECC-method it is possible to simulate a bench of internal references by adding just one of them to the NMR sample. All 28 compounds behave like they were all measured in the same NMR sample. Inert compounds that are suitable to act as internal reference and their $\log D_{\text{ref,fix}}^*$ values are summarized in Table 2-4. In the next chapter the use of the residual solvent signal of TOL-*d*₈ and THF-*d*₈ as internal reference is examined in detail.

Table 2-4. Overview of all ECC-adapted inert references that fulfill the requirement of internal references for 15 mM solutions.

MW_{calc} [g/mol]	Compound ^{a)}	TOL- <i>d</i> ₈ $\log D_{\text{ref,fix}}^*$	THF- <i>d</i> ₈ $\log D_{\text{ref,fix}}^*$
70	Cyclopentane	-8.6694	-8.6437
79	THF- <i>d</i> ₇ ^{b,f)}	--	-8.6335
88	TMS	-8.7445	-8.7018
92	TOL	--	-8.6742
99	TOL- <i>d</i> ₇ ^{d,f)}	-8.7289	--
114	TMB	-8.7963	-8.7749 ^{c)}
116	Indene	-8.7698	-8.7325
128	Naphthalene	-8.7932	-8.7461
136	ADAM ^{e)}	-8.8454 ^{c)}	--
178	Diphenylacetylene	-8.9095	-8.8535
178	Anthracene	-8.8574	-8.8129
192	9-Methylantracene	-8.8824	-8.8440
202	Pyrene	-8.8960	-8.8457
204	1-Phenylnaphthalene	-8.9184	-8.8812
228	Triphenylene	-8.9552	-8.8869
321	Si(SiMe ₃) ₄	-9.0038	-8.9773
433	Tetraphenylnaphthalene	-9.1660	-9.1054

- When a compound had more than one ^1H signal, the average diffusion coefficient was used.
- Due to the very high access of the solvent, the signal of THF- d_7 can be used as internal reference, but a higher MW_{det} error can occur, when the solvent is coordinating to *e.g.* a metal.
- The “original” $\log D_{\text{ref,fix}}$ values that were used for all ECCs.
- A the middle diffusion coefficients of the three aromatic protons was calculated. The final diffusion coefficient was calculated by middling this value with the diffusion coefficient of the methyl group at 1.73 ppm.
- ADAM has two signals in the ^1H -spectrum. For determining the diffusion coefficient, the signal of the $-\text{CH}_2$ groups with the highest intensity was used.
- The residual solvent signal of TOL- d_8 and THF- d_8 that arises from the proton of isotopomers containing one less deuterium atom than the perdeuterated solvent^[106] are referred as TOL- d_7 and THF- d_7 .

2.1.3 Quality of TOL- d_7 and THF- d_7 as Internal Reference

To compare the quality of the ECCs, MWs of all model compounds were calculated by using the $\log D_{\text{ref,fix}}^*$ values of TOL- d_7 and THF- d_7 as internal references (Table 2-4). The MWs of the model compounds were determined by using the appropriate ECCs. The MW of cyclopentane (Fig. 2-4, very left point, $MW_{\text{err}} = 7\%$) was *e.g.* determined by using ECC_{CS} and TPhN (Fig. 2-4, very right point, $MW_{\text{err}} = 0\%$) by using ECC_{ED} . Fig. 2-4 shows that the quality of MW-determination is reference-independent. It does not matter if ADAM/TMB or TOL- d_7 /THF- d_7 were used as internal reference. Both give excellent MW-predictions with a standard deviation of only $\sigma = 4\%$. The maximum error in both solvents is $MW_{\text{err}} \leq \pm 9\%$. Therefore it can be postulated that this is the maximum resolution of this DOSY-ECC-MW-determination method.

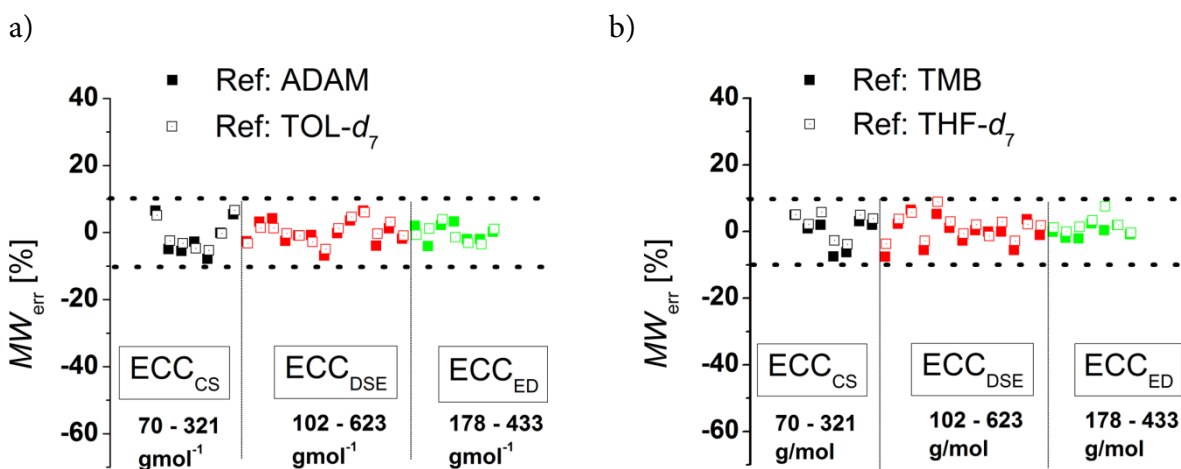


Fig. 2-4. Using a) ADAM or TOL- d_7 and b) TMB or THF- d_7 as internal reference (15 mM) gives a good MW-determination with a standard deviation of only 4%.

2.1.4 Influence of Shape

There are several modifications of the Stokes-Einstein equation which take the molecule's shape into account (by adding *e.g.* correction factors).^[79c, 99, 101] The power law derived MW-determinations distinguish mostly between compound classes,^[81a] large^[107] and small molecules,^[103] but not directly between different shapes within those molecular classes. In this chapter it will be demonstrated that the accuracy of the power law derived MW-prediction is highly affected, also for small molecules, by the analyte's shape. To validate this issue external calibration curves ECC_{ED} , ECC_{DSE} and ECC_{ED} were used for MW-determination of *all* molecules without considering their true shape (Fig. 2-5). When for example the ECC_{CS} (that is for compact spherical molecules) is used on expanded disc like molecules, the determined MW will have a massive error especially for big molecules (Fig. 2-5A).

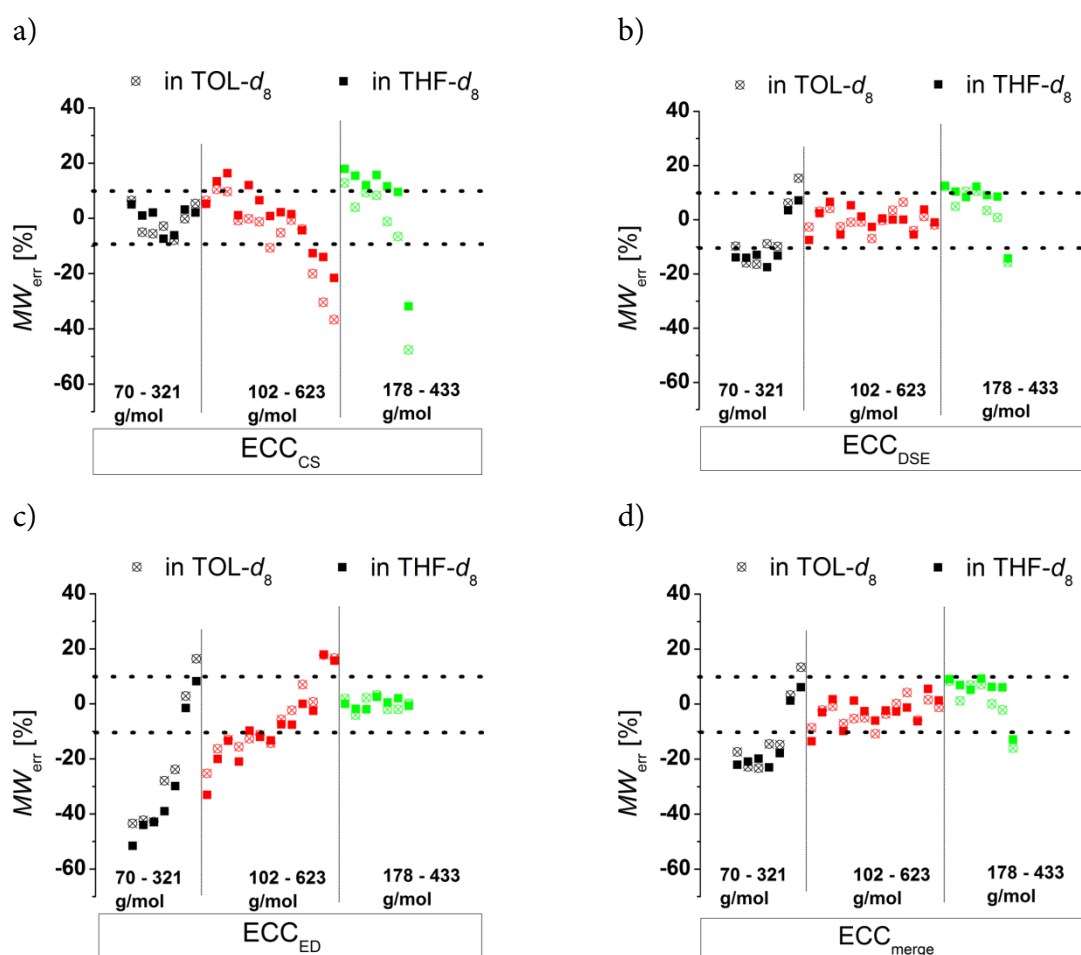


Fig. 2-5. Using exclusively a) ECC_{CS} , b) ECC_{DSE} c) ECC_{ED} and d) ECC_{merge} on *all* model compounds (15 mM) in TOL- d_8 and THF- d_8 . *E.g.* the MW-determination of TPhN (an expanded flat disc, $MW_{calc} = 433$ g/mol) in TOL- d_8 with spherically references (ECC_{CS}) would produce a MW of $MW_{det} = 639$ g/mol with an error of $MW_{err} = 48\%$. This is why it is very important to use appropriate references with right shapes for accurate MW-determinations.

Anticipating for example TPhN (an expanded flat disc, 433 g/mol) in TOL- d_8 to be spherical would produce a MW of $MW_{\text{det}} = 639$ g/mol that is a 48% overestimated mass (Fig. 2-5A). Using *e.g.* the ECC_{ED} for non-oblate molecules would produce especially for small molecules with $MW_{\text{calc}} < 170$ g/mol a large error (Fig. 2-5C). The merged calibration curve ECC_{merge} (Fig. 2-5D) determines MWs in a range of $MW_{\text{err}} = \pm 23\%$. However, the deviation is much smaller in the region of approximately 120-200 g/mol. On one hand that means that in this MW-region all molecules diffuse more or less independently from their shape. On the other hand the MW-determination (and the self-diffusion) of molecules that are outside that region, is increasingly influenced by the analyte's shape. Using the wrong calibration curve (or for example wrong references for an ICC) can produce highly erroneous MW-values. This is the reason why other calibration curves^[101, 103, 108] that correlate a bundle of different molecules without considering the right shape, lead to bigger deviations from the correct MWs in the range of $MW_{\text{err}} = \pm 30\%$. By taking the correct shape into account it is possible to determine more accurate MWs with a deviation of $MW_{\text{err}} \leq \pm 9\%$ (A-Table 6 and A-Table 7 in the appendix).

2.1.5 Influence of Concentration

All above mentioned ECCs were derived from diluted solutions (15 mM). It was important to validate how good the ECC-MW-determination works, when the concentration is much higher than 15 mM. Therefore DOSYs of some model compounds have been measured at significantly higher concentrations of 240 mM (reference and analyte each 120 mM). The results are shown in Fig. 2-6.

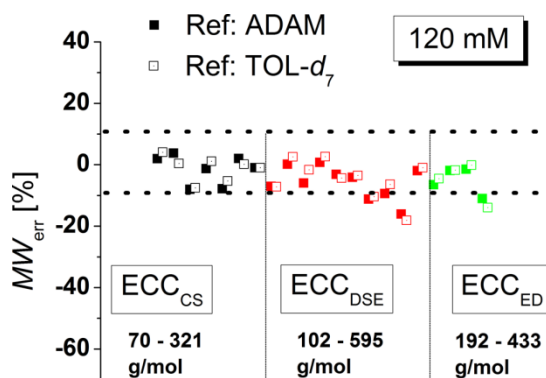


Fig. 2-6. DOSY-ECC-MW-determination of some model compounds at a concentration of 120 mM at 25°C in TOL- d_8 . ADAM was used in equimolar concentration as internal reference.

The Stokes-Einstein equation is only valid for infinite diluted solutions. Therefore the error should be bigger with high concentrated solutions. However, the average deviation of the estimated MW is only a little higher and most of the compounds are still in the $\pm 9\%$ range. The biggest error arises probably due to intermolecular interactions that result in higher estimated MWs. Especially π -interactions of big aromatic systems, at high concentrations could significantly increase the error of estimated MWs (A-Table 8 in the appendix). Anyway, all compounds without aromatic rings have been determined within $\pm 9\%$ deviation. The power law seems to be valid even for higher concentrations, if inter- or intramolecular interactions can be excluded. At lower temperatures inter- or intramolecular interactions increase. Therefore the error of MW-determination, especially for huge aromatic systems should also increase with high concentrations. This is why for low temperature measurements diluted samples should be used. Thanks to the internal reference, the ECC-MW-determination.

2.1.6 Influence of Temperature

According to the Stokes-Einstein equation the self-diffusion should be inversely proportional to the viscosity. Indeed, increasing the solvent viscosity by cooling the NMR sample from room temperature to -75°C leads to an increase of the diffusion coefficient by almost two magnitudes! Thanks to the internal reference, the ECC-MW-determination of $\text{Si}(\text{SiMe}_3)_4$ (TTS, 321 g/mol) gives in the full range of -75°C to $+100^\circ\text{C}$ still good results (Fig. 2-7).

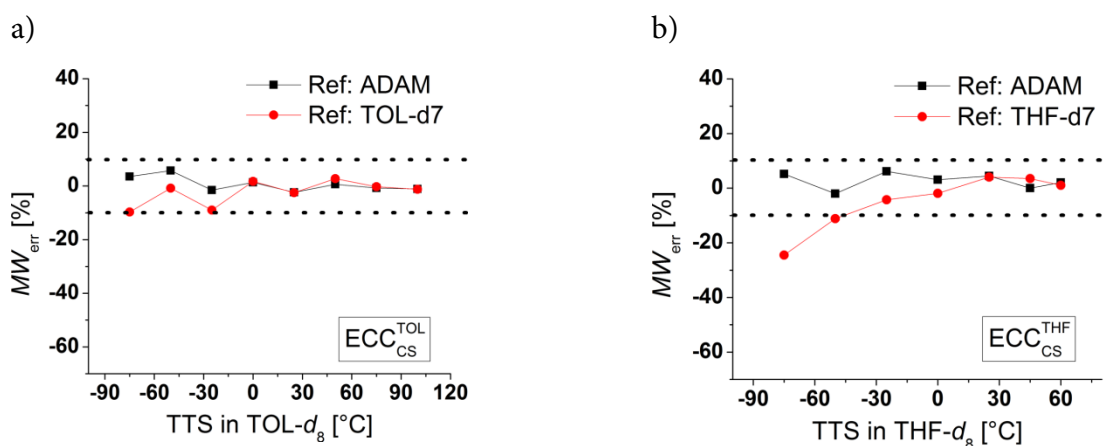


Fig. 2-7. DOSY-ECC-MW-determination of $\text{Si}(\text{SiMe}_3)_4$ (TTS, 15 mM) in a) TOL- d_8 and in b) THF- d_8 at different temperatures. Thanks to the internal reference, the ECC-MW-determination of TTS gives in the full temperature range good results. However, below -50°C the use of the residual THF proton signal THF- d_7 can be problematically, due to hydrogen bonding with residual water molecules.

The internal reference is able to compensate for viscosity changes in the solvent (see also A-Table 9 in the appendix). Notably, the MW-determination is still possible at temperatures close to the boiling point of the solvent. This would give the opportunity to observe species that are forming during reactions at elevated temperatures. Furthermore, it is obvious that the signal of TOL- d_7 is a useful internal reference for both high and low temperatures. However, using more polar THF- d_7 below -50°C can get problematically. This probably results from solvent-solvent interactions and hydrogen bonding with residual water molecules.

2.1.7 Influence of Halides and Molar Density

In the Stokes-Einstein equation the diffusion coefficient relies on the shape and on the hydrodynamic radius of the particle. The latter can be described by the volume of the surrounding solvent molecules, the electron cloud and also the volume of the atoms. One has to keep in mind that the volume of an atom is not proportional to its atom weigh. Especially halides, compared to their atomic radii, have very high atomic masses and therefore a high mass density. For instance a potassium cation has an ion radius of 138 pm and an atom weight of 39 g/mol. An iodine atom has almost the same radius of 133 pm but an atom weight of 127 g/mol that is 320% higher than that of the K^+ cation.^[109] The herein presented ECCs were elaborated with references that consist of hydrocarbons with some heteroatoms of the third period like silicon, phosphor and sulfur. Therefore especially compounds containing heavy halides will be underestimated in MW. While chlorine containing compounds are estimated with good accuracies the much denser bromides show bigger deviations from the correct MWs (Table 2-5).

Table 2-5. DOSY-ECC-MW-determination of molecules with halides.

Compound	MW_{calc} [g/mol]	MW_{det} a) [g/mol]	MW_{err} [%]	$MD_w/10^{29}$ [g/(mol·m ³)]
1-Hexylchloride	120	117	2	5.49
1-Octylchloride	149	143	4	5.29
1-Decylchloride	177	176	1	5.13
1-Propylbromide	123	82	34	9.66
Triphenylmethylbromide	323	283	12	6.45
9,10-Dibromoanthracene	336	194 ^{b)}	42	8.71
1-Butyliodide	184	102	45	11.15

a) ECC_{DSE} and b) ECC_{ED} was used to determine the MW

Especially increasing halide to carbon ratio leads to bigger errors. For example triphenylmethylbromide with one bromine atom is underestimated by 12%. But 9,10-dibromoanthracene with two bromides, a small carbon backbone and therefore a very high molar density is underestimated in MW by 42%. These examples demonstrate that the power law depends not only on the shape of the molecules but also heavily on the molecular density.

There are more or less extensive ways to calculate the density of a molecule. However, a simple but robust equation that correlates the MW to the approximated volume of a compound would be highly beneficial. Therefore equation (25) was derived:

$$MD_W = \frac{MW_{\text{calc}}}{V_{\text{sph}}}, \text{ with } V_{\text{sph}} = \sum V_W = \sum_{i=1}^n \frac{3}{4} \pi r_{w,i}^3 \quad (25)$$

where MD_W is the molar van der Waals density, MW_{calc} the calculated molecular weight of a compound, V_W the van der Waals volume and r_w the van der Waals radius of n atoms. In respect to this equation the van der Waals volumes^[110] of all atoms of a compound were calculated and summed up to one single van der Waals-sphere (V_{sph}) (A-Table 10 in the appendix). Of course this method is just an approximation without considering the real covalent bond-bond distances and the shape of the compounds. But the ratio between the MW and the sum of all van der Waals volumes (V_w , see Table 2-7, *vide infra*) leads to a

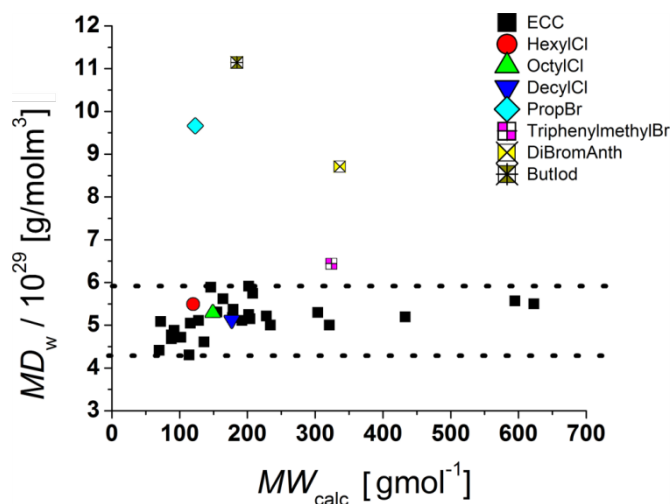


Fig. 2-8. Molar van der Waals-density (MD_w) distribution in the model compounds and molecules with heavy atoms. The ECCs presented in this thesis work well with molecules with a molar density between $4.3 \cdot 10^{29} \text{ g}/(\text{mol} \cdot \text{m}^3)$ and $5.9 \cdot 10^{29} \text{ g}/(\text{mol} \cdot \text{m}^3)$.

value that represents approximately a molar van der Waals density (MD_w) in a unit of $\text{g}/(\text{mol} \cdot \text{m}^3)$. Plotting MD_w against MW_{calc} give for all model compounds an average density distribution of around $5.2 \cdot 10^{29} \text{ g}/(\text{mol} \cdot \text{m}^3)$ (Fig. 2-8). Obviously the ECCs presented in this thesis work well with molecules with a molar density between $4.3 \cdot 10^{29} \text{ g}/(\text{mol} \cdot \text{m}^3)$ and $5.9 \cdot 10^{29} \text{ g}/(\text{mol} \cdot \text{m}^3)$. Higher molar van der Waals densities like for example 9,10-dibromoanthracene [$MD_w = 8.7 \cdot 10^{29} \text{ g}/(\text{mol} \cdot \text{m}^3)$, Table 2-5] will be underestimated and lower MD_w values will be overestimated in MW. To obtain accurate MWs for molecules with high densities it is necessary to measure new calibration curves with references of comparable molar densities and shapes. However, in order to apply a density correction on the MW_{det} value of highly densed molecules a correction factor X_{corr} can be calculated for each ECC (Table 2-6).

$$X_{\text{corr}} = \frac{MW_{\text{calc}}}{MW_{\text{det}}} \quad (26)$$

Table 2-6. DOSY-ECC-MW-determination of various compounds (DSE shape, 20 mM in THF- d_8) with high molar van der Waals densities.

		MD_w	MW_{calc}	MW_{det}	
	<i>Formula</i>	[$\text{g}/(\text{mol} \cdot \text{m}^3)$]	[g/mol]	[g/mol]	X_{corr}
1-Butylbromide	$\text{C}_4\text{H}_9\text{Br}$	8.62E+29	137	93	1.473
1-Propylbromide	$\text{C}_3\text{H}_7\text{Br}$	9.66E+29	123	82	1.500
1-Pentylbromide	$\text{C}_5\text{H}_{11}\text{Br}$	7.92E+29	151	106	1.425
1-Butyliodide	$\text{C}_4\text{H}_9\text{I}$	1.12E+30	184	102	1.804

FeCp ₂	C ₁₀ H ₁₀ Fe ₂	6.89E+29	186	153	1.216
Triphenylmethylbromide	C ₁₉ H ₁₅ Br	6.45E+29	323	290	1.114
2-Chlorobenzoxazole	C ₇ H ₄ ClNO	6.66E+29	146	124	1.177

Plotting *e.g.* the X_{corr} factor of molecules with DSE shape (Table 2-6) against their molar van der Waals density MD_{w} gives a linear dependency (Fig. 2-9):

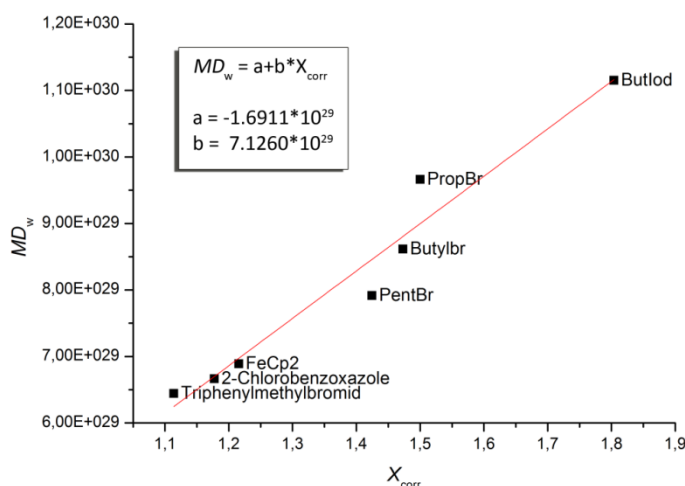


Fig. 2-9. Plot of MD_{w} vs. X_{corr} for density correction of molecules with molar van der Waals densities above $5.9 \cdot 10^{29} \text{ g}/(\text{mol} \cdot \text{m}^3)$

With parameter a and b it is possible to apply a density correction on MW_{det} values for molecules with molar van der Waals densities above $5.9 \cdot 10^{29} \text{ g}/(\text{mol} \cdot \text{m}^3)$:

$$MW_{\text{det,corr}} = MW_{\text{det}} \cdot X_{\text{corr}} \quad (27)$$

However, equation (27) should be used with caution, since its ability was not proved on a significant amount of model compounds with high molar densities.

Table 2-7. Van der Waals Volumes of selected elements.^[111]

Element	V_{w} [m ³]	Element	V_{w} [m ³]
H	5.575E-30	O	1.471E-29
Li	2.525E-29	Si	3.879E-29
Na	4.900E-29	P	2.443E-29
K	8.711E-29	S	2.443E-29
Rb	1.165E-28	Cl	2.245E-29
Cs	1.690E-28	Br	2.652E-29

Mg	2.169E-29	I	3.252E-29
C	2.058E-29		
N	1.560E-29		

2.1.8 Influence of Deuterated Compounds

The MW-estimation of the residual solvent peak (THF- d_7 , 79 g/mol) gives a MW of 63 g/mol that would be underestimated in MW ($MW_{\text{err}} = 20\%$). The determined MW fits much better to the protonated THF- h_8 species (72 g/mol, $MW_{\text{err}} = 8\%$). This is congruent to the nearly similar atomic radius of D compared to H. According to the abovementioned correlation of the atomic volume and the corresponding diffusion coefficient, it is clear that deuterated molecules diffuse approximately like their protonated counterparts, although they have slightly higher MWs. In the case of TOL- d_7 (99 g/mol) this effect is less pronounced ($MW_{\text{det}} = 96$ g/mol, $MW_{\text{err}} = 3\%$ rel. to TOL- d_7 and $MW_{\text{err}} = -5\%$ rel. to TOL- h_8) due to the relative higher MW of toluene. Moreover, especially in the case of multiple THF- d_8 -coordination it is advisable to use the molecular weight of THF- h_8 instead of THF- d_8 to have an accurate MW-determination.

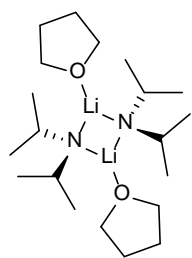
2.2 DOSY-ECC-MW-Determination of Organometallics and Metal Amides

On the one hand organometallic compounds tend to aggregate *via* coordinative bonds that are significantly longer than covalent bonds. Additionally solvent molecules can associate and dissociate in solution.^[112] Therefore the space between all atoms is less packed than in the “sigma bonded-compact spheres” model of the ECC_{CS}. On the other hand alkaline organometallics frequently adopt spherical and ellipsoidal shapes, according to the ring-stacking and laddering principle.^[11] This is why ECC_{DSE} for “dissipated spheres and ellipsoids” should be the best calibration curve for the most organometallic compounds.^[6]

2.2.1 Structure of LDA in THF Solution

THF solvated LDA is known to exist exclusively as a disolvated dimer **29** (Fig. 2-10, see also chapter 1.1.1).^[14] As a proof of principle a DOSY-ECC-MW-determination of LDA in THF- d_8 solution (15 mM) was investigated. In fact, using ECC_{DSE} for the MW-

determination of LDA ($MW_{\text{calc}} = 358 \text{ g/mol}$) in THF- d_8 gives a MW of $MW_{\text{det}} = 347 \text{ g/mol}$ with a deviation of only 3% from the calculated MW (Fig. 2-10).^[6]



29

DOSY-ECC-MW-determination:

$$MW_{\text{calc}} = 358 \text{ g/mol}$$

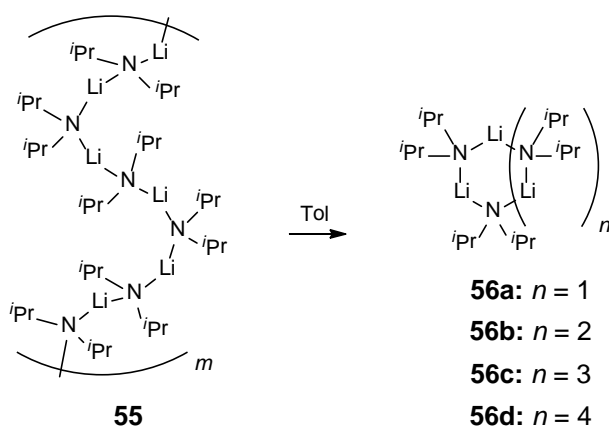
$$MW_{\text{det}} = 347 \text{ g/mol}$$

$$MW_{\text{err}} = 3\%$$

Fig. 2-10. DOSY-ECC-MW-determination of LDA (15 mM) in THF- d_8 solution by applying ECC_{DSE}. PhN (15 mM) was used as internal reference with $D_{\text{ref,fix}} = -8.8812$.

2.2.2 Structure of LDA in Toluene Solution¹¹

LDA is a very prominent reagent that plays a key role in organic synthesis, serving as a base *par excellence* for a broad range of deprotonation reactions (see *e.g.* Scheme 1-2). However, the state of aggregation in solution in the absence of donor bases was unclear. *Kim and Collum et al.* analyzed [⁶Li]LDA and [⁶Li,¹⁵N]LDA in hexane by ⁶Li and ¹⁵N NMR spectroscopy and observed a mixture of as many as five cyclic oligomers.^[12a] They anticipated that the main cyclic aggregates corresponded to dimers, trimers and higher oligomers. Unfortunately a quantification of these observations was not possible because “a severe overlap renders the effort required for a detailed study unjustifiable”. This is why these oligomers have not been characterized further.



Scheme 2-1. LDA in the solid state and in toluene solution.

¹¹ A revised version of my publication: R. Neufeld, M. John, D. Stalke, *Angew. Chem.*, **2015**, 127, 7100–7104; *Angew. Chem. Int. Ed.*, **2015**, 54, 6994–6998.

LDA is polymeric in the solid state and shows little solubility in toluene (Scheme 2-1). The highest concentrations that could be observed at RT were in the range of 7-15 mM. In the ^7Li spectrum only one broad signal at 2.81 ppm is present that broadens up with decreasing temperature. This circumstance makes it impossible to distinguish between any oligomers from the ^7Li -NMR experiment (Fig. 2-11a). However, at RT in the ^1H spectrum two sets of two main signals corresponding to the α -CH (3.12 ppm and 3.01 ppm) and $-\text{CH}_3$ group (1.14 ppm and 1.11 ppm) are present (species **A** and **B** Fig. 2-11b). A third compound with very low intensity was also evidenced by an additional α -CH signal at 3.19 ppm (species **C**). Due to its poor intensity it was not possible to determine the diffusion coefficient of this third compound at RT. Although, the other two main signals at 3.12 ppm and 3.01 ppm show some overlap, their self-diffusion was measurable *via* DOSY-NMR.

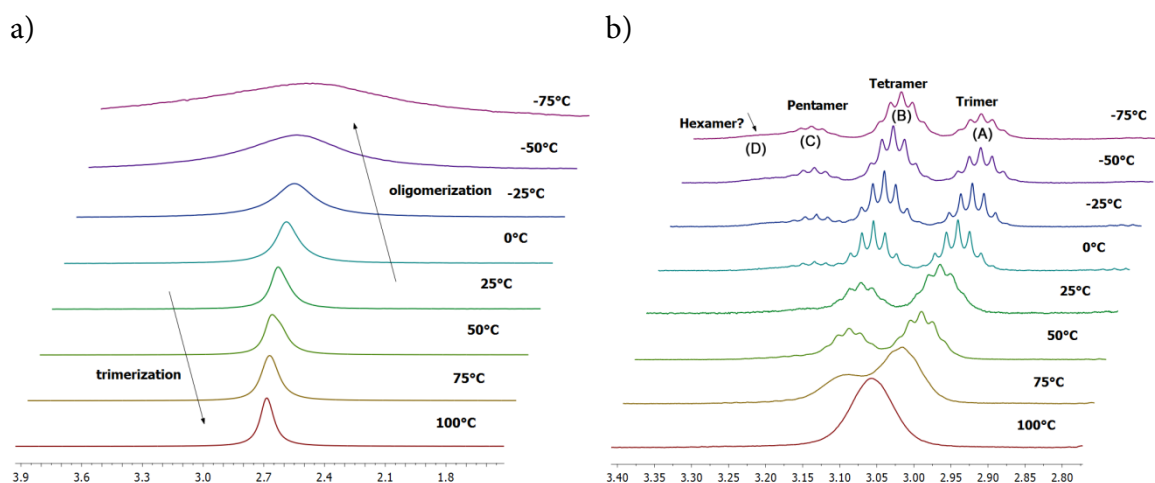


Fig. 2-11. a) ^7Li - and b) ^1H -superposition plot of LDA and its α -CH signals in TOL- d_8 at different temperatures.

From DOSY-ECC-MW-determination (Table 2-8B) species **A** agrees best with a trimer **56a** ($MW_{\text{calc}} = 321$ g/mol, $MW_{\text{det}} = 318$ g/mol, $MW_{\text{err}} = 1\%$, Scheme 2-1) and species **B** with tetramer **56b** ($MW_{\text{calc}} = 428$ g/mol, $MW_{\text{det}} = 390$ g/mol, $MW_{\text{err}} = 9\%$). Careful integration of both signals at 25°C reveals that **56a** and **56b** exist together in a ratio of 2:1 (A-Table 12 in the appendix). It is also evident that dimers, like those proposed by *Kim et al.* are not present in the mixture ($MW_{\text{err}} = -48\%$ and -143%) at any temperature. The other low field shifted species **C** with weak intensity has to be a bigger aggregate than the tetramer. At -50°C the integral of **C** increases significantly at the expense of species **A**. The signal separation was suitable for the DOSY-ECC-MW-determination (A-Figure 3 in the

appendix). Table 2-8a illustrates that **C** shows the best agreement with a pentameric LDA-aggregate **56c** ($MW_{\text{calc}} = 536 \text{ g/mol}$, $MW_{\text{det}} = 520 \text{ g/mol}$, $MW_{\text{err}} = 3\%$).

Table 2-8. DOSY-ECC-MW-determination of LDA in TOL- d_8 at various temperatures. ^{a)}

		<i>Dimer</i> (214 g/mol)	<i>Trimer</i> (321 g/mol)	<i>Tetramer</i> (428 g/mol)	<i>Pentamer</i> (536 g/mol)	<i>Hexamer</i> (643 g/mol)
	MW_{det} [g/mol]	MW_{err} [%]	MW_{err} [%]	MW_{err} [%]	MW_{err} [%]	MW_{err} [%]
a) -50°C						
Species A	332	-55	-3	22	38	48
Species B	423	-98	-32	1	21	34
Species C	520	-143	-62	-21	3	19
b) $+25^\circ\text{C}$						
Species A	318	-48	1	26	41	51
Species B	390	-82	-21	9	27	39
c) $+100^\circ\text{C}$						
Species A	333	-56	-4	22	38	48

a) ECC_{DSE}^{TOL} was used to determine the MWs. The accuracy of this method is in the range of $MW_{\text{err}} \leq \pm 9\%$. None of the species show accordance with the dimer ($MW_{\text{err}} \geq -48\%$).

The MW estimation of the residual diisopropyl amine present in solution (DA(H), $MW_{\text{calc}} = 101 \text{ g/mol}$, $MW_{\text{det}} = 100 \text{ g/mol}$, $MW_{\text{err}} = 1\%$, A-Table 11 in the appendix) was also possible. The good agreement with the calculated MW gives evidence that DA(H) does not coordinate to any oligomeric species. This result is consistent with previous investigations, which showed that DA(H) is a very poor ligand for LDA.^[14a] At -50°C an additional multiplet appears that belongs to oligomer **D** at the left hand side of the signal attributed to the pentamer **C** (Fig. 2-11a). Unfortunately this signal was too weak for a MW-determination. Further cooling did not improve the signal-to-noise ratio due to a reduced solubility of LDA in toluene at temperatures below -50°C . In 1999, *Rutherford* and *Collum* showed by low temperature ^6Li and ^{15}N NMR spectroscopy that the lighter congener of LDA, lithium diethyl amide (LiDEA) can exist as several oligomers in THF and oxetane solutions (Fig. 2-12).^[113] In neat THF or oxetane LiDEA is a cyclic dimer **57**. At lower donor base concentrations cyclic oligomers appear. At low THF concentrations (2-10 equiv.) a cyclic trimer **58** and a four-rung-ladder **59** are formed. Higher order ladders were not observed within the solubility limits of LiDEA, but at sub-stoichiometric oxetane concentrations they noticed a relatively complex LiDEA equilibrium of cyclic dimers, trimers and ladders of tetramers, pentamers and hexamers (**57-61**). While LiDEA tend to

form ladder structures, an increased bulk of the R groups favors cyclic arrangements. *E.g.* the donor base-free lithium hexamethyldisilazide adopts a cyclic trimeric structure **40** in the solid state^[39b] and exists as a cyclic tetramer- dimer mixture in hydrocarbons (see chapter 1.1.2).^[51]

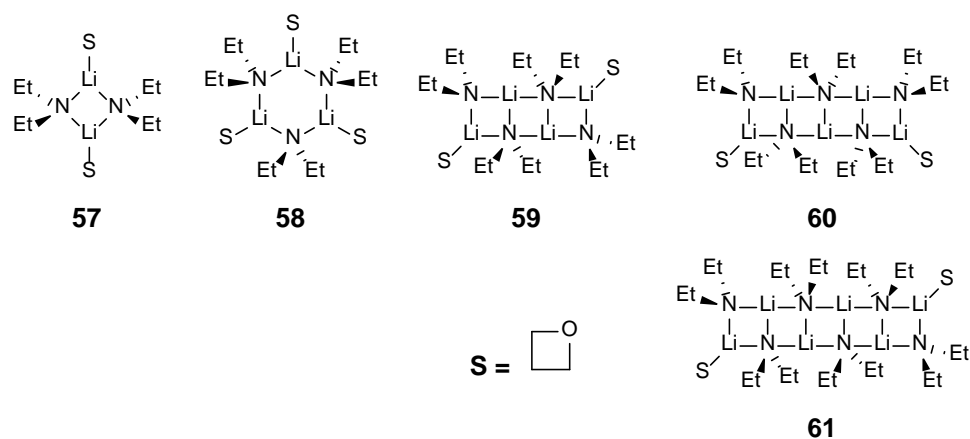


Fig. 2-12. Aggregation of lithium diethyl amide (LiDEA) in neat oxetane or pentane/toluene mixtures as cosolvent.^[113]

Similarly lithium tetramethylpiperidide adopts a cyclic trimer **31** and tetramer **32** in the solid state^[33-34] and appears to form both cyclic oligomers in pentane (see chapter 1.1.1).^[34b] In view of this trend and the bulkiness of the *t*Pr-groups, the assumption that the signal from oligomer **D** stems from the cyclic LDA-hexamer **56d** appears to be valid. Cooling the sample shifts the position of the oligomer-equilibrium. While the tetramer concentration increases, that of the trimer decreases. Obviously low temperatures stabilize the higher aggregates, due to entropy. The conversion of the trimer to the corresponding oligomers is also reflected in the ⁷Li NMR spectrum (Fig. 2-11a). The ⁷Li signal becomes broader at lower temperature. This could be due to a relatively faster quadrupolar relaxation or additionally due to the increase of oligomeric structures. Warming up the solution causes the opposite trend. The oligomer concentration decreases, while the trimer concentration increases. At +50°C a shoulder at the main ⁷Li signal is apparent, revealing two main species: the trimer **56a** and the tetramer **56b**. In the ¹H NMR spectrum at +100°C all aggregates coalesce to one set of signals at 3.06 ppm and 1.10 ppm, respectively. The ECC-MW-determination estimates a MW of $MW_{det} = 333$ g/mol that fits best to the trimeric LDA species **56a** with an MW-deviation of only $MW_{err} = -4\%$ (Table 2-8c).^[114]

2.2.3 Structure of Na-Indenide in THF Solution¹²

Alkali metal indenides are important precursors for the synthesis of metallocenes of the main group and transition metals. Without donating ligands like ethers or chelating crown ethers they build up polymeric stack structures.^[115] The solid-state structure of donor base-free Na-indenide is unknown. With donating ligands like PMDETA or crone ethers Li- and Na-indenide form contact ion pairs (CIP).^[116] With ammonia solvent separated ion pairs (SSIP) are formed.^[7] However, the aggregation of Na-indenide in solution is still unclear. One reason for that may be the relative bad NMR properties of the sodium nucleus that has a spin of 3/2. This quadrupole results in broad lines that get even broader with asymmetry in the environment of the sodium nucleus. ¹H-DOSY experiments are independent of that nucleus. Therefore, Na-indenide is an interesting candidate for discovering its aggregation in THF solution by employing the new DOSY-ECC-MW-determination methodology. The most feasible species are the THF solvated monomers (**M1-M4**) and the dimers **D1-D2** bearing *n* THF molecules (Fig. 2-13).

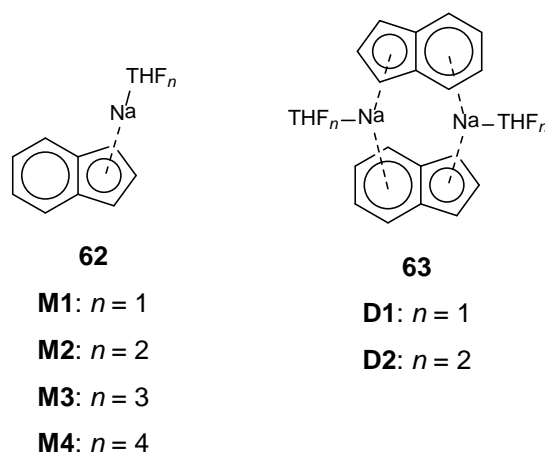


Fig. 2-13. Most plausible Na-indenide species in THF solution.

The molar density for all species is between $MD_w = 5.07$ and $5.43 \cdot 10^{29}$ g/(mol·m³) which ensures that those aggregates are suitable for all developed ECCs. At room temperature (RT) the DOSY-ECC-MW-determination estimates a MW of $MW_{det} = 331$ g/mol. The comparison of the estimated MW with the most likely Na-indenide species is shown in Table 2-9. Both dimers with two- (**D1**: $MW_{err} = 21\%$) and four THF molecules (**D2**: $MW_{err} = 41\%$) can be excluded. The same is true for the mono- (**M1**: $MW_{err} = -57\%$) and

¹² Includes revised parts of my publication: R. Neufeld, D. Stalke, *Chem. Sci.* **2015**, *6*, 3354–3364.

Table 2-9. DOSY-ECC-MW-determination of Na-indenide (15 mM) in THF-*d*₈ at various temperatures. TMB (15 mM) was used as internal reference and ECC_{DSE} to determine the MWs. ^{a)}

<i>Species</i>	<i>n</i>	<i>MW</i> _{calc} [g/mol]	<i>MW</i> _{err} [%]		
			-50°C	+25°C	+60°C
M1	1	210	-84	-57	-36
M2	2	282	-37	-17	-1
M3	3	354	-9	7	19
M4	4	426	10	22	33
D1	1	420	8 ^{b)}	21	32
D2	2	564	32	41	49
Indene		111	4	2	-30
HMDS(H)		161	-5	-5	-1

- a) DOSY-ECC-MW-determination of Na-Indenide in THF-*d*₈ solution gave following results: $MW_{\text{det}}(-50^\circ\text{C}) = 386$ g/mol, $MW_{\text{det}}(25^\circ\text{C}) = 331$ g/mol, $MW_{\text{det}}(+60^\circ\text{C}) = 286$ g/mol.
- b) The disolvated dimer **D1** ($MW_{\text{err}} = 8\%$) would also fit to the estimated MW, but this aggregation makes in this context chemically not much sense.

disolvated monomers (**M2**: $MW_{\text{err}} = -17\%$) that can also be easily excluded. The tri-solvated monomer (**M3**: $MW_{\text{err}} = 7\%$) gives the best match. Such a three-fold THF coordination fits perfectly many crystal structures of THF solvated sodium cyclopentadienide derivatives.^[117] Without difficulty it is also possible to identify the signals of remaining indene ($MW_{\text{err}} = 2\%$) and hexamethyldisilazane (HMDS(H), $MW_{\text{err}} = -5\%$). Those very accurate MWs indicate that the exchange of the latter with Na-indenide **M3** is very slow or not present. Otherwise the estimated MWs of indene or HMDS(H) should be much higher. At -50°C it is obvious that the equilibrium of Na-indenide changes to a higher MW of $MW_{\text{det}} = 386$ g/mol. That MW is right in between three- (**M3**: $MW_{\text{err}} = -9\%$) and four-fold (**M4**: $MW_{\text{err}} = 10\%$) THF-coordinated Na-indenide, indicating that a fourth THF coordination is attractive at low temperatures. Again, indene ($MW_{\text{err}} = 4\%$) and HMDS(H) ($MW_{\text{err}} = -5\%$) are not involved in that Na-indenide-THF equilibrium. By warming up the THF solution to $+60^\circ\text{C}$ the opposite trend is evident. The ECC-MW-determination estimates for Na-indenide a much lower MW of $MW_{\text{det}} = 286$ g/mol that would fit to a disolvated Na-indenide monomer (**M2**: $MW_{\text{err}} = -1\%$) but additionally the MW of indene rises significantly to ($MW_{\text{det}} = 158$ g/mol, $MW_{\text{err}} = -37\%$). This behavior indicates a rapid exchange of Na-indenide and indene at high temperatures producing a merged MW for both. Anyway, HMDS(H) is still not involved in that equilibrium ($MW_{\text{err}} = -1\%$) most likely due to its higher basicity and steric demand, compared with indene ($\text{p}K_{\text{s}} = 26$ vs 20).^[118]

2.2.4 Structure of $[t\text{-BuLi}]_4 \cdot 4[\text{Me}_2\text{NC}_6\text{H}_4\text{Li}]$ in Toluene Solution¹³

In 2012 A.-C. Pöppler *et al.* showed that *ortho* lithium dimethylanilide ($\text{Me}_2\text{NC}_6\text{H}_4\text{Li}$) crystallizes in the presence of $t\text{BuLi}$ as a separated lithium organic aggregate $[t\text{-BuLi}]_4 \cdot 4[\text{Me}_2\text{NC}_6\text{H}_4\text{Li}]$ **64** in the same crystal (Fig. 2-14).^[119] Dissolving crystals of **64** in $\text{TOL-}d_8$ resulted in an unexpectedly complicated ^7Li -NMR spectrum that shows five relatively sharp distinguishable signals over a range of nearly 2.5 ppm. In the ^7Li -DOSY experiment these species display a monotonically decreasing diffusion coefficient (Fig. 2-15).

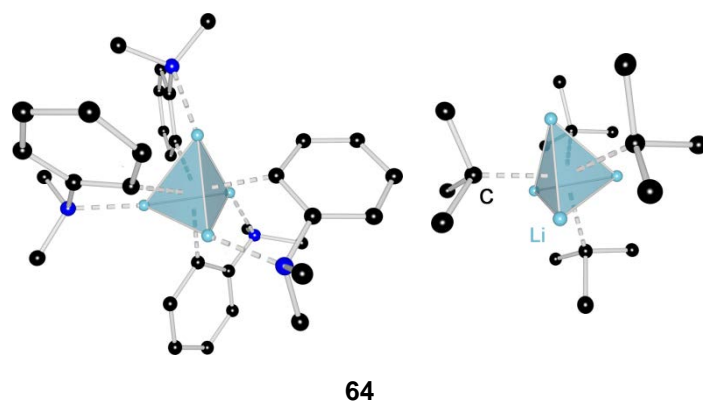


Fig. 2-14. Crystal structure of $[t\text{-BuLi}]_4 \cdot 4[\text{Me}_2\text{NC}_6\text{H}_4\text{Li}]$ **64** with hydrogen atoms omitted for clarity.

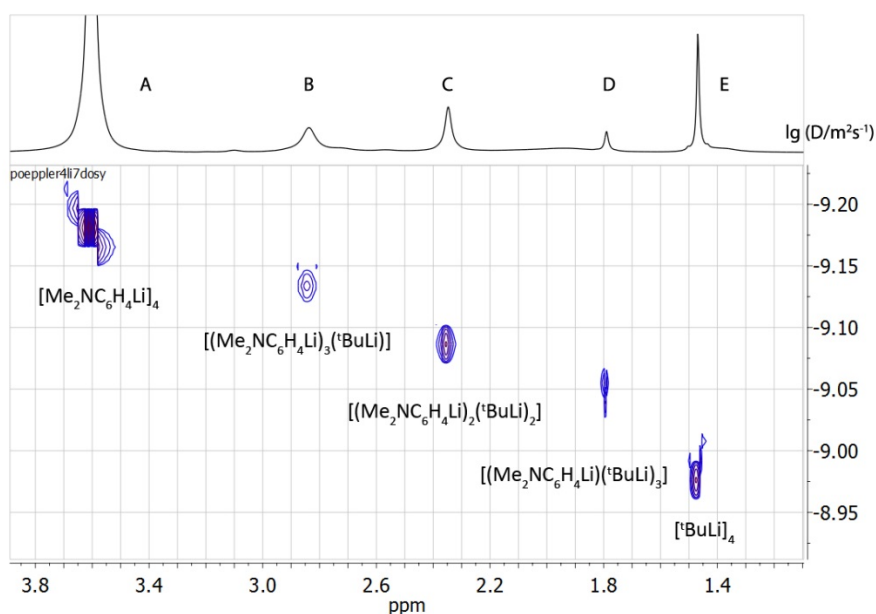


Fig. 2-15. ^7Li -DOSY spectrum of $[t\text{-BuLi}]_4 \cdot 4[\text{Me}_2\text{NC}_6\text{H}_4\text{Li}]$ **64** in $\text{TOL-}d_8$ solution.

¹³ Includes revised parts of my publication: R. Neufeld, D. Stalke, *Chem. Sci.* **2015**, *6*, 3354–3364.

It was anticipated that each species (A-E) represents a tetramer with a consecutive substitution of one *ortho* lithium anilide by one ^tBuLi moiety. However, no verifications of these results using quantitative MW determinations were performed. Reinvesting in that issue and using the diffusion measurements of A.-C. Pöppler *et al.* it was possible to determine the MWs of all species *a posteriori* by applying the DOSY-ECC-MW-determination. Taking the residual proton signal of the solvent (TOL-*d*₇) as internal reference gives very good results with the proposed structures A-E with an error smaller ±5% (Table 2-10).

Table 2-10. DOSY-ECC-MW-determination of crystalline [*t*-BuLi]₄·4[Me₂NC₆H₄Li]₄ **64** in TOL-*d*₈ solution. ECC_{DSE} and TOL-*d*₇ as internal reference with log*D*_{ref,fix} = -8.7289 were used to determine the MWs.

Species		MW _{calc}	MW _{det}	MW _{err}
		[g/mol]	[g/mol]	[%]
A	[Me ₂ NC ₆ H ₄ Li] ₄	508	527	-4
B	[(Me ₂ NC ₆ H ₄ Li) ₃ (^t BuLi)]	445	435	2
C	[(Me ₂ NC ₆ H ₄ Li) ₂ (^t BuLi) ₂]	382	367	4
D	[(Me ₂ NC ₆ H ₄ Li)(^t BuLi) ₃]	319	316	1
E	[^t BuLi] ₄	256	244	5

2.2.5 Structure of MHMDS with Ammonia as Donorbase in Toluene Solution

Previous investigations on MHMDS with ammonia as donor base revealed unprecedented aggregation motifs in the solid state (Fig. 2-16):^[1]

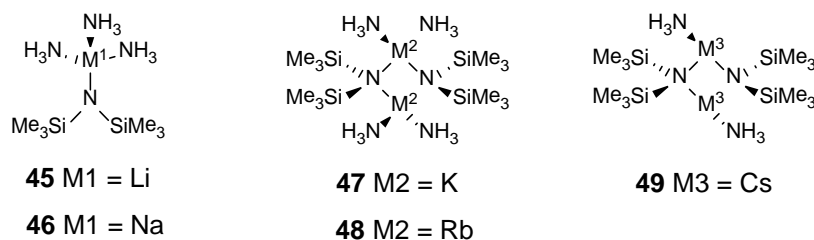


Fig. 2-16. Aggregation motifs of MHMDS (M = Li, Na, K, Rb and Cs) with ammonia as donor base in the solid state.^[1]

Li- and NaHMDS form trisolvated monomers **45** and **46**, stabilized by intermolecular hydrogen bonds (HB) enabling the possibility of HB-stabilized transition states in synthesis. Ammoniacates of KHMDS and RbHMDS form tetrasolvated dimers **47** and **48**

with two ammonia molecules which coordinate each metal cation. In the case of CsHMDS the solvation number of ammonia is decreased leading to the disolvated CsHMDS dimer **49**, where open coordination sites are stabilized by several *s*-block agnostic-like Si-CH₃...Cs interactions.^[1] All above mentioned crystal structures were derived from concentrated ammonia solutions where an excess of liquid ammonia was present. However, addition of toluene to the mother liquor and warming up the solution to 25°C and subsequent crystallization at -45°C resulted in the formation of further crystal structures which will be presented in the following section.

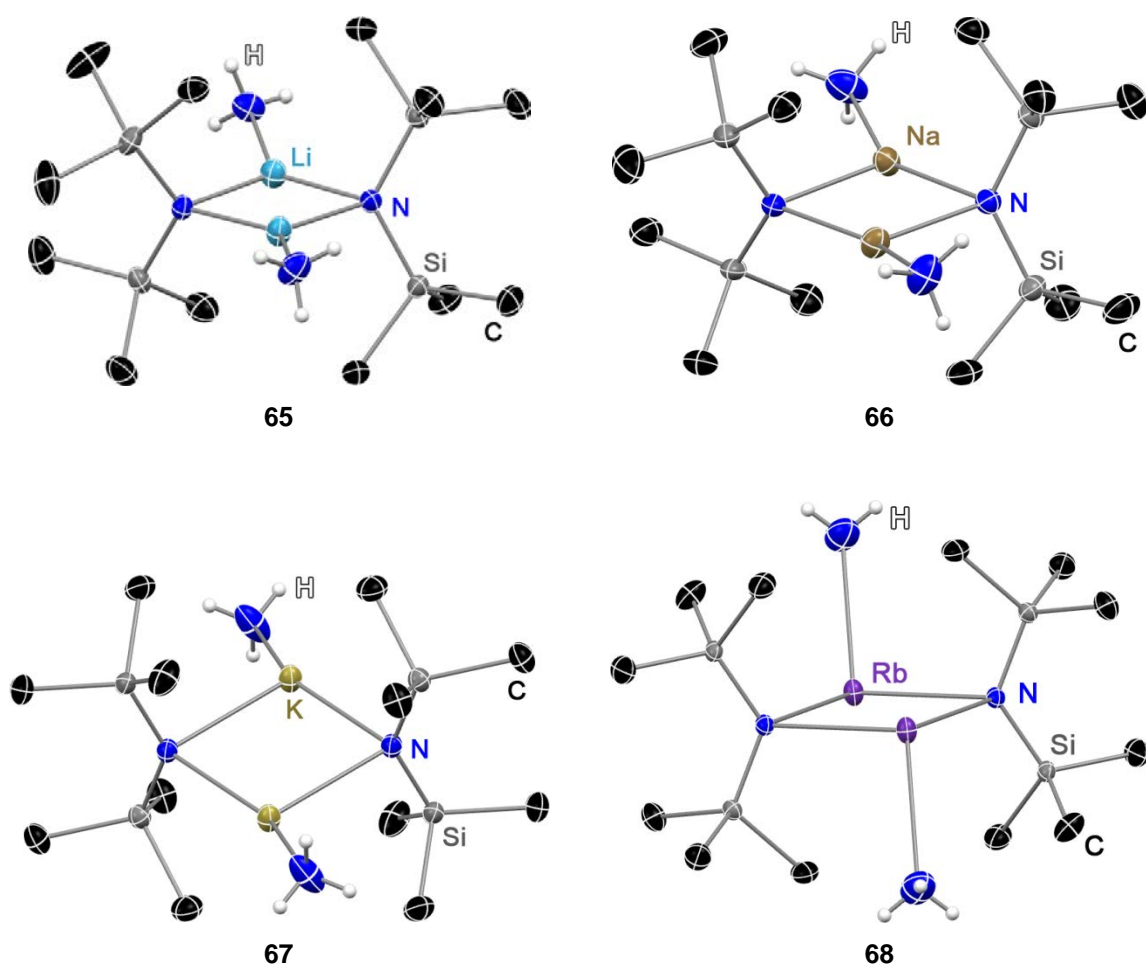


Fig. 2-17. Dimeric structure of MHMDS (M = Li, Na, K and Rb) with one equivalent of NH₃ in the solid state. Anisotropic displacement parameters are depicted at the 50% probability level. Carbon attached hydrogen atoms are omitted for clarity. Selected bond lengths, angles and crystallographic details are displayed in chapters 4.4.1 to 4.4.4.

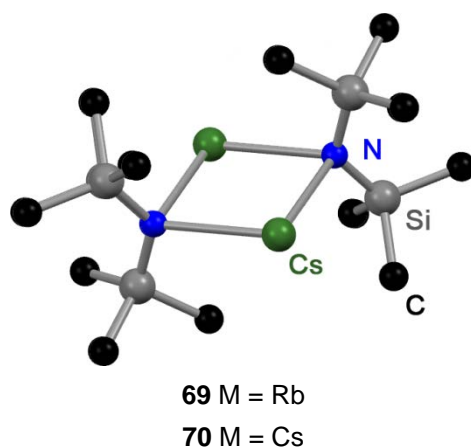
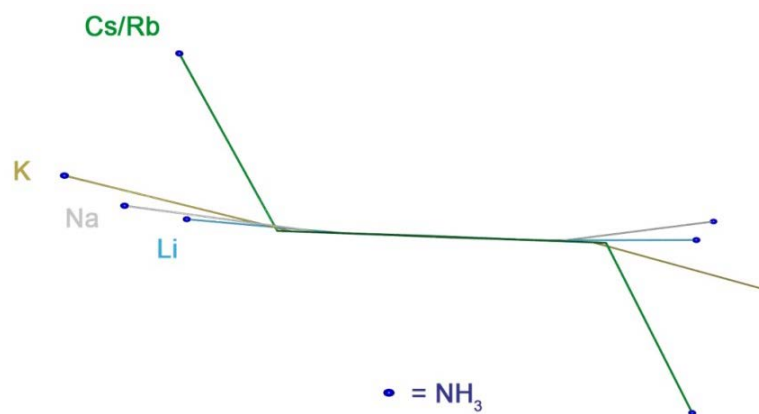


Fig. 2-18. Dimeric structure of donor-base-free Rb- and CsHMDS in the solid state.^[43] Carbon bound hydrogen atoms are omitted for clarity.

a)



b)

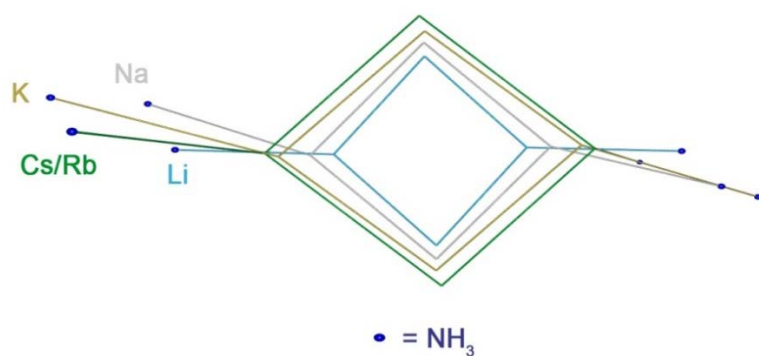


Fig. 2-19. Superposition plot of all disolvated [(NH₃)MHMDS]₂ (M = Li, Na, K, Rb and Cs) ammoniacates. a) View along the planar [N₂M₂]-ring. b) View orthogonal to the planar [N₂M₂]-ring. With increasing metal size the coordination angle of NH₃ increases, too, due to inter- and intramolecular Si-CH₃⋯M interactions which occupy the coordination sphere of the alkali metal.

Due to the increased reaction temperature (25°C instead of -33°C) excess ammonia was allowed to evaporate. Stoichiometric amounts of ammonia and MHMDS (M = Li, Na, K and Rb) yielded disolvated dimers **65-69** (Fig. 2-17) with an aggregation mode similar to that of $[(\text{H}_3\text{N})\text{CsN}(\text{SiMe}_3)_2]_2$ **49** in Fig. 2-16. In the case of CsHMDS a donor-base-free dimer **70** without any coordination of ammonia was identified (Fig. 2-18). This structure was already characterized by *Neander* and *Behrens* in 1999.^[43] Interestingly, at least in the solid state at low ammonia concentrations the Lewis soft cesium cation prefers Lewis soft Si-CH₃...Cs interactions over the coordination of Lewis hard ammonia molecules. Since there are no conspicuous bond lengths in respect to the already characterized MHMDS ammoniacates^[1] a detailed bond length discussion was redundant. However, selected bond lengths, angles and crystallographic details are given in chapters 4.4.1 to 4.4.4. In respect to the planar $[\text{M}_2\text{N}_2]$ -ring the coordination angle of the ammonia molecules grows with increasing metal size (Fig. 2-19). This is due to inter- and intramolecular Si-CH₃...M interactions which saturate the coordination sphere of the metal cation. The same was already observed in $[(\text{H}_3\text{N})\text{CsN}(\text{SiMe}_3)_2]_2$ **49**.^[1]

A unique NaHMDS intermediate **71** was crystallized from a solution which was warmed up to 0°C instead of +25°C (Fig. 2-20). Compound **71** represents an open dimer that is stabilized by an intramolecular HB of a second NaHMDS molecule.

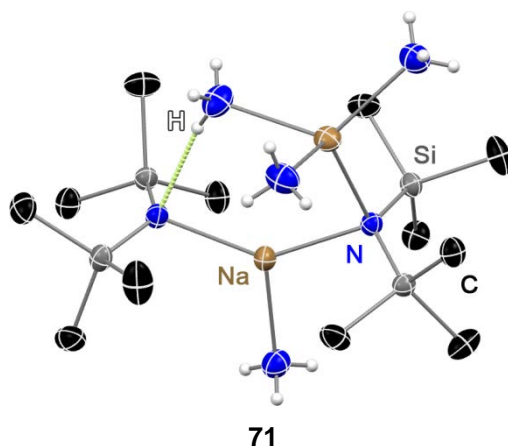
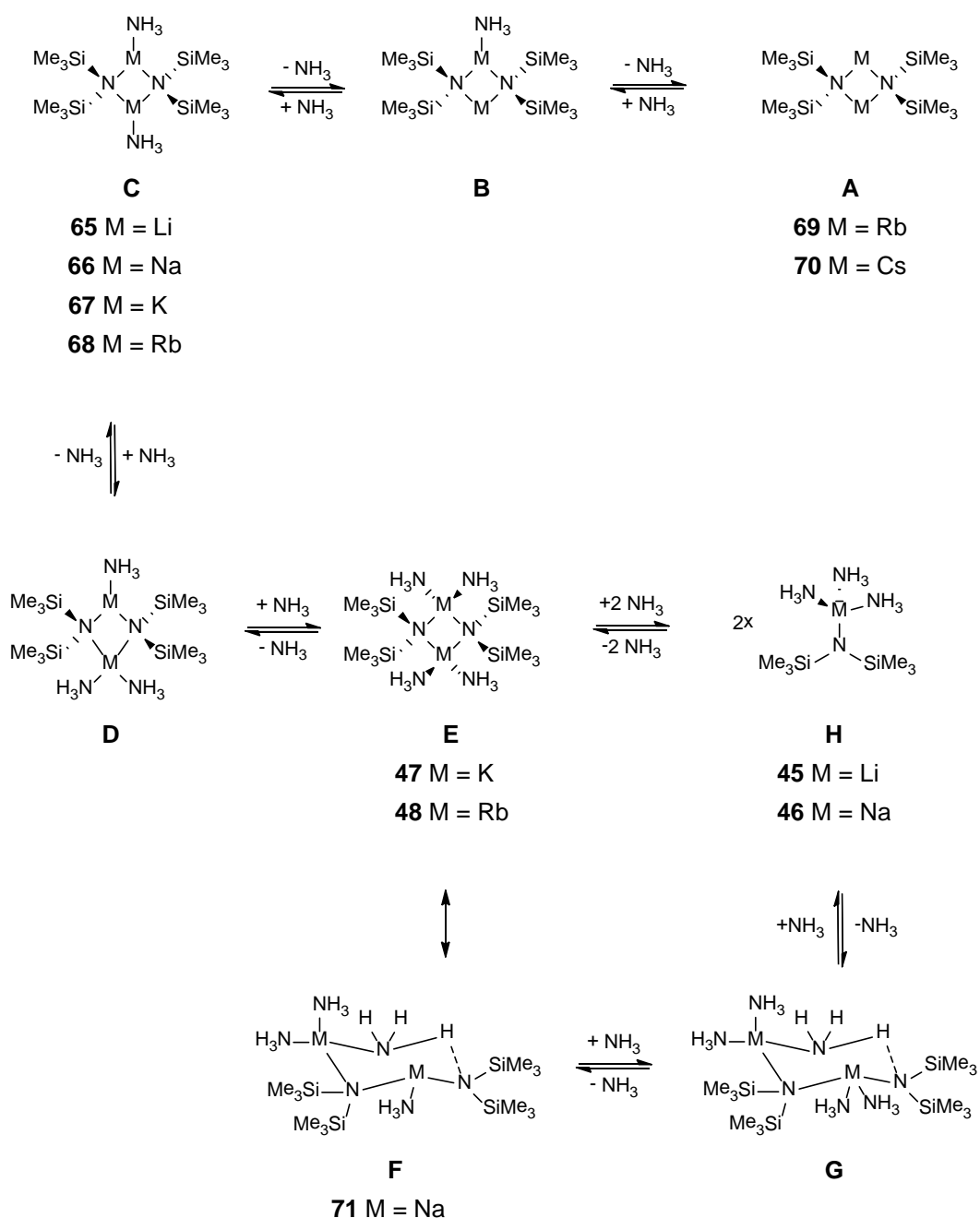


Fig. 2-20. Structure of NaHMDS intermediate **71** in the solid state. Anisotropic displacement parameters are depicted at the 50% probability level. Carbon bound hydrogen atoms are omitted for clarity. Selected bond lengths and angles and crystallographic details are displayed in chapter 4.4.5.

From MHMDS ammoniacates **65-71** an aggregation-deaggregation mechanism can be proposed that is depicted in Scheme 2-2. Successive addition of ammonia to dimer **A** would produce the monosolvated^[120] compound **B**, disolvated **C** and trisolvated **D**. The latter structure was observed in NaHMDS-3THF and also in mixed alkalimetal

HMDS·3THF aggregates (*e.g.* M1 = Li and M2 = Na, K).^[53] A fourth addition of NH₃ would result in the tetrasolvated structure E that was identified in compound 47 and 48. Migration of one NH₃ molecule to the second metal, followed by a M-N cleavage leads to structure F that represents the open dimer 71. Since the coordination sphere on one metal is still unsaturated (coordination number = 3), a fifth NH₃ molecule would coordinate to that metal giving structure G. Finally, the addition of a sixth NH₃ molecule would be accompanied by a dissociation of the dimeric structure leading to a trisolvated monomer H that structural motif was identified in ammoniacates 45 and 46.



Scheme 2-2. Proposed aggregation-deaggregation mechanism for MHMDS in the presence of ammonia.

Scheme 2-2 illustrates the impressive structural diversity of MHMDS ammoniacates in the solid state. Especially the HBs in the monomers and open dimers display a very interesting feature. HBs play a very important role in natural product synthesis. *E.g.* enzymes take advantage of HBs to achieve highly chemoselective reactions without the necessity of chiral groups on the substrate. This is why it would be very advantageous if the HBs observed in ammoniacates **45**, **46** and **71** would still be present in solution. Unfortunately, crystals from the latter are not stable at temperatures higher than -33°C . This is why it was not possible to investigate DOSY-ECC-MW-determinations of re-dissolved ammoniacate crystals. Instead, another strategy was used to obtain MHMDS in the presence of ammonia in toluene solution. Therefore, crude MHMDS was solved in TOL- d_8 (15 mM). Afterwards gaseous ND_3 was introduced to the solution (approximately one minute at $+25^{\circ}\text{C}$). Finally, the NMR-tubes were sealed and DOSY measurements were performed at RT. DOSY measurements were investigated with Li-, Na- and KHMDS at RT. All ^1H -signals are highly broadened (Fig. 2-21), indicating that more than one species could be present in solution.

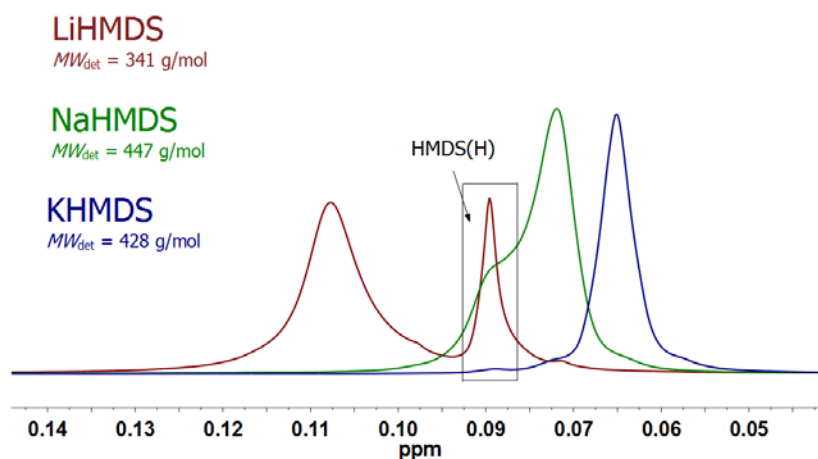


Fig. 2-21. ^1H -NMR-superposition plot of MHMDS ($M = \text{Li, Na and K}$; 15 mM) in TOL- d_8 with ammonia as donor base. The signals are significant broadened, indicating that more than one species could be present in solution.

In the solutions of Li- and NaHMDS there is also a significant concentration of protonated amine HMDS(H) that could be a results from partial protonation of MHMDS (*e.g. via* deprotonation of ND_3). However, DOSY-ECC-MW-determination on LiHMDS predicts a MW of $MW_{\text{det}} = 341 \text{ g/mol}$ giving the hint that LiHMDS could be present as dimeric structure **A**, **B** or **C** with up to two molecules of ammonia ($MW_{\text{err}} = -2\%$ to 7% , A-Table 14 in the appendix). In the case of NaHMDS the determined MW is significantly higher ($MW_{\text{det}} = 447 \text{ g/mol}$, A-Table 15 in the appendix). This MW matches with dimeric tri-

penta- solvated NaHMDS (**D-G**, $MW_{err} = -7\%$ to 1%). This result at least does not rule out the possibility of intramolecular HBs to be present in solution, since structure **F** corresponds to the open dimer **71** that was observed in the solid state.

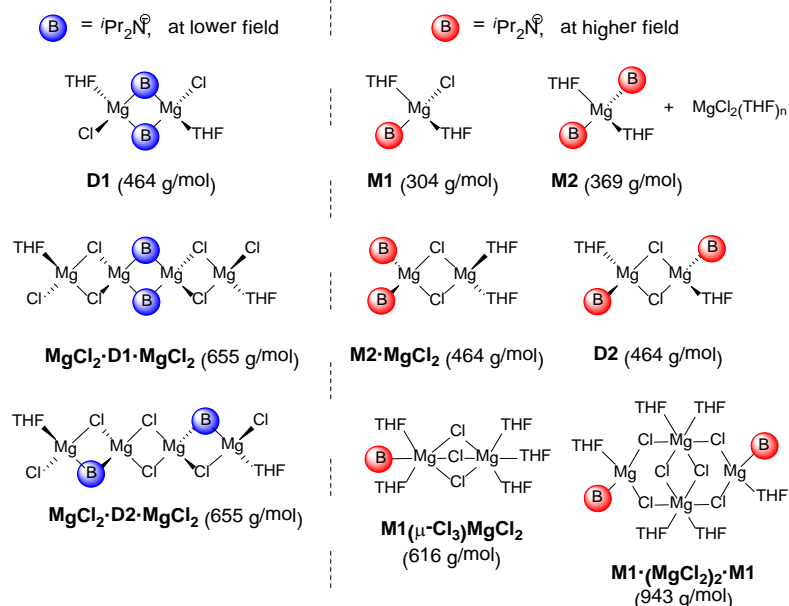
The MW-prediction of KHMDS gives a MW of $MW_{det} = 428$ g/mol that fits to dimeric mono- to- tetra solvated KHMDS (**B-E**, $MW_{err} = -3\%$ to 8% , A-Table 16 in the appendix). Structure **E** would confirm the solid state structure of $[(NH_3)_2 \cdot KN(SiMe_3)_2]_2$ (**47**).

Unfortunately these results have to be considered critically. Several factors could infect the determined MW so several aspects have to be investigated more in detail:

- 1) Intermolecular HBs between distinct species would increase the MW.
- 2) It was not cleared if HMDS(H) interacts with MHMDS ammoniacates.
- 3) Traces of ammonia could react with Li or NaHMDS.
- 4) The concentration of NH_3 and MHMDS should have a significant influence on the solution structures.
- 5) Low temperature measurements should give further information about the aggregation states.

2.2.6 Structure of Hauser Base $i\text{Pr}_2\text{NMgCl}$ in THF solution¹⁴

Chart 2-1. Most plausible aggregation modes of $i\text{Pr}_2\text{NMgCl}$ 7 in THF- d_8 solution category A



One of the most widely utilized classes of synthetic reagents are Grignard compounds that can be at the simplest level described by “ RMgX ” (where R is an organic group and X a halide). Today especially Grignard reagents with an amido ligand of the type $\text{R}_1\text{R}_2\text{NMgX}$, so called Hauser bases, and their *Turbo* derivate $\text{R}_1\text{R}_2\text{NMgX}\cdot\text{LiCl}$ play a huge role in modern chemistry (see chapter 1.1.3).

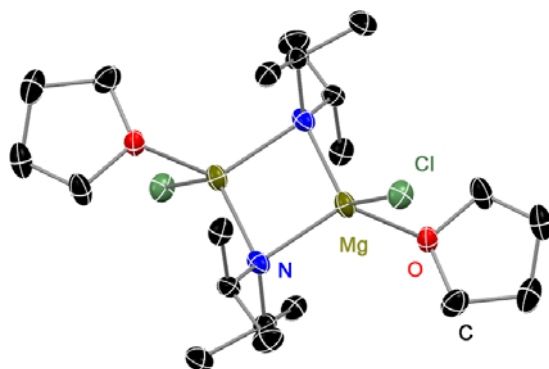


Fig. 2-22. Solid state structure of $[\text{7}\cdot\text{THF}]_2$ (**D1**) with hydrogen atoms and disorder omitted for clarity. Anisotropic displacement parameters are depicted at the 50% probability level. Selected bond lengths and angles are given in chapter 4.4.6.

¹⁴ A revised version of my publication: R. Neufeld, T. L. Teuteberg, R. Herbst-Irmer, R. A. Mata, D. Stalke, *JACS* **2016**, submitted.

However, because of their complex solution behavior, where Schlenk-type equilibria are involved, very little is known about their structure in solution. To shed light on the solution structure of $i\text{Pr}_2\text{NMgCl}$ **7** first the prominent Hauser base $i\text{Pr}_2\text{NMgCl}$ **7** was synthesized and crystallized from a THF/toluene 1:1 mixture at -6°C (see chapter 0). The crystal structure of $[\mathbf{7}\cdot\text{THF}]_2$ is shown in Fig. 2-22. TMP^[72] and HMDS^[73] Hauser bases alike all Grignard dimers^[67a, 67b, 67e, 74] show the halides in the bridging position in the solid state (like **D2**, category B in Chart 2-1). In contrast, $[\mathbf{7}\cdot\text{THF}]_2$ dimerises featuring the amido ligands in the bridging position (**D1**, category A in Chart 2-1). Searching the Cambridge Crystallography Database for Hauser bases reveals that there are only three other dimeric amido bridged Hauser bases in the literature.¹⁵ All have one in common: They feature less bulky amido ligands like Et_2N^- ,^[73a] $\text{Ph}_3\text{P}=\text{N}^-$ ^[75] and $i\text{Pr}_2\text{N}^-$.^[28] It can be concluded that in the solid state the switch from the halide to the amido bridge seems advantageous.^[64] However, solid state structures may not necessarily be maintained in solution. In synthesis organometallic compounds are predominantly used in solution. Therefore it is highly important to estimate the solution structure of $i\text{Pr}_2\text{NMgCl}$ **7**. The most plausible aggregation modes of a Hauser base in THF solution are demonstrated in Chart 2-1. A dissolved crystal of $[\mathbf{7}\cdot\text{THF}]_2$ in THF can on the one hand retain its dimeric status **D1** or isomerize to the chloride bridged dimer **D2**. On the other hand these dimers can dissociate to the monomer **M1** or rearrange according to the Schlenk-equilibrium to the diorgano-magnesium **M2** and MgCl_2 . When an excess of MgCl_2 is present, MgCl_2 co-ordinated species like $\mathbf{M1}(\mu\text{-Cl}_3)\text{MgCl}_2$, $\mathbf{M2}\cdot\text{MgCl}_2$, $\text{MgCl}_2\cdot\mathbf{D1}(\mathbf{D2})\cdot\text{MgCl}_2$ or $\mathbf{M1}\cdot(\text{MgCl}_2)_2\cdot\mathbf{M1}$ might also be present in solution. All of the mentioned species can be either distinguished by their MW or additionally by the chemical environment of the $i\text{Pr}$ -groups that is reflected in the chemical shift δ . Compared to terminal amido ligands (category B, Chart 2-1), bridging ligands (category A, Chart 2-1) show due to the presence of additional electron withdrawing metals a significant low field shift. At RT the ^1H NMR spectrum of $[\mathbf{7}\cdot\text{THF}]_2$ (Fig. 2-23) shows one broad signal set corresponding to a single species **a1** at high field (2.94/1.01 ppm for $\alpha\text{-CH/CH}_3$, category B).

¹⁵ Cambridge Structural Database CSD, version 5.36 (Updated Nov 2014), chelating amido ligands have been excluded.

Chart 2-1. Most plausible aggregation modes of ${}^i\text{Pr}_2\text{NMgCl}$ 7 in THF- d_8 solution

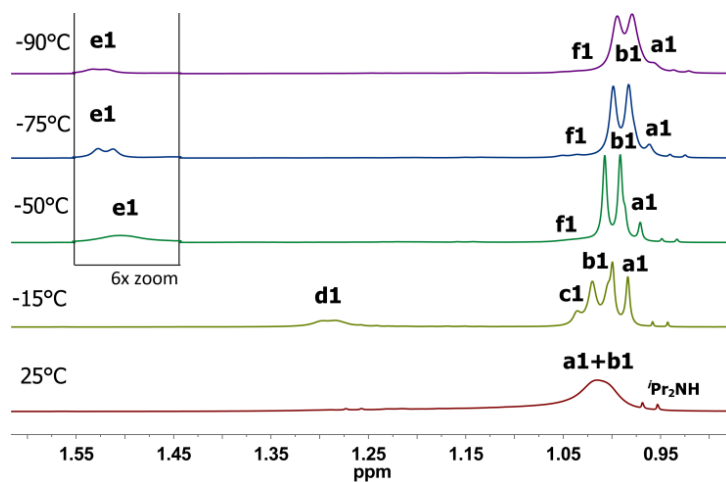
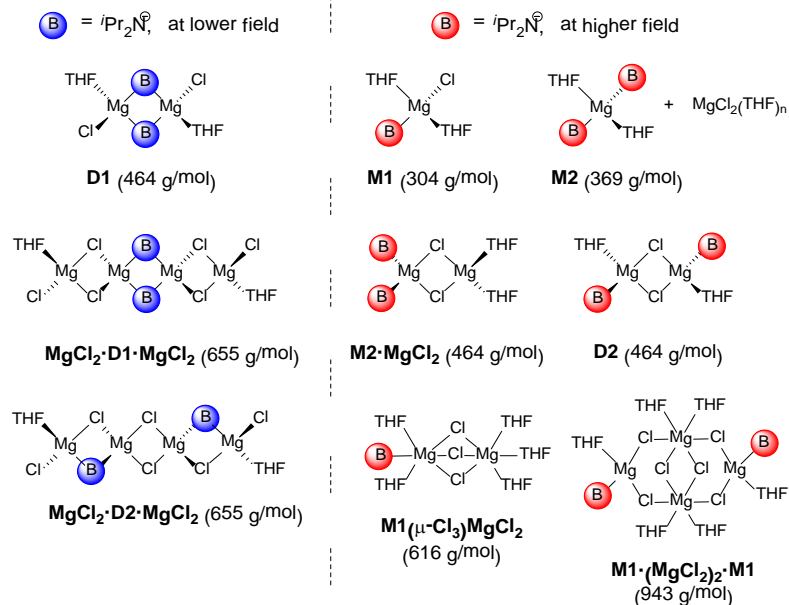


Fig. 2-23. ${}^1\text{H}$ superposition plot of crystalline $[\text{7}\cdot\text{THF}]_2$ (0.10 M, $-\text{CH}_3$ region) re-dissolved in THF- d_8 at various temperatures. For signal assignment see also Scheme 2-3. A spectrum including the $\alpha\text{-CH}$ region is displayed in A-Figure 4 in the appendix.

The ^1H -DOSY-ECC-MW-determination agrees best with the heteroleptic monomer **M1** ($MW_{\text{calc}} = 304$ g/mol, $MW_{\text{det}} = 310$ g/mol, $MW_{\text{err}} = -2\%$)¹⁶ while homoleptic monomer **M2** ($MW_{\text{err}} = 16\%$), dimeric **D2**, **M2·MgCl₂** and bigger aggregates can be easily excluded ($MW_{\text{err}} \geq 33\%$). Below 0°C two additional species **b1** (3.10/1.02 ppm, category B), **c1** (3.24/1.01 ppm, category B) at high field and **d1** (3.43/1.29 ppm, category A) at low field appear. From NMR studies on alkyl Grignard reagents it is known that homoleptic dialkylmagnesium monomers **M2** resonance at lower field, compared to heteroleptic monomers **M1**.^[121] In fact, MW-determination for species **b1** agree perfectly with the homoleptic diorganomagnesium **M2** ($MW_{\text{calc}} = 369$ g/mol, $MW_{\text{det}} = 356$, $MW_{\text{err}} = 4\%$). The MW of **c1** matches to dimeric **D2** and **M2·MgCl₂** ($MW_{\text{calc}} = 464$ g/mol, $MW_{\text{det}} = 450$ g/mol, $MW_{\text{err}} = 3\%$) that have similar MWs. Both have a comparable chemical environment and cannot be distinguished by their MWs. Both species could be present in solution but it is plausible that the equilibrium should be significantly on the side of dimer **D2** since it displays a less steric hindrance compared to **M2·MgCl₂**. In order to investigate the structure of the dimer in solution structure, electronic structure calculations were carried out by *Teuteberg* and *Mata*. The latter were performed with the B3LYP-D3 method,^[122] including solvent corrections through the use of the COSMO continuum model.^[123] Free energy differences confirm **M2·MgCl₂** to be disfavored relative to the **D2** species by 53.1 kJ/mol (A-Table 24 in the appendix). The most stable structure found corresponds in fact to a *cis*-isomer of **D2**, with both bases orientated to the same side of the Mg₂Cl₂ ring. This arrangement optimizes dispersion interactions between both the propyl moieties and the THF rings on each side. The *trans* configuration is slightly higher in energy by 7.2 kJ/mol. However, this marginal difference is not to be taken as granted since weak interactions with the solvent (which in our computations is only included as a dielectric continuum) could easily counterbalance this effect. The optimized structure of **M2·MgCl₂** shows a large N-Mg-N angle of about 146° illustrating the steric strain of both diisopropylamido groups when coordinated to the same metal center adding to the energetic disfavor (A-Figure 13 in the appendix). Species **d1**, with the highly low field shifted signal is in good agreement with the amido bridged dimer **D1** ($MW_{\text{calc}} = 464$ g/mol, $MW_{\text{det}} = 435$ g/mol, $MW_{\text{err}} = 6\%$) that is similar to the crystal structure of [7·THF]₂ in Fig. 2-22. Lowering the temperature dramatically influences the Schlenk-equilibrium of Hauser base 7. While at RT the monomer **M1**/**M2** ratio was 4:1, this ratio switches completely at -75°C (Table 2-11, 0.100 M).

¹⁶ All MW_{det} values are displayed for each species as an average value, derived from DOSY-ECC-MW measurements at various temperatures, see A-Table 17 in the appendix.

Chart 2-1. Most plausible aggregation modes of $i\text{Pr}_2\text{NMgCl}$ 7 in THF- d_8 solution

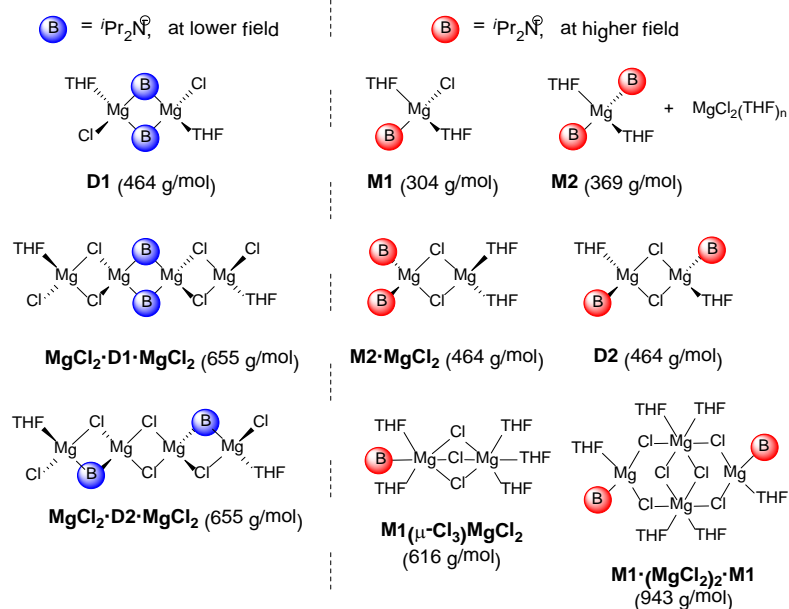


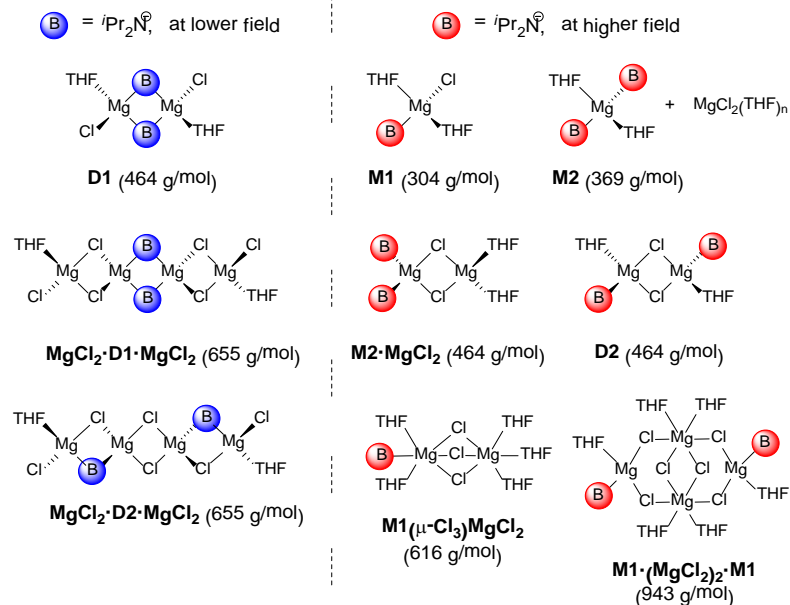
Table 2-11. The Schlenk equilibrium “constant”^{a)} K_s for the reaction $(i\text{Pr}_2\text{N})_2\text{Mg}$ (M2) + $\text{MgCl}_2 \rightleftharpoons 2 i\text{Pr}_2\text{NMgCl}$ (M1)

Temp. [°C]	K_s (0.015 M)	K_s (0.100 M)
25	25.00	16.00
0	8.16	4.43
-15	2.97	1.49
-25	1.00	0.68
-50	0.18	0.10
-75	0.12	0.05

a) Usually the Schlenk-equilibrium constant K_s is derived from ^1H integrals of $\alpha\text{-CH}$ protons with $K_s = [i\text{Pr}_2\text{NMgCl}]^2 / [(i\text{Pr}_2\text{N})_2\text{Mg}]^2$ with the approximation: $[(i\text{Pr}_2\text{N})_2\text{Mg}] \approx [\text{MgCl}_2]$. However, our results show that the concentration of $(i\text{Pr}_2\text{N})_2\text{Mg}$ is not equal to MgCl_2 because the latter is involved in further reactions with Hauser base 7. This is also reflected in our determined K_s values that show therefore a concentration dependency.

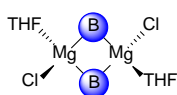
The huge population of homoleptic monomer **M2** at low temperatures stays in good agreement with the work of *Smith* and *Becker* who showed that the formation of RMgCl from R_2Mg and MgCl_2 is endothermic in THF solution.^[69] Same seems to be true for Hauser base 7. The equilibrium constants of the Schlenk-equilibrium are summarized in Table 2-11, showing that the equilibrium moves to the side of homoleptic **M2** + MgCl_2 with increasing concentration and decreasing temperature. The formation of **M2** is accompanied by the release of MgCl_2 to the solution, most probably as a monomer with up to four THF molecules.^[124] Therefore it might not be surprising when free MgCl_2 coordinates to some complexes at low temperatures. At -50°C dimers **D1** (**d1**) and **D2** (**c1**) dissipate and two new species **e1** (3.39/1.50 ppm, category A) and **f1** (3.21/ 1.04 ppm, category B) that have an even more low field shift appears. This intense shift can be attributed to an additional coordination of MgCl_2 to **M1**, **D1** or **D2**. When magnesium chloride coordinates to monomer **M1** than a structure like $\text{M1}(\mu\text{-Cl}_3)\text{MgCl}_2$ (Chart 2-1, category B) would be feasible. This coordination mode was suggested for methyl magnesium chloride by *Sakamoto* and *Imamoto et al.*^[125] With the help of coldspray ionization mass spectrometry (CSI-MS), they proposed that the $\mu\text{-Cl}_3$ bridged Grignard reagent was coordinated by four to six THF molecules, whereas the species with five THF's was the major component.^[125] Additional support is given by several crystal structures of cationic $[(\text{THF})_3\text{Mg}(\mu\text{-Cl}_3)\text{Mg}(\text{THF})_3]^+$ where MgCl_2 is also coordinated in that $\mu\text{-Cl}_3$ coordination mode.^[125] The DOSY-ECC-MW-investigation shows similar results: At -70°C the MW-determination gives for signal **f1** a MW of $MW_{\text{det}} = 512 \text{ g/mol}$ that fits to $\text{M1}(\mu\text{-Cl}_3)\text{MgCl}_2$ with four THF molecules ($MW_{\text{calc}} = 544 \text{ g/mol}$, $MW_{\text{det}} = 512 \text{ g/mol}$, $MW_{\text{err}} = 6\%$). At -80°C the MW increases significantly to $MW_{\text{det}} = 616 \text{ g/mol}$ that matches perfectly with the THF-five-fold solvated $\text{M1}(\mu\text{-Cl}_3)\text{MgCl}_2$ ($MW_{\text{calc}} = 616 \text{ g/mol}$, $MW_{\text{det}} = 616 \text{ g/mol}$, $MW_{\text{err}} = 0\%$), indicating that a higher solvation is favoured at lower temperatures. Unfortunately, below -80°C the signal was too low in intensity for further MW-determination investigations. In the literature there are several crystal structures of the type $\text{M1}(\cdot\text{MgCl}_2)_2\cdot\text{M1}$ (Chart 2-1, category B), where two monomers **M1** are bridged by two magnesium dichlorides in an open cubic aggregation mode.^[125-126] However, in solution of 7 it seems that the dissociation into smaller parts is favoured over an open cubic arrangement ($MW_{\text{calc}} = 943 \text{ g/mol}$, $MW_{\text{det}} = 616 \text{ g/mol}$, $MW_{\text{err}} = 35\%$), which was already proposed by *D. Seyferth* in 2009.^[71]

Chart 2-1. Most plausible aggregation modes of $i\text{Pr}_2\text{NMgCl}$ 7 in THF- d_8 solution



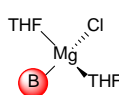
$MW_{\text{calc}} = 464 \text{ g/mol}$
 $MW_{\text{det}} = 435 \text{ g/mol}$
 $MW_{\text{err}} = 6 \%$

D1 (d1)



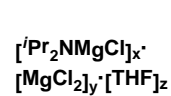
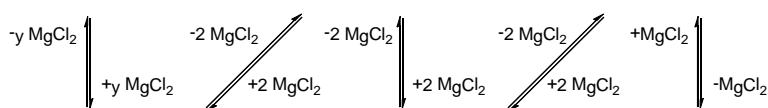
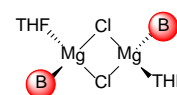
$MW_{\text{calc}} = 304 \text{ g/mol}$
 $MW_{\text{det}} = 310 \text{ g/mol}$
 $MW_{\text{err}} = -2 \%$

M1 (a1)



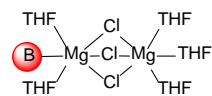
$MW_{\text{calc}} = 464 \text{ g/mol}$
 $MW_{\text{det}} = 450 \text{ g/mol}$
 $MW_{\text{err}} = 3 \%$

D2 (c1)



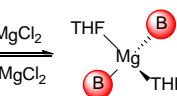
(e1)

$MW_{\text{det}} = 408\text{-}578 \text{ g/mol}$



M1(μ-Cl₃)MgCl₂ (f1)

$MW_{\text{calc}} = 616 \text{ g/mol}$
 $MW_{\text{det}} = 616 \text{ g/mol}$
 $MW_{\text{err}} = 0 \%$



M2 (b1)

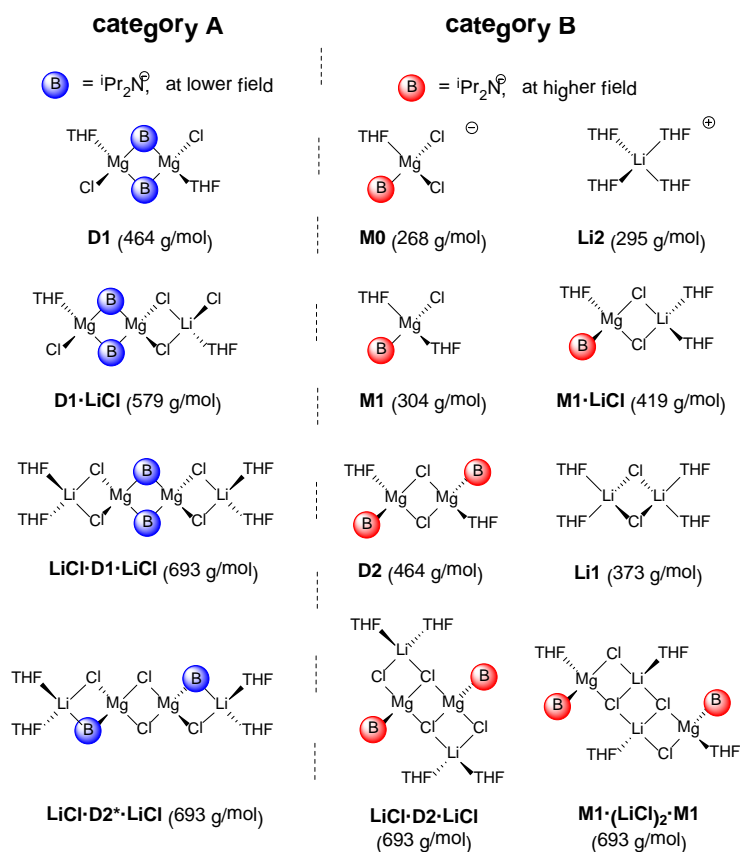
$MW_{\text{calc}} = 369 \text{ g/mol}$
 $MW_{\text{det}} = 356 \text{ g/mol}$
 $MW_{\text{err}} = 4 \%$

Scheme 2-3. DOSY-ECC-MW-determination of Hauser base $i\text{Pr}_2\text{NMgCl}$ 7 in THF- d_8 solution

Additionally to **f1**, species **e1** appears at lower field (category A). The DOSY-ECC-MW-determination shows a temperature dependent MW distribution ($MW_{\text{det}} = 409$ g/mol at -50°C , 446 g/mol at -70°C and 578 g/mol at -80°C). The addition of MgCl_2 to dimers **D1** or **D2** would produce aggregates like $\text{MgCl}_2 \cdot \text{D1} \cdot \text{MgCl}_2$ or $\text{MgCl}_2 \cdot \text{D2} \cdot \text{MgCl}_2$ (Chart 2-1, category A). However, several other MgCl_2 coordinated, amido bridged species would also be thinkable. Unfortunately, in the literature there are no crystal structures of MgCl_2 coordinated, ligand bridged Hauser bases or Grignard reagents that indicate the most plausible aggregate. The high MW of 578 g/mol at -80°C gives much room for interpretation. This is why we can only speculate how the composition of aggregate **e1** could look like. Noticeable is that in contrast to all other species, the $-\text{CH}_3$ signal of **e1** shifts to lower field with lower temperature (Fig. 2-23). This behaviour could be a result of a successive addition of MgCl_2 to **D1** or **D2**. At -80°C the shift to lower field stops and the MW of **e1** matches with dimeric $\text{MgCl}_2 \cdot \text{D1}(\text{D2}) \cdot \text{MgCl}_2$ ($MW_{\text{calc}} = 655$ g/mol, $MW_{\text{det,corr}} = 703$ g/mol, $MW_{\text{err}} = -7\%$, after molar density correction due to highly increased molar van der Waals density (MD_w) of this species, see A-Table 21 and A-Table 22 in the appendix). However, like already mentioned, this MW-agreement has to be considered with caution. Anyway, it seems that at low temperatures free, monomeric MgCl_2 is disadvantageous in solution of Hauser base 7. Instead, the coordination of MgCl_2 to monomeric and/or dimeric RMgCl molecules should be favoured like it is e.g. the case for LiCl that will be discussed in the following chapter.

2.2.7 Structure of *Turbo*-Hauser Base ${}^i\text{Pr}_2\text{NMgCl}\cdot\text{LiCl}$ in THF solution¹⁷

Chart 2-2. Most plausible aggregation modes of ${}^i\text{Pr}_2\text{NMgCl}\cdot\text{LiCl}$ **9** in THF- d_8 solution.



The impact of LiCl on the solution structure of Grignard reagents and Hauser bases is still vigorously discussed. *Knochel et al.* suggest that LiCl deaggregates RMgX oligomers^[23] and forms a more reactive bimetallic monomer $\text{RMgCl}\cdot\text{LiCl}$ that is supposed to furnish magnesiate character to the Grignard reagent in the sense of a solvent separated ion pair (SSIP) $[\text{Li}(\text{THF})_4]^+ [\text{RMg}(\text{THF})\text{Cl}_2]^-$.^[76] Crystallographic evidence of the *Turbo*-Hauser bases $\text{TMPMgCl}\cdot\text{LiCl}$ ^[72] (**M1·LiCl**, Chart 2-2 with $\text{B} = \text{TMP}^-$) and ${}^i\text{Pr}_2\text{NMgCl}\cdot\text{LiCl}$ ^[28] **9** (**LiCl·D1·LiCl**, Chart 2-2) supports the contact ion pair (CIP) coordination mode in the solid state. But still it was not clear whether the mixed metal structure really is maintained in solution or just a transient species. *García-Álvarez and Mulvey et al.* analyzed^[28] crystals of $[\mathbf{9}\cdot\text{THF}]_2$ in THF- d_8 solution at -50°C by employing the internal calibration curve (ICC) D-FW analysis that was pioneered by *Li and Williard et al.*^[77] Because of the lack of

¹⁷ A revised version of my publication: R. Neufeld, T. L. Teuteberg, R. Herbst-Irmer, R. A. Mata, D. Stalke, *JACS* **2016**, submitted.

appropriate references the accuracy of the method was not sufficient and they concluded that they were not able to “clearly establish the exact nature of the solution species”.^[28] However, the first key conclusion was that the molecular structure of crystalline $[\mathbf{9}\cdot\text{THF}]_2$ ($\text{LiCl}\cdot\mathbf{D1}\cdot\text{LiCl}$) was not retained in THF- d_8 solution and the second was that a SSIP situation like it was proposed by *Knochel*, described by negative charged magnesium ate complexes (like e.g. $\mathbf{M0}$) and free $[\text{Li}(\text{THF})_4]^+$ ($\mathbf{Li2}$) seemed most probable (category B in Chart 2-2).^[28] In this chapter some light will be shed on the complex solution structure of $\mathbf{9}$. Additionally, it will be shown that both above mentioned key conclusions have to be revised. Again the DOSY-ECC-MW-determination hand-in-hand with theoretical calculations will be applied to clarify the influence of LiCl on the Schlenk-equilibrium of $\mathbf{7}$.

Primarily it seems advisable to *a priori* rationalize which species are feasible to be present in the solution of $^i\text{Pr}_2\text{NMgCl}\cdot\text{LiCl}$ $\mathbf{9}$. A dissolved crystal of $[\mathbf{9}\cdot\text{THF}]_2$ in THF can either retain the coordination $\text{LiCl}\cdot\mathbf{D1}\cdot\text{LiCl}$ or isomerize to $\text{LiCl}\cdot\mathbf{D2}^*\cdot\text{LiCl}$ $\text{LiCl}\cdot\mathbf{D2}^*\cdot\text{LiCl}$ (Chart 2-2). In the first aggregation mode the ^iPr -groups are neighbored by compact chloride ligands, enabling a free rotation of the alkyl groups, whereas in the latter they are neighbored to a sterically demanding THF molecule that would result in a steric repulsion. This is why species $\text{LiCl}\cdot\mathbf{D1}\cdot\text{LiCl}$ should be highly favoured over $\text{LiCl}\cdot\mathbf{D2}^*\cdot\text{LiCl}$. That is again supported by calculations (A-Table 25 in the appendix). The free energy difference between $\text{LiCl}\cdot\mathbf{D1}\cdot\text{LiCl}$ and $\text{LiCl}\cdot\mathbf{D2}^*\cdot\text{LiCl}$ is 55-56 kJ/mol (the former being more stable) in the temperature range from -90°C to $+25^\circ\text{C}$. Inspection of the optimized structures confirms the steric hindrance (A-Figure 17 in the appendix). In the $\text{LiCl}\cdot\mathbf{D1}\cdot\text{LiCl}$ structure the Mg^{2+} cations are aligned with the Li^+ , resulting in a high-symmetric structure with a close to tetrahedral coordination at each metal atom. In the $\text{LiCl}\cdot\mathbf{D2}^*\cdot\text{LiCl}$ case, the Li^+ cations are forced out of this axis in order to accommodate the isopropyl groups at both ends. Another possibility to consider is that the dimer of $[\mathbf{9}\cdot\text{THF}]_2$ can dissociate into monomeric units $\mathbf{M1}\cdot\text{LiCl}$. These monomers could recombine *via* a four membered Mg_2Cl_2 ring ($\text{LiCl}\cdot\mathbf{D2}\cdot\text{LiCl}$) or by a smaller Li_2Cl_2 ring ($\mathbf{M1}\cdot(\text{LiCl})_2\cdot\mathbf{M1}$) in the centre. It is also possible that LiCl dissociates as a well-known dimer^[127] $[(\text{THF})_2\text{Li}(\mu\text{Cl})_2\text{Li}(\text{THF})_2]$ $\mathbf{Li1}$ to produce LiCl-free species $\mathbf{M1}$, $\mathbf{D1}$ or $\mathbf{D2}$ or that lithium dissociates as a solvent separated ion pair $\text{Li}(\text{THF})_4^+$ $\mathbf{Li2}$ that would produce an SSIP ate-complex like e.g. $\mathbf{M0}$, where two chlorides are coordinated to the magnesium ion (Chart 2-2).

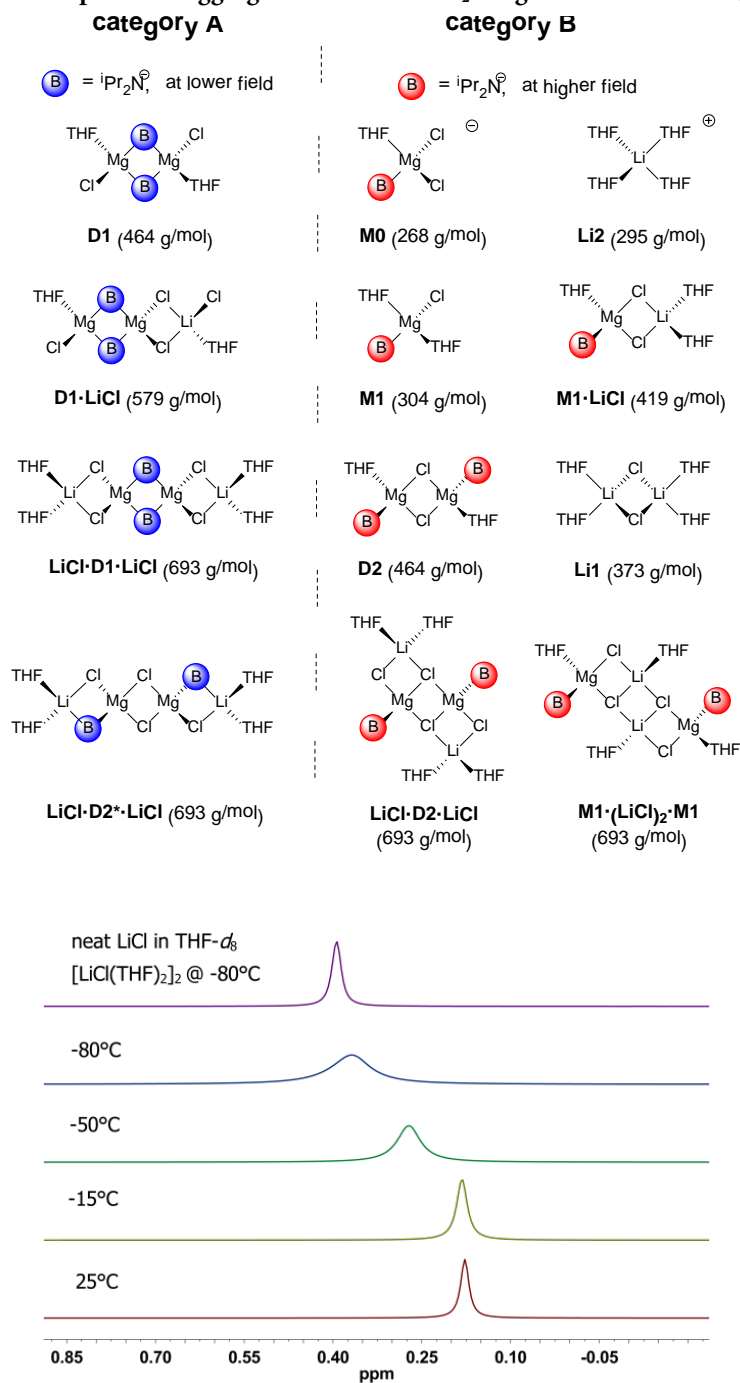
Chart 2-2. Most plausible aggregation modes of ${}^i\text{Pr}_2\text{NMgCl}\cdot\text{LiCl}$ 9 in $\text{THF-}d_8$ solution.

Fig. 2-24. ${}^7\text{Li}$ superposition plot of crystalline 9 (0.1 M) re-dissolved in $\text{THF-}d_8$ at various temperatures. On the top: ${}^7\text{Li}$ -spectrum of neat Li1 in $\text{THF-}d_8$ at -80°C .

The ^7Li spectra show at RT a singlet at 0.18 ppm (25°C) that shifts to lower field with decreasing temperature (0.38 ppm at -100°C , Fig. 2-24). The presence of LDA, where lithium coordinates directly to the diisopropyl amide, can therefore be excluded since LDA resonances in the ^7Li NMR experiment temperature independently at about 2.0 ppm (A-Figure 11 in the appendix). Additionally, the solvent separated cation $[\text{Li}(\text{THF})_4]^+$ **Li2** can be excluded to be populated at detectable concentrations too, since it is known that the solvent separated lithium ion **Li2** resonances predominately at a negative chemical shift (-1.1 ppm in THF).^[128] Further support is given by the crystal structure of **9** where the lithium cation is located near to the ^iPr -groups in a middle distance of 4.49 Å to the closest $-\text{CH}_3$ -protons.^[72] When lithium is coordinating next to the magnesium amide than such relatively close distance should be visible in a ^1H - ^7Li -HOESY experiment. In fact the ^1H - ^7Li -HOESY-spectra show at high temperature a cross peak between the ^7Li signal and the $-\text{CH}_3$ signals of species **a2**, **b2** and **c2**, indicating that *lithium does coordinate* to Hauser base 7 (Fig. 2-25).

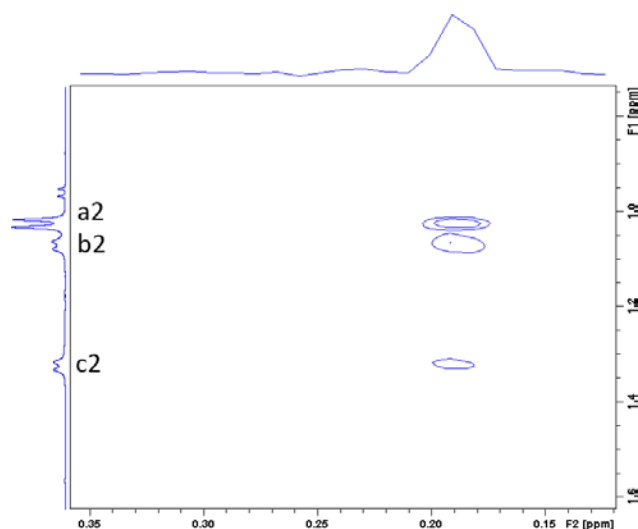


Fig. 2-25. ^1H - ^7Li -HOESY of crystalline **9** (0.03 M) re-dissolved in $\text{THF}-d_8$ at 0°C .

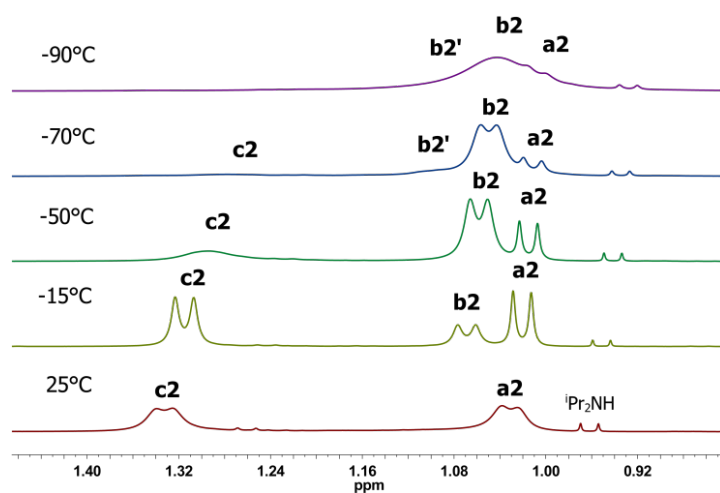
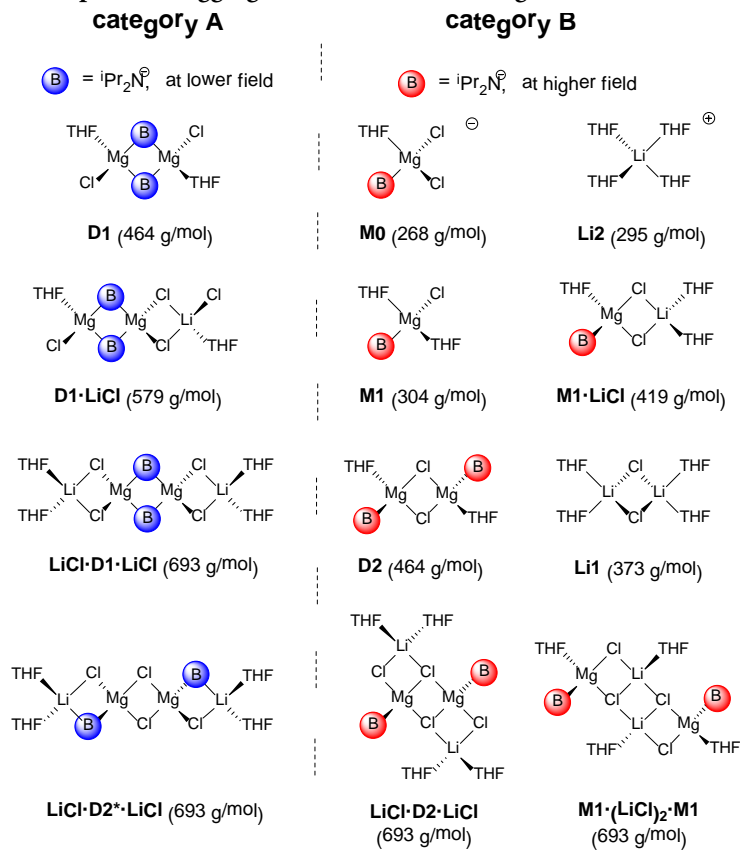
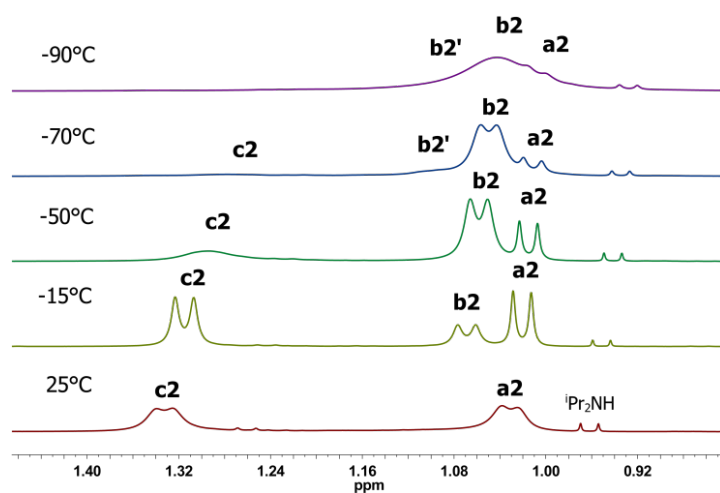
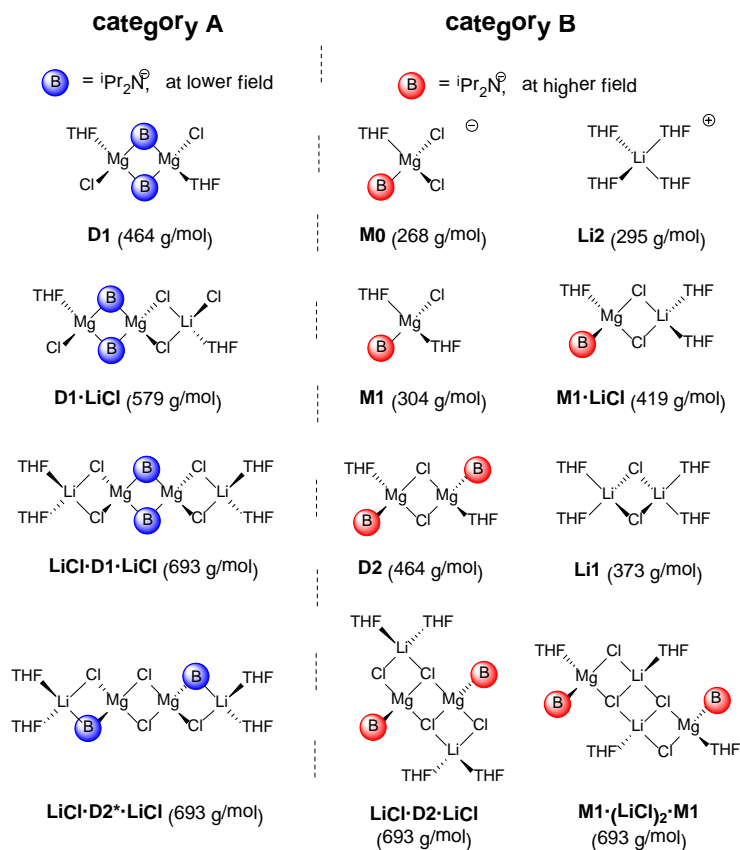
Chart 2-2. Most plausible aggregation modes of $i\text{Pr}_2\text{NMgCl}\cdot\text{LiCl}$ **9** in $\text{THF-}d_8$ solution.

Fig. 2-26. ^1H superposition plot of crystalline **9** (0.1 M, $-\text{CH}_3$ region) re-dissolved in $\text{THF-}d_8$ at various temperatures. For signal assignment see also Scheme 2-6. A spectrum including the $\alpha\text{-CH}$ signals is displayed in A-Figure 6 in the appendix.

At RT two different species (**a2**: 2.92/1.03 ppm, category B and **c2**: 3.42/1.33 ppm, category A) can be identified in the ^1H NMR spectrum of **9** (Fig. 2-26). The MW-determination of **a2** gives at all temperatures a MW that fits perfectly to the LiCl coordinated monomer **M1·LiCl** ($MW_{\text{calc}} = 419$ g/mol, $MW_{\text{det}} = 425$ g/mol, $MW_{\text{err}} = -2\%$). Compared with the salt free monomer **M1** (**a1**), the metal chloride co-coordinated monomers **M1(μ -Cl₃)MgCl₂** (**f1**) and **M1·LiCl** (**a2**) are shifted to lower field ($\Delta\delta \approx 0.02$ ppm), due to an additional coordination of electron withdrawing metal chloride. The same is true for signal **c2** that appears at the dimer region of **D1** (category A, Chart 2-2) but also low field shifted by 0.02 ppm (compared to LiCl-free dimer **D1**) indicating that **c2** corresponds to LiCl co-coordinated dimer **LiCl·D1·LiCl**. At 25°C the determined MW of **c2** ($MW_{\text{calc}} = 693$ g/mol, $MW_{\text{det}} = 525$ g/mol, $MW_{\text{err}} = 24\%$) is smaller than expected. However, with decreasing temperature the MW grows significantly ($MW_{\text{det}} = 598$ g/mol at -15°C , 618 g/mol at -40°C and 635 g/mol at -50°C) till it stops growing further at -60°C ($MW_{\text{det}} = 661$ g/mol). The same trend was already observed for species **MgCl₂·D1(D2)·MgCl₂** (**e1**) of LiCl-free Hauser base 7. In contrast to all other species of *Turbo*-Hauser base **9**, the α -CH signal of **c2** shifts like **e1** to lower field with lower temperature (A-Figure 6 in the appendix). This is why a successive coordination of LiCl to **D1** could again explain this behaviour (25°C to -40°C : av. $MW_{\text{det}} = 582$ g/mol, $MW_{\text{calc}}(\text{D1·LiCl}) = 579$ g/mol, $MW_{\text{err}} = -1\%$).¹⁸ Finally between -60°C and -70°C it is possible to determine the MW of tetra nuclear dimer **LiCl·D1·LiCl** with two lithium chlorides coordinated to dimer **D1** ($MW_{\text{calc}} = 693$ g/mol, $MW_{\text{det}} = 661$ g/mol, $MW_{\text{err}} = 5\%$). A monomer-dimer equilibrium of **a2** and **c2** was already suggested by *García-Álvarez and Mulvey et al.*^[28] Concentration experiments showed that species **a2** dominates at lower concentrations whereas **c2** is mostly populated at higher concentrations.^[28] Below -70°C the solubility limit is reached and signal **c2** disappears. With decreasing temperature a third species next to **a2** is forming (**b2**: 3.13/1.07 ppm, category B). Further cooling results in a shift of the oligomer equilibrium. The integral of **b2** increases significantly at the expense of **a2** and **c2**. The MW-determination of **b2** offers at all temperatures a MW that fits to the LiCl free dimer **D2** ($MW_{\text{calc}} = 464$ g/mol, $MW_{\text{det}} = 461$ g/mol, $MW_{\text{err}} = 1\%$).

¹⁸ This behaviour could be also attributed to a fast exchange of **LiCl·D1·LiCl** with its lithium free counterpart **D2** or to a dissociation into monomeric **M1·LiCl**. Both equilibria would produce a smaller effective MW.

Chart 2-2. Most plausible aggregation modes of $i\text{Pr}_2\text{NMgCl}\cdot\text{LiCl}$ **9** in $\text{THF-}d_8$ solution.Fig. 2-26. ^1H superposition plot of crystalline **9** (0.1 M, $-\text{CH}_3$ region) re-dissolved in $\text{THF-}d_8$ at various temperatures.

The ^1H - ^7Li HOESY experiment indicates at 0°C the interaction of **b2** with the lithium cation. However, the cross peak vanishes at lower temperatures when **b2** becomes the most populated species, indicating that **b2** would not coordinate strongly to LiCl. At -70°C , next to **b2**, a fourth species **b2'** is detectable in the ^1H experiment. At -100°C species **b2'** can be deconvoluted in the DOSY NMR experiment (Fig. 2-27) giving a MW_{det} value that fits to LiCl coordinated species $\text{LiCl}\cdot\text{D2}\cdot\text{LiCl}/\text{M1}\cdot(\text{LiCl})_2\cdot\text{M1}$ (**b2'**) ($MW_{\text{calc}} = 693$ g/mol, $MW_{\text{det}} = 641$ g/mol, $MW_{\text{err}} = 7\%$).

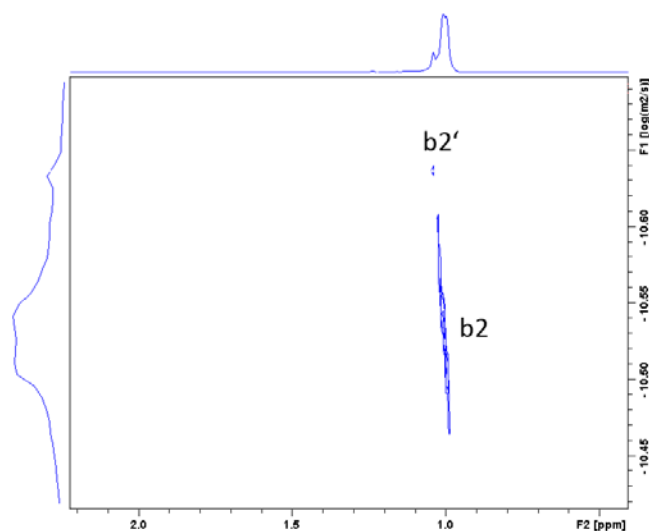


Fig. 2-27. ^1H DOSY spectrum of $^i\text{Pr}_2\text{NMgCl}\cdot\text{LiCl}$ **9** (0.10 M) at -100°C : Region of signal **b2** and **b2'**.

The ^7Li -DOSY-ECC-MW-determination experiments give further information about the aggregation behavior of **9**. All species produce only one signal that broadens up and shifts to lower field with decreasing temperature (Fig. 2-24). Only at 0°C there is a small shoulder at the ^7Li -signal, verifying that more than one Li species is present in solution of **9**. From 25°C to -40°C the ^7Li -DOSY-ECC-MW-determination gives an average-, temperature dependent MW that reflects an average value produced by all three lithium aggregates ($MW_{\text{det}} = 454\text{-}496$ g/mol). Below -60°C the MW decreases significantly without further change ($MW_{\text{det}} = 382$ g/mol at -60°C to -100°C).

Chart 2-2. Most plausible aggregation modes of $i\text{Pr}_2\text{NMgCl}\cdot\text{LiCl}$ **9** in $\text{THF-}d_8$ solution.

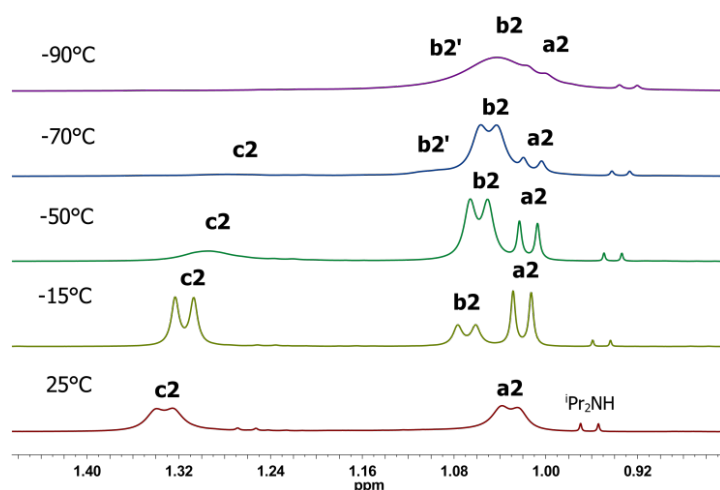
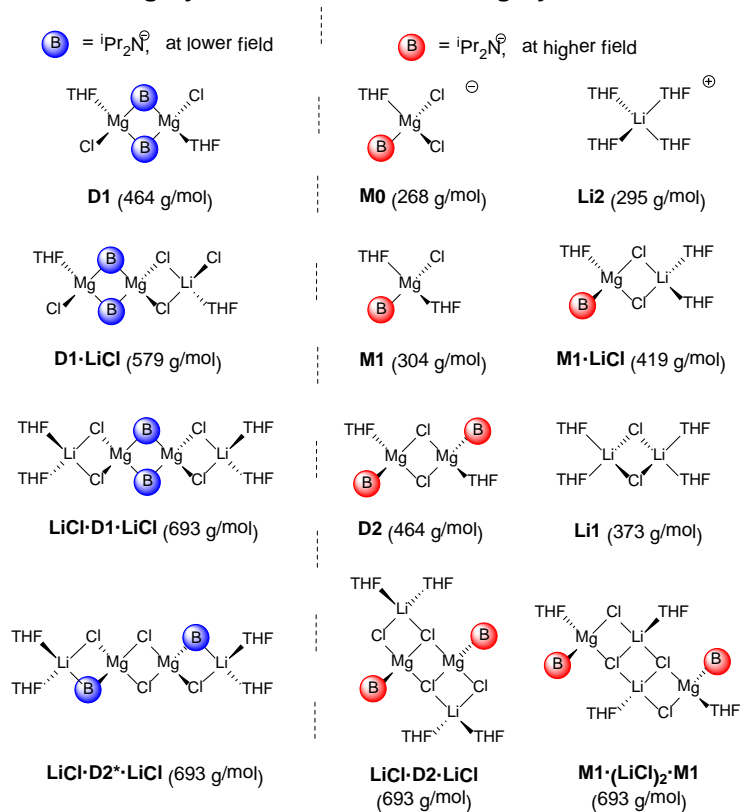
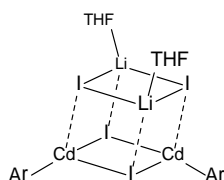


Fig. 2-26. ^1H superposition plot of crystalline **9** (0.1 M, $-\text{CH}_3$ region) re-dissolved in $\text{THF-}d_8$ at various temperatures.

This can be attributed to first **LiCl·D1·LiCl** (**c2**) precipitating from solution and the concentration of **M1·LiCl** (**a2**) decreasing significantly to very small amounts and finally second to the residual lithium chloride present in solution as the well-known [(THF)₂Li(μ-Cl)₂Li(THF)₂]-dimer **Li1** ($MW_{\text{calc}} = 373$ g/mol, $MW_{\text{det}} = 382$ g/mol, $MW_{\text{err}} = -2\%$) that becomes the most populated Li-species at low temperatures.¹⁹ The formation of significant amounts of **Li1** is also reflected in the chemical shift of the ⁷Li nucleus. With decreasing temperature the **Li1** concentration increases. This is why the ⁷Li signal moves towards the chemical shift of the LiCl dimer **Li1** (Fig. 2-24). Further, the signal gets very broadened.²⁰ At low temperature the decreased solubility could be one reason for the ⁷Li signal broadening. But additionally the formation of **LiCl·D2·LiCl/M1·(LiCl)₂·M1** from the reaction of LiCl (**Li1**) and dimer **D2** could have even a bigger impact on the signal broadening, since the chemical environment of lithium in **LiCl·D2·LiCl/M1·(LiCl)₂·M1** differs from that in **Li1**. But, how would the reaction of **Li1** and **D2** occur? Tetrameric structures **LiCl·D2·LiCl** and **M1·(LiCl)₂·M1** (Chart 2-2) were already proposed as products. In both structures two chlorides at the magnesium atoms show a coordination number of three. Searching the Cambridge Crystallography Database²¹ reveals that magnesium chlorides, with a μ-Cl₃ coordination predominantly form cubic aggregation modes in the solid state.^[126, 129]



72



Fig. 2-28. An equimolar reaction of [2,6-Pmp₂C₆H₃Li]₂ (Pmp = 2,3,4,5,6-Me₅C₆) with CdI₂ and crystallization from a saturated hexane solution at -30°C yields crystals of cubane **72**.^[130]

¹⁹ To prove the structure of LiCl in THF, DOSY measurements have been performed on anhydrous LiCl in THF-*d*₈. The ⁷Li-ECC-MW-determination confirms the dimeric structure (**Li1**) of LiCl in THF solution (from 25°C to -75°C, in av.: $MW_{\text{calc}} = 373$ g/mol, $MW_{\text{det}} = 381$ g/mol, $MW_{\text{err}} = -2\%$, see A-Table 20 in the appendix. That result stays in a very good agreement with previous work made by Reich *et al.* who categorized LiCl as a sturdy dimer (**Li1**) according to HMPA titrations: Reich, H. J.; Borst, J. P.; Dykstra, R. R.; Green, P. D. *J. Am. Chem. Soc.* **1993**, *115*, 8728–8741.

²⁰ However, a significant formation of theSSIP Li[THF]₄⁺ **Li2** can be excluded ($MW_{\text{calc}} = 295$ g/mol, $MW_{\text{det}} = 382$ g/mol, $MW_{\text{err}} = -29\%$).

²¹ Based on statistics from the Cambridge Structural Database CSD, version 5.36 (Updated Nov 2014).

Chart 2-2. Most plausible aggregation modes of $i\text{Pr}_2\text{NMgCl}\cdot\text{LiCl}$ 9 in $\text{THF-}d_8$ solution.

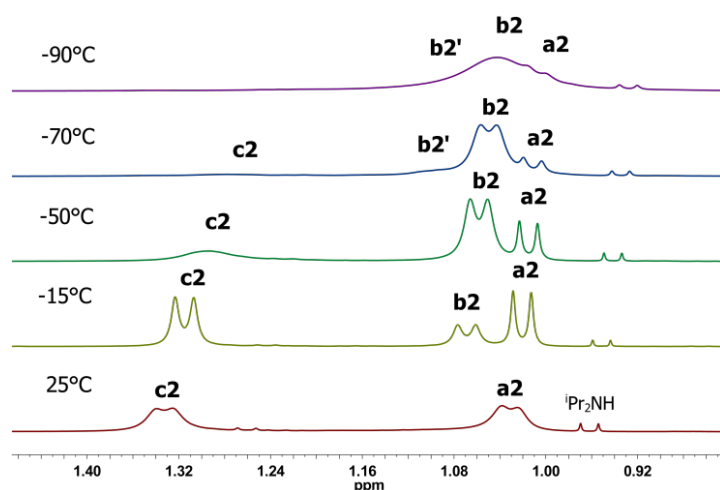
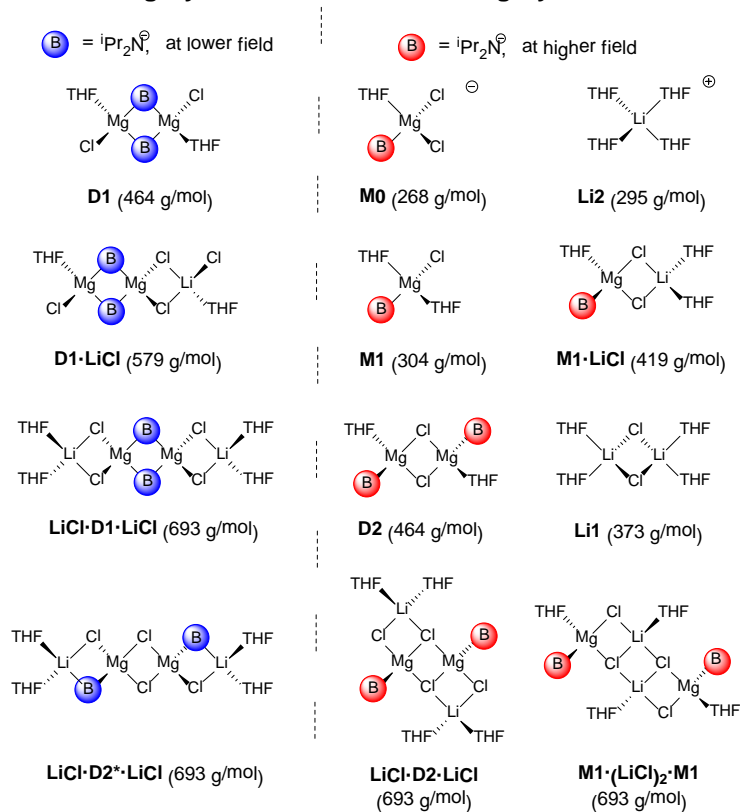
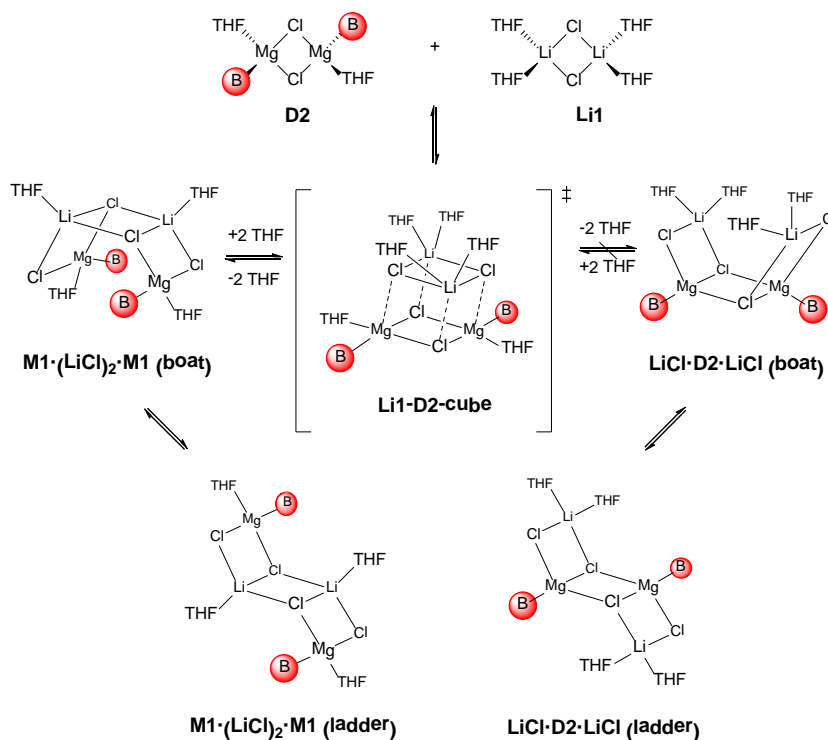


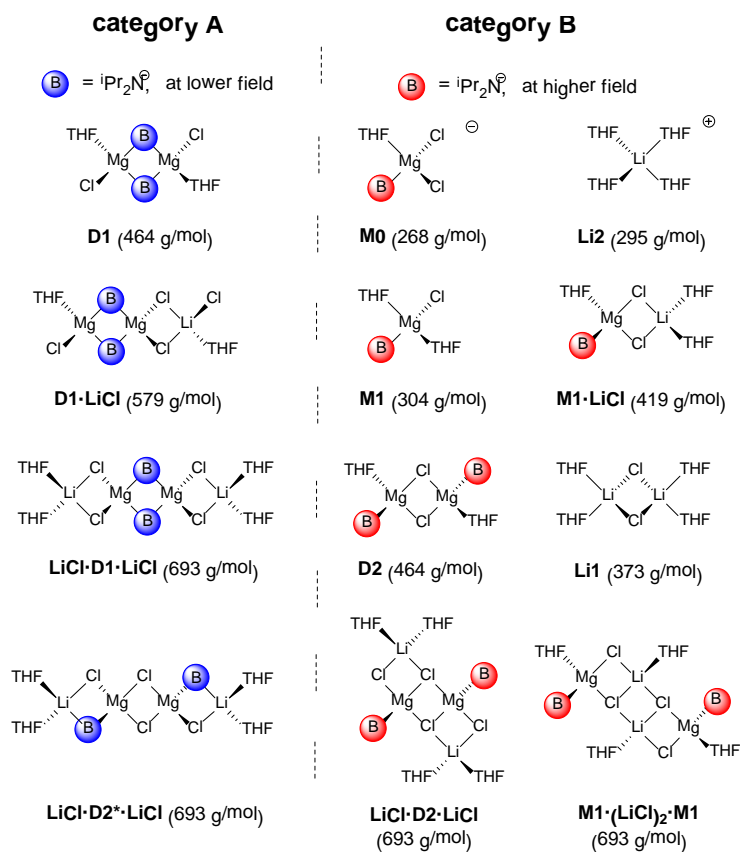
Fig. 2-26. ^1H superposition plot of crystalline 9 (0.1 M, $-\text{CH}_3$ region) re-dissolved in $\text{THF-}d_8$ at various temperatures.

Bickelhaupt and Solà et al. have shown that the most stable isomer of methylmagnesium chloride tetramers, $(\text{CH}_3\text{MgCl})_4$, is a T_d -symmetric tetranuclear cluster with a cubic $(\text{MgCl})_4$ core and terminal $-\text{CH}_3$ groups on the magnesium vertices.^[131] Li halides are also known to build stable cubic tetramers $[\text{LiX}]_4$ ($X = \text{Cl}, \text{Br}, \text{I}$)^[132] and even heteroleptic cubanes in the solid state (see compound **72** in Fig. 2-28).^[130, 133] This is why the interaction of the LiCl-dimer **Li1** with dimer **D2** could occur *via* a cubic transition state.

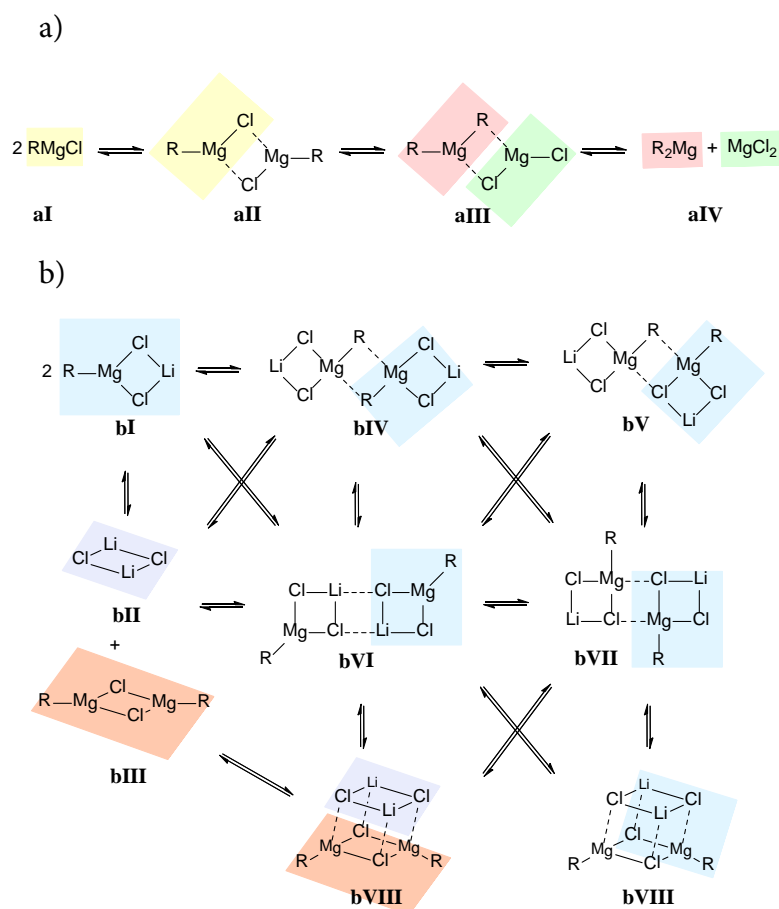


Scheme 2-4. Proposed interaction of the LiCl dimer **Li1** with the Hauser base dimer **D2**.

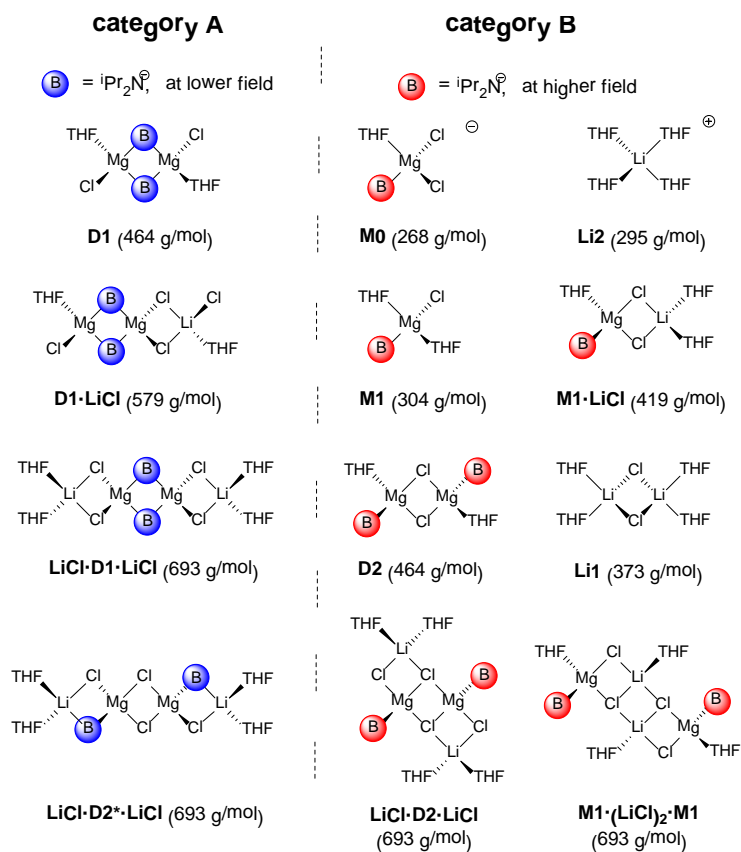
Since, the ring size of $[\text{LiCl}]_2$ and $[\text{MgCl}]_2$ differ from each other, a fast dissociation of the cubane back to the corresponding dimers would be plausible. Once the cubane is formed, it could open on one side to produce the already mentioned aggregates **LiCl·D2·LiCl** with a $[\text{MgCl}]_2$ and **M1·(LiCl)₂·M1** with a $[\text{LiCl}]_2$ core (Scheme 2-4). To find out which of those structures is the most stable in solution further calculations were carried out. These will be discussed later in the text. Additional support for the interaction of **Li1** with **D2** is given by the absence of LiCl-free species **M1** ($MW_{\text{calc}} = 304 \text{ g/mol}$) and homoleptic diorganomagnesium **M2** ($MW_{\text{calc}} = 369 \text{ g/mol}$, see Chart 2-1, $MW_{\text{det}}(\text{all species}) = 425\text{--}661 \text{ g/mol}$, $MW_{\text{err}} \geq 28\%$ and $MW_{\text{err}} \geq 13\%$). At low temperatures **M2** (Chart 2-1) is the main species in the solution of Hauser base **7**.

Chart 2-2. Most plausible aggregation modes of $i\text{Pr}_2\text{NMgCl}\cdot\text{LiCl}$ 9 in $\text{THF}-d_8$ solution.

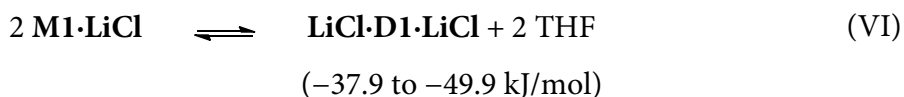
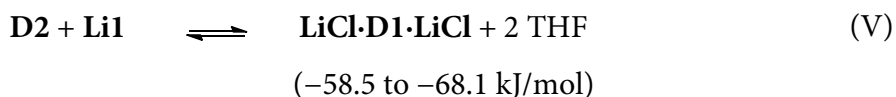
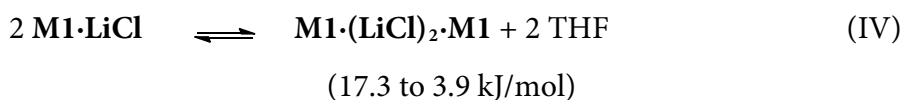
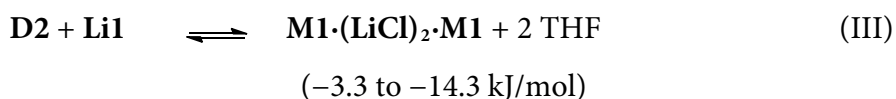
Ashby et al. proposed for the formation of **M2** a dimer based mechanism (Scheme 2-5a).^[68a] A rearrangement of dimer **aII** to an asymmetric dimer **aIII** forms two excellent leaving groups, which dissociate into the corresponding diorganomagnesium R_2Mg and $MgCl_2$ (**aIV** in Scheme 2-5a). In contrast, with LiCl as additive it is possible to rationalize several structures like **bI**-**bVIII**. Interestingly, in those structures the LiCl coordinated monomer **bI**, the LiCl-dimer **bII** and dimeric **bIII** represent always the best leaving groups (Scheme 2-5b), especially at low temperatures where monomeric LiCl and **M1** are highly unfavoured.



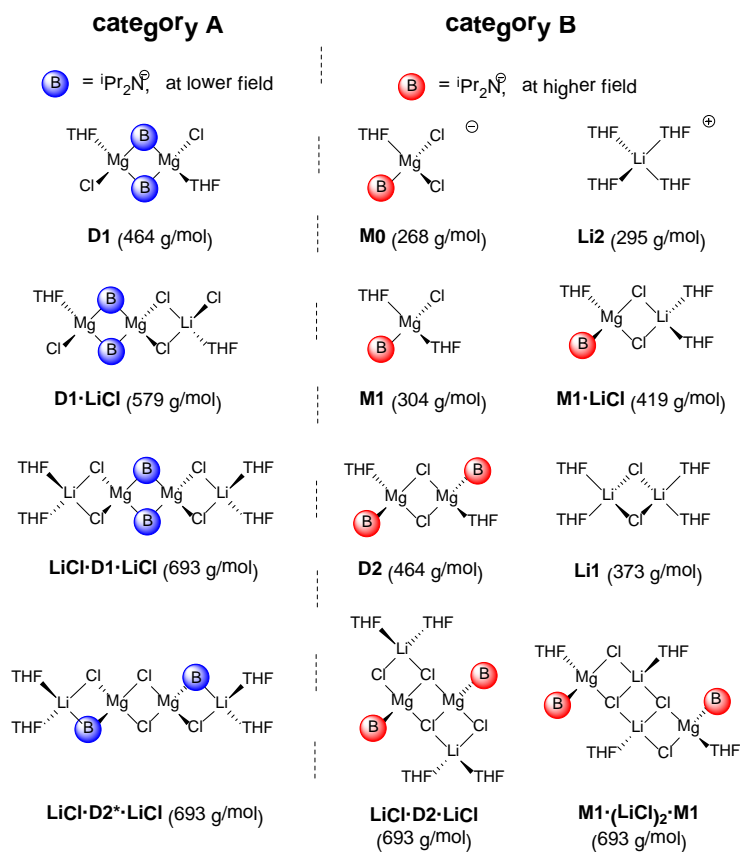
Scheme 2-5. a) Mechanism on the formation of R_2Mg and $MgCl_2$ via an asymmetric dimer **aIII** proposed by *Ashby*. b) In the presence of LiCl in various aggregation modes of **9**, **bI**, **bII** and **bIII** always the best leaving groups, suppressing the formation of homoleptic R_2Mg and $MgCl_2$ **aIV**; any solvation omitted for clarity.

Chart 2-2. Most plausible aggregation modes of $i\text{Pr}_2\text{NMgCl}\cdot\text{LiCl}$ 9 in $\text{THF-}d_8$ solution.

Further, the cleavage of MgCl_2 or R_2Mg would be accompanied by a release of solvent separated ions that would be very unfavourable since no solvent separated species were observable in solution of Hauser base **1** and **2**.²² If the LiCl dimer **Li1** (**bII**) would not communicate with dimer **D2** (**bIII**) than the formation of homoleptic **M2** (**aIV**) should be observable which is not the case.^[71] Without LiCl the dimer **D2** is only stable above -50°C . But with LiCl it is the main species below -50°C in Hauser base **2** most probably because of its interaction with the LiCl dimer **Li1**. This contrasting behaviour could be reflected in the different aggregation modes of LiCl and MgCl_2 in THF solution. The former is predominately dimeric, enabling a sufficient overlap of the $[\text{LiCl}]_2$ ring with dimer **D2**, while MgCl_2 is predominately monomeric.^[124b] This is why MgCl_2 stabilize more efficiently in a terminal coordination mode like *e.g.* in $\text{M1}(\mu\text{-Cl}_3)\text{MgCl}_2$ and $\text{MgCl}_2\cdot\text{D1}(\text{D2})\cdot\text{MgCl}_2$. To address some of the open questions regarding the interaction and aggregation of **Li1** and **D2** in THF solution, we carried out further calculations on the complexes. We started by computing the relative free energies for $\text{M1}\cdot(\text{LiCl})_2\cdot\text{M1}$ and $\text{LiCl}\cdot\text{D2}\cdot\text{LiCl}$ (depicted in Scheme 2-4). The results show that the ladder and boat configurations, both for the $\text{M1}\cdot(\text{LiCl})_2\cdot\text{M1}$ and the $\text{LiCl}\cdot\text{D2}\cdot\text{LiCl}$ isomers are very close in energy (A-Table 25 in the appendix), with differences below 3 kJ/mol (at 25°C). This is definitely within the uncertainty of the method and would indicate no particular conformational preference. However, the structures $\text{M1}\cdot(\text{LiCl})_2\cdot\text{M1}$ with an inner $[\text{LiCl}]_2$ ring are identified as the by 42.2 kJ/mol in free energy most stable species.

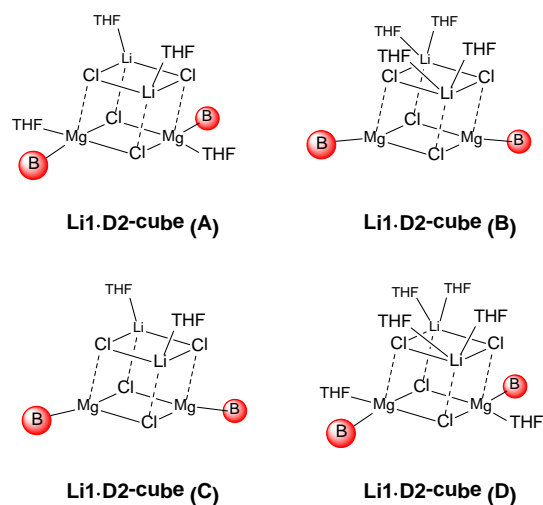
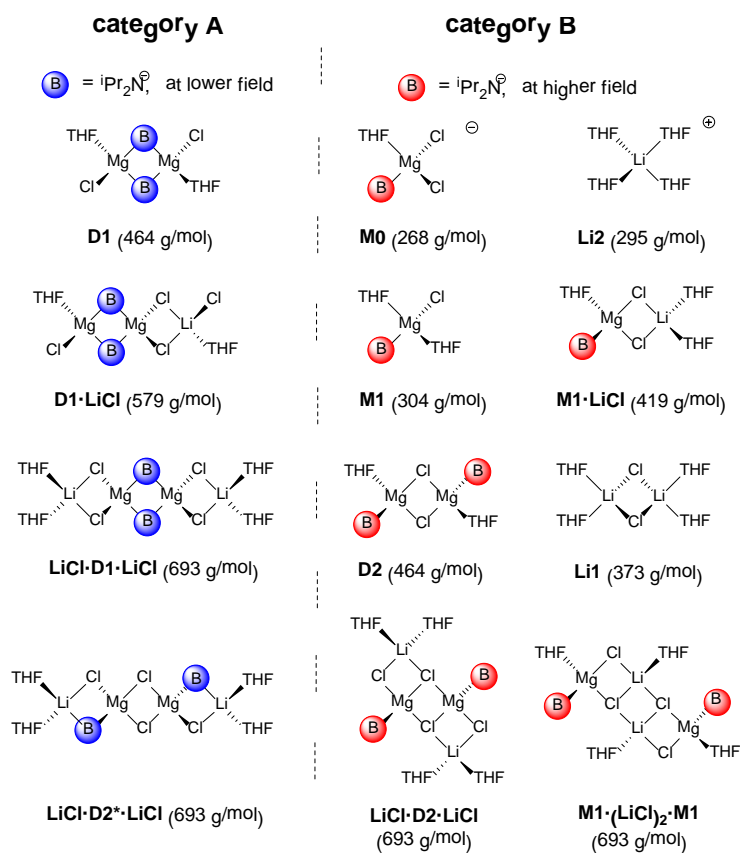


²² Grignard reagents are also known to be very weak electrolytes, see Seyferth, *Organometallics*, 2009, **28**, 1598–1605.

Chart 2-2. Most plausible aggregation modes of $i\text{Pr}_2\text{NMgCl}\cdot\text{LiCl}$ 9 in THF- d_8 solution.

The next question is whether the formation of $\mathbf{M1}\cdot(\mathbf{LiCl})_2\cdot\mathbf{M1}$ is favoured in solution as well. This complex can be formed *e.g.* by the reaction of $\mathbf{D2}$ with $\mathbf{Li1}$ (III) or by dimerization of two $\mathbf{M1}\cdot\mathbf{LiCl}$ molecules (IV). The free energies for the mixed Li-Mg dimer formation were computed in a range from -90°C to $+25^\circ\text{C}$, revealing that the dimerization process of $\mathbf{D2}$ and $\mathbf{Li1}$ (III) to give $\mathbf{M1}\cdot(\mathbf{LiCl})_2\cdot\mathbf{M1}$ at low temperature is slightly exergonic (-3.3 to -14.3 kJ/mol, from lower to higher temperature, A-Table 27 in the appendix). Species $\mathbf{M1}\cdot(\mathbf{LiCl})_2\cdot\mathbf{M1}$ (**b'**) could, as such, be formed in the solution of *Turbo*-Hauser base **9**. In contrast, the dimerization of two $\mathbf{M1}\cdot\mathbf{LiCl}$ molecules (IV) is unfavoured due to an endergonic reaction (17.3 to 3.9 kJ/mol, A-Table 29 in the appendix). Obviously such values have to be considered with certain reservations, since the molarity is changing (formally, two THF molecules are released into solution during the process, so the formation of 3 molecules from 2 starting products is present). The quantum chemical result is, therefore, strongly influenced by the translation entropy. In the gas phase, the latter can be computed from the harmonic vibrational partition function. This does not apply to the case in solution, since solvated molecules are not free to move and possess lower translational entropy than in the gas. The theoretical calculations already include a correction as suggested by *Ardura et al.* on the basis of a cell model for the change in translational degrees of freedom.^[134] However, this little energy gain for the formation of $\mathbf{M1}\cdot(\mathbf{LiCl})_2\cdot\mathbf{M1}$ stays in good agreement with the presented NMR experiments, showing that $\mathbf{D2}$ and $\mathbf{Li1}$ interact and communicate with each other but still the equilibrium is highly on the side of free $\mathbf{D2}$ and $\mathbf{Li1}$. In tune with the crystal structure of $[\mathbf{9}\cdot\text{THF}]_2$ the highest energy gain was identified for the formation of $\mathbf{LiCl}\cdot\mathbf{D1}\cdot\mathbf{LiCl}$ (V and VI). Again the reaction of $\mathbf{D2}$ and $\mathbf{Li1}$ is preferred over the dimerization of two $\mathbf{M1}\cdot\mathbf{LiCl}$ molecules by 19.4 kJ/mol.²³ Interestingly, the solubility limit of $\mathbf{LiCl}\cdot\mathbf{D1}\cdot\mathbf{LiCl}$ is reached at approximately -70°C providing small amounts of $\mathbf{M1}\cdot(\mathbf{LiCl})_2\cdot\mathbf{M1}$ that is thermodynamically less stable. One additional open question is the existence of cubic intermediates, through which the larger mixed Li-Mg aggregates could be formed. Since there is no experimental data available on such transient species, one can only postulate about different coordination motifs. Four possible cubane structures $\mathbf{Li1}\cdot\mathbf{D2}\cdot\text{cube}(\mathbf{A-D})$ are proposed (Fig. 2-29), with two available coordination sites at each Li and additional two at each Mg site. The calculations clearly identify complexes **B** and **C** as the most unstable, given the low coordination number of the Mg sites.

²³ Again with a correction to the translational entropy.

Fig. 2-29. Overview of possible cube structures of *Turbo*-Hauser base 9.Chart 2-2. Most plausible aggregation modes of ${}^i\text{Pr}_2\text{NMgCl}\cdot\text{LiCl}$ 9 in THF- d_8 solution.

A direct comparison can be in fact established between **Li1·D2-cube(A)** and **Li1·D2-cube(B)**, with **A** being favoured over **B** in the considered temperature range by about 10 kJ/mol (A-Table 24 in the appendix). For the preferred cubane structures **A** and **D** one might consider the associated equilibria given by the general equations:



with $n = 0$ for **D** and 2 for **A**. As mentioned before, the change in molarity is an obstacle in computing the free energies. By considering two equilibria simultaneously, where in one case the molarity change entropically promotes the products (**A**) and in the other the reactants (**D**). The computed free energies for dimerization according to equilibrium (VII) are given in Fig. 2-30. The dimerization of two **M1·LiCl** molecules to form **Li1·D2-cube(A-D)** (VIII) is in average 19.4 kJ/mol higher in energy (A-Table 26 and A-Table 28 in the appendix).

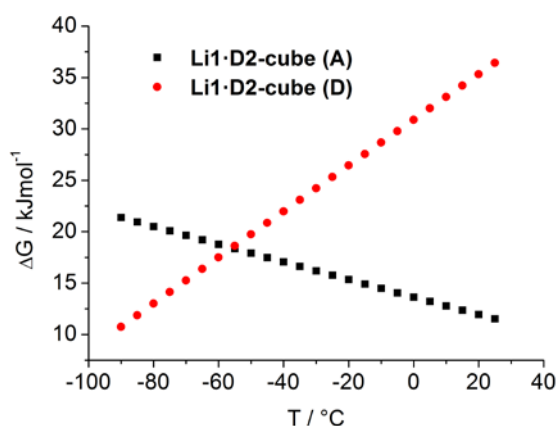
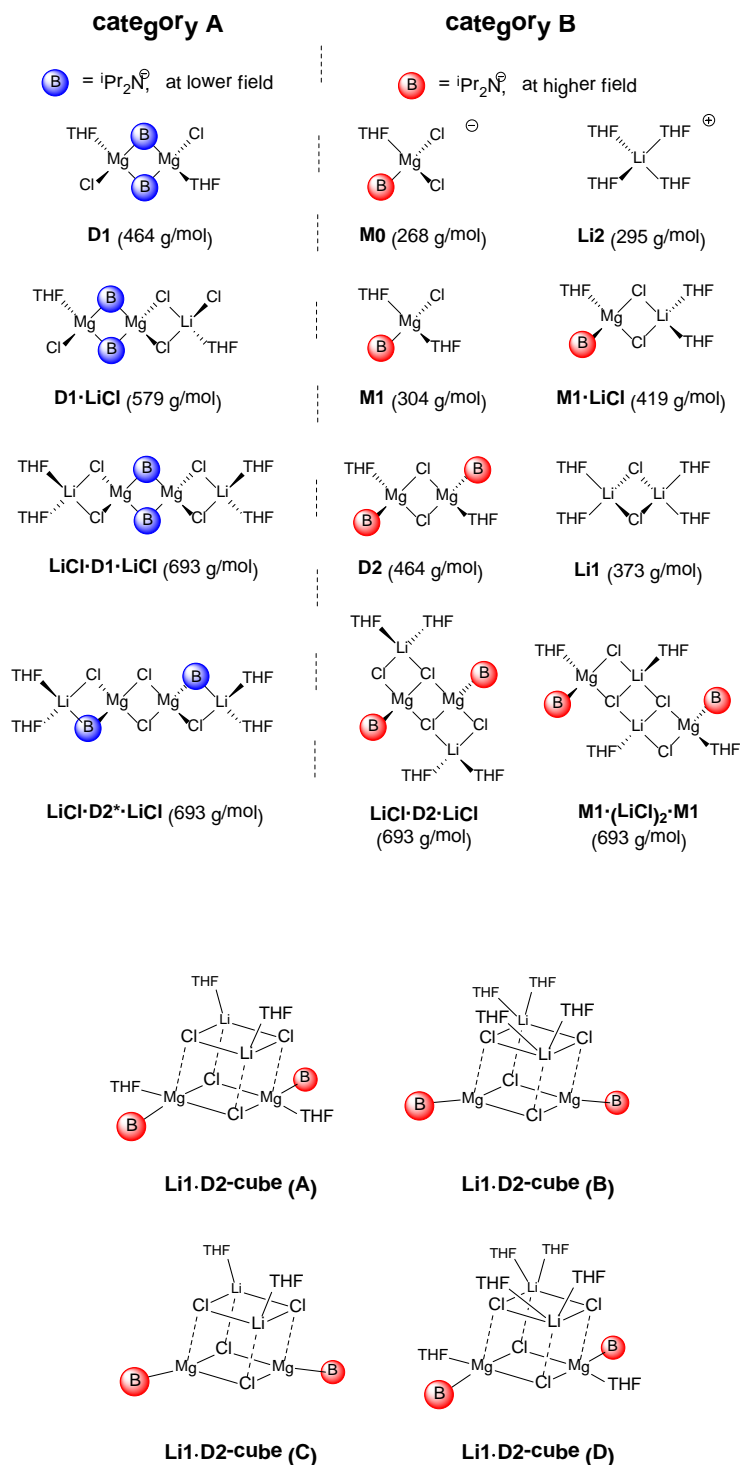
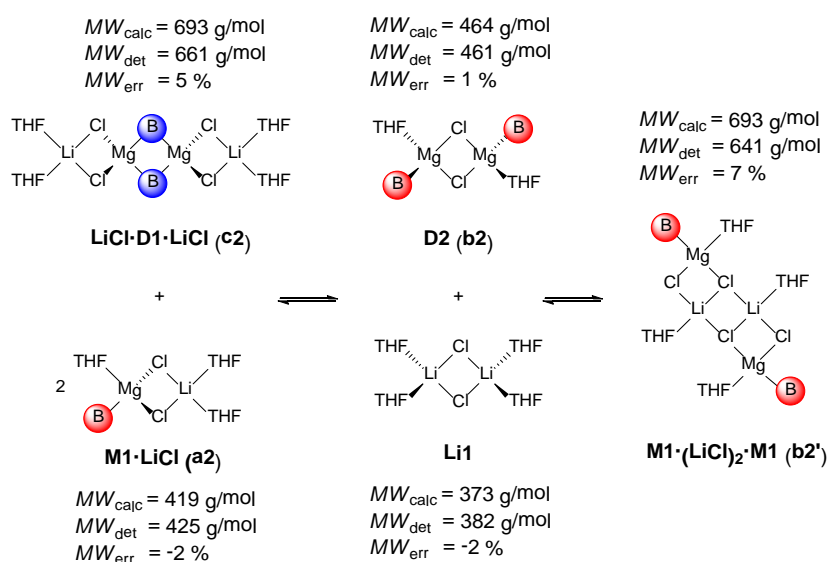


Fig. 2-30. Computed free energies for dimerization of **D2 + Li1** to give **LiCl·D2-cube (A)** and **LiCl·D2-cube(D)**.

As expected, the formation of complex **D** would be most favourable at lower temperatures. The crossing point is at about -55°C . Although the equilibrium is always shifted towards the reactants, the differences can be relatively small, as low as 10.7 kJ/mol, such that the cubic intermediate should be accessible, even if not stable relative to the metal dimer complexes **D2** and **Li1**.

Chart 2-2. Most plausible aggregation modes of $i\text{Pr}_2\text{NMgCl}\cdot\text{LiCl}$ **9** in $\text{THF-}d_8$ solution.Fig. 2-29. Overview of possible cube structures of *Turbo*-Hauser base **9**.

The presented results show that the formation of small amounts of $\text{M1}\cdot(\text{LiCl})_2\cdot\text{M1}$ (Scheme 2-6) is thermodynamically possible. Most probably, this complex is formed by dimerization of **D2** with **Li1** via a cubic intermediate, presumably $\text{Li1}\cdot\text{D2}\cdot\text{cube}(\text{D})$ at temperatures below -55°C . In addition, the NMR investigations show also that ${}^i\text{Pr}_2\text{NMgCl}\cdot\text{LiCl}$ **9** does not produce SSIPs in detectable concentrations.²⁴ Further, the proposal that the impact of LiCl on the higher reactivity of *Turbo* bases rests on the deaggregation of RMgX oligomers to monomers has to be revised. Most reactions of RMgX reagents proceed in THF solution and it is shown for long time that alkyl and aryl Grignard reagents are monomeric in THF solution.^[66] The results show that same seems to be true for Hauser base **7**.



Scheme 2-6. Schematic representation of the solution structure of **9** in $\text{THF-}d_8$ solution. The MWs were derived from ${}^1\text{H}$ - and ${}^7\text{Li}$ -DOSY-ECC-MW-determinations. At RT the equilibrium of **9** is highly located on the left side. At low temperature it moves significantly to the middle side.

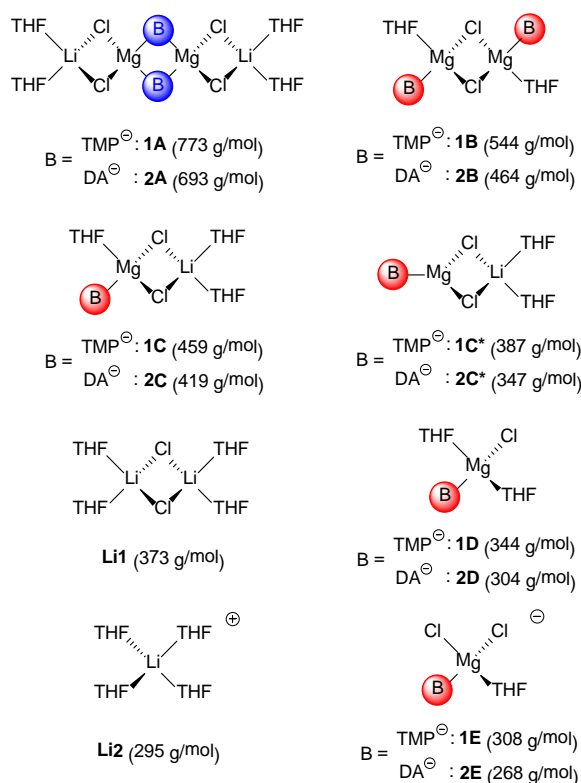
Moreover, the reason for the lower reactivity of LiCl- free Hauser bases should be reflected in the Schlenk-equilibrium. At low temperatures the equilibrium in THF solution is mostly shifted to the side of homoleptic diamidomagnesium R_2Mg where the amide ligands are highly sterically hindered in comparison with the heteroleptic RMgCl monomers and MgCl_2 co-coordinated species. These compounds that represent the most reactive species in a Hauser base solution are only present at low concentrations. This explains why it is necessary to use a large excess of Hauser bases (2-12 fold) to achieve high conversions in synthesis.^[23] The big advantage of LiCl is the ability to shift the Schlenk-equilibrium from

²⁴ Additionally, a significant formation of the SSIP $\text{Li}[\text{THF}]_4+$ **Li2** can be excluded ($MW_{\text{calc}} = 295 \text{ g/mol}$, $MW_{\text{det}} = 382 \text{ g/mol}$, $MW_{\text{err}} = -29\%$)

the homoleptic to the heteroleptic side, especially at low temperatures. The high concentration of bimetallic complexes (like monomeric **M1**·LiCl (**a1**) as well as dimeric LiCl·D1·LiCl (**c2**), D2 (**b2**) and **M1**·(LiCl)₂·**M1** (**b2'**) should provide the most influence on the reactivity, chemoselectivity and complex induced proximity effects (CIPE)^[21] of *Turbo*-Hauser bases. It is possible that this concept could also be applied to *Turbo*-Grignard reagents.

2.2.8 Structure of *Turbo*-Hauser Base TMPMgCl·LiCl in THF solution²⁵

Chart 2-3. The most plausible solution structures of **9** and **10** in THF-*d*₈ solution



Turbo-Hauser bases ⁱPr₂NMgCl·LiCl **9** and TMPMgCl·LiCl **10** show a different reactivity and regioselectivity.^[23] To understand this property and to be able to deduce informative structure-reactivity relationships it is extraordinary important to explore the solution structure of **10**. *García-Álvarez* and *Mulvey et al.* analyzed crystals of **1C** in THF-*d*₈ solution^[28] by diffusion ordered spectroscopy (DOSY) and the diffusion coefficient formula weight (D-FW) analysis that was pioneered by *Li* and *Williard et al.*^[77, 104a] This method is

²⁵ A revised version of my manuscript: R. Neufeld, D. Stalke, *Chem. Eur. J.* **2016**, submitted.

based on internal calibration curves (ICC), where many internal standards which may interfere with the reactive metal complexes are required. Because of peak overlap problems the authors had to use inappropriate internal standards,²⁶ so the molecular weight (MW) determination was prone to a relatively high error of approximately $\pm 30\%$. Consequently *García-Álvarez* and *Mulvey et al.* stated that they were not able to “clearly establish the exact nature of the solution species”.^[28] Predominantly it could not be established whether or not lithium chloride is co-coordinated to the magnesium amide. Anyhow it was concluded that a SSIP situation appeared to be the most feasible. In the following section it will be proved that LiCl does indeed coordinate to *Turbo*-Hauser Base **10**.

Primarily it seems advisable to *a priori* rationalize which species are feasible to be present in the solution of **10**. The most obvious question to be addressed in s-block organometallics of course is the amount of coordinating THF molecules to be present in the solution structure of **10**. Even from a vast number of solid state structures it is known that polar solvents like THF are necessary to coordinate such highly ionic compounds. A re-dissolved crystal of **10** in net THF could on the one hand retain its solid state structure (**1C**) or even aggregate further to combine to dimers (**1A**, **1B**) as well as dissociate to a number of smaller molecules (**1C***-**1E**, Chart 2-3). LiCl can either coordinate to the magnesium amide or dissociate as a well-known $[(\text{THF})_2\text{Li}(\mu\text{-Cl})_2\text{Li}(\text{THF})_2]$ dimer^[127] **Li1**. A solvent separated ion pair (SSIP) $\text{Li}(\text{THF})_4^+$ **Li2** would promote the formation of an ate-complex **1E** where two chloride ions coordinate a single magnesium cation. From the crystal structure of **10** it is known that the lithium cation is located at an average distance of 4.68 Å to the closest CH_3 -protons of the TMP ligand.^[72] This relatively close distance should be detectable in a ^1H - ^7Li -HOESY experiment when the structure is retained in solution.^[13b] Indeed the ^1H - ^7Li -HOESY-spectra at all temperatures display a cross peak between lithium and the CH_3 groups confirming the lithium coordination to the magnesium amide (Fig. 2-31). Similar results were observed for Hauser base **9**.

²⁶ The error of the DOSY-MW analysis depends highly on the shape of the used references as well on that of the analyte (see chapter 2.1.4). Hauser bases have an ellipsoidal shape. Therefore ellipsoid references should be used for an accurate MW-analysis. However, *García-Álvarez et al.* used references with different shapes (spherical, ellipsoidal and flat discs) that dramatically decreased the accuracy of the MW-determination.

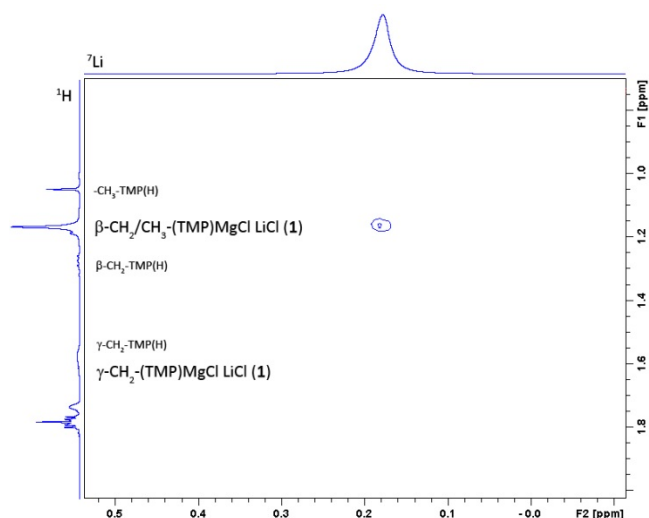
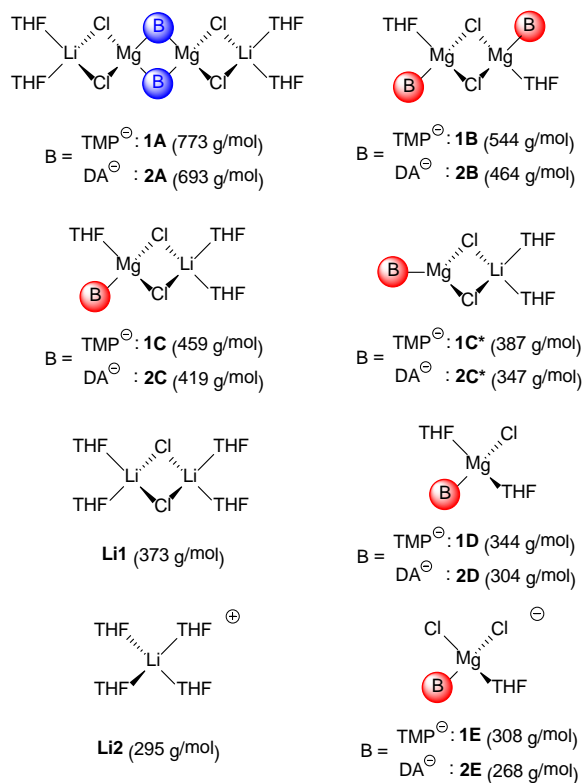


Fig. 2-31. ^1H - ^7Li -HOESY at -50°C of crystalloid **10** re-dissolved in $\text{THF-}d_8$ (20 mm) at various temperatures.

Chart 2-3. The most plausible solution structures of **9** and **10** in $\text{THF-}d_8$ solution



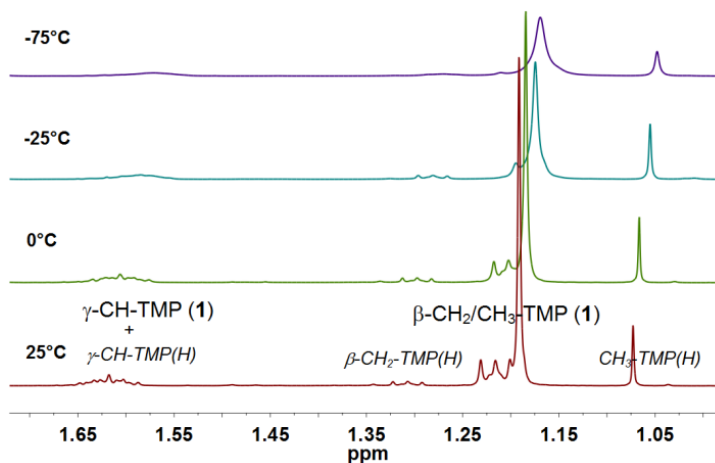


Fig. 2-32. Superposition of ^1H NMR spectra of crystalloid **10** re-dissolved in $\text{THF-}d_8$ at various temperatures.

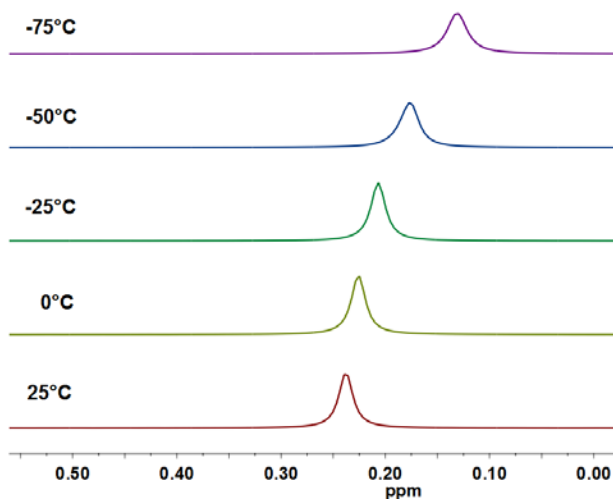


Fig. 2-33. Superposition of ^7Li NMR spectra of crystalloid **10** re-dissolved in $\text{THF-}d_8$ (20 mM) at various temperatures.

For NMR spectroscopic measurements diluted solutions of **10** (20 mM) were used by dissolving the crystals in $\text{THF-}d_8$. The ^1H NMR spectra of **10** show at all temperatures (25°C to -75°C) only one single type of TMP ligand ($\delta = 1.19/1.22/1.62$ ppm for $\text{CH}_3/\beta\text{-CH}_2/\gamma\text{-CH}$, Fig. 2-32) while the *i*Pr-Turbo-Hauser base **9** displays several oligomers.²⁷ The ^7Li NMR spectra show one singlet at about 0.2 ppm in the whole temperature range (Fig. 2-33). The presence of remaining LiTMP can be excluded since it resonates at 0.7 ppm (monomer) or at 1.3 ppm (dimer), respectively.^[35b] Additionally, the lithium

²⁷ A small amount of protonated amine TMP(H) is also present in solution. The ECC-MW-determination predicts at temperatures between 0°C and -75°C an accurate MW (in av.: $\text{MW}_{\text{calc}} = 141$ g/mol, $\text{MW}_{\text{det}} = 140$ g/mol, $\text{MW}_{\text{err}} = 1\%$). Interestingly, at RT the MW is slightly overestimated ($\text{MW}_{\text{det}} = 167$ g/mol, $\text{MW}_{\text{err}} = -18\%$), indicating a small exchange between the amide and the amine. Anyway, this interaction is neglectable at temperatures below 0°C, see A-Table 32 in the appendix.

cation $[\text{Li}(\text{THF})_4]^+$ **Li2** in aSSIP can also be excluded to be present at significant concentrations since it is known to resonate at negative field (-1.1 ppm),^[128] curtailing the plausible present species to the lithium containing dimer **1A** and the monomers **1C/1C***. Both aggregates should clearly be distinguishable *via* DOSY NMR spectroscopy

The ^1H and ^7Li -DOSY-ECC-MW-determination of **10** gives a MW of $MW_{\text{det}} = 403$ g/mol for the ^1H - und 387 g/mol for the ^7Li -nucleus (Fig. 2-34 *vide infra*).²⁸ This low MW discriminates both the lithium free aggregates **1B** ($MW_{\text{err}} = 26\%$), **1D** ($MW_{\text{err}} = -17\%$), **1E** ($MW_{\text{err}} = -31\%$) and also dimeric **1A** ($MW_{\text{err}} = 48\%$). Most interestingly the crystal structure **1C** does not keep its full integrity in THF- d_8 solution reflected by an unacceptable high error of the MW ($MW_{\text{calc}} = 459$ g/mol, $MW_{\text{det}} = 403$ g/mol, $MW_{\text{err}} = 12\%$). The smaller contact ion pair **1C*** derived from **1C** by the loss of a single THF molecule matches best the determined MW ($MW_{\text{calc}} = 387$ g/mol, $MW_{\text{det}} = 403$ g/mol, $MW_{\text{err}} = -4\%$). *Mulvey et al.* already mentioned the labile THF coordination at **1C** as the expected integrated ^1H NMR intensity THF:amide decreases from 3:1 to 2:1 when the crystals are dried *in vacuo*.^[72] From that they concluded that the powerful regioselective magnesiating ability of **10** might be a consequence of a coordinately unsaturated Mg that “could facilitate the pre-coordination of the functionalized aromatic substrate prior to magnesiation”.^[72]

Our DOSY-ECC-MW-determination fully supports this hypothesis. The labile THF ligand at the magnesium atom could be a result of steric overload from the rigid TMP ligand. Searching the Cambridge Crystallographic Database²⁹ emphasizes Mg typically to be coordinated by four to six ligands. Enlarging the bulk of the various substituents however results also in 3-coordinated magnesium amides. This is often the case when bulky SiMe_3 groups^[135] and especially when TMP ligands are involved.^[105a, 136] These investigations confirm that lithium chloride indeed co-coordinates to the magnesium amides in solution as observed in the *i*-Pr-Turbo-Hauser base **9**.^[137] A detectable population of the solvent separated lithium cation **Li2** can also be excluded for Turbo-Hauser base **10** ($MW_{\text{calc}} = 295$ g/mol, $MW_{\text{det}} = 387$ g/mol, $MW_{\text{err}} = -31\%$).

²⁸ The MW_{det} values are displayed as an average value, derived from DOSY-ECC-MW measurements at different temperatures, see A-Table 30 and A-Table 31 in the appendix.

²⁹ CSD version 5.36 (Updated Nov 2014)

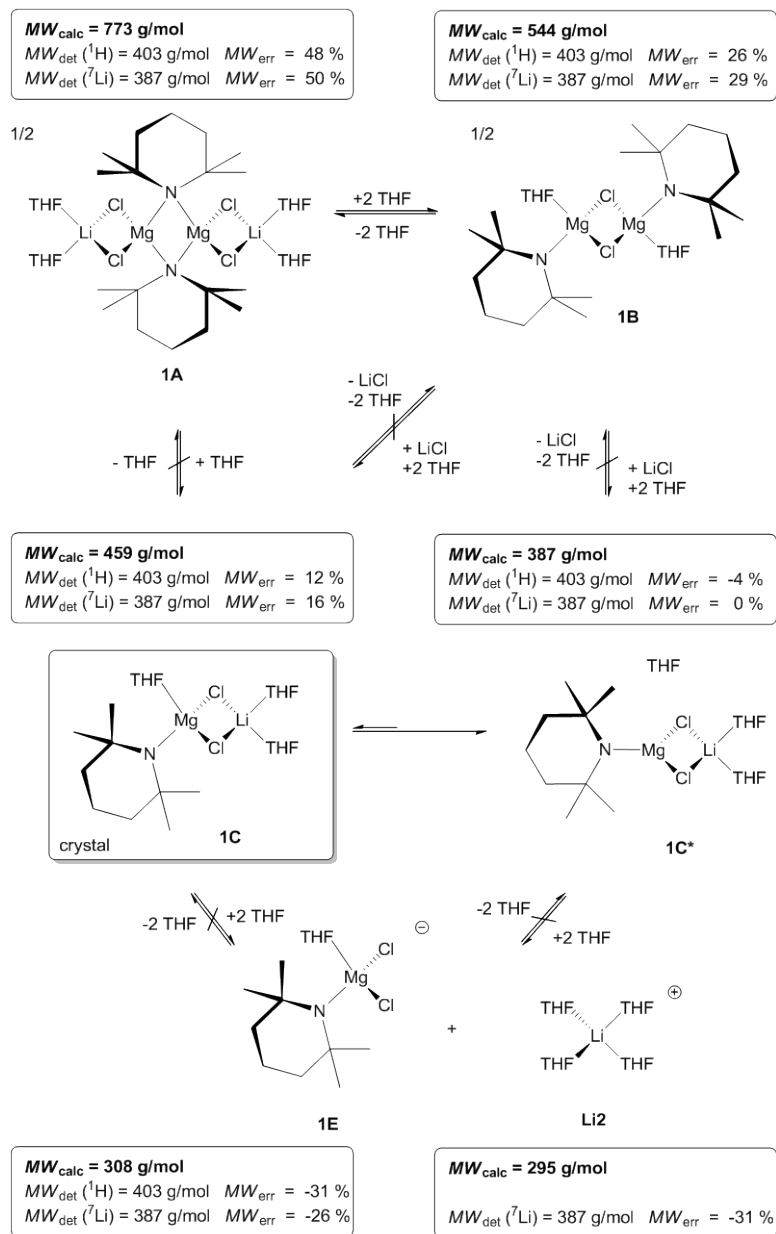


Fig. 2-34. ^1H - and ^7Li -DOSY-ECC-MW-determination of crystalloid **10** re-dissolved in $\text{THF-}d_8$ (20 mm).

3 SUMMARY AND OUTLOOK

In the first part of this Ph. D. thesis the new DOSY-ECC-MW-determination methodology was introduced. This method determines molecular weights of unknown solutes in THF- d_8 and TOL- d_8 solution with exceptional accuracy and reliability with a maximum deviation of $\pm 9\%$ and an average error of only 4% (Table 3-1). Furthermore, the influence of the internal reference, shape, concentration, temperature, heavy atoms and deuterated compounds on the MW-determination was validated in detail.^[6] Due to the normalized diffusion coefficients one internal reference is sufficient. Compared to the ICC method, this interrelation has the huge advantage that it is unnecessary to introduce multiple references into the same NMR sample. Signal overlapping, analyte-reference interaction problems, wasting chemicals and deuterated solvents can be avoided. Due to the normalized diffusion coefficients everyone is able to use the ECCs, independent of the NMR device, without the necessity of recording new calibration curves. This work facilitated consecutive research in which new ECCs for a range of further commonly used NMR solvents like DMSO- d_6 , C₆D₁₂, C₆D₆, CDCl₃ and CD₂Cl₂ were introduced.^[4] Additionally, future investigations will include the preparation of ECCs derived from molecules with high densities which contain e.g. heavy halides or transition metals. This extension could promote the ECC-method into a widely applicable standard technique to elucidate solution state structures.³⁰

Table 3-1. RMS errors for DOSY-MW-determination of small molecules by different methods.

<i>Method</i>	<i>RMS error / %</i>
Stokes-Einstein ^[101]	45
Gierer-Wirtz ^[101]	28
Chen ^[101]	18
Evans ^[101]	15
Crutchfield ^[103]	11
ECC ^[6]	4

³⁰ A simple Excel spreadsheet that implements the calculation of $\log D_{x,\text{norm}}$, allowing to estimate MWs of analytes from their diffusion coefficients is available at http://www.stalke.chemie.uni-goettingen.de/mw_det_calc/mw_det_calc.xlsx

In the second part of this Ph. D. thesis DOSY-ECC-MW-determinations were performed on several organometallic and metal amide compounds. For the first time it was possible to determine the donor-base-free solution structure of LDA in toluene (Fig. 3-1).^[5] It was shown that at room temperature LDA adopts a trimeric and tetrameric aggregation in a 2:1 ratio. This equilibrium ranges from trimers and tetramers through pentamers to higher oligomers as the temperature decreases.^[5] Additionally, it was shown that dimeric LDA as proposed by *Kim and Collum et al.*^[12a] is not present in the mixture at any temperature ($MW_{err} = -48\%$ and -143%).

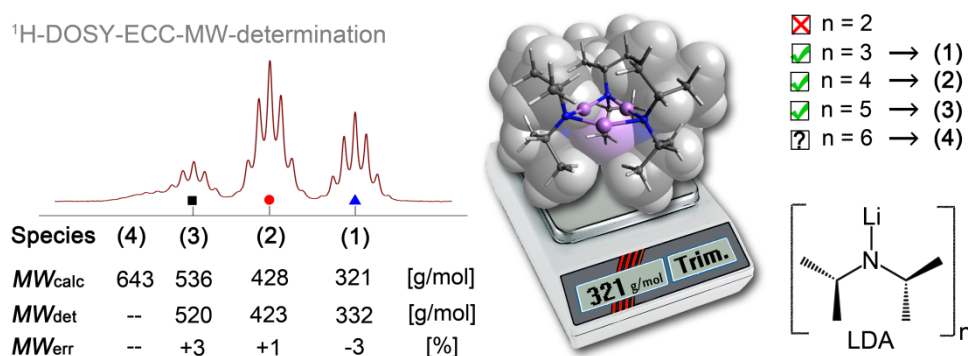


Fig. 3-1. Illustration of the DOSY-ECC-MW-determination of LDA in TOL- d_8 solution.

The ECC-approach was further used to determine the aggregation of Na-indenide. It was shown that Na-indenide is predominately a trisolvated monomer $(THF)_3 \cdot Na(C_9H_7)$ in THF- d_8 solution (Fig. 3-2).^[6] With decreasing temperature the MW increases. This behavior was attributed to a fourth THF coordination which seems to be attractive at low temperatures.

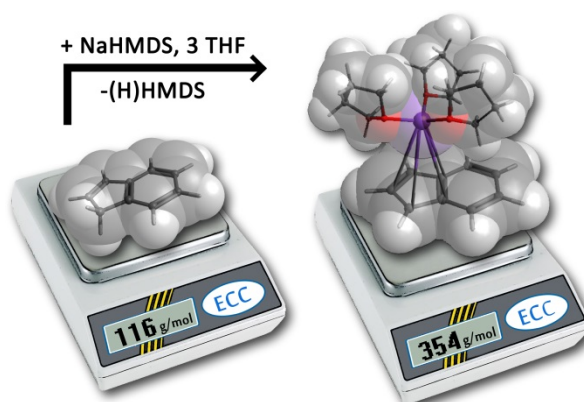


Fig. 3-2. Illustration of the DOSY-ECC-MW-determination of Na-indenide in THF- d_8 solution.

By taking the residual proton signal of the solvent (TOL- d_7) as internal reference it was possible to characterize *a posteriori* the complex solution structure of $[^t\text{BuLi}]_4 \cdot 4[\text{Me}_2\text{NC}_6\text{H}_4\text{Li}]_4$ in TOL- d_8 .^[6] The results from the DOSY-ECC-MW-determination correlate very well (error smaller than $\pm 5\%$) with the solution structures that were determined in a ^7Li -EXSY NMR experiment by A.-C. Pöppler *et al.* in 2012.^[119]

Dimeric solid state structures of MHMDS (**65-68** and **71** in Fig. 3-3) with ammonia as donor base were presented and an aggregation-deaggregation mechanism was proposed. Additionally, MW-determinations on Li-, Na- and KHMDS were performed in TOL- d_8 solution at room temperature. The measurements indicate that the latter form predominately mono- to penta- solvated dimers.

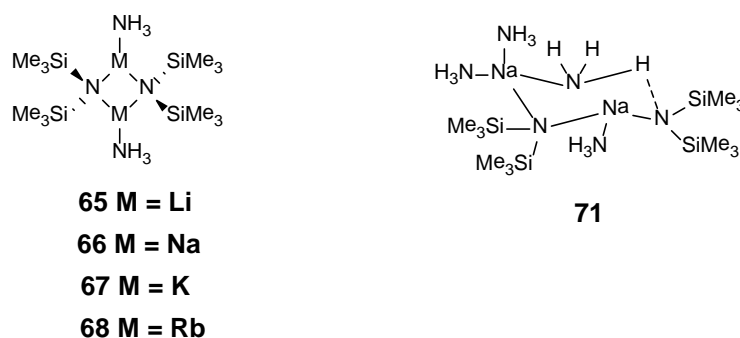


Fig. 3-3. Dimeric structure of MHMDS (M = Li, Na, K and Rb) with NH_3 in the solid state.

However, several aspects remain to be investigated in more detail. It should be proved how the concentration of NH_3 and MHMDS and the temperature influence the solution structures. The concentration of ammonia could be easily increased *e.g.* by introducing gaseous ammonia at low temperature to the NMR-sample. Finally, it would be also interesting to investigate the solution structures of the heavier analogues Rb- and CsHMDS.

Furthermore, single crystals of Hauser base $^i\text{Pr}_2\text{NMgCl}$ **7** and *Turbo* Hauser base $^i\text{Pr}_2\text{NMgCl} \cdot \text{LiCl}$ **9** were grown and analyzed in THF solution by DOSY-ECC-MW-determinations. The results show that their aggregation in THF- d_8 differs significantly and that the solution composition of the existing species is highly temperature dependent.^[137] Knowing the position of the equilibrium is of essential importance for every synthetic chemist, since Hauser bases as well as their *Turbo* analogues are used in synthetic protocols at various temperatures (-75°C to 25°C).^[16, 23] The solution structure of **7** is best represented by the common Schlenk-equilibrium with heteroleptic **M1** as the main species

at high temperatures and homoleptic **M2** at low temperatures (Fig. 3-4a). However, it was also shown that in Hauser base **7** dimeric species are also present in the THF solution although alkyl magnesium chlorides do not dimerize in that solvent. Therefore, the Hauser base **7** Schlenk-equilibrium has to be extended to dimeric amido bridged species and additionally to MgCl_2 co-coordinated species which exist only at low temperatures, where an excess of MgCl_2 is present.

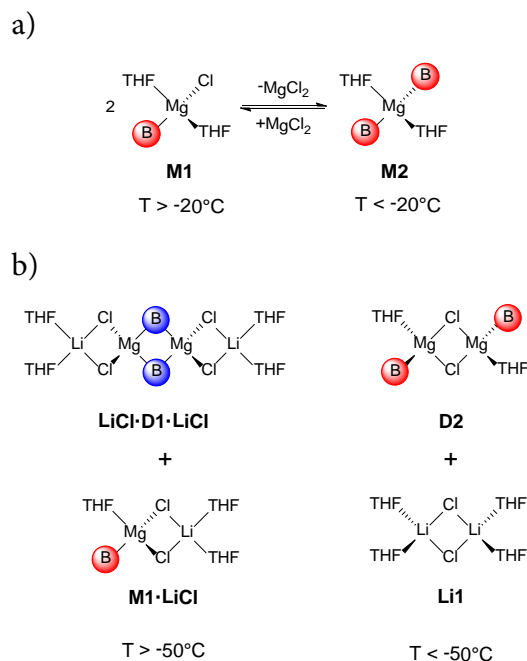


Fig. 3-4. Main species of a) Hauser base $i\text{Pr}_2\text{NMgCl}$ **7** and b) *Turbo*-Hauser base $i\text{Pr}_2\text{NMgCl}\cdot\text{LiCl}$ **9** in THF- d_8 solution with $\text{B} = i\text{Pr}_2\text{N}^-$.^[137]

It was then demonstrated that the addition of LiCl to **7** has an enormous impact on the Schlenk-equilibrium. The hypothesis that the impact of LiCl on the higher reactivity of *Turbo* bases rests on the deaggregation of RMgX oligomers to monomers^[23, 28] has to be revised. Moreover, the main advantage of LiCl is the ability to shift the Schlenk-equilibrium from the homoleptic to the heteroleptic side. At RT monomeric **M1·LiCl** and dimeric **LiCl·D1·LiCl** are the main species in solution of **9** (Fig. 3-4b), while the latter is the most populated species at high concentration (0.5 to 0.6 M). Lowering the temperature below -50°C results in the formation of **D2** and the LiCl-dimer **Li1**. The latter stabilizes the heteroleptic dimer **D2** and inhibits the formation of homoleptic $(i\text{Pr}_2\text{N})_2\text{Mg}$ (**M2**) and MgCl_2 . It is possible that this concept could also be applied to *Turbo*-Grignard reagents.

Finally, the structure of *Turbo*-Hauser base $\text{TMPMgCl}\cdot\text{LiCl}$ **10** was investigated in $\text{THF-}d_8$ solution. DOSY-ECC-MW-determinations and $^1\text{H-}^7\text{Li}$ -HOESY experiments confirm that lithium chloride indeed co-coordinates to the magnesium amides in solution as observed in the *Turbo*-Hauser base **9**.^[137] A detectable population of the solvent separated lithium cation **Li2** can also be excluded for *Turbo*-Hauser base **10** ($MW_{\text{calc}} = 295 \text{ g/mol}$, $MW_{\text{det}} = 387 \text{ g/mol}$, $MW_{\text{err}} = -31\%$).

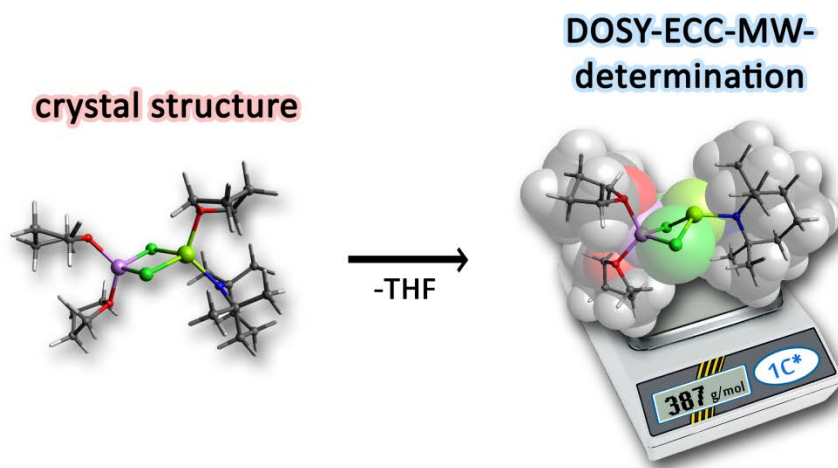


Fig. 3-5. Illustration of the DOSY-ECC-MW-determination of *Turbo*-Hauser base $\text{TMPMgCl}\cdot\text{LiCl}$ **10** in $\text{THF-}d_8$ solution.

The results show that changing the steric demand and the electronic properties of the amide strongly controls the structural features, both in the solid state as well as in solution. While **10** is a monomer in the solid state and in solution, **9** is a dimer in the crystal structure and forms predominately dimeric aggregates in THF-solution.^[137] From our measurements the different reactivities can be rationalized as followed: The TMP ligand in $\text{TMPMgCl}\cdot\text{LiCl}$ **10** is bulky enough to prevent dimerization and to promote a LiCl solubilized monomer **1C*** (Fig. 3-5).^[137] Similarly the considerable steric demand provided by the fixed methyl groups facilitates the cleavage of a labile THF ligand and induces an unsaturated magnesium site. In $^i\text{Pr}_2\text{NMgCl}\cdot\text{LiCl}$ **9** the rigid TMP ligand is replaced by two floppy diisopropyl groups and the methyl groups are not fixed in a static position relative to the metal. This flexibility permits both, a direct THF coordination at the Mg cation *and* a dimerization of the lithium stabilized monomer **M1·LiCl** to form the tetranuclear dimer **LiCl·D1·LiCl**. The latter is at high concentrations the main aggregate in solution.^[28, 137] That would also explain the limited solubility of dimeric **9** in THF (0.6 M) compared to the TMP-*Turbo*-Hauser base **10** (1.2 M) that is monomeric at all concentrations. Therefore, reactions of **10** should predominately involve a monomeric and those of **9** mainly a dimeric attack at the reactant.^[137] Beside the unsaturated magnesium atom in **10** this explains the

extreme high reactivity of **10**, reminiscent of the general higher reactivity of monomeric organometallics in comparison to their oligomeric analogues.^[138]

In summary, this work illustrates that the DOSY-ECC-method adds profound conceptual value to study aggregation in solution. Additionally, the presented organometallic solution structures provide details on reaction conditions which should have a tremendous impact on modified reaction protocols.

4 EXPERIMENTAL PART

4.1 Techniques and Experiments

4.1.1 Handling of Air- and Moisture Sensitive Compounds

All air- and moisture sensitive compounds were manipulated with standard Schlenk techniques^[139] either in an inert atmosphere of purified and dry argon or in an argon glove box. The glassware was dried at 140°C, assembled hot and cooled down under high vacuum. All solvents were dried with standard drying techniques over sodium, potassium or sodium-potassium alloy and were distilled prior to use.

4.1.2 NMR Experiments

NMR experiments were recorded either on Bruker Avance 400 spectrometer equipped with an observe broadband probe with z-axis gradient coil with maximum gradient strength of 57 G/cm or on Bruker Ascend 400 spectrometer equipped with an inverse broadband probe with z-axis gradient coil with maximum gradient strength of 51 G/cm. All spectra were acquired using 5 mm NMR tubes, which were not spun during the measurements. Chemical shifts (δ) are given in ppm relative to TMS using the residual solvent signals as internal standards. Coupling constants (J) are reported in Hz and standard abbreviations indicating multiplicity are used as follows:

s = singlet, d = doublet, t = triplet, sept = septet, m = multiplet and br = broad.

4.1.2.1 DOSY-NMR-Experiments

Dry TOL-*d*₈ or THF-*d*₈ kept with 4 Å molecular sieves under argon was used. The NMR samples were prepared by solving either purified or crystalline compounds (0.015-0.120 M) and a DOSY reference under argon atmosphere in the deuterated NMR solvent. In the case of Li-, Na-, and KHMDS gaseous ND₃ was introduced to the solution (approximately one minute at +25°C). Finally, the NMR-tubes were sealed and DOSY measurements were performed at RT. For all DOSY-NMR measurements the diffusion coefficient of the analyte was normalized to the fixed diffusion value of the internal reference. All DOSY experi-

ments were performed using a double stimulated echo sequence with bipolar gradient pulses and three spoil gradients with convection compensation (dstebpgp3s).^[91, 96] The duration of the magnetic field pulse gradients was adjusted for every temperature in a range of $\delta/2 = 400\text{--}3500\ \mu\text{s}$. The diffusion time was $\Delta = 0.1\ \text{s}$. The delay for gradient recovery was 0.2 ms and the eddy current delay 5 ms. In each PFG NMR experiment, a series of 16 spectra on 32 K data points were collected. The pulse gradients were incremented from 2 to 98% of the maximum gradient strength in a linear ramp. After Fourier transformation and baseline correction, the diffusion dimension was processed with the Topspin 3.1 software. Diffusion coefficients, processed with a line broadening of 2 Hz, were calculated by Gaussian fits with the T1/T2 software of Topspin.

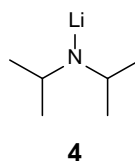
4.1.3 Computational Details

All structures included in this Ph. D. thesis were optimized at the B3LYP-D3/def2-SVP level of theory^[122] (the dispersion corrections were computed with *Becke-Johnson* type damping).^[140] The electronic energies were recomputed with the def2-TZVP basis set.^[122b] Solvation effects were included through the use of the COSMO continuum model^[123] both in the energy and optimization runs. All stationary points were confirmed to be true minima on the potential energy surface through harmonic vibrational calculations. All thermodynamic correction terms were derived from the latter. In order to deal with the large errors associated with low-energy vibrational modes (particularly in large complexes) we applied the quasi-rigid rotor harmonic oscillator formula proposed by *Grimme*,^[141] with a cutoff parameter of $100\ \text{cm}^{-1}$. Furthermore, corrections were included to the entropy to account for the overestimation of translational freedom in solution. The latter was included taking a cell model for the change in translational degrees of freedom.^[134] All reported energy values, unless otherwise noted, correspond to free energies. All calculations were carried out with the Orca 3.0.3 program package.^[142]

4.2 Synthesis and Crystallization

4.2.1 Donor-Base-Free LDA

Diisopropyl amine (15.58 g, 0.15 mol, 1.07 equiv) was dissolved in dry pentane (150 mL). At 0°C n BuLi (5.64 mol/L, 25 mL, 0.14 mol, 1.00 equiv) was added dropwise to the solution. After 20 min the reaction mixture was warmed up to RT and then stirred for 1 h. The reaction mixture was then slowly cooled down to -78°C . After 3 h the mother liquor was removed via a syringe. Finally the solvent was evaporated at RT under vacuum (approx. 6 h) to afford **4** as a white solid (10.41 g, 0.10 mol, 71%).



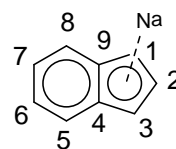
$^1\text{H-NMR}$ δ (ppm) = 0.99 (d, $^3J_{\text{HH}} = 6.5$ Hz, 12H, $-\text{CH}_3$), 3.02 (sept, $^3J_{\text{HH}} = 6.3$ Hz, 2H, $-\text{CH}$).
(400.13 MHz, $\text{THF-}d_8$, 25°C):

$^7\text{Li-NMR}$ δ (ppm) = 2.03 (s).
(155.51 MHz, $\text{THF-}d_8$, 25°C):

$^{13}\text{C}\{^1\text{H}\}\text{-NMR}$ δ (ppm) = 26.7 (s, $-\text{CH}_3$), 51.1 (s, $-\text{CH}$).
(100.62 MHz, $\text{THF-}d_8$, 25°C):

4.2.2 Na-Indenide

NaHMDS (0.73 g, 4.00 mmol, 1.00 equiv) was dissolved in dry pentane (22 mL). At RT indene (0.56 g, 4.80 mmol, 1.20 equiv) was added dropwise and the reaction mixture was warmed up to +70°C and stirred for 30 min at this temperature. Finally, the product was washed at RT with pentane (2x 15 mL) and dried under vacuum (approx. 6 h) to afford **73** as reddish solid (0.45 g, 3.24 mmol, 81%).



73

¹H-NMR

(400.13 MHz, THF-*d*₈, 25°C): δ (ppm) = 5.90 (d, $^3J_{\text{HH}} = 3.1$ Hz, 2H, H1/H3), 6.36 (m, 2H, H6/H7), 6.56 (t, $^3J_{\text{HH}} = 3.0$ Hz, 1H, H2), 7.27 (m, 2H, H5/H8).

¹³C{¹H}-NMR

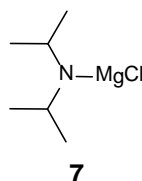
(100.62 MHz, THF-*d*₈, 25°C): δ (ppm) = 91.2 (s, C1, C3), 112.4 (s, C5, C8), 115.5 (s, C2), 118.3 (s, C6, C7), 128.4 (s, C4, C9).

4.2.3 MHMDS-Ammoniacates (M = Li, Na, K, Rb and Cs)

Each of the described complexes was prepared in a similar manner. MHMDS (*m* = 0.5 g) was kept under argon atmosphere due to its hygroscopic character. After cooling the flask to -78°C gaseous ammonia (approx. 15 mL) was condensed in the crystallization Schlenk flask till all MHMDS was dissolved. After dissolving, the ammonia solution was overfilled with dry toluene (15 mL). Finally the colorless solution was warmed to +25°C so excess ammonia could evaporate. Afterwards storage at -45°C afforded colorless crystals of **65-68** within some days which finally were suitable for X-ray structure analysis (see chapter 4.4.1 to 4.4.5). Intermediate **71** was crystallized from a solution which was warmed up to 0°C instead of +25°C. Unfortunately, the crystals were not stable at temperatures higher than -33°C. This is why it was not possible to investigate in NMR measurements of re-dissolved ammoniacate crystals.

4.2.4 $i\text{Pr}_2\text{NMgCl}$

$i\text{PrMgCl}$ (62.10 mmol, 31.05 mL, 2 M in THF, 1.0 equiv) was dropped to bulk diisopropylamine $i\text{Pr}_2\text{NH}$ (68.31 mmol, 9.60 mL, 1.1 equiv) at RT. Stirring overnight and removal of the solvent *in vacuo* yielded an offwhite powder (11.68 g, 96%, considering the loss of one molecule of THF). To receive crystalline product a saturated THF solution (24 mL) of $[7\cdot\text{THF}]_2$ was prepared at RT. After reducing the solvent, addition of 5 mL toluene and storage at -6°C $[7\cdot\text{THF}]_2$ was isolated as colourless crystals which were suitable for single crystal X-ray analysis (see chapter 4.4.6).

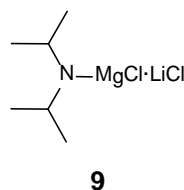


$^1\text{H-NMR}$ δ (ppm) = 1.01 (d, $^3J_{\text{HH}} = 6.1$ Hz, 12H, $-\text{CH}_3$), 2.94 (400.13 MHz, THF- d_8 , 25°C): (sept, $^3J_{\text{HH}} = 6.4$ Hz, 2H, $-\text{CH}$).

$^{13}\text{C}\{^1\text{H}\}\text{-NMR}$ δ (ppm) = 26.9 (s, $-\text{CH}_3$), 50.8 (s, $-\text{CH}$). (100.62 MHz, THF- d_8 , 25°C):

4.2.5 $i\text{Pr}_2\text{NMgCl}\cdot\text{LiCl}$

In a modified preparation route of *Armstrong*,^[28] the *Turbo*-Hauser base $[9\cdot\text{THF}]_2$ was synthesized by reaction of LDA (0.43 g, 4.00 mmol, 1.0 equiv) and a suspension of MgCl_2 (0.38 g, 4.00 mmol, 1.0 equiv) in dry THF (10 mL) and stirring the mixture at RT overnight. Removing the solvent *in vacuo* and recrystallization (2x) in a 1:1 mixture of THF/hexane at -45°C afforded $[9\cdot\text{THF}]_2$ as colourless crystals. The mother liquor was removed *via* a syringe at -45°C and the crystals were washed with cold hexane (2x 10 mL). Finally, the structure was proven *via* X-Ray diffraction: Space group $P2_1/n$; $a = 10.317 \text{ \AA}$, $b = 16.658 \text{ \AA}$, $c = 11.859 \text{ \AA}$; $\beta = 109.14^\circ$.^[28]



$^1\text{H-NMR}$ *Monomer:* δ (ppm) = 1.03 (d, $^3J_{\text{HH}} = 6.2$ Hz, 12H, $-\text{CH}_3$), 2.93 (400.13 MHz, THF- d_8 , 25°C):

(sept, $^3J_{\text{HH}} = 6.1$ Hz, 2H, $-\text{CH}$).

Dimer:

δ (ppm) = 1.33 (d, $^3J_{\text{HH}} = 5.5$ Hz, 12H, $-\text{CH}_3$), 3.42 (br, 2H, $-\text{CH}$).

^7Li -NMR

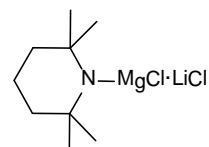
(155.51 MHz, THF- d_8 , 25°C): δ (ppm) = 0.18 (s)

$^{13}\text{C}\{^1\text{H}\}$ -NMR

(100.62 MHz, THF- d_8 , 25°C): δ (ppm) = 27.4 ($-\text{CH}_3$), 48.1 ($-\text{CH}$), 53.2 ($-\text{CH}$).

4.2.6 TMPMgCl·LiCl

In a modified preparation route of *Álvarez*,^[72] the *Turbo*-Hauser base $\mathbf{10}\cdot(\text{THF})_3$ was synthesized by reaction of LiTMP (0.59 g, 4.00 mmol, 1.0 equiv) and a suspension of MgCl_2 (0.38 g, 4 mmol, 1.0 equiv) in dry THF (10 mL) and stirring the mixture at RT overnight. Removing the solvent *in vacuo* and recrystallization (2x) in a 1:1 mixture of THF/hexane at -45°C afforded $\mathbf{10}\cdot(\text{THF})_3$ as colourless crystals. The mother liquor was removed *via* a syringe at -45°C and the crystals were washed with cold hexane (2x 10 mL). Finally, the structure was proven via X-Ray diffraction: Space group $P2_1/c$; $a = 8.313$ Å, $b = 26.214$ Å, $c = 14.116$ Å; $\beta = 120.53^\circ$.^[72]



10

^1H -NMR

(400.13 MHz, THF- d_8 , 25°C): δ (ppm) = 1.18 (s, 12H, $-\text{CH}_3$), 1.20 (t, $^3J_{\text{HH}} = 6.1$ Hz, 4H, β - CH_2), 1.60 (m, 2H, γ - CH_2).

^7Li -NMR

(155.51 MHz, THF- d_8 , 25°C): δ (ppm) = 0.24 (s)

$^{13}\text{C}\{^1\text{H}\}$ -NMR

(100.62 MHz, THF- d_8 , 25°C): δ (ppm) = 21.0 (γ - CH_2), 36.2 ($-\text{CH}_3$), 43.0 (β - CH_2), 52.3 (α - CH_2).

4.3 Preparation of DOSY-NMR-Samples

4.3.1 Internal References

In THF- d_8 : Internal reference TMB and analyte (see A-Table 7 in the appendix) were dissolved in equimolar ratio (each 15 mM) and DOSY measurements were performed immediately at 25°C. Low temperature measurements were performed at -75 to +60°C with TTS and ADAM as internal reference (each 15 mM).

In TOL- d_8 : Internal reference ADAM and analyte (see A-Table 6 in the appendix) were dissolved in equimolar ratio (each 15 mM) and DOSY measurements were performed immediately at 25°C. For high concentration measurements ADAM and analytes were dissolved in equimolar ratio (each 120 mM) to give a final concentration of 240 mM. Low temperature measurements were performed at -75 to +100°C with TTS and ADAM as internal reference (each 15 mM).

4.3.2 LDA

In THF- d_8 : Internal reference TMB and donor-base-free LDA (see chapter 4.2.1) were dissolved in equimolar ratio (each 15 mM) and DOSY measurements were performed at 25°C.

In TOL- d_8 : Internal reference ADAM and donor-base-free LDA (see chapter 4.2.1) were dissolved in equimolar ratio (each 15 mM) and DOSY measurements were performed at 25°C, -50°C and finally at +100°C.

4.3.3 Na-Indenide

Internal reference TMB and donor-base-free Na-indenide (see chapter 0) were dissolved in THF- d_8 (each 15 mM). DOSY spectra were collected at 25°C to -50°C and finally at +60°C.

4.3.4 MHMDS-Ammoniacates (M = Li, Na and K)

Internal reference ADAM and MHMDS were dissolved in TOL- d_8 (each 15 mM). Under Schlenk conditions gaseous ND_3 was introduced for approximately 1 min to the NMR sample at 25°C. Finally, the NMR-tubes were sealed and DOSY measurements were performed at 25°C.

4.3.5 $^i\text{Pr}_2\text{NMgCl}$ and $^i\text{Pr}_2\text{NMgCl}\cdot\text{LiCl}$

Internal reference PhN (20 mM) and crystalline $[\mathbf{7}\cdot\text{THF}]_2$ or $[\mathbf{9}\cdot\text{THF}]_2$ (100 mM) were dissolved in THF- d_8 . DOSY spectra were collected at 25°C to -100°C.

4.3.6 $\text{TMPMgCl}\cdot\text{LiCl}$

Internal reference PhN and crystalline $\mathbf{10}\cdot(\text{THF})_3$ (each 20 mM) were dissolved in THF- d_8 . DOSY spectra were collected at 25°C to -75°C.

4.4 X-Ray Analysis

Single crystals were selected due to their sensitivity and reactivity in inert perfluorinated oil.^[143] The X-ray data sets of **65** and **66** were collected at 100(2) K on a Bruker Smart Apex II Ultra diffractometer equipped with a Bruker Rotating Anode with Mo- K_α radiation ($\lambda = 0.71073 \text{ \AA}$). The X-ray data sets of $[\mathbf{7}\cdot\text{THF}]_2$, **67**, **68** and **71** were collected at 100(2) K on a Bruker Smart Apex II Quazar diffractometer with an Incoatec micro source^[144] equipped with mirror-monochromated Mo- K_α radiation ($\lambda = 0.71073 \text{ \AA}$). The data were integrated with SAINT^[145] and a semi-empirical absorption correction with SADABS^[146] was applied. The structures were solved by direct methods with SHELXT^[147] and refined by full-matrix least-squares on F^2 for all data with SHELXL.^[148] Non-hydrogen atoms were refined with anisotropic displacement parameters. Nitrogen-attached hydrogen atoms were located in the difference Fourier map and refined isotropically using distance similarity restraints for all N-H and H...H-1,2-distances. All other hydrogen atoms were placed in calculated positions and refined using a riding model.^[149]

4.4.1 $[\text{NH}_3 \cdot \text{LiN}(\text{SiMe}_3)_2]_2 \cdot \text{TOL}$

4.4.1.1 Crystal Data

Formula: $\text{C}_{19}\text{H}_{50}\text{Li}_2\text{N}_4\text{Si}_4$, $M = 460.87$ g/mol, triclinic space group $P\bar{1}$, $a = 9.561(2)$, $b = 11.710(2)$, $c = 15.437(3)$ Å, $\alpha = 92.96(2)^\circ$, $\beta = 105.26(2)^\circ$, $\gamma = 110.88(2)^\circ$, $V = 1537.5(6)$ Å³, $Z = 2$, $\mu(\text{MoK}\alpha) = 0.205$ mm⁻¹, 70826 reflections collected, 6034 independent reflections ($R_{\text{int}} = 1.88\%$), $\theta_{\text{max}} = 26.02^\circ$, 293 parameters refined, 30 restraints used, $R_1[I > 2\sigma(I)] = 4.64\%$, $wR_2(\text{all data}) = 11.87\%$, GooF = 1.231, largest diff. peak and hole 0.386 and -0.322 eÅ⁻³.

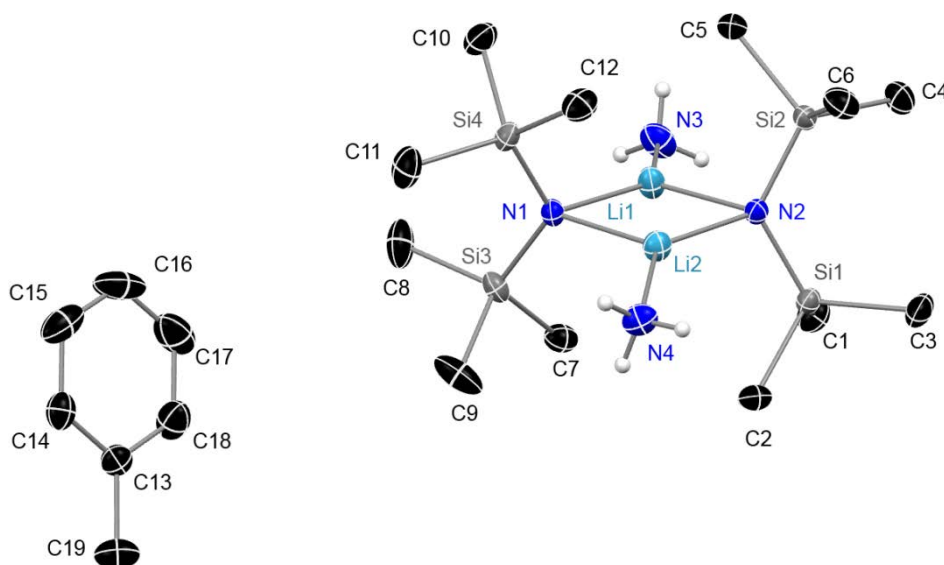


Fig. 4-1. Asymmetric unit of **65**·TOL with carbon bound hydrogen atoms omitted for clarity. Anisotropic displacement parameters are depicted at the 50% probability level.

Selected bond lengths (Å) and angles (°): N1–Si1 1.696(2), N1–Si2 1.698(2), N1–Li2 2.032(5), N1–Li1 2.044(5), N2–Li1 2.029(5), N2–Si3 1.695(2), N2–Si4 1.697(2), N2–Li2 2.031(5), N3–Li1 2.044(5), N4–Li2 2.046(5); Si1–N1–Si2 123.6(1), Si3–N2–Si4 122.7(1), N2–Li2–N1 105.6(2), N2–Li1–N1 105.2(2), Li2–N1–Li1 74.4(2), Li1–N2–Li2 74.7(2).

4.4.2 $[\text{NH}_3 \cdot \text{NaN}(\text{SiMe}_3)_2]_2$

4.4.2.1 Crystal Data

Formula: $\text{C}_{12}\text{H}_{42}\text{N}_4\text{Na}_2\text{Si}_4$, $M = 400.83$ g/mol, triclinic space group $P\bar{1}$, $a = 9.459(2)$, $b = 10.088(2)$, $c = 14.539(3)$ Å, $\alpha = 72.76(2)^\circ$, $\beta = 84.69(2)^\circ$, $\gamma = 84.69(2)^\circ$, $V = 84.69(2)^\circ$ Å³, $Z = 2$, $\mu(\text{MoK}\alpha) = 0.260$ mm⁻¹, 83314 reflections collected, 5797 independent reflections ($R_{\text{int}} = 2.16\%$), $\theta_{\text{max}} = 27.12^\circ$, 230 parameters refined, 30 restraints used, $R_1[I > 2\sigma(I)] = 3.25\%$, $wR_2(\text{all data}) = 8.51\%$, GooF = 1.158, largest diff. peak and hole 0.418 and -0.301 eÅ⁻³.

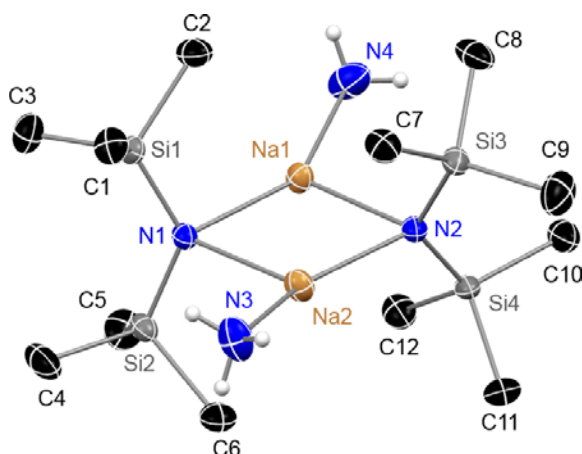


Fig. 4-2. Asymmetric unit of **66** with carbon bound hydrogen atoms omitted for clarity. Anisotropic displacement parameters are depicted at the 50% probability level.

The structure of **66** was refined as a twin with BASF = 0.5. Selected bond lengths (Å) and angles (°): N1–Si1 1.684(2), N1–Si1 1.684(2), N1–Si2 1.682(2), N1–Na1 2.401(2), N1–Na2 2.396(2), N2–Si3 1.683(2), N2–Si3 1.683(2), N2–Na1 2.407(2), N2–Na2 2.384(2), N3–Na2 2.402(2), N4–Na1 2.420(2); Si2–N1–Si1 127.31(9), Si2–N1–Si1 127.31(9), N1–Na1–N2 100.00(5), N2–Na2–N1 100.82(5), Na2–N1–Na1 79.53(5), Na2–N2–Na1 79.64(5).

4.4.3 $[\text{NH}_3 \cdot \text{KN}(\text{SiMe}_3)_2]_2$

4.4.3.1 Crystal Data

Formula: $\text{C}_{12}\text{H}_{42}\text{K}_2\text{N}_4\text{Si}_4$, $M = 433.05$ g/mol, monoclinic space group $P2_1/n$, $a = 9.339(2)$, $b = 9.065(2)$, $c = 15.950(3)$ Å, $\beta = 97.92(2)^\circ$, $V = 1337.4(5)$ Å³, $Z = 2$, $\mu(\text{MoK}\alpha) = 0.536$ mm⁻¹, 44595 reflections collected, 3059 independent reflections ($R_{\text{int}} = 3.47\%$), $\theta_{\text{max}} = 27.48^\circ$, 134 parameters refined, 127 restraints used, $R_1[I > 2\sigma(I)] = 2.51\%$, $wR_2(\text{all data}) = 6.45\%$, GooF = 1.081, largest diff. peak and hole 0.272 and -0.191 eÅ⁻³.

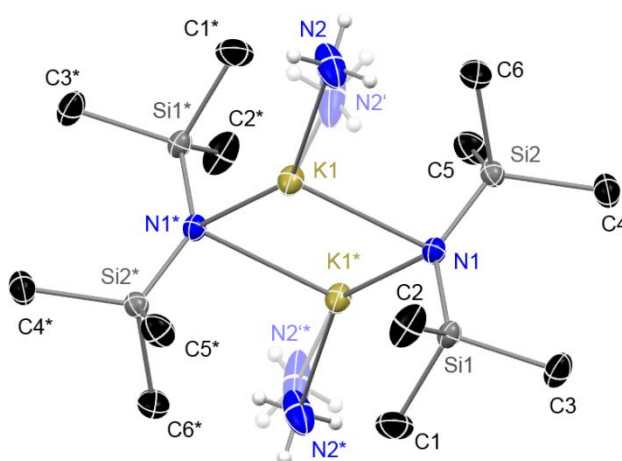


Fig. 4-3. Asymmetric unit of **67** with carbon bound hydrogen atoms omitted for clarity. Anisotropic displacement parameters are depicted at the 50% probability level.

Disorder of N2 and N2' was refined with restraints for K–N and H...K 1,2-distances an occupancy ratio of 0.570:0.430. Selected bond lengths (Å) and angles (°): N1–Si1 1.669(1), N1–Si2 1.669(1), N1–K1 2.792(1), N1–K1* 2.834(1), N2–K1 2.829(6), N2'–K1 2.839(8); N1–K1–N1* 92.76(3), K1–N1–K1* 87.23(3), Si1–N1–Si2 135.46(7). Atoms highlighted with an asterisk are symmetry generated by $2-x, 1-y, 1-z$.

4.4.4 $[\text{NH}_3 \cdot \text{RbN}(\text{SiMe}_3)_2]_2$

4.4.4.1 Crystal Data

Formula: $\text{C}_{12}\text{H}_{42}\text{N}_4\text{Rb}_2\text{Si}_4$, $M = 525.79$ g/mol, monoclinic space group $P2_1/c$, $a = 8.825(2)$, $b = 12.597(2)$, $c = 12.410(3)$ Å, $\beta = 106.88(2)^\circ$, $V = 12.410(3)$ Å³, $Z = 2$, $\mu(\text{MoK}\alpha) = 2.095$ mm⁻¹, 48496 reflections collected, 3043 independent reflections ($R_{\text{int}} = 10.21\%$), $\theta_{\text{max}} = 21.46^\circ$, 118 parameters refined, 40 restraints used, $R_1[I > 2\sigma(I)] = 2.52\%$, $wR_2(\text{all data}) = 5.00\%$, GooF = 1.018, largest diff. peak and hole 0.387 and -0.394 eÅ⁻³.

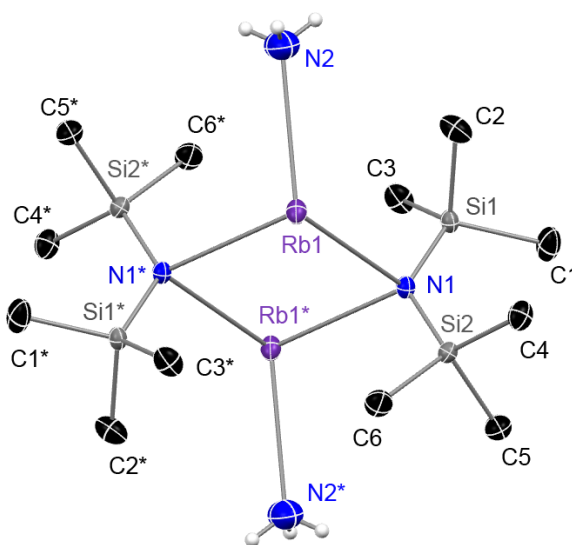


Fig. 4-4. Asymmetric unit of **68** with carbon bound hydrogen atoms omitted for clarity. Anisotropic displacement parameters are depicted at the 50% probability level.

Selected bond lengths (Å) and angles ($^\circ$): N1–Si1 1.676(2), N1–Si2 1.672(2), N1–Rb1 2.908(2), N1–Rb1* 3.016(2), N2–Rb1 3.014(3); N1–Rb1–N1* 95.83(4), Rb1–N1–Rb1* 84.17(4), Si2–N1–Si1 125.6(1). Atoms highlighted with an asterisk are symmetry generated by $-x, 1-y, -z$.

4.4.5 $(\text{NH}_3)_4 \cdot [\text{NaN}(\text{SiMe}_3)_2]_2$

4.4.5.1 Crystal Data

Formula: $\text{C}_{12}\text{H}_{48}\text{N}_6\text{Na}_2\text{Si}_4$, $M = 434.90$ g/mol, monoclinic space group $P2_1/n$, $a = 19.146(2)$, $b = 9.876(2)$, $c = 30.726(3)$ Å, $\beta = 91.82(2)^\circ$, $V = 5806.9(14)$ Å³, $Z = 8$, $\mu(\text{MoK}\alpha) = 0.242$ mm⁻¹, 205785 reflections collected, 11875 independent reflections ($R_{\text{int}} = 6.21\%$), $\theta_{\text{max}} = 26.37^\circ$, 529 parameters refined, 552 restraints used, $R_1[I > 2\sigma(I)] = 3.31\%$, $wR_2(\text{all data}) = 8.98\%$, GooF = 1.042, largest diff. peak and hole 0.510 and -0.232 eÅ⁻³.

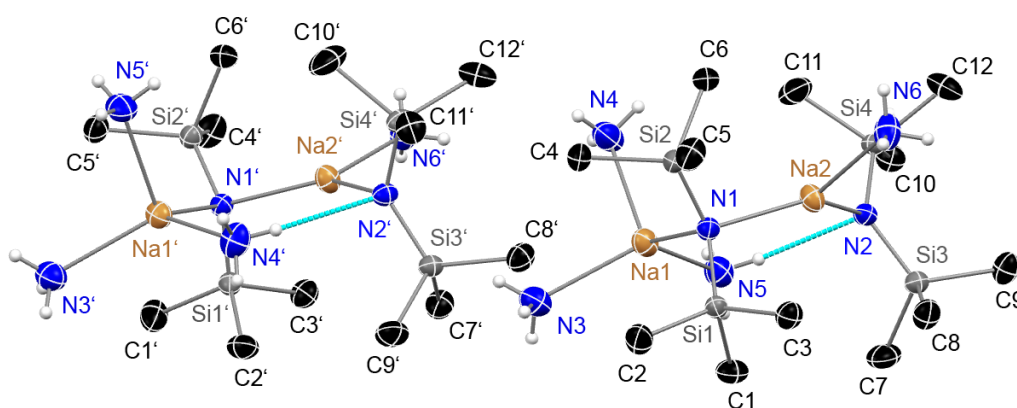


Fig. 4-5. Asymmetric unit of **71** with carbon bound hydrogen atoms omitted for clarity. The asymmetric unit contains two molecules. Anisotropic displacement parameters are depicted at the 50% probability level.

Selected bond lengths (Å) and angles ($^\circ$): N1–Si1 1.689(1), N1–Si2 1.685(1), N1–Na1 2.450(1), N1–Na2 2.387(1), N2–Si3 1.679(1), N2–Si4 1.670(1), N2–Na2 2.339(1), N3–Na1 2.472(2), N4–Na1 2.469(2), N5–Na1 2.432(2), N6–Na2 2.418(2), N5–N2 3.219(2), N5–H...N2 2.39(1); N5–H–N2 172(2), Si2–N1–Si1 125.35(8), Si4–N2–Si3 127.95(8), Na2–N1–Na1 95.34(5), N5–Na1–N1 111.71(5), N2–Na2–N1 137.77(5); N1'–Si1' 1.691(1), N1'–Si2' 1.683(1), N1'–Na1' 2.440(1), N1'–Na2' 2.386(1), N2'–Si3' 1.679(1), N2'–Si4' 1.669(1), N2'–Na2' 2.335(1), N3'–Na1' 2.469(2), N4'–Na1' 2.437(2), N5'–Na1' 2.477(2), N6'–Na2' 2.401(2), N4'–N2' 3.225(2), N4'–H...N2' 2.40(1); N4'–H–N2' 170(2), Si2'–N1'–Si1' 126.17(8), Si4'–N2'–Si3' 128.59(8), Na2'–N1'–Na1' 95.73(5), N5'–Na1'–N1' 116.92(6), N2'–Na2'–N1' 139.99(5).

4.4.6 [(THF)ClMg(μ -ⁱPr₂N)]₂

4.4.6.1 Crystal Data

Formula: C₂₀H₄₄Cl₂Mg₂N₂O₂, $M = 464.09$ g/mol, monoclinic, space group $P2_1/n$, $a = 9.766(2)$, $b = 9.648(2)$, $c = 14.138(3)$ Å, $\beta = 110.00(2)^\circ$, $V = 1251.8(4)$ Å³, $Z = 2$, $\mu(\text{MoK}\alpha) = 0.327$ mm⁻¹, 33818 reflections collected, 2666 independent reflections ($R_{\text{int}} = 3.91\%$), $\theta_{\text{max}} = 26.75^\circ$, 230 parameters refined, 686 restraints used, $R_1[I > 2\sigma(I)] = 3.00\%$, $wR_2(\text{all data}) = 7.96\%$, GooF = 1.067, largest diff. peak and hole 0.285 and -0.167 eÅ⁻³. Crystallographic data for compound [7·THF]₂ have been deposited at the Cambridge Crystallographic Data Centre (CCDC) 1423230.

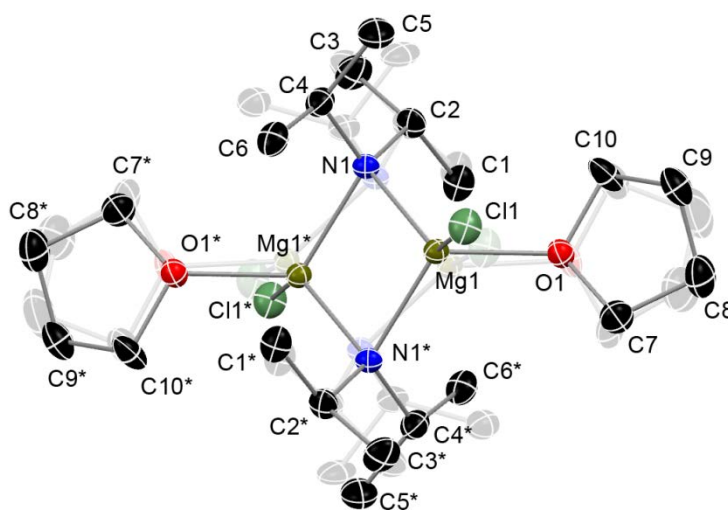


Fig. 4-6. Asymmetric unit of [7·THF]₂ with hydrogen atoms omitted for clarity. Anisotropic displacement parameters are depicted at the 50% probability level.

Selected bond lengths (Å) and angles (°): Mg1–N1 2.142(1), Mg1–N1* 2.142(3), Mg1–Cl1 2.324(1), Mg1–O1 2.070(6), N1–C2 1.510(3), N1–C4 1.503(3), O1–Mg1–N1 113.5(2), O1–Mg1–Cl1 91.8(1), N1*–Mg1–N1 96.9(1), Mg1*–N1–Mg1 83.2(1), N1–Mg1–N1*–Mg1' 0.0. Atoms highlighted with an asterisk are symmetry generated by $1-x, 1-y, 1-z$.

The structure is severely disordered and refined with distances restraints and restraints for the anisotropic displacement parameters.^[149] However, the disorder was deconvoluted and refined successfully. The occupancy ratio was refined to 0.809:0.191. This disorder seems to be an inherent problem with this structure, since *García-Álvarez* and *Mulvey et al.* had also problems to crystallize non-disordered crystals of the related LiCl coordinated compound **LiCl·D1·LiCl**.^[28]

5 Appendix

Estimating the Maximum Error of $\log D_{x,\text{norm}}$ in TOL- d_8 and THF- d_8

All measurements were performed at 25°C. All compounds have been measured in 15 mM solutions of analyte and reference in an equimolar ratio. The absolute diffusion coefficients (D_x) of all compounds are different on each NMR device. But the normalized diffusion coefficients $\log D_{x,\text{norm}}$ shows on all devices nearly the same value with a small average standard deviation of $\sigma = 0.0028$ in TOL- d_8 and $\sigma = 0.0020$ in THF- d_8 , see A-Table 1 and A-Table 2.

A-Table 1. Diffusion parameter measured on two different NMR-devices (in TOL- d_8 with ADAM as internal reference).

Compound	Device 1 ^{a)}			Device 2 ^{b)}			Average	std. dev
	$\log D_x$	$\log D_{x,\text{norm}}$	$\log D_{\text{ref}}$	$\log D_x$	$\log D_{x,\text{norm}}$	$\log D_{\text{ref}}$	$\log D_{x,\text{norm}}$	σ
TMS	-8.6449	-8.7453	-8.7450	-8.7445	-8.7437	-8.8462	-8.7445	0.0012
ADAM	-8.7450	-8.8454	-8.7450	-8.8462	-8.8454	-8.8462	-8.8454	0.0000
N(SiMe ₃) ₃	-8.8570	-8.9525	-8.7498	-8.9454	-8.9421	-8.8486	-8.9473	0.0074
Si(SiMe ₃) ₄	-8.9090	-9.0077	-8.7467	-9.0031	-8.9998	-8.8486	-9.0038	0.0056
Cyclopentane	-8.5712	-8.6702	-8.7464	-8.6664	-8.6686	-8.8431	-8.6694	0.0011
THF	-8.5753	-8.6752	-8.7455	-8.6743	-8.6698	-8.8499	-8.6725	0.0038
TOL- d_7	-8.6334	-8.7338	-8.7450	-8.7366	-8.7358	-8.8462	-8.7348	0.0014
Indene	-8.6733	-8.7705	-8.7481	-8.7742	-8.7691	-8.8505	-8.7698	0.0010
Naphthaline	-8.7018	-8.7966	-8.7506	-8.7962	-8.7898	-8.8517	-8.7932	0.0048
2-Phenylpyridine	-8.7625	-8.8592	-8.7486	-8.8598	-8.8559	-8.8492	-8.8576	0.0023
1-Phenylnaphthaline	-8.8239	-8.9182	-8.7510	-8.9255	-8.9186	-8.8523	-8.9184	0.0003
Tri(o-tolyl)phosphine	-8.9562	-9.0476	-8.7540	-9.0499	-9.0402	-8.8551	-9.0439	0.0053
BINAP	-9.1258	-9.2235	-8.7476	-9.2339	-9.2337	-8.8456	-9.2286	0.0072
Anthracene	-8.7630	-8.8580	-8.7503	-8.8580	-8.8569	-8.8465	-8.8574	0.0008
9-Methylanthracene	-8.7820	-8.8790	-8.7484	-8.8900	-8.8858	-8.8496	-8.8824	0.0048
Pyrene	-8.7972	-8.8937	-8.7488	-8.9030	-8.8982	-8.8502	-8.8960	0.0031
Triphenylene	-8.8593	-8.9556	-8.7491	-8.9590	-8.9548	-8.8496	-8.9552	0.0006
TPhN	-9.0772	-9.1656	-8.7570	-9.1778	-9.1664	-8.8567	-9.1660	0.0006
a) Uncalibrated gradients							Average	0.0028
b) Calibrated gradients								

A-Table 2. Diffusion parameter measured on two different NMR-devices (in THF- d_8 and TMB as internal standard).

Compound	Device 1 ^{a)}			Device 2 ^{b)}			Average	std. dev
	$\log D_x$	$\log D_{x,\text{norm}}$	$\log D_{\text{ref}}$	$\log D_x$	$\log D_{x,\text{norm}}$	$\log D_{\text{ref}}$	$\log D_{x,\text{norm}}$	σ
TMS	-8.5969	-8.6993	-8.6724	-8.7018	-8.7043	-8.7724	-8.7018	0.0035
TMB	-8.6724	-8.7749	-8.6724	-8.7724	-8.7749	-8.7724	-8.7749	0.0000
N(SiMe ₃) ₃	-8.8091	-8.9124	-8.6716	-8.8993	-8.9018	-8.7724	-8.9071	0.0075
Si(SiMe ₃) ₄	-8.8765	-8.9787	-8.6726	-8.9767	-8.9759	-8.7757	-8.9773	0.0020
Cyclopentane	-8.5381	-8.6439	-8.6690	-8.6428	-8.6435	-8.7742	-8.6437	0.0003
THF- d_7	-8.5303	-8.6328	-8.6724	-8.6368	-8.6393	-8.7724	-8.6360	0.0046
Indene	-8.6276	-8.7326	-8.6698	-8.7306	-8.7323	-8.7731	-8.7325	0.0002
Naphthaline	-8.6432	-8.7458	-8.6722	-8.7459	-8.7464	-8.7744	-8.7461	0.0004
2-Phenylpyridine	-8.6950	-8.7996	-8.6702	-8.7968	-8.7980	-8.7737	-8.7988	0.0011
1-Phenylnaphthalin	-8.7762	-8.8799	-8.6712	-8.8918	-8.8812	-8.7854	-8.8806	0.0009
Tri(o-tolyl)phosphine	-8.8904	-8.9914	-8.6739	-8.9965	-8.9957	-8.7757	-8.9935	0.0030
BINAP	-9.0678	-9.1666	-8.6761	-9.1670	-9.1661	-8.7757	-9.1663	0.0003
Anthracene	-8.7083	-8.8140	-8.6692	-8.8118	-8.8117	-8.7749	-8.8129	0.0016
Pyrene	-8.7453	-8.8436	-8.6765	-8.8503	-8.8479	-8.7773	-8.8457	0.0030
Triphenylene	-8.7904	-8.8889	-8.6763	-8.8852	-8.8849	-8.7752	-8.8869	0.0028
TPhN	-9.0082	-9.1057	-8.6774	-9.1103	-9.1050	-8.7802	-9.1054	0.0005
							Average	0.0020

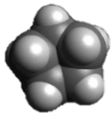
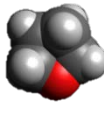

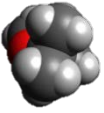
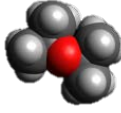
a) Uncalibrated gradients

b) Calibrated gradients

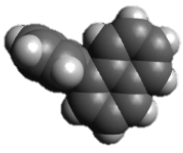
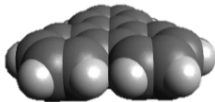

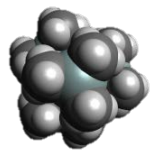
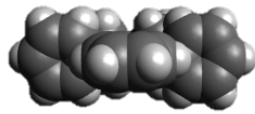
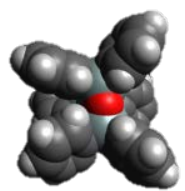
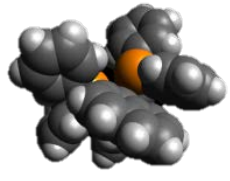
Overview of the Used Model Compounds for ECCs

Three dimensional models that were geometry optimized with the program Avogadro 1.1.0 have been generated. Of course the transitions between the shapes are not sharp but there are clear systematic trends that can be rationalized. A-Table 3 displays, that compact spherical (CS) molecules have nearly the same radius in all dimensions with a highly filled space. Dissipated spheres and ellipsoids (DSE) have an elongated main-axis and a less filled space. Small annelated aromatic compounds like toluene (92 g/mol), indene (116 g/mol) or naphthalene (128 g/mol) with $MW < 150$ g/mol diffuse DSE-like. Also diphenylacetylene (178 g/mol) that has an elongated molecule is still in the range of a DSE shape. The significance of one and two dimensional shapes begins approximately at $MW > 178$ g/mol. This is why the ECC_{ED} for extended discs (ED) begins with anthracene that has a MW of 178 g/mol.

A-Table 3. Classification of all model compounds appropriate to their shapes.

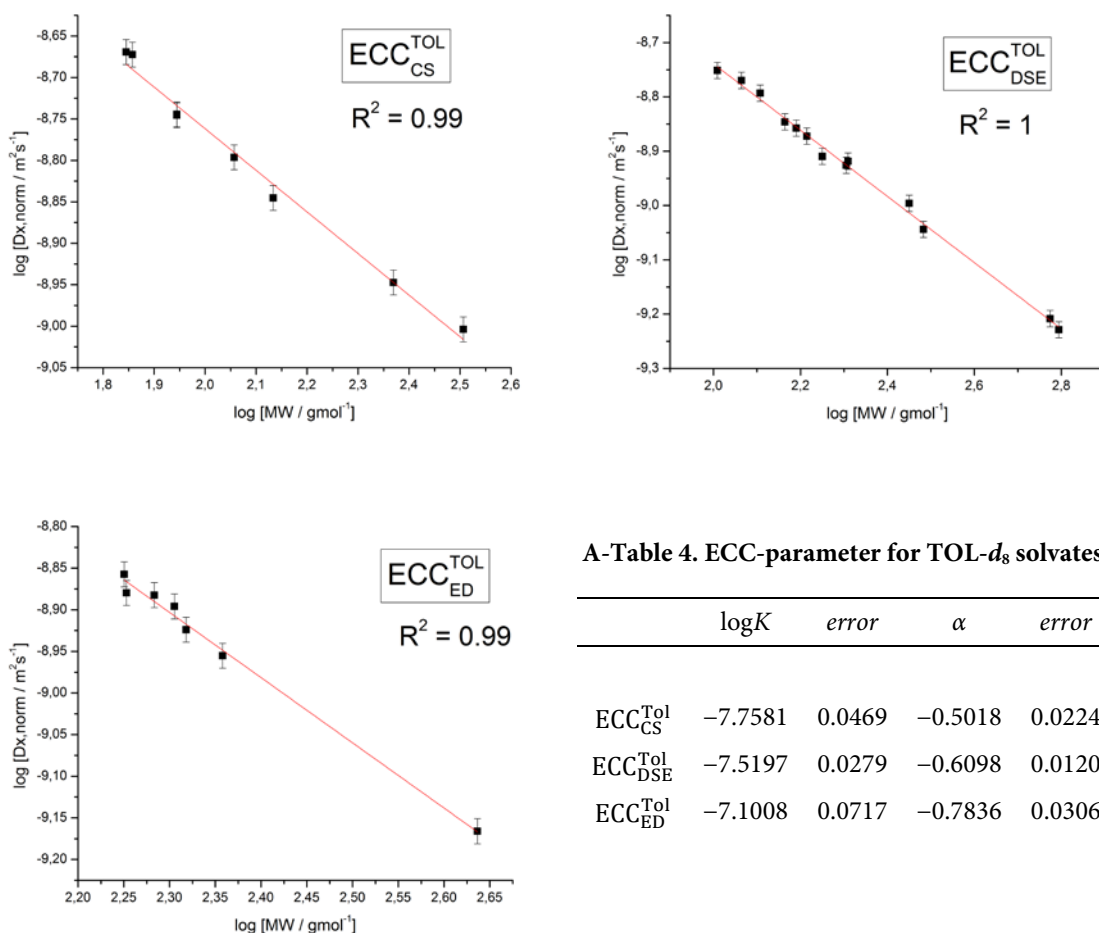
MW_{calc} [g/mol]	Compact Spheres [g/mol]	Dissipated Spheres and Ellipsoids [g/mol]	Expanded Discs [g/mol]
70-90	 Cyclopentane (70)		
	 THF (72)		
	 TMS (88)		
	 MTBE (88)		
100			 Diisopropylether (102)

MW_{calc} [g/mol]	Compact Spheres [g/mol]	Dissipated Spheres and Ellipsoids [g/mol]	Expanded Discs [g/mol]	
100	TMB (114)	Indene (116)		
	ADAM (136)	Naphthaline (128)		
		1,3-Indandione (146)		
		2-Phenylpyridine (155)		
			Anthracene (178)	
		Tetramethoxypropane (164)	Acridine (179)	
		Diphenylacetylene (178)	9-Methylanthracene (192)	
	200			Pyrene (202)
		N(SiMe ₃) ₃ (234)	Diphenylsulfoxide (202)	Anthtacinone (208)

MW_{calc} [g/mol]	Compact Spheres [g/mol]	Dissipated Spheres and Ellipsoids [g/mol]	Expanded Discs [g/mol]
200		 1-Phenylnaphthalene (204)	 Triphenylene (228)
300		 Tri(o-tolyl)phosphine (304)	
	 S(SiMe ₃) ₄ (321)		
400			 Tetraphenylnaphthalene (433)
500		 Hexaphenyltrisiloxane (595)	
600		 BINAP (623)	

External Calibration Curves

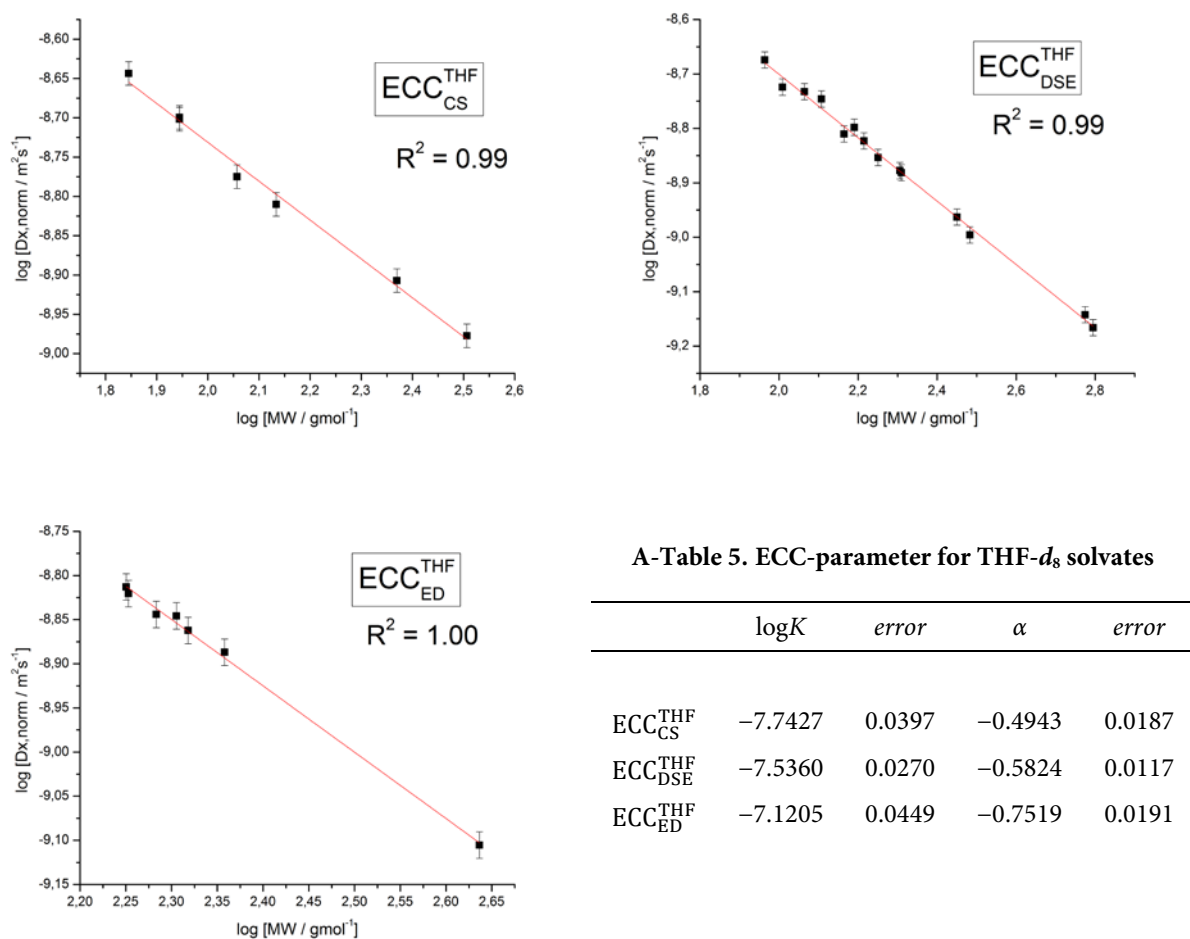
The maximum deviation of $\log D_{x,\text{norm}}$ was 0.0075, which is approximately the width at half maximum of a DOSY signal. This is the reason why the maximum $\Delta \log D_{x,\text{norm}}$ was defined as 2×0.0075 which is reflected in the error bars in the calibration plots:



A-Table 4. ECC-parameter for TOL- d_8 solvates.

	$\log K$	<i>error</i>	α	<i>error</i>
$\text{ECC}_{\text{CS}}^{\text{Tol}}$	-7.7581	0.0469	-0.5018	0.0224
$\text{ECC}_{\text{DSE}}^{\text{Tol}}$	-7.5197	0.0279	-0.6098	0.0120
$\text{ECC}_{\text{ED}}^{\text{Tol}}$	-7.1008	0.0717	-0.7836	0.0306

A-Figure 1. Plots of $\log D_{x,\text{norm}}$ vs $\log MW$ in TOL- d_8 of all model compounds sorted by their molecular shape. The linear fits show very high accuracy indicated by corr. $R^2 \geq 0.99$.



A-Figure 2. Plots of $\log D_{x,\text{norm}}$ vs $\log MW$ in THF-*d*₈ of all model compounds sorted by their molecular shape. The linear fits show very high accuracy indicated by corr. $R^2 \geq 0.99$.

A-Table 6. Overview of the used model compounds for ECC^{TOL} and their normalized diffusion coefficients $\log D_{x,norm}$, the determined MW_{det} and the deviation from the real molecular weight MW_{err} .^{a)} ADAM was used as the internal reference with $\log D_{ref,fix}$ (ADAM) = -8.8454 . All compounds have been measured in 15 mM solutions of analyte and ADAM in an equimolar ratio.

MW_{calc} [g/mol]	<i>Compact Spheres, ECC_{CS}</i>	$D_{x,norm}$ [m ² /s]	$\log D_{x,norm}$	$\log MW_{det}$	MW_{det} [g/mol]	MW_{err} [%]
70	Cyclopentane	2.1411E-09	-8.6694	1.8157	65	7
72	THF	2.1258E-09	-8.6725	1.8220	66	8
88	TMS	1.8010E-09	-8.7445	1.9655	92	-5
88	MTBE	1.7965E-09	-8.7456	1.9676	93	-5
114	TMB	1.5985E-09	-8.7963	2.0687	117	-3
136	ADAM ^{b)}	1.4277E-09	-8.8454	2.1665	147	-8
234	N(SiMe ₃) ₃	1.1290E-09	-8.9473	2.3696	234	0
321	Si(SiMe ₃) ₄	9.9135E-10	-9.0038	2.4821	303	5
<i>Dissipated Spheres & Ellipsoids, ECC_{DSE}</i>						
102	Diisopropylether	1.7727E-09	-8.7514	2.0199	105	-3
116	Indene	1.6990E-09	-8.7698	2.0501	112	3
128	Naphthaline	1.6099E-09	-8.7932	2.0885	123	4
146	1,3 Indandione	1.4257E-09	-8.8460	2.1750	150	-2
155	2-Phenylpyridine	1.3882E-09	-8.8576	2.1941	156	-1
164	Tetramethoxypropane	1.3420E-09	-8.8722	2.2181	165	-1
178	Diphenylacetylene	1.2316E-09	-8.9095	2.2793	190	-7
202	Diphenylsulfoxid	1.1859E-09	-8.9260	2.3062	202	0
204	1-Phenylnaphthaline	1.2067E-09	-8.9184	2.2938	197	4
304	Tri(o-tolyl)phosphine	9.0389E-10	-9.0439	2.4996	316	-4
595	Hexaphenyltrisiloxane	6.1914E-10	-9.2082	2.7691	588	1
623	BINAP	5.9079E-10	-9.2286	2.8025	635	-2
<i>Expanded Discs, ECC_{ED}</i>						
178	Anthracene	1.3885E-09	2.2504	-8.8574	2.2417	2
179	Acridine	1.3190E-09	2.2529	-8.8797	2.2701	-4
192	9-Methylanthracene	1.3110E-09	2.2833	-8.8824	2.2735	2
202	Pyrene	1.2707E-09	2.3054	-8.8960	2.2908	3
208	Anthraquinone	1.1915E-09	2.3181	-8.9239	2.3265	-2
228	Triphenylene	1.1087E-09	2.3579	-8.9552	2.3664	-2
433	Tetraphenylnaphthaline	6.8229E-10	2.6365	-9.1660	2.6355	0
				Std. dev.	σ	4

- a) When a compound had more than one signal in the ¹H-NMR, the average diffusion coefficient was used.
- b) For determining the diffusion coefficient, we used the signal of the -CH₂ groups with the highest intensity.

A-Table 7. Overview of the used model compounds for ECC^{THF} and their normalized diffusion coefficients $\log D_{x,norm}$, the determined MW_{det} and the deviation MW_{err} . TMB was used as the internal reference with $\log D_{ref,fix}$ (TMB) = -8.7749 . All compounds have been measured in 15 mM solutions of analyte and TMB in an equimolar ratio.^{a)}

MW_{calc} [g/mol]	Compact Spheres, ECC_{CS}	$D_{x,norm}$ [m ² /s]	$\log D_{x,norm}$	$\log MW_{det}$	MW_{det} [g/mol]	MW_{err} [%]
70	Cyclopentane	2.2713E-09	-8.6437	1.8229	67	5
88	TMS	1.9870E-09	-8.7018	1.9404	87	1
88	MTBE	1.9980E-09	-8.6994	1.9356	86	2
114	TMB	1.6793E-09	-8.7749	2.0882	123	-7
136	ADAM ^{b)}	1.5481E-09	-8.8102	2.1597	144	-6
234	N(SiMe ₃) ₃	1.2386E-09	-8.9071	2.3557	227	3
321	Si(SiMe ₃) ₄	1.0537E-09	-8.9773	2.4977	315	2
<i>Dissipated Spheres & Ellipsoids, ECC_{DSE}</i>						
92	Toluol	2.1175E-09	-8.6742	1.9543	90	2
102	Diisopropylether	1.8871E-09	-8.7242	2.0402	110	-8
116	Indene	1.8515E-09	-8.7325	2.0544	113	2
128	Naphthaline	1.7943E-09	-8.7461	2.0778	120	7
146	1,3 Indandione	1.5478E-09	-8.8103	2.1880	154	-6
155	2-Phenylpyridine	1.5921E-09	-8.7980	2.1670	147	5
164	Tetramethoxypropane	1.5028E-09	-8.8231	2.2100	162	1
178	Diphenylacetylene	1.4013E-09	-8.8535	2.2622	183	-3
202	Diphenylsulfoxid	1.3256E-09	-8.8776	2.3035	201	0
204	1-Phenyl-naphthaline	1.3146E-09	-8.8812	2.3098	204	0
304	Tri(o-tolyl)phosphine	1.0100E-09	-8.9957	2.5063	321	-6
595	Hexaphenyltrisiloxane	7.2042E-10	-9.1424	2.7583	573	4
623	BINAP	6.8215E-10	-9.1661	2.7990	629	-1
<i>Expanded Discs, ECC_{ED}</i>						
178	Anthracene	1.5386E-09	-8.8129	2.2509	178	0
179	Acridine	1.5119E-09	-8.8205	2.2610	182	-2
192	9-Methylanthracene	1.4321E-09	-8.8440	2.2923	196	-2
202	Pyrene	1.4265E-09	-8.8457	2.2946	197	2
208	Anthrachinone	1.3734E-09	-8.8622	2.3165	207	0
228	Triphenylene	1.2975E-09	-8.8869	2.3493	224	2
433	Tetraphenyl-naphthaline	7.8459E-10	-9.1054	2.6399	436	-1
				Std. dev.	σ	4

a) When a compound had more than one signal in the ¹H-NMR, the average diffusion coefficient was used.

b) For determining the diffusion coefficient, we used the signal of the -CH₂ groups with the highest intensity.

Influence of High Concentration

A-Table 8. ECC^{TOL} from 15 mM solutions were used to determine the MW of compounds that were measured in concentrated TOL- d_8 solutions (120 mM). The deviation MW_{err} is a little higher than in the dilute solutions but still in a good range. ADAM was used as the internal reference with $\log D_{ref,fix}$ (ADAM) = -8.8454 .^{a)}

MW_{calc} [g/mol]	Compact Spheres, ECC_{CS}	$D_{x,norm}$ [m ² /s]	$\log D_{x,norm}$	$\log MW_{det}$	MW_{det} [g/mol]	MW_{err} [%]
70	Cyclopentane	2.0900E-09	-8.6799	1.8367	69	2
72	THF	2.0805E-09	-8.6818	1.8406	69	4
88	MTBE	1.7751E-09	-8.7508	1.9780	95	-8
88	TMS	1.8331E-09	-8.7368	1.9502	89	-1
136	ADAM ^{b)}	1.4277E-09	-8.8454	2.1665	147	-8
234	N(SiMe ₃) ₃	1.1410E-09	-8.9427	2.3605	229	2
321	Si(SiMe ₃) ₄	9.5908E-10	-9.0181	2.5108	324	-1
<i>Dissipated Spheres & Ellipsoids, ECC_{DSE}</i>						
102	Diisopropylether	1.7278E-09	-8.7625	2.0382	109	-7
116	Indene	1.6664E-09	-8.7782	2.0639	116	0
146	Indandione	1.3971E-09	-8.8548	2.1895	155	-6
155	2-Phenylpyridine	1.4019E-09	-8.8533	2.1871	154	1
161	HMDS	1.3379E-09	-8.8736	2.2203	166	-3
164	tetramethoxythane	1.3153E-09	-8.8810	2.2324	171	-4
178	Diphenylacetylene	1.2020E-09	-8.9201	2.2966	198	-11
204	PhN	1.1174E-09	-8.9518	2.3486	223	-9
304	Tri(o-tolyl)phosphine	8.4481E-10	-9.0732	2.5477	353	-16
595	Hexaphenyltrisiloxane	6.0717E-10	-9.2167	2.7830	607	-2
<i>Expanded Discs, ECC_{ED}</i>						
192	9-Methylantracene	1.2259E-09	-8.9116	2.3107	205	-7
202	Pyrene	1.2195E-09	-8.9138	2.3136	206	-2
228	Triphenylene	1.1129E-09	-8.9535	2.3643	231	-1
433	Tetraphenylnaphthaline	6.2746E-10	-9.2024	2.6819	481	-11
				Std. dev.	σ	5

- a) When a compound had more than one signal in the ¹H-NMR, the average diffusion coefficient was used.
- b) For determining the diffusion coefficient, we used the signal of the -CH₂ groups with the highest intensity.

Testing the Influence of the Temperature on ECCs

A-Table 9. ECC-MW-determination of $\text{Si}(\text{SiMe}_3)_4$ (321 g/mol) in TOL- d_8 and in THF- d_8 . ADAM was used as internal reference in 15mM solutions.

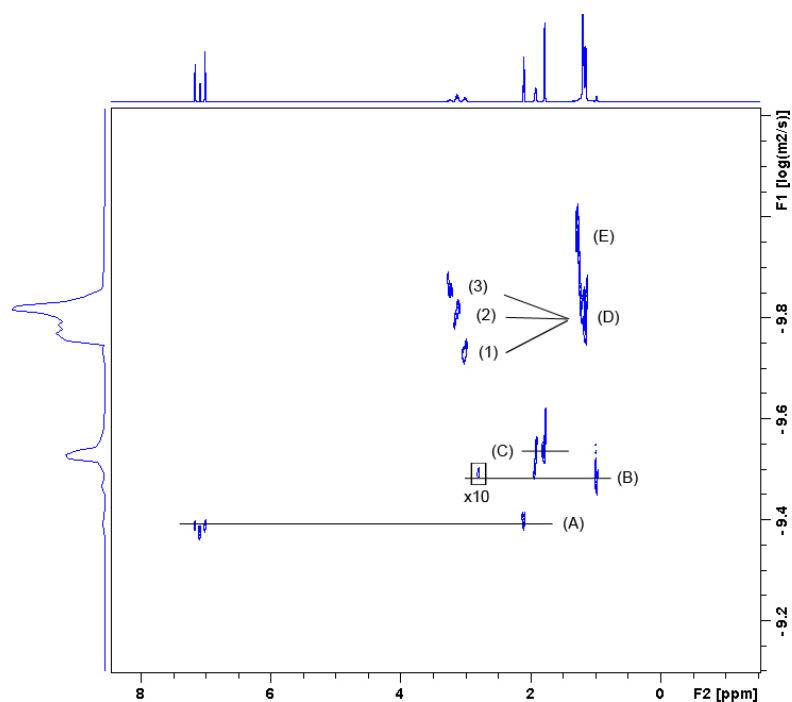
TOL- d_8					
<i>Temp</i> [°C]	$D_{x,\text{norm}}$ [m ² /s]	$\log D_{x,\text{norm}}$	$\log MW_{\text{det}}$	MW_{det} [g/mol]	MW_{err} [%]
100	9.5854E-10	-9.0184	2.5113	325	-1
75	9.6025E-10	-9.0176	2.5097	323	-1
50	9.6687E-10	-9.0146	2.5038	319	1
25	9.5261E-10	-9.0211	2.5166	329	-2
0	9.7043E-10	-9.0130	2.5006	317	1
-25	9.5640E-10	-9.0194	2.5132	326	-2
-50	9.9297E-10	-9.0031	2.4807	302	6
-75	9.8113E-10	-9.0083	2.4911	310	3

THF- d_8					
<i>Temp</i> [°C]	$D_{x,\text{norm}}$ [m ² /s]	$\log D_{x,\text{norm}}$	$\log MW_{\text{det}}$	MW_{det} [g/mol]	MW_{err} [%]
60	1.0540E-09	-8.9772	2.4975	314	2
45	1.0433E-09	-8.9816	2.5065	321	0
25	1.0671E-09	-8.9718	2.4866	307	4
0	1.0594E-09	-8.9749	2.4930	311	3
-25	1.0766E-09	-8.9680	2.4788	301	6
-50	1.0331E-09	-8.9859	2.5151	327	-2
-75	1.0710E-09	-8.9702	2.4835	304	5

Calculation of the Molar Van der Waals Density MD_w

A-Table 10. Calculation of the molar van der Waals density MD_w using equation (25).

<i>Compound</i>	<i>Formula</i>	MW_{calc} [g/mol]	MD_w [g/(mol·m ³)]	ΣV_w [m ³]
Cyclopentane	C5H10	70	4.41E+29	1.59E-28
THF	C4H8O	72	5.08E+29	1.42E-28
TMS	C4H12Si	88	4.68E+29	1.88E-28
MTBE	C5H12O	88	4.77E+29	1.85E-28
TMB	C8H18	114	4.30E+29	2.65E-28
ADAM	C10H16	136	4.61E+29	2.95E-28
N(SiMe ₃) ₃	C9H27NSi3	234	5.00E+29	4.68E-28
Si(SiMe ₃) ₄	C12H36Si5	321	5.00E+29	6.42E-28
Toluol	C7H8	92	4.88E+29	1.89E-28
Diisopropylether	C6H14O	102	4.72E+29	2.16E-28
Indene	C9H8	116	5.05E+29	2.30E-28
Naphthaline	C10H8	128	5.11E+29	2.50E-28
1,3 Indandione	C9H6O2	146	5.89E+29	2.48E-28
2-Phenylpyridine	C11H9N	155	5.31E+29	2.92E-28
Tetramethoxypropane	C7H16O4	164	5.61E+29	2.92E-28
Diphenylacetylene	C14H10	178	5.18E+29	3.44E-28
Diphenylsulfoxid	C12H10OS	202	5.91E+29	3.42E-28
1-Phenylnaphthaline	C16H12	204	5.15E+29	3.96E-28
Tri(o-tolyl)phosphine	C21H21P	304	5.30E+29	5.74E-28
Hexaphenyltrisiloxane	C36H30O3Si3	595	5.57E+29	1.07E-27
BINAP	C44H32P2	623	5.50E+29	1.13E-27
Anthracene	C14H10	178	5.18E+29	3.44E-28
Acridine	C13H9N	179	5.37E+29	3.33E-28
9-Methylanthracene	C15H12	192	5.11E+29	3.76E-28
Pyrene	C16H10	202	5.25E+29	3.85E-28
Anthrachinone	C14H8O2	208	5.74E+29	3.62E-28
Triphenylene	C18H12	228	5.21E+29	4.37E-28
Tetraphenylnaphthaline	C34H24	433	5.19E+29	8.34E-28
1-Hexylchloride	C6H13Cl	120	5.49E+29	2.18E-28
1-Octylchloride	C8H17Cl	149	5.29E+29	2.82E-28
1-Decylchloride	C10H21Cl	177	5.13E+29	3.45E-28
1-Propylbromide	C3H7Br	123	9.66E+29	1.27E-28
Dibromoanthracene	C14H8Br2	336	8.71E+29	3.86E-28
Triphenylmethylbromid	C19H15Br	323	6.45E+29	5.01E-28

DOSY-Spectrum of LDA in TOL- d_8 at -50°C A-Figure 3. DOSY-Spectrum of LDA in TOL- d_8 at -50°C .A-Table 11. DOSY-ECC-MW-determination of LDA in TOL- d_8 at -50°C .

Entry	Compound (g/mol)	$D/10^{-10}$ [m^2/s]	$\log D_x$	$\log D_{x,\text{norm}}$	$MW_{\text{det}}^{\text{a)}}$ [g/mol]	MW_{err} [%]
(A)	TOL- d_8 (92) ^{b)}	3.723	-9.4291	-8.6992	86	7
(B)	Diisopropylamine (101)	3.402	-9.4683	-8.7383	100	1
(C)	ADAM (136) ^{c)}	2.659	-9.5753	-8.8454	147	-8
(D)	Mix of (1), (2), (3)					
(1)	Trimer (321)	1.632	-9.7873	-9.0574	332	-3
(2)	Tetramer (428)	1.409	-9.8511	-9.1212	423	1
(3)	Pentamer (536)	1.243	-9.9055	-9.1756	520	3
(E)	Higher oligomers					

a) All MWs were calculated by using ECC_{DSE}.

b) Deuterated species diffuse like their protonated counterparts.

c) The MW of ADAM, a highly spherical and compact molecule, was calculated by using ECC_{CS}.

A-Table 12. Relative proton intensities of the α -CH signals of LDA in TOL- d_8 at various temperatures.^{a)}

<i>Temp</i> [°C]	<i>Trimer</i> A	<i>Tetramer</i> B	<i>Pentamer</i> C	<i>Oligomer</i> D
-75	4	8	5	5
-50	5	8	5	4
-25	6	8	4	4
0	10	8	2	2
+25	12	8		4 ^{b)}
+50	12	8		3 ^{b)}
+75	28	8		2 ^{b)}
+100	One coalesced signal			

- a) Sum of the α -CH protons: trimer (6 H), tetramer (8 H), pentamer (10 H). Due to signal overlap the sum of the integrals is not always constant.
- b) Pentamer and higher oligomers are not separated.

¹H-DOSY-ECC-MW-determination parameters of MHMDS (M = Li, Na and K) in TOL- d_8 with ammonia as donor base

A-Table 13. DOSY-ECC-MW-determination parameters of MHMDS in TOL- d_8 (15 mM) with ammonia as donor base. ADAM was used as internal reference (15 mM) and ECC_{DSE} to determine the MWs.

	<i>LiHMDS</i>	<i>NaHMDS</i>	<i>KHMDS</i>
D_x	9.4180E-10	8.8640E-10	8.1480E-10
$\log D_x$	-9.0260	-9.0524	-9.0889
$\log D_{x,\text{norm}}$	-9.0643	-9.1356	-9.1243
D_{ref} (ADAM)	1.5590E-09	1.7290E-09	1.5485E-09
$\log D_{\text{ref}}$ (ADAM)	-8.8072	-8.7622	-8.8101
MW_{det} [g/mol]	341	447	428

A-Table 14. DOSY-ECC-MW-determination of LiHMDS in TOL- d_8 (15 mm) with ammonia as donor base. ADAM was used as internal reference (15 mm) and ECC_{DSE} to determine the MWs.

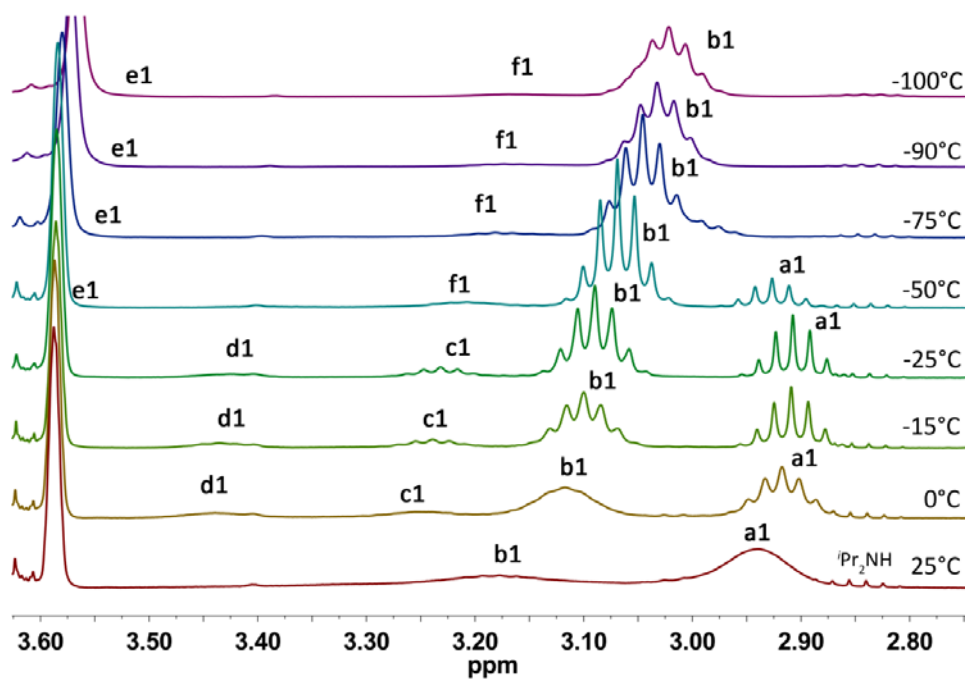
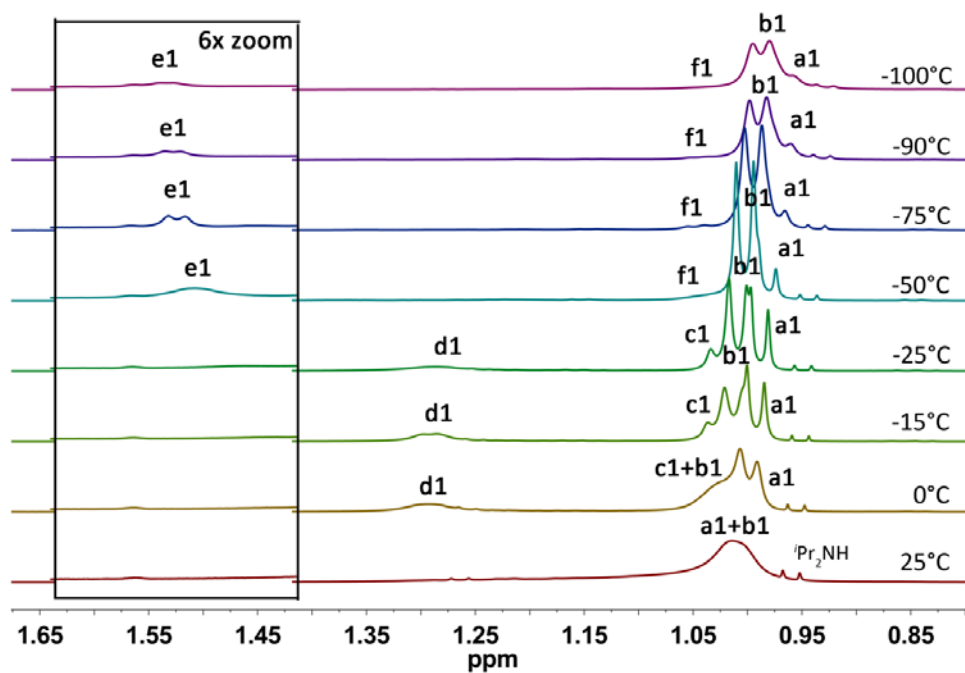
	<i>Species</i>	MW_{calc} [g/mol]	MW_{err} [g/mol]	MW_{det} 341 g/mol
A	[LiHMDS] ₂	335	-2	
B	(NH ₃) · [LiHMDS] ₂	352	3	
C	(NH ₃) ₂ · [LiHMDS] ₂	369	7	
D	(NH ₃) ₃ · [LiHMDS] ₂	386	12	
E/F	(NH ₃) ₄ · [LiHMDS] ₂	403	15	
G	(NH ₃) ₅ · [LiHMDS] ₂	420	19	
H	(NH ₃) ₃ · LiHMDS	218	-56	

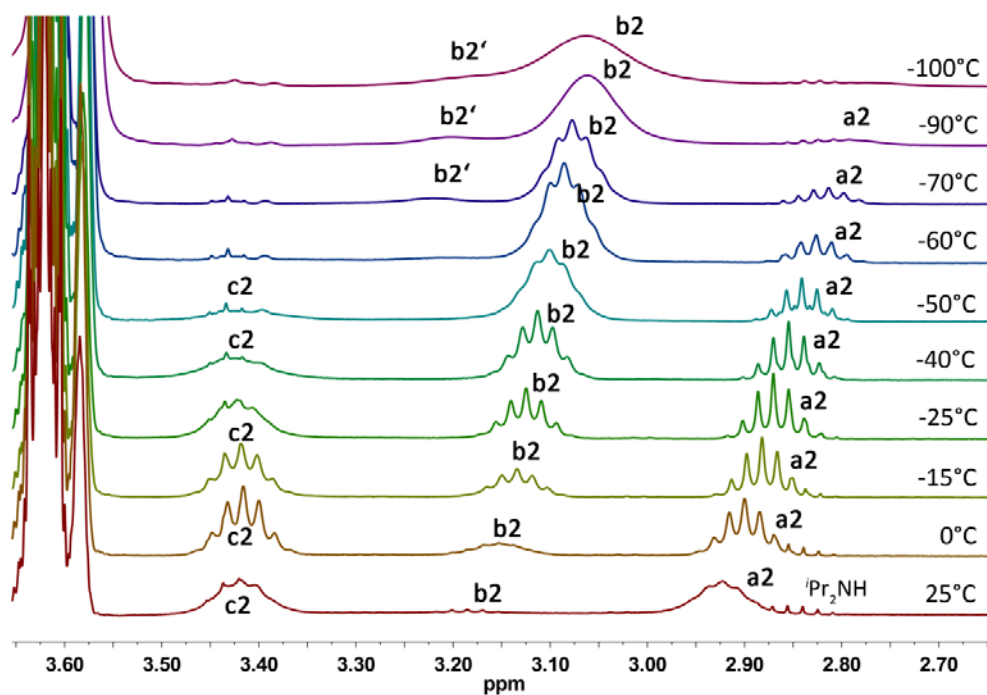
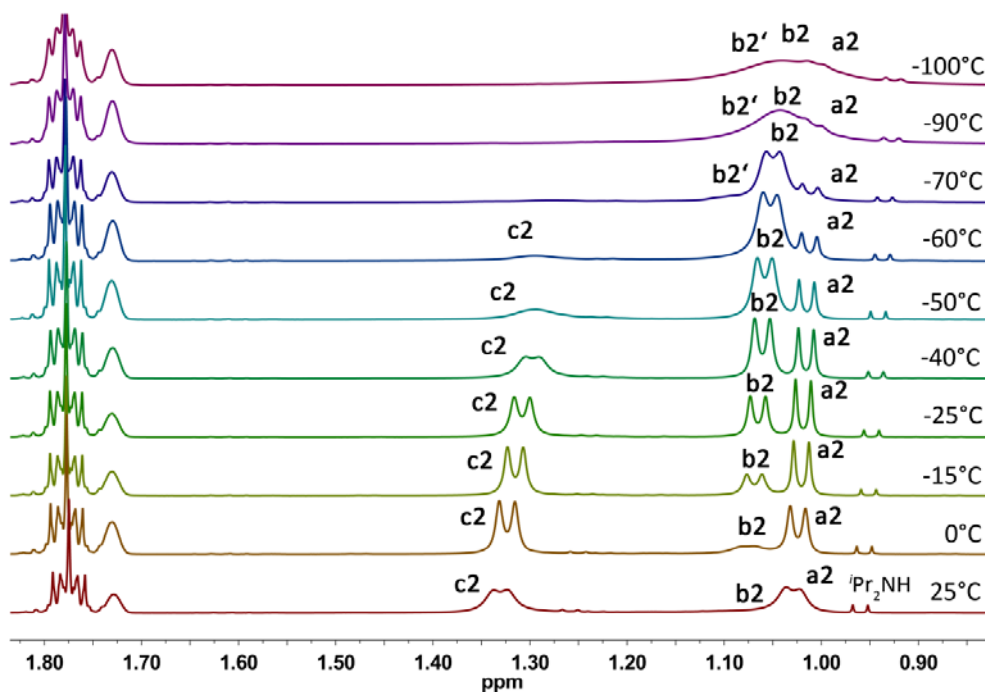
A-Table 15. DOSY-ECC-MW-determination of NaHMDS in TOL- d_8 (15 mm) with ammonia as donor base. ADAM was used as internal reference (15 mm) and ECC_{DSE} to determine the MWs.

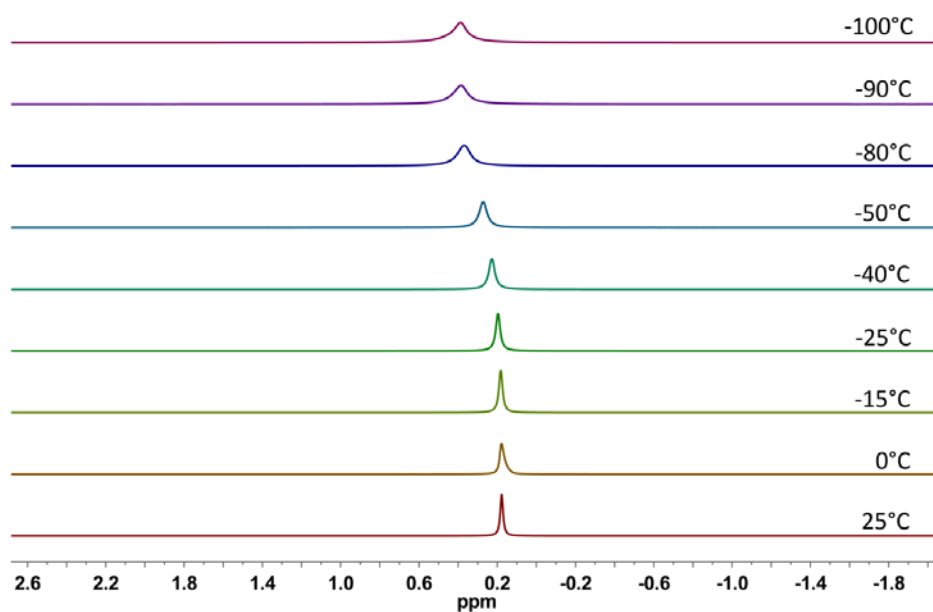
	<i>Species</i>	MW_{calc} [g/mol]	MW_{err} [g/mol]	MW_{det} 447 g/mol
A	[NaHMDS] ₂	367	-22	
B	(NH ₃) · [NaHMDS] ₂	384	-16	
C	(NH ₃) ₂ · [NaHMDS] ₂	401	-11	
D	(NH ₃) ₃ · [NaHMDS] ₂	418	-7	
E/F	(NH ₃) ₄ · [NaHMDS] ₂	435	-3	
G	(NH ₃) ₅ · [NaHMDS] ₂	452	1	
H	(NH ₃) ₃ · NaHMDS	234	-90	

A-Table 16. DOSY-ECC-MW-determination of KHMDS in TOL- d_8 (15 mm) with ammonia as donor base. ADAM was used as internal reference (15 mm) and ECC_{DSE} to determine the MWs.

	<i>Species</i>	MW_{calc} [g/mol]	MW_{err} [g/mol]	MW_{det} 428 g/mol
A	[KHMDS] ₂	399	-7	
B	(NH ₃) · [KHMDS] ₂	416	-3	
C	(NH ₃) ₂ · [KHMDS] ₂	433	1	
D	(NH ₃) ₃ · [KHMDS] ₂	450	5	
E/F	(NH ₃) ₄ · [KHMDS] ₂	467	8	
G	(NH ₃) ₅ · [KHMDS] ₂	484	12	
H	(NH ₃) ₃ · KHMDS	251	-71	

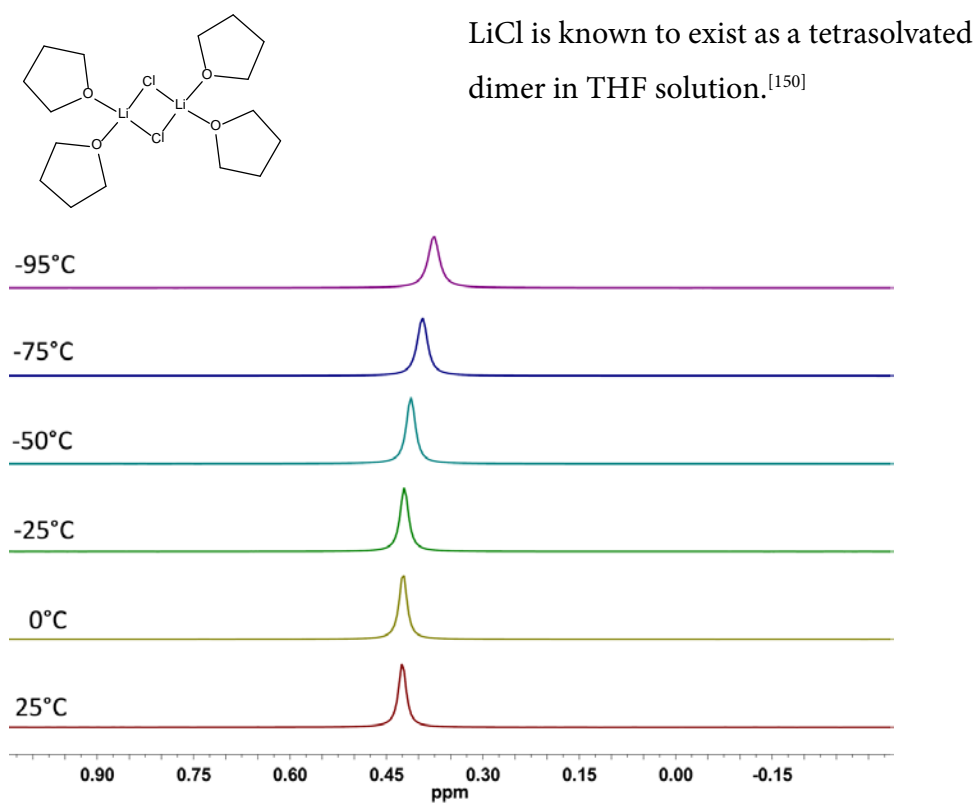
^1H spectra of $^i\text{Pr}_2\text{NMgCl}$ 7 in $\text{THF-}d_8$ A-Figure 4. ^1H spectrum of $^i\text{Pr}_2\text{NMgCl}$ 7 (0.10 M) in $\text{THF-}d_8$. (α -CH region).A-Figure 5. ^1H spectrum of $^i\text{Pr}_2\text{NMgCl}$ 7 (0.10 M) in $\text{THF-}d_8$. ($-\text{CH}_3$ region).

^1H and ^7Li spectra of ${}^i\text{Pr}_2\text{NMgCl}\cdot\text{LiCl}$ 9 in $\text{THF-}d_8$ **A-Figure 6.** ${}^1\text{H}$ spectrum of ${}^i\text{Pr}_2\text{NMgCl}\cdot\text{LiCl}$ 9 (0.10 M) in $\text{THF-}d_8$. ($\alpha\text{-CH}$ region).**A-Figure 7.** ${}^1\text{H}$ spectrum of ${}^i\text{Pr}_2\text{NMgCl}\cdot\text{LiCl}$ 9 (0.10 M) in $\text{THF-}d_8$. ($-\text{CH}_3$ region).

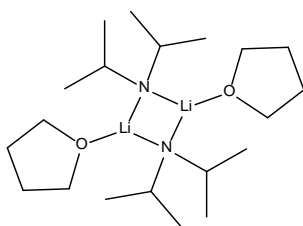


A-Figure 8. ^7Li spectra of $^i\text{Pr}_2\text{NMgCl}\cdot\text{LiCl}$ **9** (0.10 M) in THF- d_8 .

^7Li Spectra of LiCl in THF- d_8



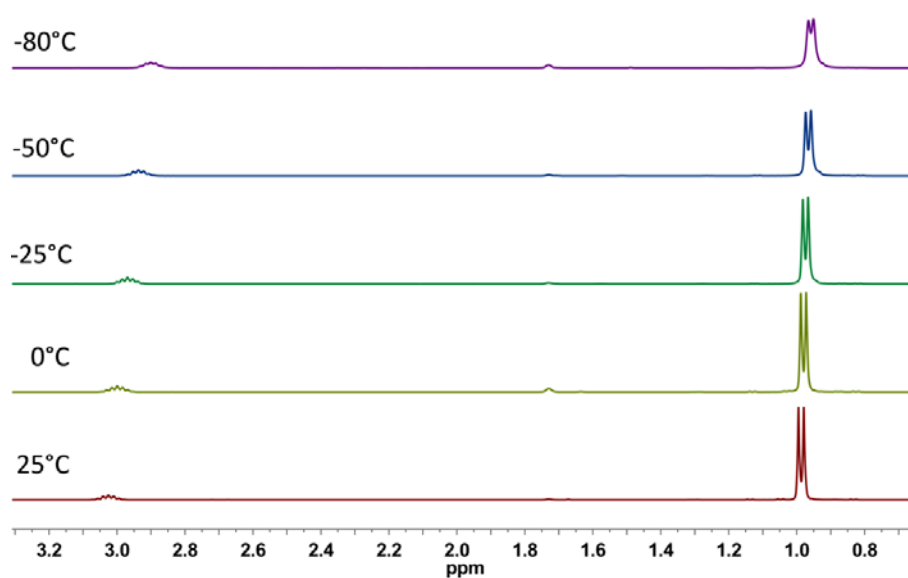
A-Figure 9. ^7Li spectra of LiCl (0.03 M) in THF- d_8 .

^1H and ^7Li Spectra of Lithiumdiisopropylamide (LDA) in THF- d_8 

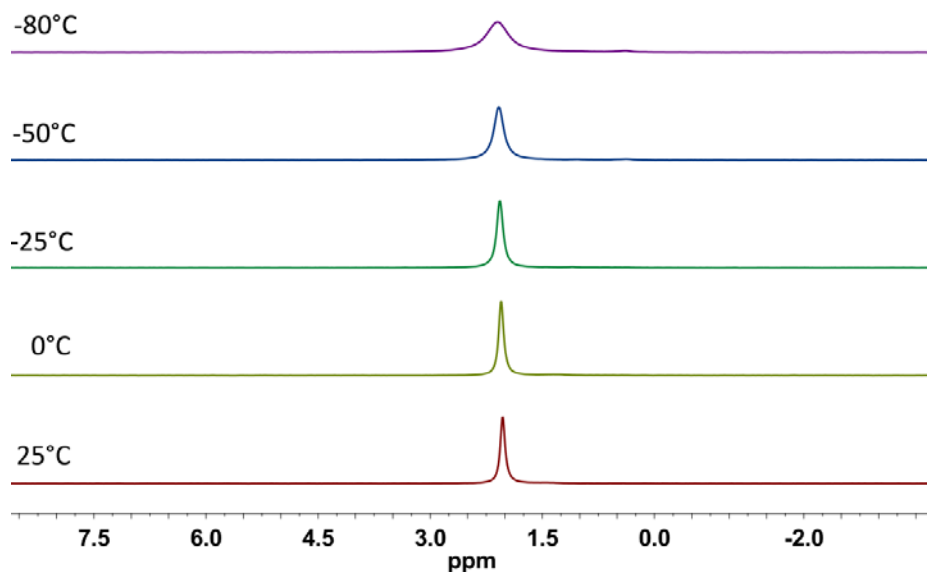
LDA is known to exist exclusively as a disolvated dimer in THF solution.^[151]

Lithium species of **9** resonances at a chemical shift region of 0.18 ppm to 0.38 ppm in the ^7Li experiment.

LDA can be excluded to be present in solution of **9**, because it resonances at around 2 ppm.



A-Figure 10. ^1H spectrum of LDA (0.10 M) in THF- d_8 .



A-Figure 11. ^7Li spectrum of LDA (0.10 M) in $\text{THF-}d_8$.

^1H -DOSY-ECC-MW-determination parameters of $^i\text{Pr}_2\text{NMgCl}$ 7

A-Table 17. ^1H -DOSY-ECC-MW-determination of $^i\text{Pr}_2\text{NMgCl}$ 7 in $\text{THF-}d_8$ (0.10 M). PhN (0.02 M) was used as internal reference with $\log D_{\text{ref,fix}}(\text{PhN}) = -8.8812$. The accuracy of this method is in the range of $MW_{\text{err}} < \pm 9\%$.

^1H -DOSY					25°C
	Signal	a	Species	MW_{calc} [g/mol]	MW_{err} [%]
D_x (a)	1.1250E-09		$\text{MgCl}_2 \cdot \text{D1(D2)} \cdot \text{MgCl}_2$	655	50
$\log D_x$ (a)	-8.9488		D1	464	30
$\log D_{x,\text{norm}}$ (a)	-8.9999		$\text{M1} \cdot (\text{MgCl}_2)_2 \cdot \text{M1}$	943	65
D_{ref} (PhN)	1.4787E-09		$(\mu\text{-Cl3})\text{-M1} \cdot \text{MgCl}_2$	616	47
$\log D_{\text{ref}}$ (PhN)	-8.8301		D2	464	30
MW_{det} [g/mol]	326		M2	369	12
			M1	304	-7
	Signal	b	Species	MW_{calc} [g/mol]	MW_{err} [%]
D_x (b)	1.0600E-09		$\text{MgCl}_2 \cdot \text{D1(D2)} \cdot \text{MgCl}_2$	655	45
$\log D_x$ (b)	-8.9747		D1	464	22
$\log D_{x,\text{norm}}$ (b)	-9.0258		$\text{M1} \cdot (\text{MgCl}_2)_2 \cdot \text{M1}$	943	62
D_{ref} (PhN)	1.4787E-09		$(\mu\text{-Cl3})\text{-M1} \cdot \text{MgCl}_2$	616	41
$\log D_{\text{ref}}$ (PhN)	-8.8301		D2	464	22
MW_{det} [g/mol]	361		M2	369	2
			M1	304	-19

-15°C					
	<i>Signal</i>	a	<i>Species</i>	MW_{calc} [g/mol]	MW_{err} [%]
D_x (a)	5.3190E-10		MgCl ₂ ·D1(D2)·MgCl ₂	655	53
log D_x (a)	-9.2742		D1	464	34
log $D_{x,\text{norm}}$ (a)	-8.9833		M1·(MgCl ₂) ₂ ·M1	943	68
D_{ref} (PhN)	6.7280E-10		(μ-Cl3)-M1·MgCl ₂	616	50
log D_{ref} (PhN)	-9.1721		D2	464	34
MW_{det} [g/mol]	305		M2	369	17
			M1	304	0
	<i>Signal</i>	b	<i>Species</i>	MW_{calc} [g/mol]	MW_{err} [%]
D_x (b)	4.6230E-10		MgCl ₂ ·D1(D2)·MgCl ₂	655	41
log D_x (b)	-9.3351		D1	464	16
log $D_{x,\text{norm}}$ (b)	-9.0442		M1·(MgCl ₂) ₂ ·M1	943	59
D_{ref} (PhN)	6.7280E-10		(μ-Cl3)-M1·MgCl ₂	616	37
log D_{ref} (PhN)	-9.1721		D2	464	16
MW_{det} [g/mol]	389		M2	369	-5
			M1	304	-28
	<i>Signal</i>	c	<i>Species</i>	MW_{calc} [g/mol]	MW_{err} [%]
D_x (c)	4.2840E-10		MgCl ₂ ·D1(D2)·MgCl ₂	655	32
log D_x (c)	-9.3682		D1	464	5
log $D_{x,\text{norm}}$ (c)	-9.0772		M1·(MgCl ₂) ₂ ·M1	943	53
D_{ref} (PhN)	6.7280E-10		(μ-Cl3)-M1·MgCl ₂	616	28
log D_{ref} (PhN)	-9.1721		D2	464	5
MW_{det} [g/mol]	443		M2	369	-20
			M1	304	-46
	<i>Signal</i>	d	<i>Species</i>	MW_{calc} [g/mol]	MW_{err} [%]
D_x (d)	4.3580E-10		MgCl ₂ ·D1(D2)·MgCl ₂	655	34
log D_x (d)	-9.3607		D1	464	7
log $D_{x,\text{norm}}$ (d)	-9.0698		M1·(MgCl ₂) ₂ ·M1	943	54
D_{ref} (PhN)	6.7280E-10		(μ-Cl3)-M1·MgCl ₂	616	30
log D_{ref} (PhN)	-9.1721		D2	464	7
MW_{det} [g/mol]	430		M2	369	-17
			M1	304	-41
-25°C					
	<i>Signal</i>	a	<i>Species</i>	MW_{calc} [g/mol]	MW_{err} [%]
D_x (a)	4.2320E-10		MgCl ₂ ·D1(D2)·MgCl ₂	655	52
log D_x (a)	-9.3735		D1	464	33
log $D_{x,\text{norm}}$ (a)	-8.9883		M1·(MgCl ₂) ₂ ·M1	943	67
D_{ref} (PhN)	5.4157E-10		(μ-Cl3)-M1·MgCl ₂	616	49

Appendix

$\log D_{\text{ref}}$ (PhN)	-9.2663		D2	464	33
MW_{det} [g/mol]	312		M2	369	16
			M1	304	-2
	<i>Signal</i>	b	<i>Species</i>	MW_{calc} [g/mol]	MW_{err} [%]
D_x (b)	3.8110E-10		MgCl ₂ ·D1(D2)·MgCl ₂	655	43
$\log D_x$ (b)	-9.4190		D1	464	20
$\log D_{x,\text{norm}}$ (b)	-9.0338		M1·(MgCl ₂) ₂ ·M1	943	60
D_{ref} (PhN)	5.4157E-10		(μ-Cl3)-M1·MgCl ₂	616	39
$\log D_{\text{ref}}$ (PhN)	-9.2663		D2	464	20
MW_{det} [g/mol]	373		M2	369	-1
			M1	304	-23
	<i>Signal</i>	c	<i>Species</i>	MW_{calc} [g/mol]	MW_{err} [%]
D_x (c)	3.3890E-10		MgCl ₂ ·D1(D2)·MgCl ₂	655	30
$\log D_x$ (c)	-9.4699		D1	464	2
$\log D_{x,\text{norm}}$ (c)	-9.0848		M1·(MgCl ₂) ₂ ·M1	943	52
D_{ref} (PhN)	5.4157E-10		(μ-Cl3)-M1·MgCl ₂	616	26
$\log D_{\text{ref}}$ (PhN)	-9.2663		D2	464	2
MW_{det} [g/mol]	456		M2	369	-24
			M1	304	-50
	<i>Signal</i>	d	<i>Species</i>	MW_{calc} [g/mol]	MW_{err} [%]
D_x (d)	3.4580E-10		MgCl ₂ ·D1(D2)·MgCl ₂	655	33
$\log D_x$ (d)	-9.4612		D1	464	5
$\log D_{x,\text{norm}}$ (d)	-9.0760		M1·(MgCl ₂) ₂ ·M1	943	53
D_{ref} (PhN)	5.4157E-10		(μ-Cl3)-M1·MgCl ₂	616	28
$\log D_{\text{ref}}$ (PhN)	-9.2663		D2	464	5
MW_{det} [g/mol]	441		M2	369	-20
			M1	304	-45
					-50°C
	<i>Signal</i>	a	<i>Species</i>	MW_{calc} [g/mol]	MW_{err} [%]
D_x (a)	2.3360E-10		MgCl ₂ ·D1(D2)·MgCl ₂	655	53
$\log D_x$ (a)	-9.6315		D1	464	33
$\log D_{x,\text{norm}}$ (a)	-8.9862		M1·(MgCl ₂) ₂ ·M1	943	67
D_{ref} (PhN)	2.9747E-10		(μ-Cl3)-M1·MgCl ₂	616	50
$\log D_{\text{ref}}$ (PhN)	-9.5266		D2	464	33
MW_{det} [g/mol]	309		M2	369	16
			M1	304	-2

Appendix

	<i>Signal</i>	b	<i>Species</i>	MW_{calc} [g/mol]	MW_{err} [%]
D_x (b)	2.1800E-10		MgCl ₂ ·D1(D2)·MgCl ₂	655	47
log D_x (b)	-9.6615		D1	464	25
log $D_{x,\text{norm}}$ (b)	-9.0162		M1·(MgCl ₂) ₂ ·M1	943	63
D_{ref} (PhN)	2.9747E-10		(μ-Cl3)-M1·MgCl ₂	616	43
log D_{ref} (PhN)	-9.5266		D2	464	25
MW_{det} [g/mol]	348		M2	369	6
			M1	304	-14
	<i>Signal</i>	c+d	no signal		
	<i>Signal</i>	e	<i>Species</i>	MW_{calc} [g/mol]	MW_{err} [%]
D_x (e)	1.9850E-10		MgCl ₂ ·D1(D2)·MgCl ₂	655	24
log D_x (e)	-9.7022		D1	464	-7
log $D_{x,\text{norm}}$ (e)	-9.0569		M1·(MgCl ₂) ₂ ·M1	943	47
D_{ref} (PhN)	2.9747E-10		(μ-Cl3)-M1·MgCl ₂	616	19
log D_{ref} (PhN)	-9.5266		D2	464	-7
$MW_{\text{det,corr}}$ [g/mol]	497		M2	369	-35
MW_{det} [g/mol]	409		M1	304	-63
	<i>Signal</i>	f	<i>Species</i>	MW_{calc} [g/mol]	MW_{err} [%]
D_x (f)	1.9330E-10		MgCl ₂ ·D1(D2)·MgCl ₂	655	35
log D_x (f)	-9.7138		D1	464	8
log $D_{x,\text{norm}}$ (f)	-9.0684		M1·(MgCl ₂) ₂ ·M1	943	55
D_{ref} (PhN)	2.9747E-10		(μ-Cl3)-M1·MgCl ₂	616	31
log D_{ref} (PhN)	-9.5266		D2	464	8
MW_{det} [g/mol]	428		M2	369	-16
			M1	304	-41
					-70°C
	<i>Signal</i>	a	<i>Species</i>	MW_{calc} [g/mol]	MW_{err} [%]
D_x (a)	1.1650E-10		MgCl ₂ ·D1(D2)·MgCl ₂	655	55
log D_x (a)	-9.9337		D1	464	36
log $D_{x,\text{norm}}$ (a)	-8.9763		M1·(MgCl ₂) ₂ ·M1	943	68
D_{ref} (PhN)	1.4503E-10		(μ-Cl3)-M1·MgCl ₂	616	52
log D_{ref} (PhN)	-9.8385		D2	464	36
MW_{det} [g/mol]	297		M2	369	19
			M1	304	2

	<i>Signal</i>	b	<i>Species</i>	MW_{calc} [g/mol]	MW_{err} [%]
D_x (b)	1.0720E-10		$\text{MgCl}_2 \cdot \text{D1(D2)} \cdot \text{MgCl}_2$	655	48
$\log D_x$ (b)	-9.9698		D1	464	26
$\log D_{x,\text{norm}}$ (b)	-9.0125		$\text{M1} \cdot (\text{MgCl}_2)_2 \cdot \text{M1}$	943	64
D_{ref} (PhN)	1.4503E-10		$(\mu\text{-Cl3})\text{-M1} \cdot \text{MgCl}_2$	616	44
$\log D_{\text{ref}}$ (PhN)	-9.8385		D2	464	26
MW_{det} [g/mol]	343		M2	369	7
			M1	304	-13
	<i>Signal</i>	c+d	no signal		
	<i>Signal</i>	e	<i>Species</i>	MW_{calc} [g/mol]	MW_{err} [%]
D_x (e)	9.1980E-11		$\text{MgCl}_2 \cdot \text{D1(D2)} \cdot \text{MgCl}_2$	655	17
$\log D_x$ (e)	-1.0036E+01		D1	464	-17
$\log D_{x,\text{norm}}$ (e)	-9.0790		$\text{M1} \cdot (\text{MgCl}_2)_2 \cdot \text{M1}$	943	42
D_{ref} (PhN)	1.4503E-10		$(\mu\text{-Cl3})\text{-M1} \cdot \text{MgCl}_2$	616	12
$\log D_{\text{ref}}$ (PhN)	-9.8385		D2	464	-17
$MW_{\text{det,corr}}$ [g/mol]	542		M2	369	-47
MW_{det} [g/mol]	446		M1	304	-78
	<i>Signal</i>	f	<i>Species</i>	MW_{calc} [g/mol]	MW_{err} [%]
D_x (f)	8.4910E-11		$\text{MgCl}_2 \cdot \text{D1(D2)} \cdot \text{MgCl}_2$	655	22
$\log D_x$ (f)	-1.0071E+01		D1	464	-10
$\log D_{x,\text{norm}}$ (f)	-9.1137		$\text{M1} \cdot (\text{MgCl}_2)_2 \cdot \text{M1}$	943	46
D_{ref} (PhN)	1.4503E-10		$(\mu\text{-Cl3})\text{-M1} \cdot \text{MgCl}_2^{(4\text{THF})}$	544	6
$\log D_{\text{ref}}$ (PhN)	-9.8385		D2	464	-10
MW_{det} [g/mol]	512		M2	369	-39
			M1	304	-68
	<i>Signal</i>	a	too weak in intensity		-80°C
	<i>Signal</i>	b	<i>Species</i>	MW_{calc} [g/mol]	MW_{err} [%]
D_x (b)	7.3170E-11		$\text{MgCl}_2 \cdot \text{D1(D2)} \cdot \text{MgCl}_2$	655	47
$\log D_x$ (b)	-1.0136E+01		D1	464	25
$\log D_{x,\text{norm}}$ (b)	-9.0147		$\text{M1} \cdot (\text{MgCl}_2)_2 \cdot \text{M1}$	943	63
D_{ref} (PhN)	9.9497E-11		$(\mu\text{-Cl3})\text{-M1} \cdot \text{MgCl}_2$	616	44
$\log D_{\text{ref}}$ (PhN)	-1.0002E+01		D2	464	25
MW_{det} [g/mol]	346		M2	369	6
			M1	304	-14
	<i>Signal</i>	c+d	no signal		

Appendix

	<i>Signal</i>	e	<i>Species</i>	MW_{calc} [g/mol]	MW_{err} [%]
D_x (e)	5.4260E-11		MgCl ₂ ·D1(D2)·MgCl ₂	655	-7
log D_x (e)	-1.0266E+01		D1	464	-51
log $D_{x,\text{norm}}$ (e)	-9.1445		M1·(MgCl ₂) ₂ ·M1	943	25
D_{ref} (PhN)	9.9497E-11		(μ-Cl3)-M1·MgCl ₂	616	-14
log D_{ref} (PhN)	-1.0002E+01		D2	464	-51
$MW_{\text{det,corr}}$ [g/mol]	703		M2	369	-91
MW_{det} [g/mol]	578		M1	304	-131
	<i>Signal</i>	f	<i>Species</i>	MW_{calc} [g/mol]	MW_{err} [%]
D_x (f)	5.2290E-11		MgCl ₂ ·D1(D2)·MgCl ₂	655	6
log D_x (f)	-1.0282E+01		D1	464	-33
log $D_{x,\text{norm}}$ (f)	-9.1606		M1·(MgCl ₂) ₂ ·M1	943	35
D_{ref} (PhN)	9.9497E-11		(μ-Cl3)-M1·MgCl ₂	616	0
log D_{ref} (PhN)	-1.0002E+01		D2	464	-33
MW_{det} [g/mol]	616		M2	369	-67
			M1	304	-102
<i>Signal</i>		a	too weak in intensity		-90°C
<i>Signal</i>		b	<i>Species</i>	MW_{calc} [g/mol]	MW_{err} [%]
D_x (b)	4.5770E-11		MgCl ₂ ·D1(D2)·MgCl ₂	655	47
log D_x (b)	-1.0339E+01		D1	464	26
log $D_{x,\text{norm}}$ (b)	-9.0139		M1·(MgCl ₂) ₂ ·M1	943	63
D_{ref} (PhN)	6.2133E-11		(μ-Cl3)-M1·MgCl ₂	616	44
log D_{ref} (PhN)	-1.0207E+01		D2	464	26
MW_{det} [g/mol]	345		M2	369	7
			M1	304	-13
<i>Signal</i>		c+d	no signal		
<i>Signal</i>		e+f	too weak in intensity		
<i>Signal</i>		a	too weak in intensity		-100°C
<i>Signal</i>		b	<i>Species</i>	MW_{calc} [g/mol]	MW_{err} [%]
D_x (b)	2.6840E-11		MgCl ₂ ·D1(D2)·MgCl ₂	655	48
log D_x (b)	-1.0571E+01		D1	464	26
log $D_{x,\text{norm}}$ (b)	-9.0122		M1·(MgCl ₂) ₂ ·M1	943	64
D_{ref} (PhN)	3.6287E-11		(μ-Cl3)-M1·MgCl ₂	616	44
log D_{ref} (PhN)	-1.0440E+01		D2	464	26
MW_{det} [g/mol]	342		M2	369	7
			M1	304	-13
<i>Signal</i>		c+d	no signal		
<i>Signal</i>		e+f	too weak in intensity		

¹H-DOSY-ECC-MW-determination parameters of ¹Pr₂NMgCl·LiCl 9

A-Table 18. ¹H-DOSY-ECC-MW-determination of ¹Pr₂NMgCl·LiCl 9 in THF-*d*₈ (0.10 M). PhN (0.02 M) was used as internal reference with $\log D_{\text{ref,fix}}(\text{PhN}) = -8.8812$. The accuracy of this method is in the range of $MW_{\text{err}} < \pm 9\%$.

¹ H-DOSY					25°C
	<i>Signal</i>	a2	<i>Species</i>	<i>MW</i> _{calc} [g/mol]	<i>MW</i> _{err} [%]
<i>D</i> _x (a2)	9.2820E-10		LiCl·D1·LiCl	693	38
$\log D_x$ (a2)	-9.0324		D1	464	8
$\log D_{x,\text{norm}}$ (a2)	-9.0693		LiCl·D2·LiCl	693	38
<i>D</i> _{ref} (PhN)	1.4313E-09		D2	464	8
$\log D_{\text{ref}}$ (PhN)	-8.8443		M1·LiCl	419	-3
<i>MW</i> _{det} [g/mol]	429		M1	304	-41
			M0	268	-60
	<i>Signal</i>	b2	too low in intensity		
	<i>Signal</i>	c2	<i>Species</i>	<i>MW</i> _{calc} [g/mol]	<i>MW</i> _{err} [%]
<i>D</i> _x (c2)	8.2560E-10		LiCl·D1·LiCl	693	24
$\log D_x$ (c2)	-9.0832		D1	464	-13
$\log D_{x,\text{norm}}$ (c2)	-9.1202		LiCl·D2·LiCl	693	24
<i>D</i> _{ref} (PhN)	1.4313E-09		D2	464	-13
$\log D_{\text{ref}}$ (PhN)	-8.8443		M1·LiCl	419	-25
<i>MW</i> _{det} [g/mol]	525		M1	304	-73
			M0	268	-96
					0°C
	<i>Signal</i>	a2	<i>Species</i>	<i>MW</i> _{calc} [g/mol]	<i>MW</i> _{err} [%]
<i>D</i> _x (a2)	6.1450E-10		LiCl·D1·LiCl	693	39
$\log D_x$ (a2)	-9.2115		D1	464	9
$\log D_{x,\text{norm}}$ (a2)	-9.0647		LiCl·D2·LiCl	693	39
<i>D</i> _{ref} (PhN)	9.3753E-10		D2	464	9
$\log D_{\text{ref}}$ (PhN)	-9.0280		M1·LiCl	419	-1
<i>MW</i> _{det} [g/mol]	421		M1	304	-39
			M0	268	-58
	<i>Signal</i>	b2	<i>Species</i>	<i>MW</i> _{calc} [g/mol]	<i>MW</i> _{err} [%]
<i>D</i> _x (b2)	5.5940E-10		LiCl·D1·LiCl	693	29
$\log D_x$ (b2)	-9.2523		D1	464	-7
$\log D_{x,\text{norm}}$ (b2)	-9.1055		LiCl·D2·LiCl	693	29
<i>D</i> _{ref} (PhN)	9.3753E-10		D2	464	-7
$\log D_{\text{ref}}$ (PhN)	-9.0280		M1·LiCl	419	-18
<i>MW</i> _{det} [g/mol]	495		M1	304	-63

			M0	268	-85
	<i>Signal</i>	c2	<i>Species</i>	MW_{calc} [g/mol]	MW_{err} [%]
D_x (c2)	5.0700E-10		LiCl·D1·LiCl	693	15
$\log D_x$ (c2)	-9.2950		D1	464	-26
$\log D_{x,\text{norm}}$ (c2)	-9.1482		LiCl·D2·LiCl	693	15
D_{ref} (PhN)	9.3753E-10		D2	464	-26
$\log D_{\text{ref}}$ (PhN)	-9.0280		M1·LiCl	419	-40
MW_{det} [g/mol]	586		M1	304	-93
			M0	268	-119
-15°C					
	<i>Signal</i>	a2	<i>Species</i>	MW_{calc} [g/mol]	MW_{err} [%]
D_x (a2)	4.5560E-10		LiCl·D1·LiCl	693	39
$\log D_x$ (a2)	-9.3414		D1	464	9
$\log D_{x,\text{norm}}$ (a2)	-9.0650		LiCl·D2·LiCl	693	39
D_{ref} (PhN)	6.9570E-10		D2	464	9
$\log D_{\text{ref}}$ (PhN)	-9.1576		M1·LiCl	419	-1
MW_{det} [g/mol]	422		M1	304	-39
			M0	268	-58
	<i>Signal</i>	b2	<i>Species</i>	MW_{calc} [g/mol]	MW_{err} [%]
D_x (b2)	4.3210E-10		LiCl·D1·LiCl	693	33
$\log D_x$ (b2)	-9.3644		D1	464	0
$\log D_{x,\text{norm}}$ (b2)	-9.0880		LiCl·D2·LiCl	693	33
D_{ref} (PhN)	6.9570E-10		D2	464	0
$\log D_{\text{ref}}$ (PhN)	-9.1576		M1·LiCl	419	-10
MW_{det} [g/mol]	462		M1	304	-52
			M0	268	-73
	<i>Signal</i>	c2	<i>Species</i>	MW_{calc} [g/mol]	MW_{err} [%]
D_x (c2)	3.7190E-10		LiCl·D1·LiCl	693	14
$\log D_x$ (c2)	-9.4296		D1	464	-29
$\log D_{x,\text{norm}}$ (c2)	-9.1532		LiCl·D2·LiCl	693	14
D_{ref} (PhN)	6.9570E-10		D2	464	-29
$\log D_{\text{ref}}$ (PhN)	-9.1576		M1·LiCl	419	-43
MW_{det} [g/mol]	598		M1	304	-97
			M0	268	-124

-40°C					
	<i>Signal</i>	a2	<i>Species</i>	MW_{calc} [g/mol]	MW_{err} [%]
D_x (a2)	2.6880E-10		LiCl·D1·LiCl	693	39
$\log D_x$ (a2)	-9.5706		D1	464	9
$\log D_{x,\text{norm}}$ (a2)	-9.0658		LiCl·D2·LiCl	693	39
D_{ref} (PhN)	4.1120E-10		D2	464	9
$\log D_{\text{ref}}$ (PhN)	-9.3859		M1·LiCl	419	-1
MW_{det} [g/mol]	423		M1	304	-39
			M0	268	-58
	<i>Signal</i>	b2	<i>Species</i>	MW_{calc} [g/mol]	MW_{err} [%]
D_x (b2)	2.5450E-10		LiCl·D1·LiCl	693	33
$\log D_x$ (b2)	-9.5943		D1	464	0
$\log D_{x,\text{norm}}$ (b2)	-9.0896		LiCl·D2·LiCl	693	33
D_{ref} (PhN)	4.1120E-10		D2	464	0
$\log D_{\text{ref}}$ (PhN)	-9.3859		M1·LiCl	419	-11
MW_{det} [g/mol]	465		M1	304	-53
			M0	268	-74
	<i>Signal</i>	c2	<i>Species</i>	MW_{calc} [g/mol]	MW_{err} [%]
D_x (c2)	2.1570E-10		LiCl·D1·LiCl	693	11
$\log D_x$ (c2)	-9.6661		D1	464	-33
$\log D_{x,\text{norm}}$ (c2)	-9.1614		LiCl·D2·LiCl	693	11
D_{ref} (PhN)	4.1120E-10		D2	464	-33
$\log D_{\text{ref}}$ (PhN)	-9.3859		M1·LiCl	419	-48
MW_{det} [g/mol]	618		M1	304	-103
			M0	268	-131
-60°C					
	<i>Signal</i>	a2	<i>Species</i>	MW_{calc} [g/mol]	MW_{err} [%]
D_x (a2)	1.3470E-10		LiCl·D1·LiCl	693	37
$\log D_x$ (a2)	-9.8706		D1	464	5
$\log D_{x,\text{norm}}$ (a2)	-9.0748		LiCl·D2·LiCl	693	37
D_{ref} (PhN)	2.1037E-10		D2	464	5
$\log D_{\text{ref}}$ (PhN)	-9.6770		M1·LiCl	419	-5
MW_{det} [g/mol]	439		M1	304	-44
			M0	268	-64
	<i>Signal</i>	b2	<i>Species</i>	MW_{calc} [g/mol]	MW_{err} [%]
D_x (b2)	1.3190E-10		LiCl·D1·LiCl	693	34
$\log D_x$ (b2)	-9.8798		D1	464	2
$\log D_{x,\text{norm}}$ (b2)	-9.0839		LiCl·D2·LiCl	693	34
D_{ref} (PhN)	2.1037E-10		D2	464	2

$\log D_{\text{ref}}(\text{PhN})$	-9.6770		M1·LiCl	419	-9
$MW_{\text{det}} [\text{g/mol}]$	455		M1	304	-50
			M0	268	-70
	<i>Signal</i>	c2	<i>Species</i>	$MW_{\text{calc}} [\text{g/mol}]$	$MW_{\text{err}} [\%]$
$D_x (\text{c2})$	1.0610E-10		LiCl·D1·LiCl	693	5
$\log D_x (\text{c2})$	-9.9743		D1	464	-42
$\log D_{x,\text{norm}} (\text{c2})$	-9.1785		LiCl·D2·LiCl	693	5
$D_{\text{ref}} (\text{PhN})$	2.1037E-10		D2	464	-42
$\log D_{\text{ref}}(\text{PhN})$	-9.6770		M1·LiCl	419	-58
$MW_{\text{det}} [\text{g/mol}]$	661		M1	304	-117
			M0	268	-147
-70°C					
	<i>Signal</i>	a2	<i>Species</i>	$MW_{\text{calc}} [\text{g/mol}]$	$MW_{\text{err}} [\%]$
$D_x (\text{a2})$	9.9060E-11		LiCl·D1·LiCl	693	40
$\log D_x (\text{a2})$	-1.0004E+01		D1	464	10
$\log D_{x,\text{norm}} (\text{a2})$	-9.0625		LiCl·D2·LiCl	693	40
$D_{\text{ref}} (\text{PhN})$	1.5037E-10		D2	464	10
$\log D_{\text{ref}}(\text{PhN})$	-9.8228		M1·LiCl	419	0
$MW_{\text{det}} [\text{g/mol}]$	418		M1	304	-37
			M0	268	-56
	<i>Signal</i>	b2	<i>Species</i>	$MW_{\text{calc}} [\text{g/mol}]$	$MW_{\text{err}} [\%]$
$D_x (\text{b2})$	9.7030E-11		LiCl·D1·LiCl	693	38
$\log D_x (\text{b2})$	-1.0013E+01		D1	464	7
$\log D_{x,\text{norm}} (\text{b2})$	-9.0714		LiCl·D2·LiCl	693	38
$D_{\text{ref}} (\text{PhN})$	1.5037E-10		D2	464	7
$\log D_{\text{ref}}(\text{PhN})$	-9.8228		M1·LiCl	419	-3
$MW_{\text{det}} [\text{g/mol}]$	433		M1	304	-42
			M0	268	-62
	<i>Signal</i>	c2	<i>Species</i>	$MW_{\text{calc}} [\text{g/mol}]$	$MW_{\text{err}} [\%]$
$D_x (\text{c2})$	7.5890E-11		LiCl·D1·LiCl	693	5
$\log D_x (\text{c2})$	-1.0120E+01		D1	464	-42
$\log D_{x,\text{norm}} (\text{c2})$	-9.1782		LiCl·D2·LiCl	693	5
$D_{\text{ref}} (\text{PhN})$	1.5037E-10		D2	464	464
$\log D_{\text{ref}}(\text{PhN})$	-9.8228		M1·LiCl	419	-58
$MW_{\text{det}} [\text{g/mol}]$	660		M1	304	-117
			M0	268	-147

	<i>Signal</i>	a2	too low in intensity	-90°C	
	<i>Signal</i>	b2	<i>Species</i>	MW_{calc} [g/mol]	MW_{err} [%]
D_x (b2)	4.2360E-11		LiCl·D1·LiCl	693	33
$\log D_x$ (b2)	-1.0373E+01		D1	464	0
$\log D_{x,\text{norm}}$ (b2)	-9.0890		LiCl·D2·LiCl	693	33
D_{ref} (PhN)	6.8357E-11		D2	464	0
$\log D_{\text{ref}}$ (PhN)	-1.0165E+01		M1·LiCl	419	-11
MW_{det} [g/mol]	464		M1	304	-53
			M0	268	-73
	<i>Signal</i>	c2	no signal		
	<i>Signal</i>	a2	too low in intensity	-100°C	
	<i>Signal</i>	b2	<i>Species</i>	MW_{calc} [g/mol]	MW_{err} [%]
D_x (b2)	2.9330E-11		LiCl·D1·LiCl	693	35
$\log D_x$ (b2)	-1.0533E+01		D1	464	3
$\log D_{x,\text{norm}}$ (b2)	-9.0818		LiCl·D2·LiCl	693	35
D_{ref} (PhN)	4.6550E-11		D2	464	3
$\log D_{\text{ref}}$ (PhN)	-1.0332E+01		M1·LiCl	419	-8
MW_{det} [g/mol]	451		M1	304	-48
			M0	268	-69
	<i>Signal</i>	b2'	<i>Species</i>	MW_{calc} [g/mol]	MW_{err} [%]
D_x (b2')	2.3890E-11		LiCl·D1·LiCl	693	7
$\log D_x$ (b2')	-1.0622E+01		D1	464	-38
$\log D_{x,\text{norm}}$ (b2')	-9.1709		LiCl·D2·LiCl	693	7
D_{ref} (PhN)	4.6550E-11		D2	464	-38
$\log D_{\text{ref}}$ (PhN)	-1.0332E+01		M1·LiCl	419	-53
MW_{det} [g/mol]	641		M1	304	-111
			M0	268	-140
	<i>Signal</i>	c2	no signal		

⁷Li-DOSY-ECC-MW-determination parameters of ⁱPr₂NMgCl·LiCl 9

A-Table 19. ⁷Li-DOSY-ECC-MW-determination of ⁱPr₂NMgCl·LiCl 9 in THF-*d*₈ (0.10 M). PhN (0.02 M) was used as internal reference with $\log D_{\text{ref,fix}}(\text{PhN}) = -8.8812$. The accuracy of this method is in the range of $MW_{\text{err}} < \pm 9\%$.

⁷ Li-DOSY		25°C		
		<i>Species</i>	<i>MW</i> _{calc} [g/mol]	<i>MW</i> _{err} [%]
<i>D</i> (Li)	8.7220E-10	LiCl·D1·LiCl	693	31
$\log D_x$ (Li)	-9.0594	LiCl·D2·LiCl	693	31
$\log D_{x,\text{norm}}$ (Li)	-9.0963	M1·LiCl	419	-14
<i>D</i> _{ref} (PhN)	1.4313E-09	LiCl-Dimer	373	-28
$\log D_{\text{ref}}$ (PhN)	-8.8443	Li(THF) ₄	295.38	-62
<i>MW</i> _{det}	478			
+0°C				
		<i>Species</i>	<i>MW</i> _{calc} [g/mol]	<i>MW</i> _{err} [%]
<i>D</i> (Li)	5.5920E-10	LiCl·D1·LiCl	693	29
$\log D_x$ (Li)	-9.2524	LiCl·D2·LiCl	693	29
$\log D_{x,\text{norm}}$ (Li)	-9.1056	M1·LiCl	419	-18
<i>D</i> _{ref} (PhN)	9.3753E-10	LiCl-Dimer	373	-33
$\log D_{\text{ref}}$ (PhN)	-9.0280	Li(THF) ₄	295.38	-68
<i>MW</i> _{det}	496			
-15°C				
		<i>Species</i>	<i>MW</i> _{calc} [g/mol]	<i>MW</i> _{err} [%]
<i>D</i> (Li)	4.1750E-10	LiCl·D1·LiCl	693	29
$\log D_x$ (Li)	-9.3793	LiCl·D2·LiCl	693	29
$\log D_{x,\text{norm}}$ (Li)	-9.1030	M1·LiCl	419	-17
<i>D</i> _{ref} (PhN)	6.9570E-10	LiCl-Dimer	373	-31
$\log D_{\text{ref}}$ (PhN)	-9.1576	Li(THF) ₄	295.38	-66
<i>MW</i> _{det}	490			
-40°C				
		<i>Species</i>	<i>MW</i> _{calc} [g/mol]	<i>MW</i> _{err} [%]
<i>D</i> (Li)	2.5810E-10	LiCl·D1·LiCl	693	34
$\log D_x$ (Li)	-9.5882	LiCl·D2·LiCl	693	34
$\log D_{x,\text{norm}}$ (Li)	-9.0835	M1·LiCl	419	-8
<i>D</i> _{ref} (PhN)	4.1120E-10	LiCl-Dimer	373	-22
$\log D_{\text{ref}}$ (PhN)	-9.3859	Li(THF) ₄	295.38	-54
<i>MW</i> _{det}	454			

-60°C				
		<i>Species</i>	MW_{calc} [g/mol]	MW_{err} [%]
D (Li)	1.4340E-10	LiCl·D1·LiCl	693	43
$\log D_x$ (Li)	-9.8435	LiCl·D2·LiCl	693	43
$\log D_{x,\text{norm}}$ (Li)	-9.0476	M1·LiCl	419	6
D_{ref} (PhN)	2.1037E-10	LiCl-Dimer	373	-6
$\log D_{\text{ref}}$ (PhN)	-9.6770	Li(THF)4	295	-33
MW_{det}	394			
-70°C				
		<i>Species</i>	MW_{calc} [g/mol]	MW_{err} [%]
D (Li)	1.0740E-10	LiCl·D1·LiCl	693	48
$\log D_x$ (Li)	-9.9690	LiCl·D2·LiCl	693	48
$\log D_{x,\text{norm}}$ (Li)	-9.0273	M1·LiCl	419	13
D_{ref} (PhN)	1.5037E-10	LiCl-Dimer	373	3
$\log D_{\text{ref}}$ (PhN)	-9.8228	Li(THF)4	295	-23
MW_{det}	364			
-90°C				
		<i>Species</i>	MW_{calc} [g/mol]	MW_{err} [%]
D (Li)	4.7090E-11	LiCl·D1·LiCl	693	44
$\log D_x$ (Li)	-1.0327E+01	LiCl·D2·LiCl	693	44
$\log D_{x,\text{norm}}$ (Li)	-9.0431	M1·LiCl	419	8
D_{ref} (PhN)	6.8357E-11	LiCl-Dimer	373	-4
$\log D_{\text{ref}}$ (PhN)	-1.0165E+01	Li(THF)4	295	-31
MW_{det}	387			
-100°C				
		<i>Species</i>	MW_{calc} [g/mol]	MW_{err} [%]
D (Li)	3.2170E-11	LiCl·D1·LiCl	693	44
$\log D_x$ (Li)	-1.0493E+01	LiCl·D2·LiCl	693	44
$\log D_{x,\text{norm}}$ (Li)	-9.0417	M1·LiCl	419	8
D_{ref} (PhN)	4.6550E-11	LiCl-Dimer	373	-3
$\log D_{\text{ref}}$ (PhN)	-1.0332E+01	Li(THF)4	295.38	-30
MW_{det}	385			

A-Table 20. DOSY-ECC-MW-determination of anhydrous LiCl in THF-*d*₈ (0.015 M). 2,2,3,3-tetramethylbutane (TMB) was used as internal reference with $\log D_{\text{ref,fix}}(\text{TMB}) = -8.7749$.

	25°C	0°C	-25°C	-50°C	-75°C	av.
$D_{\text{ref}}(\text{TMB})$	2.003E-09	1.319E-09	8.821E-10	4.806E-10	2.299E-10	
$D_x(\text{Li})$	1.102E-09	7.318E-10	4.790E-10	2.631E-10	1.204E-10	
MW_{calc} [g/mol]	373	373	373	373	373	373
MW_{det} [g/mol]	374	369	382	377	401	381
MW_{err} [%]	0	1	-2	-1	-7	-2

Aggregate $\text{M1} \cdot (\text{MgCl}_2)_2 \cdot \text{M1}$ ($MW_{\text{calc}} = 943$ g/mol) show an increased van der Waals value of $MD_w = 6.26 \cdot 10^{29}$ (A-Table 21). This aggregate would be underestimated in MW by approximately 10%, $\Delta MW = 94$ g/mol. However, the highest MW we could observe was $MW_{\text{det}} = 578$ g/mol so aggregate $\text{M1} \cdot (\text{MgCl}_2)_2 \cdot \text{M1}$ can be excluded to be present in solution of 7.

A-Table 21. Calculation of the molar van der Waals density MD_w of all ¹Pr₂NMgCl 7 species.

Species	Formula	MW_{calc} [g/mol]	$MD_w/10^{29}$ [g/(mol·m ³)]	
	$\text{M1} \cdot (\text{MgCl}_2)_2 \cdot \text{M1}$	C36H76Cl6Mg4N2O6	943	6.26
e1	$\text{MgCl}_2 \cdot \text{D1}(\text{D2}) \cdot \text{MgCl}_2$	C20H44Cl6Mg4N2O2	655	6.98
f1	$(\mu\text{-Cl3})\text{-M1} \cdot \text{MgCl}_2$	C26H54Cl3Mg2NO5	616	5.95
d1	D1	C20H44Cl2Mg2N2O2	464	5.76
c1	D2	C20H44Cl2Mg2N2O2	464	5.76
b1	M2	C20H44MgN2O2	369	4.99
a1	M1	C14H30ClMgNO2	304	5.58

Compound $\text{MgCl}_2 \cdot \text{D1}(\text{D2}) \cdot \text{MgCl}_2$ ($MW_{\text{calc}} = 655$ g/mol) has a very huge van der Waals density. This is why this aggregate would be highly underestimated in MW by approximately 20%, $\Delta MW = 131$ g/mol. For species **e1** a MW of $MW_{\text{det}} = 578$ g/mol was measured that is in the 20% region of compound $\text{MgCl}_2 \cdot \text{D1}(\text{D2}) \cdot \text{MgCl}_2$. This is why a density correction was done (see chapter 2.1.7). The results are shown in A-Table 22:

A-Table 22. Density correction of species e1.

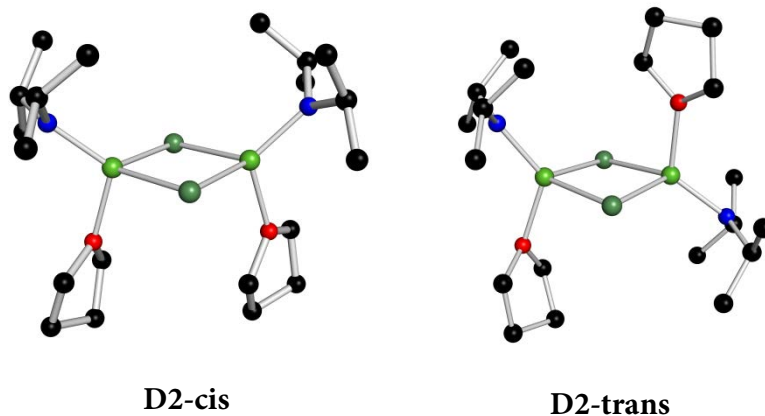
Species e1	T[°C]	MW_{calc}	MW_{det}	X_{corr}	$MW_{\text{det,corr}}$
		[g/mol]	[g/mol]		[g/mol]
$\text{MgCl}_2 \cdot \text{D1(D2)} \cdot \text{MgCl}_2$	-80	655	578	1.22	703
$MD_w = 6.98 \cdot 10^{29}$	-70	655	446	1.22	542
	-60	655	409	1.22	497

A-Table 23. Calculation of the molar van der Waals density MD_w of all ${}^i\text{Pr}_2\text{NMgCl} \cdot \text{LiCl}$ 9 species.

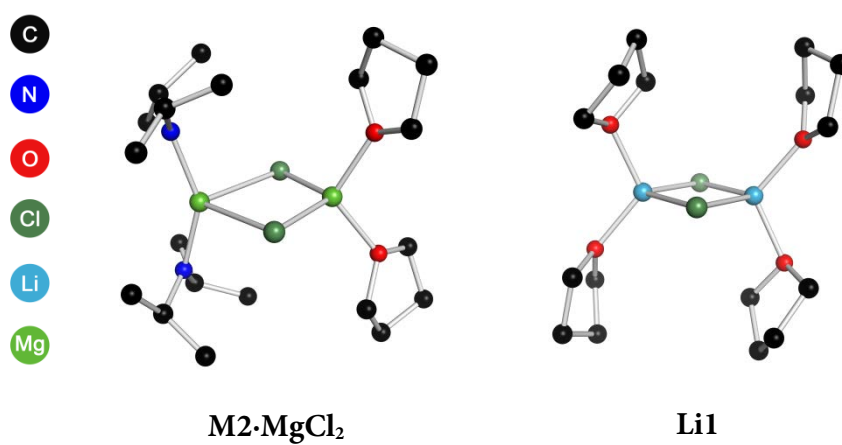
Species	Formula	MW_{calc}	$MD_w/10^{29}$	
		[g/mol]	[g/(mol·m ³)]	
b'	M1·(LiCl)₂·M1	C28H60Cl4Li2Mg2N2O4	693	5.85
c	LiCl·D1·LiCl	C28H60Cl4Li2Mg2N2O4	693	5.85
	D1	C20H44Cl2Mg2N2O2	464	5.76
b	D2	C20H44Cl2Mg2N2O2	464	5.76
a	M1·LiCl	C18H38Cl2LiMgNO3	418	5.70
Li	Li1	C16H32Cl2Li2O4	373	5.64
	M1	C14H30ClMgNO2	304	5.58
	Li2	C16H32LiO4	295	4.99
	M0	C10H22Cl2MgNO	268	6.30

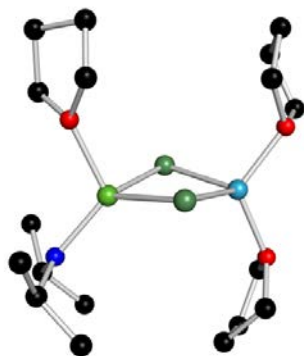
In the case of ${}^i\text{Pr}_2\text{NMgCl} \cdot \text{LiCl}$ 9 all van der Waals densities are in the desired range (A-Table 23) of $MD_w = 4.3 \cdot 10^{29}$ g/(mol·m³) and $MD_w = 5.9 \cdot 10^{29}$ g/(mol·m³). Only species **M0** ($MW_{\text{calc}} = 268$ g/mol) would be underestimated in MW by approximately 20%, $\Delta MW = 54$ g/mol. However, the smallest MW we could observe was $MW_{\text{det}} = 364$ g/mol, so species **M0** can be excluded to be present in solution of 9.

Optimized Structures from theoretical calculations



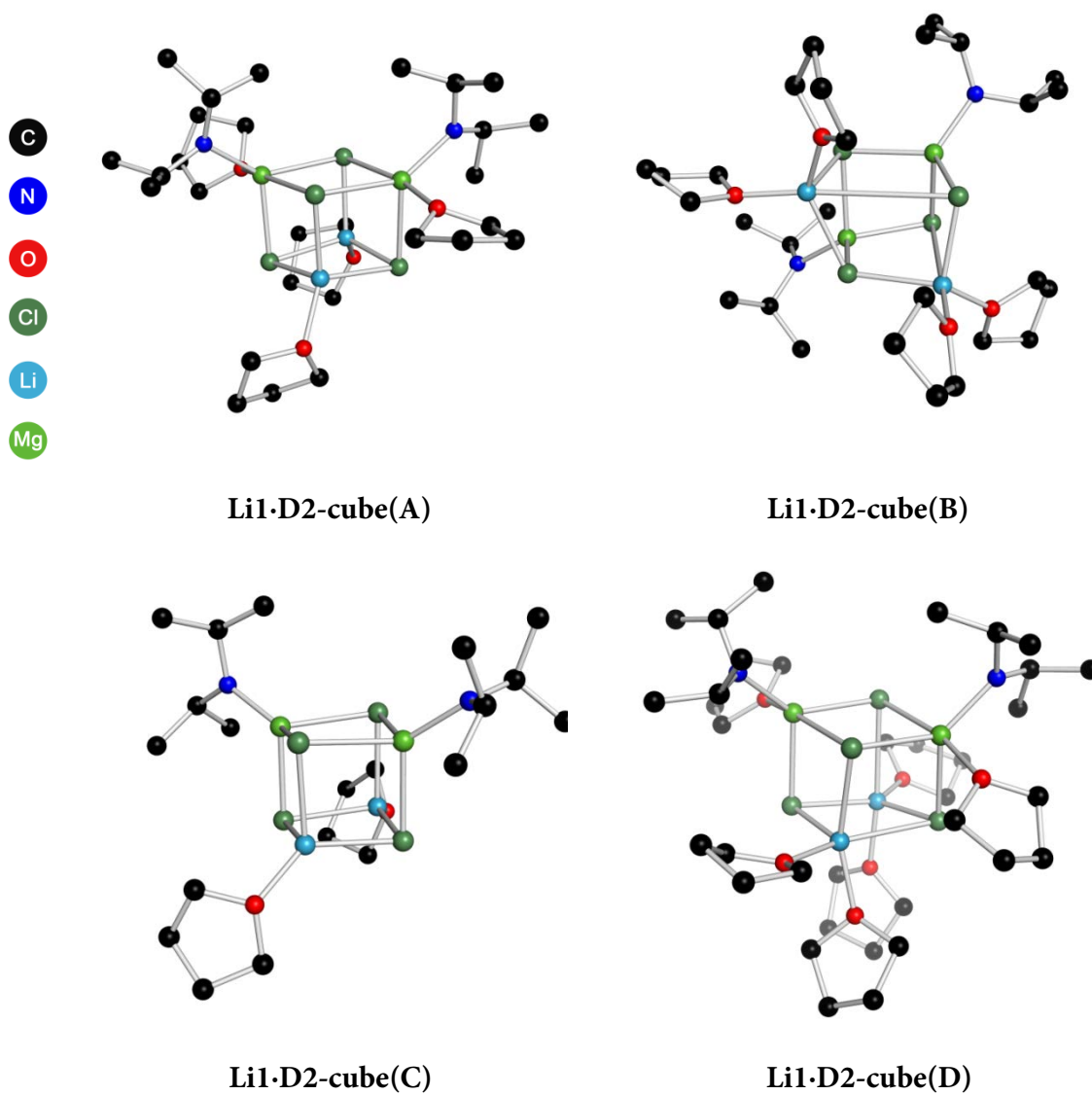
A-Figure 12. B3LYP-D3/def2-SVP optimized structures of D2 (cis and trans).

A-Figure 13. B3LYP-D3/def2-SVP optimized structures of M2·MgCl₂ and Li1.

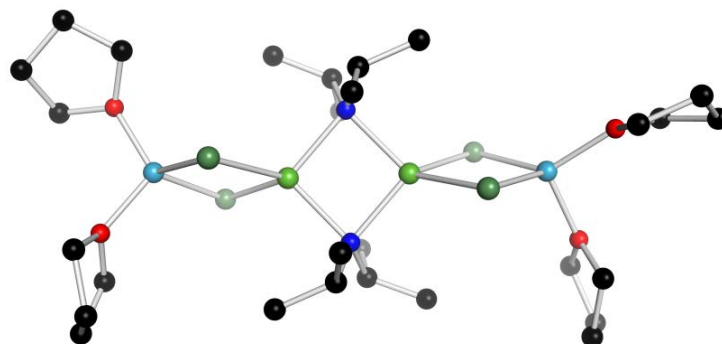


M1-LiCl

A-Figure 14. B3LYP-D3/def2-SVP optimized structure of M1-LiCl.

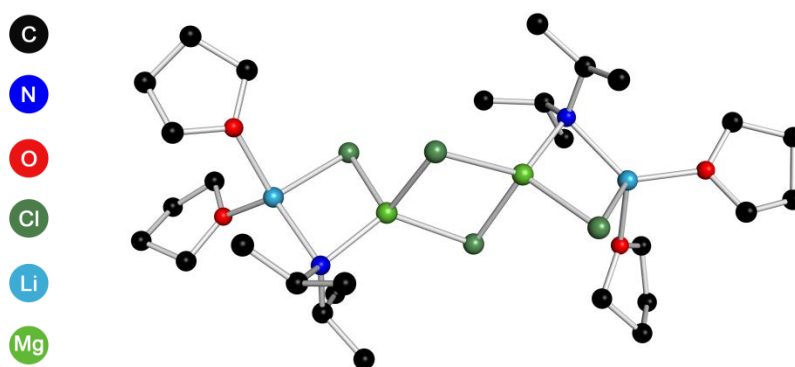


A-Figure 15. B3LYP-D3/def2-SVP optimized structures of Li1-D2-cube(A-D).



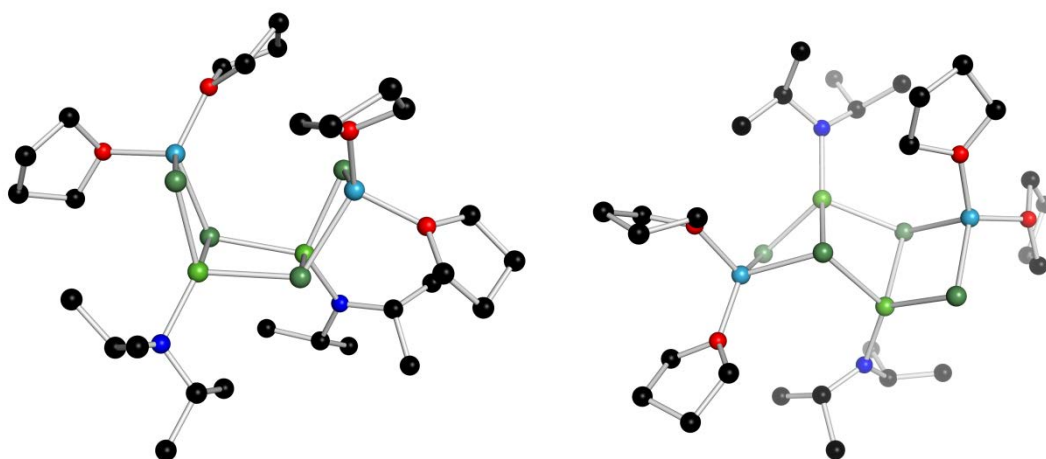
LiCl·D1·LiCl

A-Figure 16. B3LYP-D3/def2-SVP optimized structures of LiCl·D1·LiCl.



LiCl·D2*·LiCl

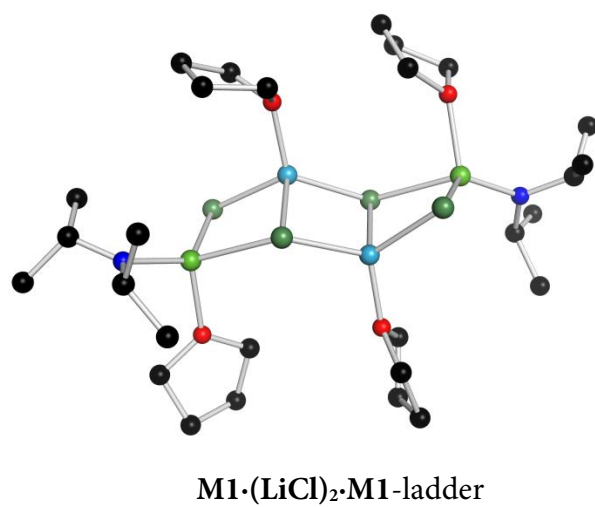
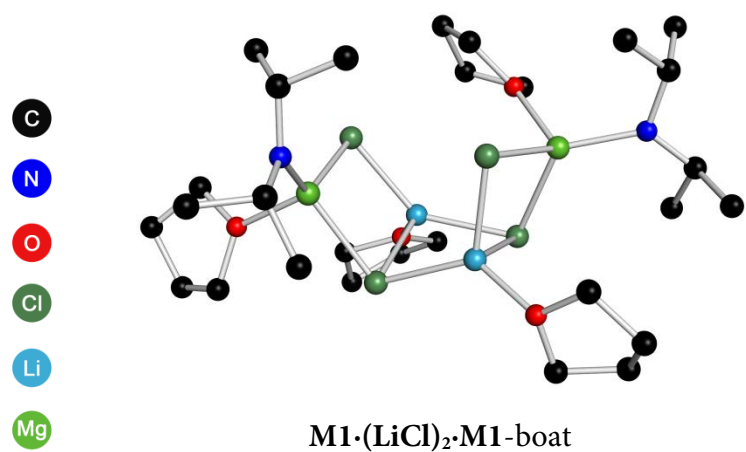
A-Figure 17. B3LYP-D3/def2-SVP optimized structures of LiCl·D2*·LiCl.



LiCl·D2·LiCl-boat

LiCl·D2·LiCl-ladder

A-Figure 18. B3LYP-D3/def2-SVP optimized structures of LiCl·D2·LiCl (boat and ladder).



A-Figure 19. B3LYP-D3/def2-SVP optimized structures of M1·(LiCl)₂·M1 (boat and ladder).

Free Enthalpies of computed species**A-Table 24. Relative free enthalpies ΔG in kJ/mol. (left: D2-cis and right Cube D was used as reference)**

<i>T</i> [°C]	<i>D2-cis</i>	<i>D2-trans</i>	<i>M2·MgCl₂</i>	<i>Cube A</i>	<i>Cube B</i>	<i>Cube C</i>	<i>Cube D</i>
-90	0	5.5	53.7	10.6	20.4	51.5	0.0
-85	0	5.6	53.7	9.1	18.9	48.4	0.0
-80	0	5.7	53.6	7.5	17.3	45.2	0.0
-75	0	5.7	53.6	5.9	15.7	42.1	0.0
-70	0	5.8	53.6	4.4	14.2	39.1	0.0
-65	0	5.9	53.6	2.8	12.6	36.0	0.0
-60	0	6.0	53.6	1.3	11.1	32.9	0.0
-55	0	6.0	53.6	0.0	9.8	30.1	0.3
-50	0	6.1	53.6	0.0	9.8	28.6	1.8
-45	0	6.2	53.5	0.0	9.8	27.0	3.4
-40	0	6.3	53.5	0.0	9.8	25.5	4.9
-35	0	6.3	53.5	0.0	9.8	24.0	6.5
-30	0	6.4	53.5	0.0	9.8	22.5	8.0
-25	0	6.5	53.4	0.0	9.8	21.0	9.6
-20	0	6.6	53.4	0.0	9.9	19.5	11.1
-15	0	6.7	53.4	0.0	9.9	18.0	12.7
-10	0	6.7	53.4	0.0	9.9	16.5	14.2
-5	0	6.8	53.3	0.0	9.9	15.0	15.7
0	0	6.9	53.3	0.0	9.9	13.5	17.3
5	0	7.0	53.3	0.0	9.9	12.0	18.8
10	0	7.1	53.3	0.0	10.0	10.5	20.3
15	0	7.1	53.2	0.0	10.0	9.1	21.9
20	0	7.2	53.2	0.0	10.0	7.6	23.4
25	0	7.3	53.2	0.0	10.0	6.1	24.9

A-Table 25. Relative free enthalpies ΔG for mixed dimers of LiCl and ${}^i\text{Pr}_2\text{NMgCl}$ in kJ/mol, with LiCl·D1·LiCl as reference.

T [°C]	<i>LiCl·D2·LiCl-</i> <i>boat</i>	<i>LiCl·D2·LiCl-</i> <i>ladder</i>	<i>M1·(LiCl)₂·M-</i> <i>boat</i>	<i>M1·(LiCl)₂·M1-</i> <i>ladder</i>	<i>LiCl·D1·LiCl</i>
-90	95.7	97.6	55.2	57.8	0.0
-85	95.7	97.5	55.1	57.8	0.0
-80	95.7	97.5	55.1	57.7	0.0
-75	95.7	97.4	55.0	57.6	0.0
-70	95.7	97.3	54.9	57.6	0.0
-65	95.7	97.2	54.9	57.5	0.0
-60	95.7	97.2	54.8	57.5	0.0
-55	95.7	97.1	54.8	57.4	0.0
-50	95.7	97.0	54.7	57.3	0.0
-45	95.7	97.0	54.6	57.3	0.0
-40	95.8	96.9	54.6	57.2	0.0
-35	95.8	96.8	54.5	57.1	0.0
-30	95.8	96.8	54.5	57.1	0.0
-25	95.8	96.7	54.4	57.0	0.0
-20	95.8	96.6	54.3	56.9	0.0
-15	95.8	96.6	54.3	56.9	0.0
-10	95.8	96.5	54.2	56.8	0.0
-5	95.9	96.4	54.2	56.7	0.0
0	95.9	96.3	54.1	56.6	0.0
5	95.9	96.3	54.0	56.6	0.0
10	95.9	96.2	54.0	56.5	0.0
15	95.9	96.1	53.9	56.4	0.0
20	96.0	96.1	53.9	56.4	0.0
25	96.0	96.0	53.8	56.3	0.0

Free Reaction enthalpies for the reaction of D2 and Li1**A-Table 26. Free Reaction enthalpies for the reaction of D2 and Li1 in kJ/mol.**

<i>T</i> [°C]	<i>CUBE A</i>	<i>CUBE B</i>	<i>CUBE C</i>	<i>CUBE D</i>
-90	21.4	31.2	62.2	10.7
-85	20.9	30.7	60.2	11.9
-80	20.5	30.3	58.3	13.0
-75	20.1	29.9	56.3	14.1
-70	19.6	29.4	54.3	15.3
-65	19.2	29.0	52.3	16.4
-60	18.8	28.6	50.4	17.5
-55	18.3	28.1	48.4	18.6
-50	17.9	27.7	46.5	19.7
-45	17.5	27.3	44.5	20.9
-40	17.1	26.9	42.6	22.0
-35	16.6	26.4	40.6	23.1
-30	16.2	26.0	38.7	24.2
-25	15.8	25.6	36.8	25.3
-20	15.3	25.2	34.8	26.5
-15	14.9	24.8	32.9	27.6
-10	14.5	24.4	31.0	28.7
-5	14.1	24.0	29.1	29.8
0	13.6	23.5	27.1	30.9
5	13.2	23.1	25.2	32.0
10	12.8	22.7	23.3	33.1
15	12.4	22.3	21.4	34.2
20	11.9	21.9	19.5	35.3
25	11.5	21.5	17.6	36.4

A-Table 27. Free Reaction enthalpies for the reaction of D2 and Li1 in kJ/mol.

T [°C]	$\text{LiCl}\cdot\text{D}_2\cdot\text{LiCl}$ - <i>boat</i>	$\text{LiCl}\cdot\text{D}_2\cdot\text{LiCl}$ - <i>ladder</i>	$\text{M1}\cdot(\text{LiCl})_2\cdot\text{M1}$ - <i>boat</i>	$\text{M1}\cdot(\text{LiCl})_2\cdot\text{M1}$ - <i>ladder</i>	$\text{LiCl}\cdot\text{D1}\cdot\text{LiCl}$
-90	37.1	39.1	-3.3	-0.7	-58.5
-85	36.7	38.6	-3.8	-1.2	-58.9
-80	36.3	38.1	-4.3	-1.7	-59.4
-75	35.9	37.6	-4.8	-2.2	-59.8
-70	35.5	37.1	-5.3	-2.6	-60.2
-65	35.0	36.6	-5.8	-3.1	-60.7
-60	34.6	36.1	-6.3	-3.6	-61.1
-55	34.2	35.6	-6.7	-4.1	-61.5
-50	33.8	35.1	-7.2	-4.6	-61.9
-45	33.4	34.6	-7.7	-5.1	-62.3
-40	33.0	34.1	-8.2	-5.6	-62.8
-35	32.6	33.6	-8.7	-6.1	-63.2
-30	32.2	33.1	-9.2	-6.6	-63.6
-25	31.8	32.7	-9.6	-7.0	-64.0
-20	31.4	32.2	-10.1	-7.5	-64.4
-15	31.0	31.7	-10.6	-8.0	-64.9
-10	30.6	31.2	-11.1	-8.5	-65.3
-5	30.2	30.7	-11.5	-9.0	-65.7
0	29.8	30.2	-12.0	-9.5	-66.1
5	29.4	29.8	-12.5	-9.9	-66.5
10	29.0	29.3	-12.9	-10.4	-66.9
15	28.6	28.8	-13.4	-10.9	-67.3
20	28.2	28.3	-13.9	-11.4	-67.7
25	27.8	27.9	-14.3	-11.8	-68.1

Free Reaction enthalpies for the reaction of 2 M1·LiCl**A-Table 28. Free Reaction enthalpies for the reaction 2 M1·LiCl in kJ/mol.**

<i>T</i> [°C]	<i>CUBE A</i>	<i>CUBE B</i>	<i>CUBE C</i>	<i>CUBE D</i>
-90	42.0	51.7	82.8	31.3
-85	41.4	51.2	80.7	32.4
-80	40.9	50.7	78.6	33.4
-75	40.4	50.1	76.6	34.4
-70	39.8	49.6	74.5	35.5
-65	39.3	49.1	72.4	36.5
-60	38.8	48.6	70.4	37.5
-55	38.3	48.0	68.3	38.5
-50	37.7	47.5	66.3	39.6
-45	37.2	47.0	64.2	40.6
-40	36.7	46.5	62.2	41.6
-35	36.1	45.9	60.1	42.6
-30	35.6	45.4	58.1	43.6
-25	35.1	44.9	56.1	44.6
-20	34.5	44.4	54.0	45.7
-15	34.0	43.9	52.0	46.7
-10	33.5	43.4	50.0	47.7
-5	32.9	42.8	48.0	48.7
0	32.4	42.3	45.9	49.7
5	31.9	41.8	43.9	50.7
10	31.4	41.3	41.9	51.7
15	30.8	40.8	39.9	52.7
20	30.3	40.3	37.9	53.7
25	29.8	39.8	35.9	54.7

A-Table 29. Free Reaction enthalpies for the reaction of 2 M1·LiCl in kJ/mol.

<i>T</i> [°C]	<i>LiCl</i> · <i>D2</i> · <i>LiCl</i> - <i>boat</i>	<i>LiCl</i> · <i>D2</i> · <i>LiCl</i> - <i>ladder</i>	<i>M1</i> ·(<i>LiCl</i>) ₂ · <i>M1</i> - <i>boat</i>	<i>M1</i> ·(<i>LiCl</i>) ₂ · <i>M1</i> - <i>ladder</i>	<i>LiCl</i> · <i>D1</i> · <i>LiCl</i>
-90	57.7	59.7	17.3	19.9	-37.9
-85	57.2	59.1	16.7	19.3	-38.5
-80	56.7	58.5	16.1	18.7	-39.0
-75	56.2	57.9	15.5	18.1	-39.5
-70	55.7	57.3	14.9	17.6	-40.0
-65	55.1	56.7	14.3	17.0	-40.6
-60	54.6	56.1	13.7	16.4	-41.1
-55	54.1	55.5	13.2	15.8	-41.6
-50	53.6	54.9	12.6	15.2	-42.1
-45	53.1	54.3	12.0	14.6	-42.6
-40	52.6	53.7	11.4	14.0	-43.2
-35	52.1	53.1	10.8	13.4	-43.7
-30	51.6	52.6	10.3	12.8	-44.2
-25	51.1	52.0	9.7	12.3	-44.7
-20	50.6	51.4	9.1	11.7	-45.2
-15	50.1	50.8	8.5	11.1	-45.8
-10	49.6	50.2	7.9	10.5	-46.3
-5	49.1	49.6	7.4	9.9	-46.8
0	48.6	49.0	6.8	9.3	-47.3
5	48.1	48.5	6.2	8.7	-47.8
10	47.6	47.9	5.6	8.2	-48.3
15	47.1	47.3	5.1	7.6	-48.9
20	46.6	46.7	4.5	7.0	-49.4
25	46.1	46.1	3.9	6.4	-49.9

¹H-DOSY-ECC-MW-determination parameters of TMPMgCl·LiCl 10 at 25°C to -75°C

A-Table 30. ¹H-DOSY-ECC-MW-determination of TMPMgCl·LiCl 10 in THF-*d*₈ (20 mM). PhN was used as internal reference in equimolar ratio with $\log D_{\text{ref,fix}}(\text{PhN}) = -8.8812$.

¹ H DOSY		25°C		
		<i>Species</i>	<i>MW</i> _{calc} [g/mol]	<i>MW</i> _{err} [%]
<i>D</i> _x	9.3030E-10	1A	773	49
$\log D_x$	-9.0314	1B	544	28
$\log D_{x,\text{norm}}$	-9.0476	1C	459	14
<i>D</i> _{ref} (PhN)	1.3647E-09	1C*	387	-2
$\log D_{\text{ref}}(\text{PhN})$	-8.8650	1D	344	-14
<i>MW</i> _{det} [g/mol]	394	1E	308	-28
+0°C				
		<i>Species</i>	<i>MW</i> _{calc} [g/mol]	<i>MW</i> _{err} [%]
<i>D</i> _x	6.7670E-10	1A	773	50
$\log D_x$	-9.1696	1B	544	29
$\log D_{x,\text{norm}}$	-9.0418	1C	459	16
<i>D</i> _{ref} (PhN)	9.7947E-10	1C*	387	0
$\log D_{\text{ref}}(\text{PhN})$	-9.0090	1D	344	-12
<i>MW</i> _{det} [g/mol]	385	1E	308	-25
-25°C				
		<i>Species</i>	<i>MW</i> _{calc} [g/mol]	<i>MW</i> _{err} [%]
<i>D</i> _x	3.8980E-10	1A	773	48
$\log D_x$	-9.4092	1B	544	26
$\log D_{x,\text{norm}}$	-9.0533	1C	459	12
<i>D</i> _{ref} (PhN)	5.7933E-10	1C*	387	-4
$\log D_{\text{ref}}(\text{PhN})$	-9.2371	1D	344	-17
<i>MW</i> _{det} [g/mol]	403	1E	308	-31
-50°C				
		<i>Species</i>	<i>MW</i> _{calc} [g/mol]	<i>MW</i> _{err} [%]
<i>D</i> _x	2.1200E-10	1A	773	47
$\log D_x$	-9.6737	1B	544	24
$\log D_{x,\text{norm}}$	-9.0595	1C	459	10
<i>D</i> _{ref} (PhN)	3.1960E-10	1C*	387	-7
$\log D_{\text{ref}}(\text{PhN})$	-9.4954	1D	344	-20
<i>MW</i> _{det} [g/mol]	413	1E	308	-34

		-75°C		
		<i>Species</i>	MW_{calc} [g/mol]	MW_{err} [%]
D_x	1.1030E-10	1A	773	46
$\log D_x$	-9.9574	1B	544	23
$\log D_{x,\text{norm}}$	-9.0625	1C	459	9
D_{ref} (PhN)	1.6743E-10	1C*	387	-8
$\log D_{\text{ref}}$ (PhN)	-9.7762	1D	344	-21
MW_{det} [g/mol]	418	1E	308	-36

⁷Li-DOSY-ECC-MW-determination parameters of TMPMgCl·LiCl 10 at 25°C to -75°C

A-Table 31. ⁷Li-DOSY-ECC-MW-determination of TMPMgCl·LiCl 10 in THF-*d*₈ (20 mm). PhN was used as internal reference in equimolar ratio with $\log D_{\text{ref,fix}}(\text{PhN}) = -8.8812$.

⁷ Li DOSY		25°C		
		<i>Species</i>	MW_{calc} [g/mol]	MW_{err} [%]
D (Li)	9.3330E-10	1A	773	49
$\log D_x$ (Li)	-9.0300	1C	459	15
$\log D_{x,\text{norm}}$ (Li)	-9.0462	Li1	373	-5
D_{ref} (PhN)	1.3647E-09	1C*	387	-1
$\log D_{\text{ref}}$ (PhN)	-8.8650	Li2	295	-33
MW_{det}	392			
		+0°C		
		<i>Species</i>	MW_{calc} [g/mol]	MW_{err} [%]
D (Li)	6.7490E-10	1A	773	50
$\log D_x$ (Li)	-9.1708	1C	459	16
$\log D_{x,\text{norm}}$ (Li)	-9.0430	Li1	373	-4
D_{ref} (PhN)	9.7947E-10	1C*	387	0
$\log D_{\text{ref}}$ (PhN)	-9.0090	Li2	295	-31
MW_{det}	387			
		-25°C		
		<i>Species</i>	MW_{calc} [g/mol]	MW_{err} [%]
D (Li)	3.9330E-10	1A	773	49
$\log D_x$ (Li)	-9.4053	1C	459	14
$\log D_{x,\text{norm}}$ (Li)	-9.0494	Li1	373	-6
D_{ref} (PhN)	5.7933E-10	1C*	387	-3
$\log D_{\text{ref}}$ (PhN)	-9.2371	Li2	295	-34
MW_{det}	397			

		-50°C		
		<i>Species</i>	MW_{calc} [g/mol]	MW_{err} [%]
D (Li)	2.1940E-10	1A	773	50
$\log D_x$ (Li)	-9.6588	1C	459	15
$\log D_{x,\text{norm}}$ (Li)	-9.0446	Li1	373	-4
D_{ref} (PhN)	3.1960E-10	1C*	387	-1
$\log D_{\text{ref}}$ (PhN)	-9.4954	Li2	295	-32
MW_{det}	389			
		-75°C		
		<i>Species</i>	MW_{calc} [g/mol]	MW_{err} [%]
D (Li)	1.1840E-10	1A	773	52
$\log D_x$ (Li)	-9.9266	1C	459	19
$\log D_{x,\text{norm}}$ (Li)	-9.0317	Li1	373	1
D_{ref} (PhN)	1.6743E-10	1C*	387	4
$\log D_{\text{ref}}$ (PhN)	-9.7762	Li2	295	-25
MW_{det}	370			

¹H-DOSY-ECC-MW-determination parameters of TMP(H) at 25°C to -75°C

A-Table 32. ¹H-DOSY-ECC-MW-determination of the protonated amine TMP(H) in THF-*d*₈ (20 mM). PhN was used as internal reference in equimolar ratio with $\log D_{\text{ref,fix}}(\text{PhN}) = -8.8812$. The MW of TMP(H), a highly spherical and compact molecule was calculated by using ECC_{CS}.

¹ H DOSY		25°C		
		<i>Species</i>	MW_{calc} [g/mol]	MW_{err} [%]
D (TMP(H))	1.4980E-09	TMP(H)	141	-18
$\log D$ (TMP(H))	-8.824488187			
$\log D_{x,\text{norm}}$ (TMP(H))	-8.8407			
D_{ref} (PhN)	1.3647E-09			
$\log D_{\text{ref}}$ (PhN)	-8.8650			
MW_{det}	167			
		+0°C		
		<i>Species</i>	MW_{calc} [g/mol]	MW_{err} [%]
D (TMP(H))	1.1400E-09	TMP(H)	141	-5
$\log D$ (TMP(H))	-8.943095149			
$\log D_{x,\text{norm}}$ (TMP(H))	-8.8153			
D_{ref} (PhN)	9.7947E-10			
$\log D_{\text{ref}}$ (PhN)	-9.0090			
MW_{det}	148			

				-25°C
		<i>Species</i>	MW_{calc} [g/mol]	MW_{err} [%]
D (TMP(H))	6.7950E-10	TMP(H)	141	-3
$\log D$ (TMP(H))	-9.167810539			
$\log D_{x,\text{norm}}$ (TMP(H))	-8.8119			
D_{ref} (PhN)	5.7933E-10			
$\log D_{\text{ref}}$ (PhN)	-9.2371			
MW_{det}	146			

				-50°C
		<i>Species</i>	MW_{calc} [g/mol]	MW_{err} [%]
D (TMP(H))	3.8820E-10	TMP(H)	141	4
$\log D$ (TMP(H))	-9.410944469			
$\log D_{x,\text{norm}}$ (TMP(H))	-8.7968			
D_{ref} (PhN)	3.1960E-10			
$\log D_{\text{ref}}$ (PhN)	-9.4954			
MW_{det}	136			

				-75°C
		<i>Species</i>	MW_{calc} [g/mol]	MW_{err} [%]
D (TMP(H))	2.0622E-10	TMP(H)	141	7
$\log D$ (TMP(H))	-9.685669217			
$\log D_{x,\text{norm}}$ (TMP(H))	-8.7907			
D_{ref} (PhN)	1.6743E-10			
$\log D_{\text{ref}}$ (PhN)	-9.7762			
MW_{det}	132			

A-Table 33. Calculation of the molar van der Waals density MD_w of all TMP species.

Species	Formula	MW_{calc}	MD_w [g/(mol·m ³)]	ΣV_w [m ³]
1A	C ₃₄ H ₆₈ Cl ₄ Li ₂ Mg ₂ N ₂ O ₄	773	5.72E+29	1.35E-27
1B	C ₂₆ H ₅₂ Cl ₂ Mg ₂ N ₂ O ₂	544	5.59E+29	9.74E-28
1C	C ₂₁ H ₄₂ Cl ₂ LiMgNO ₃	459	5.61E+29	8.18E-28
1C*	C ₁₇ H ₃₄ Cl ₂ LiMgNO ₂	387	5.72E+29	6.76E-28
Li1	C ₁₆ H ₃₂ Cl ₂ Li ₂ O ₄	373	5.64E+29	6.62E-28
1D	C ₁₇ H ₃₄ ClMgNO ₂	344	5.47E+29	6.29E-28
Li2	C ₁₆ H ₃₂ LiO ₄	295	4.99E+29	5.92E-28
1E	C ₁₃ H ₂₆ Cl ₂ MgNO	308	6.05E+29	5.09E-28

In the DOSY-ECC-MW-determination of TMPMgCl·LiCl **10** no species with MWs lower than 308 g/mol were observed, so aggregate **1E** can be neglected. All other species work very well with the used ECCs.

6 REFERENCES

- [1] R. Neufeld, R. Michel, R. Herbst-Irmer, R. Schöne, D. Stalke, *Chem. Eur. J.* **2016**, submitted.
- [2] R. Neufeld, T. L. Teuteberg, R. Herbst-Irmer, R. A. Mata, D. Stalke, *JACS* **2016**, accepted.
- [3] R. Neufeld, D. Stalke, *Chem. Eur. J.* **2016**, submitted.
- [4] S. Bachmann, R. Neufeld, M. Dzemski, D. Stalke, *Chem. Eur. J.* **2016**, accepted.
- [5] R. Neufeld, M. John, D. Stalke, *Angew. Chem.* **2015**, *127*, 7100-7104; *Angew. Chem. Int. Ed.* **2015**, *54*, 6994-6998.
- [6] R. Neufeld, D. Stalke, *Chem. Sci.* **2015**, *6*, 3354-3364.
- [7] R. Michel, T. Nack, R. Neufeld, J. M. Dieterich, R. A. Mata, D. Stalke, *Angew. Chem.* **2013**, *125*, 762-766; *Angew. Chem. Int. Ed.* **2013**, *52*, 734-738.
- [8] a) E. Carl, D. Stalke, in *Lithium Compounds in Organic Synthesis – From Fundamentals to Applications* (Eds.: Renzo Luisi, V. Capriati), Wiley-VCH, Weinheim, **2014**, pp. 1-31; b) T. Stey, D. Stalke, in *The Chemistry of Organolithium Compounds* (Eds.: Z. Rappoport, I. Marek), John Wiley & Sons, New York, **2004**, pp. 47-120.
- [9] a) D. L. Comins, J. M. Nolan, I. D. Bori, *Tetrahedron Lett.* **2005**, *46*, 6697-6699; b) M. T. Reetz, in *Encyclopedia of Reagents for Organic Synthesis*, John Wiley & Sons, Ltd, **2001**; c) D. C. Bradley, I. M. Thomas, *J. Chem. Soc.* **1960**, 3857-3861.
- [10] R. E. Mulvey, S. D. Robertson, *Angew. Chem.* **2013**, *125*, 11682-11700; *Angew. Chem. Int. Ed.* **2013**, *52*, 11470-11487.
- [11] a) R. E. Mulvey, *Chem. Soc. Rev.* **1991**, *20*, 167-209; b) D. R. Armstrong, D. Barr, W. Clegg, S. M. Hodgson, R. E. Mulvey, D. Reed, R. Snaith, D. S. Wright, *J. Am. Chem. Soc.* **1989**, *111*, 4719-4727; c) D. R. Armstrong, D. Barr, W. Clegg, R. E. Mulvey, D. Reed, R. Snaith, K. Wade, *J. Chem. Soc., Chem. Comm.* **1986**, 869-870.
- [12] a) Y. J. Kim, M. P. Bernstein, A. S. G. Roth, F. E. Romesberg, P. G. Williard, D. J. Fuller, A. T. Harrison, D. B. Collum, *J. Org. Chem.* **1991**, *56*, 4435-4439; b) E. Nakamura, K. Hashimoto, I. Kuwajima, *Tetrahedron Lett.* **1978**, *19*, 2079-2082.
- [13] a) A.-C. Pöppler, M. Granitzka, R. Herbst-Irmer, Y.-S. Chen, B. B. Iversen, M. John, R. A. Mata, D. Stalke, *Angew. Chem.* **2014**, *126*, 13498-13503; *Angew. Chem. Int. Ed.* **2014**, *53*, 13282-13287; b) M. Granitzka, A.-C. Pöppler, E. K. Schwarze, D. Stern, T. Schulz, M. John, R. Herbst-Irmer, S. K. Pandey, D. Stalke, *J. Am. Chem. Soc.* **2012**, *134*, 1344-1351; c) D. B. Collum, A. J. McNeil, A. Ramirez, *Angew. Chem.* **2007**, *17*, 3060-3077; *Angew. Chem. Int. Ed.* **2007**, *46*, 3002-3017; d) J. F. Remenar, D. B. Collum, *J. Am. Chem. Soc.* **1998**, *120*, 4081-4086.
- [14] a) J. L. Rutherford, D. B. Collum, *J. Am. Chem. Soc.* **2000**, *123*, 199-202; b) J. F. Remenar, B. L. Lucht, D. B. Collum, *J. Am. Chem. Soc.* **1997**, *119*, 5567-5572; c) F. E. Romesberg, D. B. Collum, *J. Am. Chem. Soc.* **1994**, *116*, 9198-9202.
- [15] R. R. Fraser, M. Bresse, T. S. Mansour, *J. Chem. Soc., Chem. Comm.* **1983**, 620-621.
- [16] R. Li-Yuan Bao, R. Zhao, L. Shi, *Chem. Commun.* **2015**, *51*, 6884-6900.
- [17] C. R. Hauser, H. G. Walker, *J. Am. Chem. Soc.* **1947**, *69*, 295-297.
- [18] P. E. Eaton, C. H. Lee, Y. Xiong, *J. Am. Chem. Soc.* **1989**, *111*, 8016-8018.
- [19] M. Shilai, Y. Kondo, T. Sakamoto, *J. Chem. Soc. Perkin Trans. 1* **2001**, 442-444.

- [20] Y. Kondo, A. Yoshida, T. Sakamoto, *J. Chem. Soc. Perkin Trans. 1* **1996**, 2331-2332.
- [21] M. C. Whisler, S. MacNeil, V. Snieckus, P. Beak, *Angew. Chem.* **2004**, *116*, 2256-2276; *Angew. Chem. Int. Ed.* **2004**, *43*, 2206-2225.
- [22] a) F. M. Piller, P. Appukkuttan, A. Gavryushin, M. Helm, P. Knochel, *Angew. Chem.* **2008**, *120*, 6907-6911; *Angew. Chem. Int. Ed.* **2008**, *47*, 6802-6806; b) J. P. Snyder, *J. Am. Chem. Soc.* **1995**, *117*, 11025-11026; c) T. Stemmler, J. E. Penner-Hahn, P. Knochel, *J. Am. Chem. Soc.* **1993**, *115*, 348-350; d) D. Stern, N. Finkelmeier, D. Stalke, *Chem. Commun.* **2011**, *47*, 2113-2115.
- [23] A. Krasovskiy, V. Krasovskaya, P. Knochel, *Angew. Chem.* **2006**, *118*, 3024-3027; *Angew. Chem. Int. Ed.* **2006**, *45*, 2958-2961.
- [24] a) D. Tilly, F. Chevallier, F. Mongin, P. C. Gros, *Chem. Rev.* **2014**, *114*, 1207-1257; b) T. Klatt, J. T. Markiewicz, C. Sämann, P. Knochel, *J. Org. Chem.* **2014**, *79*, 4253-4269; c) F. Mongin, A. Harrison-Marchand, *Chem. Rev.* **2013**, *113*, 7563-7727; d) G. C. Clososki, C. J. Rohbogner, P. Knochel, *Angew. Chem. Int. Ed.* **2007**, *46*, 7681-7684.
- [25] J. Clayden, C. C. Stimson, M. Keenan, *Chem. Commun.* **2006**, 1393-1394.
- [26] T. Bresser, P. Knochel, *Angew. Chem.* **2011**, *123*, 1954 – 1958; *Angew. Chem. Int. Ed.* **2011**, *50*, 1914-1917.
- [27] F. M. Piller, P. Knochel, *Synthesis* **2011**, *2011*, 1751-1758.
- [28] D. R. Armstrong, P. García-Álvarez, A. R. Kennedy, R. E. Mulvey, J. A. Parkinson, *Angew. Chem.* **2010**, *122*, 3253-3256; *Angew. Chem. Int. Ed.* **2010**, *49*, 3185-3188.
- [29] T. L. Rathman, J. A. Schwindeman, *Org. Process Res. Dev.* **2014**, *18*, 1192-1210.
- [30] N. D. R. Barnett, R. E. Mulvey, W. Clegg, P. A. O'Neil, *J. Am. Chem. Soc.* **1991**, *113*, 8187-8188.
- [31] Y. Ma, A. C. Hoepker, L. Gupta, M. F. Faggin, D. B. Collum, *J. Am. Chem. Soc.* **2010**, *132*, 15610-15623.
- [32] a) X. Sun, D. B. Collum, *J. Am. Chem. Soc.* **2000**, *122*, 2452-2458; b) J. F. Remenar, D. B. Collum, *J. Am. Chem. Soc.* **1997**, *119*, 5573-5582.
- [33] M. F. Lappert, M. J. Slade, A. Singh, J. L. Atwood, R. D. Rogers, R. Shakir, *J. Am. Chem. Soc.* **1983**, *105*, 302-304.
- [34] a) E. Hevia, A. R. Kennedy, R. E. Mulvey, D. L. Ramsay, S. D. Robertson, *Chem. Eur. J.* **2013**, *19*, 14069-14075; b) B. L. Lucht, D. B. Collum, *J. Am. Chem. Soc.* **1994**, *116*, 7949-7950.
- [35] a) P. L. Hall, J. H. Gilchrist, A. T. Harrison, D. J. Fuller, D. B. Collum, *J. Am. Chem. Soc.* **1991**, *113*, 9575-9585; b) P. Renaud, M. A. Fox, *J. Am. Chem. Soc.* **1988**, *110*, 5702-5705.
- [36] D. B. Collum, *Acc. Chem. Res.* **1993**, *26*, 227-234.
- [37] F. E. Romesberg, J. H. Gilchrist, A. T. Harrison, D. J. Fuller, D. B. Collum, *J. Am. Chem. Soc.* **1991**, *113*, 5751-5757.
- [38] a) J. F. Remenar, B. L. Lucht, D. Kruglyak, F. E. Romesberg, D. B. Collum, *J. Org. Chem.* **1997**, *62*, 5748-5754; b) F. E. Romesberg, D. B. Collum, *J. Am. Chem. Soc.* **1995**, *117*, 2166-2178; c) P. G. Williard, Q. Y. Liu, *J. Am. Chem. Soc.* **1993**, *115*, 3380-3381.
- [39] a) R. D. Rogers, J. L. Atwood, R. Grüning, *J. Organomet. Chem.* **1978**, *157*, 229-237; b) D. Mootz, A. Zinnius, B. Böttcher, *Angew. Chem.* **1969**, *81*, 398-399; *Angew. Chem. Int. Ed.* **1969**, *8*, 378-379.
- [40] a) M. Driess, H. Pritzkow, M. Skipinski, U. Winkler, *Organometallics* **1997**, *16*, 5108-5112; b) J. Knizek, I. Krossing, H. Nöth, H. Schwenk, T. Seifert, *Chem. Ber.* **1997**, *130*, 1053-1062.
- [41] R. Grüning, J. L. Atwood, *J. Organomet. Chem.* **1977**, *137*, 101-111.

- [42] a) K. F. Tesh, T. P. Hanusa, J. C. Huffman, *Inorg. Chem.* **1990**, 29, 1584-1586; b) P. Williard, *Acta Crystallogr. C* **1988**, 44, 270-272.
- [43] S. Neander, U. Behrens, *Z. Anorg. Allg. Chem.* **1999**, 625, 1429-1434.
- [44] T. Fjeldberg, P. B. Hitchcock, M. F. Lappert, A. J. Thorne, *J. Chem. Soc., Chem. Comm.* **1984**, 822-824.
- [45] J. C. Green, M. Payne, E. A. Seddon, R. A. Andersen, *J. Chem. Soc., Dalton Trans.* **1982**, 887-892.
- [46] a) G. C. Forbes, A. R. Kennedy, R. E. Mulvey, P. J. A. Rodger, R. B. Rowlings, *J. Chem. Soc., Dalton Trans.* **2001**, 1477-1484; b) K. W. Henderson, P. G. Williard, *Organometallics* **1999**, 18, 5620-5626; c) K. W. Henderson, A. E. Dorigo, Q.-Y. Liu, P. G. Williard, *J. Am. Chem. Soc.* **1997**, 119, 11855-11863; d) H. Mack, G. Frenzen, M. Bendikov, M. S. Eisen, *J. Organomet. Chem.* **1997**, 549, 39-43.
- [47] a) C. Knapp, E. Lork, T. Borrmann, W.-D. Stohrer, R. Mews, *Z. Anorg. Allg. Chem.* **2005**, 631, 1885-1892; b) G. C. Forbes, A. R. Kennedy, R. E. Mulvey, P. J. A. Rodger, *Chem. Commun.* **2001**, 1400-1401; c) M. Karl, G. Seybert, W. Massa, K. Harms, S. Agarwal, R. Maleika, W. Stelter, A. Greiner, W. H. B. Neumüller, K. Dehnicke, *Z. Anorg. Allg. Chem.* **1999**, 625, 1301-1309; d) F. T. Edelman, F. Pauer, M. Wedler, D. Stalke, *Inorg. Chem.* **1992**, 31, 4143-4146.
- [48] a) M. S. Hill, G. Kociok-Kohn, D. J. MacDougall, *Inorg. Chem.* **2011**, 50, 5234-5241; b) P. L. Arnold, I. J. Casely, Z. R. Turner, R. Bellabarba, R. B. Tooze, *Dalton Trans.* **2009**, 7236-7247.
- [49] a) D. M. Cousins, M. G. Davidson, C. J. Frankis, D. Garcia-Vivo, M. F. Mahon, *Dalton Trans.* **2010**, 39, 8278-8280; b) N. M. Clark, P. Garcia-Alvarez, A. R. Kennedy, C. T. O'Hara, G. M. Robertson, *Chem. Commun.* **2009**, 5835-5837; c) P. P. Power, X. Xiaojie, *J. Chem. Soc., Chem. Comm.* **1984**, 358-359.
- [50] a) W. J. Evans, D. B. Rego, J. W. Ziller, *Inorg. Chem.* **2006**, 45, 3437-3443; b) A. M. Domingos, G. M. Sheldrick, *Acta Crystallogr. B* **1974**, 30, 517-519.
- [51] B. Y. Kimura, T. L. Brown, *J. Organomet. Chem.* **1971**, 26, 57-67.
- [52] a) B. L. Lucht, D. B. Collum, *Acc. Chem. Res.* **1999**, 32, 1035-1042; b) B. L. Lucht, M. P. Bernstein, J. F. Remenar, D. B. Collum, *J. Am. Chem. Soc.* **1996**, 118, 10707-10718.
- [53] P. G. Williard, M. A. Nichols, *J. Am. Chem. Soc.* **1991**, 113, 9671-9673.
- [54] a) P. Woidy, M. Buhl, F. Kraus, *Dalton Trans.* **2015**, 44, 7332-7337; b) T. G. Müller, F. Karau, W. Schnick, F. Kraus, *Angew. Chem.* **2014**, 126, 13913-13915; *Angew. Chem. Int. Ed.* **2014**, 53, 13695-13697; c) M. Neumeier, F. Fendt, S. Gärtner, C. Koch, T. Gärtner, N. Korber, R. M. Gschwind, *Angew. Chem.* **2013**, 125, 4579-4582; *Angew. Chem. Int. Ed.* **2013**, 52, 4483-4486; d) H. Nuss, M. Jansen, *Angew. Chem.* **2006**, 118, 4476-4479; *Angew. Chem. Int. Ed.* **2006**, 45, 4369-4371.
- [55] a) J. Hey, D. M. Andrada, R. Michel, R. A. Mata, D. Stalke, *Angew. Chem.* **2013**, 125, 10555-10559; *Angew. Chem. Int. Ed.* **2013**, 52, 10365-10369; b) R. Michel, R. Herbst-Irmer, D. Stalke, *Organometallics* **2010**, 29, 6169-6171.
- [56] P. Ji, J. Atherton, M. I. Page, *J. Org. Chem.* **2011**, 76, 1425-1435.
- [57] C. G. A. Inc., *Handbook of compressed gases*, Kluwer Academic Publishers Group, Dordrecht, Netherlands, **1999**.
- [58] A. F. Holleman, N. Wiberg, *Lehrbuch der Anorganischen Chemie, Vol. 102*, de Gruyter, Berlin, **2007**.
- [59] L. V. Coulter, J. R. Sinclair, A. G. Cole, G. C. Roper, *J. Am. Chem. Soc.* **1959**, 81, 2986-2989.
- [60] E. J. Behrman, *J. Chem. Educ.* **2006**, 83, 1290.
- [61] T. Francis, *CRC Handbook of Chemistry and Physics, Vol. 87*, Boca Raton, **2006**.

- [62] a) T. M. Harris, C. M. Harris, *J. Org. Chem.* **1966**, *31*, 1032-1035; b) T. H. Vaughn, G. F. Hennion, R. R. Vogt, J. A. Nieuwland, *J. Org. Chem.* **1937**, *02*, 1-22; c) L. H. Baldinger, J. A. Nieuwland, *J. Am. Chem. Soc.* **1933**, *55*, 2851-2853.
- [63] U. Wannagat, H. Niederprüm, *Angew. Chem.* **1959**, *71*, 574-574.
- [64] J. F. Allan, W. Clegg, K. W. Henderson, L. Horsburgh, A. R. Kennedy, *J. Organomet. Chem.* **1998**, *559*, 173-179.
- [65] W. Schlenk, W. Schlenk, *Chem. Ber.* **1929**, *62*, 920-924.
- [66] F. W. Walker, E. C. Ashby, *J. Am. Chem. Soc.* **1969**, *91*, 3845-3850.
- [67] a) Ö. Seven, M. Bolte, H.-W. Lerner, *Acta Crystallogr. E* **2013**, *69*, m424-m424; b) M. A. Nesbit, D. L. Gray, G. S. Girolami, *Acta Crystallogr. E* **2012**, *68*, m942; c) W. Ren, G. Zi, D.-C. Fang, M. D. Walter, *Chem. Eur. J.* **2011**, *17*, 12669-12682; d) A. G. Avent, C. F. Caro, P. B. Hitchcock, M. F. Lappert, Z. Li, X.-H. Wei, *Dalton Trans.* **2004**, 1567-1577; e) A. L. Spek, P. Voorbergen, G. Schat, C. Blomberg, F. Bickelhaupt, *J. Organomet. Chem.* **1974**, *77*, 147-151; f) L. J. Guggenberger, R. E. Rundle, *J. Am. Chem. Soc.* **1968**, *90*, 5375-5378.
- [68] a) E. C. Ashby, M. B. Smith, *J. Am. Chem. Soc.* **1964**, *86*, 4363-4370; b) E. C. Ashby, W. E. Becker, *J. Am. Chem. Soc.* **1963**, *85*, 118-119.
- [69] M. B. Smith, W. E. Becker, *Tetrahedron* **1967**, *23*, 4215-4227.
- [70] a) E. C. Ashby, J. Nackashi, G. E. Parris, *J. Am. Chem. Soc.* **1975**, *97*, 3162-3171; b) E. C. Ashby, G. E. Parris, *J. Am. Chem. Soc.* **1971**, *93*, 1206-1213; c) E. C. Ashby, S. Yu, *J. Organometal. Chem.* **1971**, *29*, 339-348.
- [71] D. Seyferth, *Organometallics* **2009**, *28*, 1598-1605.
- [72] P. García-Álvarez, D. V. Graham, E. Hevia, A. R. Kennedy, J. Klett, R. E. Mulvey, C. T. O'Hara, S. Weatherstone, *Angew. Chem.* **2008**, *120*, 8199-8201; *Angew. Chem. Int. Ed.* **2008**, *47*, 8079-8081.
- [73] a) K.-C. Yang, C.-C. Chang, J.-Y. Huang, C.-C. Lin, G.-H. Lee, Y. Wang, M. Y. Chiang, *J. Organomet. Chem.* **2002**, *648*, 176-187; b) R. A. Bartlett, M. M. Olmstead, P. P. Power, *Inorg. Chem.* **1994**, *33*, 4800-4803.
- [74] A. R. Kennedy, R. E. Mulvey, S. D. Robertson, *Dalton Trans.* **2010**, *39*, 9091-9099.
- [75] A. S. Batsanov, P. D. Bolton, R. C. B. Copley, M. G. Davidson, J. A. K. Howard, C. Lustig, R. D. Price, *J. Organomet. Chem.* **1998**, *550*, 445-448.
- [76] a) A. Krasovskiy, B. F. Straub, P. Knochel, *Angew. Chem.* **2006**, *118*, 165-169; *Angew. Chem. Int. Ed.* **2006**, *45*, 159-162; b) A. Krasovskiy, P. Knochel, *Angew. Chem.* **2004**, *116*, 3396-3399; *Angew. Chem. Int. Ed.* **2004**, *43*, 3333-3336.
- [77] D. Li, I. Keresztes, R. Hopson, P. G. Williard, *Acc. Chem. Res.* **2008**, *42*, 270-280.
- [78] a) E. O. Stejskal, J. E. Tanner, *J. Chem. Phys.* **1965**, *42*, 288-292; b) J. E. Tanner, *Rev. Sci. Instrum.* **1965**, *36*, 1086-1087; c) E. O. Stejskal, *J. Chem. Phys.* **1965**, *43*, 3597-3603.
- [79] a) P. Pregosin, *Acta Crystallogr. C* **2013**, *69*, 1433-1436; b) K. A. Heisel, J. J. Goto, V. V. Krishnan, *AJAC* **2012**, *3*, 401-409; c) A. Macchioni, G. Ciancaleoni, C. Zuccaccia, D. Zuccaccia, *Chem. Soc. Rev.* **2008**, *37*, 479-489; d) P. S. Pregosin, P. G. A. Kumar, I. Fernández, *Chem. Rev.* **2005**, *105*, 2977-2998.
- [80] a) I. V. Nesmelova, V. D. Fedotov, *BBA* **1998**, *1383*, 311-316; b) D. Jayawickrama, S. Zink, D. V. Velde, R. I. Effiong, C. K. Larive, *J. Biomol. Struct. Dyn.* **1995**, *13*, 229-244.

- [81] a) S. Augé, P.-O. Schmit, C. A. Crutchfield, M. T. Islam, D. J. Harris, E. Durand, M. Clemancey, A.-A. Quoineaud, J.-M. Lancelin, Y. Prigent, F. Taulelle, M.-A. Delsuc, *J. Phys. Chem., B* **2009**, *113*, 1914-1918; b) S. Viel, D. Capitani, L. Mannina, A. Segre, *Biomacromolecules* **2003**, *4*, 1843-1847; c) A. Chen, D. Wu, C. S. Johnson, *J. Am. Chem. Soc.* **1995**, *117*, 7965-7970.
- [82] a) H. C. Gaede, K. Gawrisch, *Magn. Reson. Chem.* **2004**, *42*, 115-122; b) M. Braun, U. Hartnagel, E. Ravanelli, B. Schade, C. Böttcher, O. Vostrowsky, A. Hirsch, *Eur. J. Org. Chem.* **2004**, *2004*, 1983-2001; c) H. Ihm, J.-S. Ahn, M. S. Lah, Y. H. Ko, K. Paek, *Org. Lett.* **2004**, *6*, 3893-3896.
- [83] a) S. C. Hunter, S.-J. Chen, C. A. Steren, M. G. Richmond, Z.-L. Xue, *Organometallics* **2015**; b) M. M. Kireenko, E. A. Kuchuk, K. V. Zaitsev, V. A. Tafeenko, Y. F. Oprunenko, A. V. Churakov, E. K. Lermontova, G. S. Zaitseva, S. S. Karlov, *Dalton Trans.* **2015**, *44*, 11963-11976; c) E. Weisheim, C. G. Reuter, P. Heinrichs, Y. V. Vishnevskiy, A. Mix, B. Neumann, H.-G. Stammler, N. W. Mitzel, *Chem. Eur. J.* **2015**, *21*, 12436-12448; d) C. Su, R. Hopson, P. G. Williard, *Eur. J. Inorg. Chem.* **2013**, *2013*, 4136-4141; e) S. E. Baillie, W. Clegg, P. García-Álvarez, E. Hevia, A. R. Kennedy, J. Klett, L. Russo, *Organometallics* **2012**, *31*, 5131-5142.
- [84] A. Einstein, R. Furth, A. D. Cowper, *Investigations on the Theory of the Brownian Movement*, Courier Dover Publications, Mineola, NY, **1956**.
- [85] E. L. Hahn, *Phys. Rev.* **1950**, *80*, 580-594.
- [86] J. E. Tanner, *J. Chem. Phys.* **1970**, *52*, 2523-2526.
- [87] D. E. Woessner, *J. Chem. Phys.* **1961**, *34*, 2057-2061.
- [88] D. H. Wu, A. D. Chen, C. S. Johnson, *J. Magn. Reson.* **1995**, *115*, 260-264.
- [89] S. J. Gibbs, C. S. Johnson Jr, *Journal of Magnetic Resonance (1969)* **1991**, *93*, 395-402.
- [90] M. D. Pelta, G. A. Morris, M. J. Stchedroff, S. J. Hammond, *Magn. Reson. Chem.* **2002**, *40*, 147-152.
- [91] A. Jerschow, N. Müller, *J. Magn. Reson.* **1997**, *125*, 372-375.
- [92] M. Nilsson, G. A. Morris, *Chem. Commun.* **2007**, 933-935.
- [93] K. F. Morris, C. S. Johnson, *J. Am. Chem. Soc.* **1992**, *114*, 3139-3141.
- [94] M. Nilsson, A. M. Gil, I. Delgadillo, G. A. Morris, *Chem. Commun.* **2005**, 1737-1739.
- [95] B. Vitorge, D. Jeanneat, *Anal. Chem.* **2006**, *78*, 5601-5606.
- [96] A. Jerschow, N. Müller, *J. Magn. Reson.* **1996**, *123*, 222-225.
- [97] A. R. Waldeck, P. W. Kuchel, A. J. Lennon, B. E. Chapman, *Prog. Nucl. Magn. Reson. Spectrosc.* **1997**, *30*, 39-68.
- [98] A. Spornol, K. Z. Wirtz, *Z. Naturforsch., A Astrophys., Phys., Phys. Chem.* **1953**, *8*, 522-532.
- [99] H. C. Chen, S. H. Chen, *J. Phys. Chem.* **1984**, *88*, 5118-5121.
- [100] F. Perrin, *J. Phys. Radium* **1936**, *7*, 1-11.
- [101] R. Evans, Z. Deng, A. K. Rogerson, A. S. McLachlan, J. J. Richards, M. Nilsson, G. A. Morris, *Angew. Chem.* **2013**, *125*, 3281-3284; *Angew. Chem. Int. Ed.* **2013**, *52*, 3199-3202.
- [102] D. K. Wilkins, S. B. Grimshaw, V. Receveur, C. M. Dobson, J. A. Jones, L. J. Smith, *Biochemistry* **1999**, *38*, 16424-16431.
- [103] C. A. Crutchfield, D. J. Harris, *J. Magn. Reson.* **2007**, *185*, 179-182.

- [104] a) J. Guang, R. Hopson, P. G. Williard, *J. Org. Chem.* **2015**, *80*, 9102-9107; b) C. Su, R. Hopson, P. G. Williard, *J. Am. Chem. Soc.* **2013**, *135*, 14367-14379; c) G. Kagan, W. Li, R. Hopson, P. G. Williard, *Org. Lett.* **2009**, *11*, 4818-4821; d) D. Li, G. Kagan, R. Hopson, P. G. Williard, *J. Am. Chem. Soc.* **2009**, *131*, 5627-5634; e) D. Li, R. Hopson, W. Li, J. Liu, P. G. Williard, *Org. Lett.* **2008**, *10*, 909-911.
- [105] a) A. J. Martinez-Martinez, D. R. Armstrong, B. Conway, B. J. Fleming, J. Klett, A. R. Kennedy, R. E. Mulvey, S. D. Robertson, C. T. O'Hara, *Chem. Sci.* **2014**, *5*, 771-781; b) D. R. Armstrong, A. R. Kennedy, R. E. Mulvey, S. D. Robertson, *Dalton Trans.* **2013**, *42*, 3704-3711; c) D. R. Armstrong, P. García-Álvarez, A. R. Kennedy, R. E. Mulvey, S. D. Robertson, *Chem. Eur. J.* **2011**, *17*, 6725-6730; d) P. García-Álvarez, R. E. Mulvey, J. A. Parkinson, *Angew. Chem.* **2011**, *123*, 9842-9845; *Angew. Chem. Int. Ed.* **2011**, *50*, 9668-9671.
- [106] G. R. Fulmer, A. J. M. Miller, N. H. Sherden, H. E. Gottlieb, A. Nudelman, B. M. Stoltz, J. E. Bercaw, K. I. Goldberg, *Organometallics* **2010**, *29*, 2176-2179.
- [107] S. Floquet, S. Brun, J.-F. Lecomte, M. Henry, M.-A. Delsuc, Y. Prigent, E. Cadot, F. Taulelle, *J. Am. Chem. Soc.* **2009**, *131*, 17254-17259.
- [108] M. A. Jacobson, I. Keresztes, P. G. Williard, *J. Am. Chem. Soc.* **2005**, *127*, 4965-4975.
- [109] P. Paetzold, *Chemie: Eine Einführung*, Walter de Gruyter, Berlin, **2009**.
- [110] A. Bondi, *J. Phys. Chem.* **1964**, *68*, 441-451.
- [111] The van der Waals radii were taken from: A. Bondi, *J. Phys. Chem.* **1964**, *68*, 441-451.
- [112] D. Stern, N. Finkelmeier, K. Meindl, J. Henn, D. Stalke, *Angew. Chem.* **2010**, *122*, 7021-7024; *Angew. Chem. Int. Ed.* **2010**, *49*, 6869-6872.
- [113] J. L. Rutherford, D. B. Collum, *J. Am. Chem. Soc.* **1999**, *121*, 10198-10202.
- [114] P. Zhao, D. B. Collum, *J. Am. Chem. Soc.* **2003**, *125*, 4008-4009.
- [115] R. E. Dinnebier, S. Neander, U. Behrens, F. Olbrich, *Organometallics* **1999**, *18*, 2915-2918.
- [116] a) R. Michel, R. Herbst-Irmer, D. Stalke, *Organometallics* **2011**, *30*, 4379-4386; b) T. Kähler, U. Behrens, S. Neander, F. Olbrich, *J. Organomet. Chem.* **2002**, *649*, 50-54; c) R. E. Dinnebier, U. Behrens, F. Olbrich, *Organometallics* **1997**, *16*, 3855-3858.
- [117] a) T. Nishinaga, D. Yamazaki, H. Stahr, A. Wakamiya, K. Komatsu, *J. Am. Chem. Soc.* **2003**, *125*, 7324-7335; b) Z. Hou, Y. Zhang, H. Tezuka, P. Xie, O. Tardif, T.-a. Koizumi, H. Yamazaki, Y. Wakatsuki, *J. Am. Chem. Soc.* **2000**, *122*, 10533-10543.
- [118] R. R. Fraser, T. S. Mansour, S. Savard, *J. Org. Chem.* **1985**, *50*, 3232-3234.
- [119] A.-C. Pöppler, M. M. Meinholz, H. Faßhuber, A. Lange, M. John, D. Stalke, *Organometallics* **2012**, *31*, 42-45.
- [120] Y. Sarazin, S. J. Coles, D. L. Hughes, M. B. Hursthouse, M. Bochmann, *Eur. J. Inorg. Chem.* **2006**, 3211-3220.
- [121] Z. Rappoport, I. Marek, *The Chemistry of Organomagnesium Compounds, Part I*, John Wiley & Sons Ltd, West Sussex, England, **2008**.
- [122] a) S. Grimme, J. Antony, S. Ehrlich, H. Krieg, *J. Chem. Phys.* **2010**, *132*, 154104; b) F. Weigend, R. Ahlrichs, *Phys. Chem. Chem. Phys.* **2005**, *7*, 3297-3305; c) A. D. Becke, *J. Chem. Phys.* **1993**, *98*, 5648-5652; d) A. D. Becke, *Phys. Rev. A* **1988**, *38*, 3098-3100; e) C. Lee, W. Yang, R. G. Parr, *Phys. Rev. B* **1988**, *37*, 785-789.
- [123] A. Klamt, G. Schuurmann, *J. Chem. Soc. Perkin Trans. 2* **1993**, 799-805.

- [124] a) D. Stern, M. Granitzka, T. Schulz, D. Stalke, *Z. Naturforsch.* **2010**, *65b*, 719-724; b) J. Tammiku-Taul, P. Burk, A. Tuulmets, *J. Phys. Chem. A* **2004**, *108*, 133-139.
- [125] S. Sakamoto, T. Imamoto, K. Yamaguchi, *Org. Lett.* **2001**, *3*, 1793-1795.
- [126] F. Blasberg, M. Bolte, M. Wagner, H.-W. Lerner, *Organometallics* **2012**, *31*, 1001-1005.
- [127] a) A. V. Yakimansky, A. H. E. Müller, M. Van Beylen, *Macromolecules* **2000**, *33*, 5686-5692; b) W. Ming Keong, A. I. Popov, *J. Inorg. Nucl. Chem.* **1972**, *34*, 3615-3622; c) S. H. Bauer, T. Ino, R. F. Porter, *J. Chem. Phys.* **1960**, *33*, 685-691.
- [128] C. Elschenbroich, F. Hensel, H. Hopf, *Organometallchemie*, Vol. 6, B. G. Teubner Verlag, Wiesbaden, **2008**.
- [129] a) J. Vollet, J. R. Hartig, K. Baranowska, H. Schnöckel, *Organometallics* **2006**, *25*, 2101-2103; b) U. Casellato, F. Ossola, *Organometallics* **1994**, *13*, 4105-4108.
- [130] B. M. Gridley, T. J. Blundell, G. J. Moxey, W. Lewis, A. J. Blake, D. L. Kays, *Chem. Commun.* **2013**, *49*, 9752-9754.
- [131] J. O. C. Jiménez-Halla, F. M. Bickelhaupt, M. Solà, *J. Organomet. Chem.* **2011**, *696*, 4104-4111.
- [132] a) M. Brym, C. Jones, P. C. Junk, M. Kloth, *Z. Anorg. Allg. Chem.* **2006**, *632*, 1402-1404; b) S. Courtenay, P. Wei, D. W. Stephan, *Can. J. Chem.* **2003**, *81*, 1471-1476; c) F. Neumann, F. Hampel, P. v. R. Schleyer, *Inorg. Chem.* **1995**, *34*, 6553-6555.
- [133] a) A. D. Sutton, T. Ngyuen, J. C. Fettinger, M. M. Olmstead, G. J. Long, P. P. Power, *Inorg. Chem.* **2007**, *46*, 4809-4814; b) A. S. Batsanov, M. G. Davidson, J. A. K. Howard, S. Lamb, C. Lustig, R. D. Price, *Chem. Commun.* **1997**, 1211-1212; c) N. H. Buttrus, C. Eaborn, M. N. A. El-Kheli, P. B. Hitchcock, J. D. Smith, A. C. Sullivan, K. Tavakkoli, *J. Chem. Soc., Dalton Trans.* **1988**, 381-391.
- [134] D. Ardura, R. López, T. L. Sordo, *J. Phys. Chem., B.* **2005**, *109*, 23618-23623.
- [135] a) J. Francos, B. J. Fleming, P. Garcia-Alvarez, A. R. Kennedy, K. Reilly, G. M. Robertson, S. D. Robertson, C. T. O'Hara, *Dalton Trans.* **2014**, *43*, 14424-14431; b) B. Baishya, *J. Organomet. Chem.* **2014**, *769*, 112-118.
- [136] E. Hevia, A. R. Kennedy, R. E. Mulvey, S. Weatherstone, *Angew. Chem.* **2004**, *116*, 1741-1744; *Angew. Chem. Int. Ed.* **2004**, *43*, 1709-1712.
- [137] R. Neufeld, T. L. Teuteberg, R. Herbst-Irmer, R. A. Mata, D. Stalke, *JACS* **2016**, accepted.
- [138] A. C. Jones, A. W. Sanders, M. J. Bevan, H. J. Reich, *J. Am. Chem. Soc.* **2007**, *129*, 3492-3493.
- [139] W. Schlenk, J. Holtz, *Ber. Dtsch. Chem. Ges.* **1917**, *50*, 262-274.
- [140] a) E. R. Johnson, A. D. Becke, *J. Chem. Phys.* **2006**, *124*, 174104; b) A. D. Becke, E. R. Johnson, *J. Chem. Phys.* **2005**, *123*, 154101; c) E. R. Johnson, A. D. Becke, *J. Chem. Phys.* **2005**, *123*, 024101.
- [141] S. Grimme, *Chem. Eur. J.* **2012**, *18*, 9955-9964.
- [142] F. Neese, *WIREs Comput. Mol. Sci.* **2012**, *2*, 73-78.
- [143] a) D. Stalke, *Chem. Soc. Rev.* **1998**, *27*, 171-178; b) T. Kottke, D. Stalke, *J. Appl. Crystallogr.* **1993**, *26*, 615-619.
- [144] T. Schulz, K. Meindl, D. Leusser, D. Stern, J. Graf, C. Michaelson, M. Ruf, G. M. Sheldrick, D. Stalke, *J. Appl. Crystallogr.* **2009**, *42*, 885 - 891.
- [145] SAINT v8.30c in Bruker APEX2 v2012.2, Bruker AXS Inst. Inc., Madison, USA, **2012**.
- [146] G. M. Sheldrick, SADABS-2015/1, Universität Göttingen, Germany, **2012**.
- [147] G. M. Sheldrick, *Acta Crystallogr.* **2015**, *A71*, 3-8.
- [148] G. M. Sheldrick, *Acta Crystallogr.* **2015**, *C71*, 3-8.

- [149] a) A. Thorn, B. Dittrich, G. M. Sheldrick, *Acta Cryst.* **2012**, A68, 448–451; b) L. Krause, R. Herbst-Irmer, G. M. Sheldrick, D. Stalke, *J. Appl. Crystallogr.* **2015**, 48, 3–10; c) P. Müller, R. Herbst-Irmer, A. L. Spek, T. R. Schneider, M. R. Sawaya, *Crystal Structure Refinement—A Crystallographer's Guide to SHELXL*, Oxford University Press, Oxford (England), **2006**.
- [150] H. J. Reich, J. P. Borst, R. R. Dykstra, P. D. Green, *J. Am. Chem. Soc.* **1993**, 115, 8728–8741.
- [151] A. S. Galiano-Roth, D. B. Collum, *J. Am. Chem. Soc.* **1989**, 111, 6772–6778.

Danksagung

Viele Menschen haben zum Gelingen dieser Doktorarbeit beigetragen. Bei ihnen möchte ich mich hiermit nochmals bedanken:

An erster Stelle danke ich Herrn Prof. Dr. Dietmar Stalke für die Möglichkeit, bei ihm arbeiten und forschen zu dürfen und für die Freiheit, die er mir damit gelassen hat.

Herrn Prof. Dr. Sven Schneider danke ich für die Übernahme des Korreferats dieser Arbeit. Des Weiteren sei den Mitgliedern der Prüfungskommission gedankt.

Prof. Ricardo Mata und Thorsten Teuteberg danke ich für die wertvollen Ergebnisse aus theoretischen Rechnungen und für die tolle Zusammenarbeit.

Sebastian Bachmann, Thomas Niklas und Peter Stollberg danke ich für das Korrekturlesen dieser Arbeit. Ich danke euch ebenfalls für die vielen anregenden und teilweise auch sehr lustigen Diskussionen.

Dem gesamten Arbeitskreis danke ich für die angenehme Atmosphäre und die zahlreichen, leckeren Kaffee- und Kuchenpausen.

Den vielen „Diffraktometerschraubern“ und Martin Schlote sei ebenfalls vielmals für ihr Engagement und ihre Hilfestellung gedankt.

Michael John danke ich für die Beratung rund um das Thema NMR und Regine Herbst-Irmer für die Unterstützung rund um das Thema Kristallografie.

Ein weiterer Dank gilt Annegret Lehmberg, Benjamin Neding, Hendrik Alexander Schwenson und Sinja Pagel für die Herstellung der Hauser Base im Rahmen des MaWi-Praktikums.

Des Weiteren danke ich meinen Forschungspraktikanten Markus Kinauer, Mona Wilken und Martin Dzemski für die unterstützende Hand bei der Forschungsarbeit.

Der größte Dank gilt meiner Frau Nadine. Ohne deine Unterstützung und deinen Rückhalt hätte ich mich während meiner Promotion niemals so entfalten können. Ich bin sehr froh, dass ich dich habe.

Meinen Freunden danke ich vielmals für die Unterstützung und die schöne Ablenkung.

Zu guter Letzt danke ich meiner Familie. Ich danke euch für alles!

Curriculum Vitae

Personal Data

Name: Roman Neufeld
Date of birth: 29.03.1985 in Pavlodar/Kazakhstan
Nationality: German
Marital status: Married to Nadine Wolf-Neufeld
Address: Nelkenwinkel 5, 37081 Göttingen
E-mail: rneufeld@uni.de



Scientific Career

09.2012 – 03.2016 Ph. D. thesis “*DOSY External Calibration Curve Molecular Weight Determination as a Valuable Methodology in Characterizing Reactive Intermediates in Solution*” in Prof. Dr. D. Stalke’s workgroup at the Institute of Inorganic Chemistry at Georg-August-University Göttingen (Grade “*summa cum laude*”)

09.2012 – 02.2016 Scientific researcher with Prof. Dr. D. Stalke within the Georg-August-University School of Science (GAUSS) doctoral programme with funding by Centre for Materials Crystallography (CMC) as part of the Danish National Research Foundation (DNRF93)

10.2011 – 04.2012 Master’s thesis “*Neuartige Alkalimetall-Amid-Ammoniakate*” within Prof. Dr. D. Stalke’s workgroup at the Institute of Inorganic Chemistry at Georg-August-University Göttingen (Grade 1.0)

10.2009 – 05.2012 Master of Science in Chemistry at Georg-August-University Göttingen (Grade 1.7)

04.2009 – 08.2009 Bachelor’s thesis “*Palladium-katalysierte Kupplungsreaktionen zur Synthese von C-Glycosiden*” in Dr. D. B. Werz’s workgroup at the Institute of Organic and Biomolecular Chemistry at Georg-August-University Göttingen (Grade 1.7)

10.2006 – 08.2009 Bachelor of Science in Chemistry at Georg-August-University Göttingen (Grade 2.3)

10.2005 – 06.2006 Guest student in Nanostructure Sciences at University of Kassel.

09.1997 – 06.2005 A-level at Gustav-Stresemann-Gymnasium, Bad Wildungen (Grade 2.4)

Experience in University and Abroad

09.2012 – 02.2016	Scientific researcher with Prof. Dr. D. Stalke
03.2013 – 02.2016	Radiation protection commissioner within the group of Prof. Dr. D. Stalke
06.2015 – 02.2016	Supervision of practical labwork of major chemistry students (<i>Inorganic Synthesis</i>)
06.2014 – 06.2015	Supervision of practical labwork of material science students (<i>Inorganic Material Synthesis</i>)
09.2012 – 06.2014	Development of the chemistry labwork course <i>Inorganic Material Synthesis</i> for material science students.
09.2007 – 06.2013	IT service and network administrator at the Student Hostel <i>ROKO</i> , Göttingen
09.2011 – 06.2012	Supervision of practical labwork (incl. seminars) of medical and dental students (<i>Chemistry for Medical and Dental Students</i>)
04.2003 – 04.2005	Ice cream manufacturer at ice cream shop <i>San Marco</i> , Waldeck

Awards

07.2015	Winner of the award “ <i>Bester Vortrag</i> ” at Jung Chemiker Forum, Georg-August-University, Göttingen
06.2015	Second winner of the “ <i>Winterfeldt-Preis</i> ” at Leibniz University, Hannover
12.2014	Winner of the award “ <i>Preis für die beste nichtselbstständige Lehre am Institut für Anorganische Chemie</i> ” at Georg-August-University, Göttingen
10.2011	Winner of the “ <i>Paint Club Urban Art Battle Göttingen</i> ”

Skills and Interests

Languages	German (native), English (fluent), Russian and French (basics)
EDV	Microsoft Office Scientific data processing software (ChemDraw, Origin, Topspin, MestreNova) Adobe Photoshop
Radiation protection	Qualification: S1.1, S1.2, S1.3, S2.1, S2.2, S5, S6.1 (StrSchV) and R2.1 (RöV)
Expertise	According to §5 Chemikalienverbotsordnung
Hobbies	Biking, football, table tennis, photography and image editing

Scientific Conference Participations

1. *Jung Chemiker Forum 2015*, Göttingen, Germany–Talk “*Akkurate Molekulgewichtsbestimmungen zur Charakterisierung reaktiver metallorganischer Verbindungen mittels einer neuen DOSY-NMR-Methode*”
2. *Winterfeldt-Preis 2015*, Hanover, Germany–Talk (invited) “*Charakterisierung reaktiver metallorganischer Verbindungen mittels einer neuen DOSY-NMR-Methode*”
3. *European Congress on Magnetic Resonance (EUROMAR) 2015*, Prag, Czech Republic–Poster (Student Grant) “*Accurate Molecular Weight Determination via DOSY-NMR*”
4. *41st International Conference on Coordination Chemistry (ICCC-41) 2014*, Singapur–Poster “*Alkali Metal Coordinated Hexamethyldisilazides from Liquid Ammonia*”
5. *Center for Materials Crystallography Conference (CMC) 2014*, Göttingen, Germany–Talk “*Structural Insight into Ammonia Solvated Alkalimetal-HMDS*”
6. *20th EuCheMS Conference on Organometallic Chemistry (EuCOMC XX) 2013*, St. Andrews, United Kingdom–Poster (Travel Grant) “*Tune-up Aggregation of Alkali-HMDS with Ammonia*”
7. *Jung Chemiker Forum 2013*, Göttingen, Germany–Poster “*Ammonia, a Powerful Donorbase for Alkali Metal Hexamethyldisilazides*”

Scientific Publications in Print

1. R. Neufeld, T. L. Teuteberg, R. Herbst-Irmer, R. A. Mata, D. Stalke “*Solution Structures of Hauser Base ${}^i\text{Pr}_2\text{NMgCl}$ and Turbo-Hauser Base ${}^i\text{Pr}_2\text{NMgCl}\cdot\text{LiCl}$ in THF and the Influence of LiCl on the Schlenk-Equilibrium*” *JACS* **2016**, accepted.
2. R. Neufeld, D. Stalke “*Solution Structure of Turbo-Hauser Base $\text{TMPMgCl}\cdot\text{LiCl}$ in THF- d_6* ” *Chem. Eur. J.* **2016**, submitted.
3. R. Neufeld, R. Michel, R. Herbst-Irmer, R. Schöne, D. Stalke “*Introducing a Hydrogen Bond Donor Into a Non Nucleophilic Brønsted Base: Structural insight into Ammonia Coordinated Alkali Metal Hexamethyldisilazide (HMDS, metal = Li, Na, K, Rb and Cs)*” *Chem. Eur. J.* **2016**, submitted.
4. S. Bachmann, R. Neufeld, M. Dzemski, D. Stalke “*New External Calibration Curves (ECCs) for the Determination of Molecular Weights in Various Common NMR Solvents*” *Chem. Eur. J.* **2016**, accepted.
5. R. Neufeld, M. John, D. Stalke “*The Donor-Base-Free Aggregation of Lithium Diisopropyl Amide in Hydrocarbons Revealed by a DOSY Method*” *Angew. Chem. Int. Ed.* **2015**, 54, 6994–6998; *Angew. Chem.* **2015**, 127, 7100–7104, Frontispiece Cover.

6. R. Neufeld, D. Stalke “Accurate Molecular Weight Determination of Small Molecules via DOSY-NMR by Using External Calibration Curves with Normalized Diffusion Coefficients” *Chem. Sci.* **2015**, 6, 3354–3364.
7. P. P. Samuel, R. Neufeld, K. C. Mondal, H. W. Roesky, R. Herbst-Irmer, D. Stalke, S. Demeshko, F. Meyer, V. C. Rojisha, S. De, P. Parameswaran, A. C. Stuckl, W. Kaim, J. H. Christian, J. K. Bindra, N. S. Dalal “Cr(I)Cl as well as Cr⁺ are stabilised between two cyclic alkyl amino carbenes” *Chem. Sci.* **2015**, 6, 3148–3153.
8. P. P. Samuel, K. C. Mondal, N. Amin Sk, H. W. Roesky, E. Carl, R. Neufeld, D. Stalke, S. Demeshko, F. Meyer, L. Ungur, L. F. Chibotaru, J. Christian, V. Ramachandran, J. van Tol, N. S. Dalal “Electronic Structure and Slow Magnetic Relaxation of Low-Coordinate Cyclic Alkyl(amino) Carbene Stabilized Iron(I) Complexes” *J. Am. Chem. Soc.* **2014**, 136, 11964–11971.
9. J. Wallbaum, R. Neufeld, D. Stalke, D. B. Werz “A Domino Approach to Dibenzopentafulvalenes by Quadruple Carbopalladation” *Angew. Chem. Int. Ed.* **2013**, 52, 13243–13246; *Angew. Chem.* **2013**, 125, 13485–13488.
10. R. Michel, T. Nack, R. Neufeld, J. M. Dieterich, R. A. Mata, D. Stalke “The Layered Structure of [Na(NH₃)₄][Indenide] Containing a Square-Planar Na(NH₃)₄⁺ Cation” *Angew. Chem. Int. Ed.* **2013**, 52, 734–738; *Angew. Chem.* **2013**, 125, 762–766.
11. D. C. Koester, M. Leibeling, R. Neufeld, D. B. Werz “A Pd-Catalyzed Approach to (1→6)-Linked C-Glycosides” *Org. Lett.* **2010**, 12, 3934–3937.

Göttingen, March 31, 2016